Modeling and Optimization of Rechargeable Sensor Networks

Liguang Xie

Dissertation submitted to the Faculty of the
Virginia Polytechnic Institute and State University
in partial fulfillment of the requirements for the degree of

Doctor of Philosophy
in
Computer Engineering

Y. Thomas Hou, Chair
Wenjing Lou
Hanif D. Sherali
Yi Shi
Anil Vullikanti
Yaling Yang

August 16, 2013
Blacksburg, Virginia

Keywords: Wireless Sensor Networks, Wireless Energy Transfer,
Energy, Networking, Modeling, Optimization

Modeling and Optimization of Rechargeable Sensor Networks

Liguang Xie

Abstract

Over the past fifteen years, advances in Micro-Electro-Mechanical Systems (MEMS) technology have enabled rapid development of wireless sensor networks (WSNs). A WSN consists of a large number of sensor nodes that are typically powered by batteries. Each sensor node collects useful information from its environment, and forwards this data to a base station through wireless communications. Applications of WSNs include environmental monitoring, industrial monitoring, agriculture, smart home monitoring, military surveillance, to name a few.

Due to battery constraint at each sensor node, a fundamental challenge for a WSN is its limited operational lifetime – the amount of time that the network can remain operational before some or all of the sensor nodes run out of battery. To conserve energy and prolong the lifetime of a WSN, there have been active research efforts across all network layers. Although these efforts help conserve energy usage and prolong network lifetime to some extent, energy and lifetime remain fundamental bottlenecks and are the key factors that hinder the wide-scale deployment of WSNs.

This dissertation addresses the energy problem of a WSN by exploiting a recent breakthrough in wireless energy transfer (WET) technology. This breakthrough WET technology is based on the so-called magnetic resonant coupling (MRC), which allows electric energy to be transferred from a source coil to a receive coil without any plugs or wires. The advantages of MRC are high energy transfer efficiency even under omni-direction, not requiring line-of-sight (LOS), and being robust against environmental conditions.

Inspired by this enabling WET technology, this dissertation focuses on applying MRC to a WSN and on studying how to optimally use this technology to address lifetime problem for a WSN. The goal is to fundamentally remove lifetime bottleneck for a WSN. The main contributions of this

dissertation are summarized as follows:

1. **Single-node Charging for a Sparse WSN.** We first investigate how MRC can be applied to a WSN so as to remove the lifetime performance bottleneck in a WSN, i.e., allowing a WSN to remain operational forever. We consider the scenario of a mobile wireless charging vehicle (WCV) periodically traveling inside the sensor network and charging each sensor node's battery wirelessly. We introduce the concept of renewable energy cycle and offer both necessary and sufficient conditions for a sensor node to maintain its renewable energy cycle. We study an optimization problem, with the objective of maximizing the ratio of the WCV's vacation time over the cycle time. For this problem, we prove that the optimal traveling path for the WCV is the shortest Hamiltonian cycle and uncover a number of important properties. Subsequently, we develop a near-optimal solution by a piecewise linear approximation technique and prove its performance guarantee. This first study shows that network lifetime bottleneck can be fundamentally resolved by WET.

2. **Multi-node Charging for a Dense WSN.** We next exploit recent advances in MRC that allows multiple sensor nodes to be charged at the same time, and show how MRC with multi-node charging capability can address the scalability problem associated with the single-node charging technology. We consider a WCV that periodically travels inside a WSN and can charge multiple sensor nodes simultaneously. Based on the charging range of the WCV, we propose a cellular structure that partitions the two-dimensional plane into adjacent hexagonal cells. We pursue a formal optimization framework by jointly optimizing the traveling path of the WCV, flow routing among the sensor nodes, and the charging time with each hexagonal cell. By employing discretization and a novel Reformulation-Linearization Technique (RLT), we develop a provably near-optimal solution for any desired level of accuracy. Through numerical results, we demonstrate that our solution can indeed address the scalability problem for WET in a dense WSN.

3. **Bundling Mobile Base Station and Wireless Energy Transfer: The Pre-planned Path**

Case. Our aforementioned work is based on the assumption that the location of base station is fixed and known in the WSN. On the other hand, it has been recognized that a mobile base station (MBS) can offer significant advantages over a fixed one. But employing two separate vehicles, one for WET and one for MBS, could be expensive and hard to manage. So a natural question to ask is: can we bundle WET and MBS on the same vehicle? This is the focus of this study. Here, our goal is to minimize energy consumption of the entire system while ensuring that none of the sensor nodes runs out of energy. To simplify the problem, we assume that the path for the vehicle is given *a priori*. We develop a mathematical model for this problem. Instead of studying the general problem formulation (called CoP-t), which is time-dependent, we show that it is sufficient to study a special subproblem (called CoP-s), which only involves space-dependent variables. Subsequently, we develop a provable near-optimal solution to CoP-s with the development of several novel techniques including discretizing a continuous path into a finite number of segments and representing each segment with worst-case energy bounds.

4. **Bundling Mobile Base Station and Wireless Energy Transfer: The Unconstrained Path Case.** Based on our experience for the pre-planned path case, we further study the problem where the traveling path of the WCV (also carrying the MBS) can be unconstrained. That is, we study an optimization problem that jointly optimizes the traveling path, stopping points, charging schedule, and flow routing. For this problem, we propose a two-step solution. First, we study an idealized problem that assumes zero traveling time, and develop a provably near-optimal solution to this idealized problem. In the second step, we show how to develop a practical solution with non-zero traveling time and quantify the performance gap between this solution and the unknown optimal solution to the original problem.

This dissertation offers the first systematic investigation on how WET (in particular, the MRC technology) can be exploited to address lifetime bottleneck of a WSN. It lays the foundation of exploring WET for WSNs and other energy-constrained wireless networks. On the mathematical

side, we have developed or applied a number of powerful techniques such as piecewise linear approximation, RLT, time-space transformation, discretization, and logical point representation that may be applicable to address a broad class of optimization problems in wireless networks. We expect that this dissertation will open up new research directions on many interesting networking problems that can take advantage of the WET technology.

To the most significant people in my life.

My parents whose endless love has enabled me to live my dreams,

and

my wife who has supported me in every aspect of my life.

When the going gets tough, the tough get going.
Joseph P. Kennedy

Acknowledgments

My Ph.D. life at Virginia Tech has been an extremely enjoyable experience. I have had the opportunity to stay in the most beautiful college town, work with the best minds, and build up my own family. There are many people that I want to acknowledge. First and foremost, I would like to thank my advisor, Prof. Tom Hou, for all his guidance, inspiration, and support throughout my Ph.D life. He arranged my enrollment in the Electrical and Computer Engineering Department, took care of my funding, and supervised this dissertation with great wisdom and consideration. His vision helped me to identify this important research topic, and his insightful advice contributed substantially to the results of this dissertation. He has always encouraged me to think deeper, write and speak more clearly, and challenge myself much more than I would have, for which I am now immensely grateful. I will always be grateful to him for believing in my abilities, and hope that I can continue living up to his high standard.

I would like to express my sincere thanks to the rest of my dissertation committee – Dr. Yi Shi, Prof. Hanif Sherali, and Prof. Wenjing Lou, Prof. Yaling Yang, Prof. Anil Vullikanti. Dr. Shi has offered valuable feedback on almost all my Ph.D. research. His precise comments made sure that I did not lapse into theoretical trap, and helped me to greatly improve the quality of this dissertation. I would like to especially thank Prof. Sherali for taking a genuine interest in my work. His view has had a remarkable influence on my research, and his invaluable advice shaped the direction of the majority of solutions in this dissertation. Without his insightful advice, my research would have left far behind what was desired. To me, he is a truly a role model in research excellence, professionalism, and humility. I also thank Prof. Lou for her encouragement and insights, Profs. Yang and Vullikanti for their service on my dissertation committee.

I would also like to thank all the colleagues and friends in the Complex Networks and Security

Research (CNSR) Lab, specifically Sushant Sharma, Jia Liu, Canming Jiang, Huacheng Zeng, Xu Yuan, Borhan Jalaeain, Xiaoqi Qin, and Amr Nabil. Their friendship has made my Ph.D. life both fun and memorable.

There is no way to thank my wife, Ye, enough for everything she has done to support me during all these years, from relocating to Blacksburg, to giving up her own career opportunity, to putting up with my nocturnal schedule, to raising our adorable but somewhat naughty son Allen. She is truly wonderful!

Finally, and most importantly, I would like to thank my parents, Yiwei Xie and Yinghui Chen, for their unconditional and boundless love and support. They have always supported me regardless of what happened, and have believed in me every step along the way. I hope that I have become the son that makes them proud of. Words simply cannot describe my gratitude to them. This dissertation is dedicated to them with the utmost love and respect.

Contents

List of Figures

List of Tables

Chapter 1

Introduction

1.1 Wireless Sensor Networks

As Micro-Electro-Mechanical Systems (MEMS) technology advances, wireless sensor networks (WSNs) have emerged. There is a wide range of applications for WSNs, from battlefield surveillance, to intelligent transportation, to environmental and industrial monitoring, and to home automation. A WSN generally consists of a large number of small, embedded, low-power sensor nodes. Each sensor node collects useful information (e.g. temperature, humidity and barometric pressure), and forwards such data to a base station through wireless communications. A sensor node is typically powered by battery, which can only store limited energy. This leads to limited lifetime for a WSN to remain operational before some or all of the sensor nodes run out of battery. Therefore, energy is widely regarded as the fundamental performance bottleneck of a WSN.

To conserve energy for sensor nodes and prolong network lifetime, there have been active research efforts at all layers, from topology control [36, 51, 65], physical [17, 52, 55], media access control (MAC) [18, 46, 63], network [11, 23, 49] and all the way up to the application layer. Although these efforts help conserve energy usage and prolong network lifetime to some extent, energy and lifetime remain fundamental bottlenecks and are the key factors that prevent its widespread deployment.

Figure 1.1: Nikola Tesla and his Wardenclyffe project in Long Island, New York in early 1900 (URL: www.teslasociety.com).

Although energy-harvesting (or energy scavenging) techniques (see, e.g., [2], [9], [28], [30], [39], [43]) were proposed to extract energy from the environment, their success for WSNs remains limited in practice. This is because the proper operation of any energy-harvesting technique is heavily dependent on the environment. Further, the size of an energy-harvesting device may pose a concern on deployment, particularly when the size of such a device is of much larger scale than the sensor node that it is attempting to power.

1.2 Wireless Energy Transfer

Recently, wireless energy transfer (WET) – transferring electric power between two electrical devices without any plugs or wires – is undergoing a revolution. Especially, the recent breakthrough by Kurs *et al.* [31] offers a new opportunity to address energy constraints for a WSN. To familiarize readers with the WET technology, we give a concise review of its history and its recent advances.

Table 1.1: A comparison of WET technologies.

WET technologies		Strengths	Weaknesses	Example applications
Inductive Coupling		Simple, high power transfer efficiency in centimeter range	Short charging distance, requiring accurate alignment in charging direction	Electric toothbrush, charging pad for cell phones and laptops
EM radiation	Omnidirectional	Tiny receiver size	Rapid drop of power transfer efficiency over distance, ultra low-power reception	Charging a WSN for environmental monitoring (temperature, moisture, light etc.)
	Unidirectional (microwave/ laser)	Effective power transmission over long distance (kilometer-range)	Requiring LOS and complicated tracking mechanisms, inherently large scale of devices	SHARP unmanned plane
Magnetic resonant coupling (MRC)		High efficiency over several meters under omni-direction, not requiring LOS, and insensitive to weather conditions	High efficiency only within several-meter ranges	Charging mobile devices, electric vehicles, implantable devices and WSNs

The idea of WET was envisioned in the early 20th century (earlier than electric power grids). Nikola Tesla, a pioneering electrical engineer, experimented with large scale wireless power distribution by building the world's first power station in Long Island, New York [57]. He planned to use the power station, called Wardenclyffe Tower (see Fig. 1.1), to transmit not only signals but also wireless electricity. Unfortunately, due to its large electric fields, which significantly diminished the power transfer efficiency, Tesla's invention was not successful and was never put into practical use.

In the late 20th century, the need for WET re-emerged when mobile electronic devices (e.g. laptops, cell phones, PDAs, tablets) became popular. Due to these demands, there have been many active efforts to develop efficient WET technologies. Recently, the Wireless Power Consortium [68] was established by the industry to set the international standards for interoperable wireless charging. Member companies in the consortium include IC manufactories, mobile phone makers, and mobile telecom operators. These standardization efforts will help accelerate the pace of

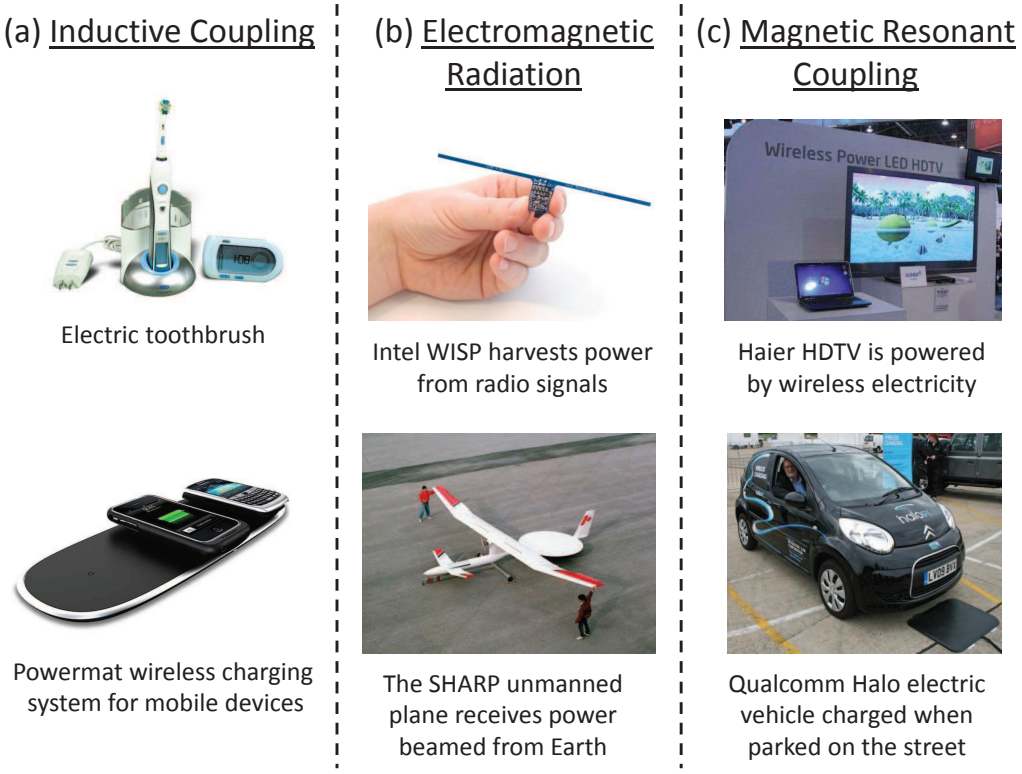

Figure 1.2: Example applications of WET.

bringing WET technologies to the market place.

To date, there are three categories of WET technologies, namely, inductive coupling, electromagnetic (EM) radiation, and MRC. For each technology, we review its physical characteristics, and discuss its strengths and weaknesses and possible applications. Table 1.1 gives a summary of the three WET technologies.

1.2.1 Inductive Coupling

Inductive coupling works by magnetic field induction, i.e., an alternating current in a primary coil (connected to a source) generates a varying magnetic field that induces a voltage across the terminals of a secondary coil at the receiver. An electrical transformer is a good example of inductive coupling. Due to its simplicity, convenience, and safety, inductive coupling has been an important

and popular technology to transfer power without wires [62]. It has been successfully commercialized to a number of products, including RFID tags [16, 27], electric toothbrush, charging pad for cell phone or laptop [45] (see Fig. 1.2(a)), and medical implants [64]. In 2010, the Wireless Power Consortium approved the world's first wireless charging standard (Qi) for low-power inductive charging (< 5W). Today, inductive coupling is considered a mature technology, and is a stepping stone to the new WET technologies such as MRC (see Section 1.2.3).

Under inductive coupling, power transfer falls off sharply even over a very short distance. It works the best when the charging node and power receiving node are close in contact (usually less than a coil diameter, e.g., centimeter-range) and have accurate alignment in the charging direction. Due to these limitations, inductive coupling is not suitable for WSNs.

1.2.2 Electromagnetic Radiation

EM radiation emits energy from a power source to a power receiver via radiative EM waves. Depending on the energy-emitting direction, it can be classified into omnidirectional radiation and unidirectional radiation. For omnidirectional radiation, a transmitter broadcasts EM waves in an assigned ISM band (e.g., 850 MHz – 950 MHz [45] or 902 MHz – 928 MHz [48] in the U.S.,[1] both with a center frequency of 915 MHz), and a receiver (e.g, RFID tags) tunes to the same frequency band to harvest radio power (see Fig. 1.2(b)). Although suitable for transferring information, omnidirectional radiation suffers from a serious efficiency problem in energy transfer since EM waves decay quickly over distance. For example, it was reported in [21] that power transfer efficiency was only about 1.5% when a receiver is 30 cm away from its RF transmitter. Moreover, to prevent potential health hazards to humans from EM radiation, omnidirectional radiation is only appropriate for ultra low-power sensor nodes (e.g., up to 10 mW [45, 48]) that have very low sensing activities (e.g., temperature, moisture and light).

When a clear line-of-sight (LOS) path exists, unidirectional radiation can achieve high power trans-

[1] ISM bands may differ in world regions and countries.

mission over a much longer distance (e.g., kilometer-range) through a microwave or laser beam. For most microwave-based systems, wireless power is transmitted on frequencies of either 2.45 or 5.8 GHz, both in the ISM frequency band. Laser-based systems, still considered less mature than microwave-based systems, transmit power under the visible or near infrared frequency spectrum (i.e., from several THz to several hundred THz) [56]. In the 1980s, a prototype aircraft, designed as a communications relay by Canada's Communications Research Center, was able to receive power beamed from a large (about 80 m in diameter) ground-based microwave transmitter. A rectifying antenna, mounted on the lower body of the plane, receives and converts microwave power (at a frequency of 2.45 GHz) to DC electricity. The unmanned plane, called the Stationary High Altitude Relay Platform (SHARP) [29], flew at an altitude of about 21 km and in circles of 1 km in radius so that it could stay in the transmission range of a ground-based transmitter (see Fig. 1.2(b)). Unidirectional radiation is not suitable for a WSN due to several undesirable requirements, such as LOS, complicated tracking mechanisms, and the large physical size of devices.

1.2.3 Magnetic Resonant Coupling

The third category of WET technology is MRC, which was a recent breakthrough developed by Kurs *et al.* [31]. This technology is based on the well-known principle of resonant coupling, i.e., by having magnetic resonant coils operate at the same resonance frequency so that they are strongly coupled via nonradiative magnetic resonance induction. Intuitively, the effect of magnetic resonance is analogous to the classical mechanical resonance, under which a string, when tuned to a certain tone, can be excited to vibration by a faraway sound generator if there is a match between their resonance frequencies.

Under resonant coupling, energy can be transferred efficiently from a source coil to a receiver coil with little loss of energy to extraneous off-resonant objects. A highlight of Kurs' experiment was to power a 60 W light bulb from a distance of 2 meters away, with about 40% power transfer

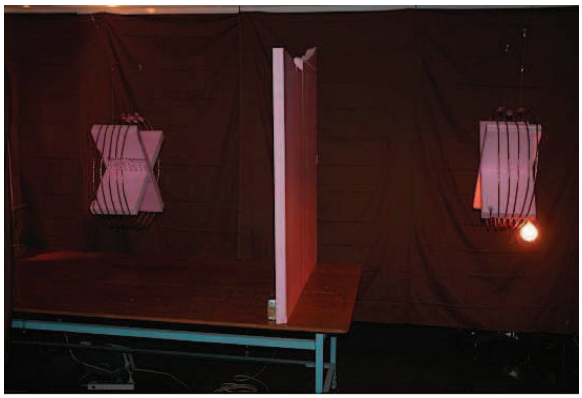

(a) Demonstrated by Kurs *et al.* [31]

(b) MRC with flat coils by Intel [25]

(c) MRC for cell phones by Witricity [67]

Figure 1.3: Magnetic Resonant Coupling: Invention and recent advances.

efficiency (see Fig. 1.3),[2] which significantly differs from inductive coupling that was limited to very close range, or EM radiation that was restricted to low-power ($\sim$mW) energy transfer. The diameter of both source and receiving coils was 0.5 m, which means that the charging distance can be four times the coil diameter.

At first glance, this technology reminds us of inductive coupling, and in some sense, it can be considered as a special case of inductive coupling where the primary and secondary coils are tuned in resonance by adding compensation capacitors. However, there are some fundamental advantages for MRC. Compared to inductive coupling, MRC can achieve higher transfer efficiency while significantly extending the charging distance from a very close range (i.e., distance less than the coil diameter, usually several centimeters) to several times the coil diameter (e.g., two meters in Kurs' experiments). Compared to EM radiation, MRC has the advantages of offering a much higher power transfer efficiency even under omni-direction, and not requiring LOS.

Although preliminary experiments by Kurs *et al.* showed the great potential of MRC, a number of technical challenges (such as orientation and interference) still exist before transitioning this technology to a successful commercial product. First, the maximum charging distance can be achieved only when source and receiving coils are aligned coaxially (along their axis). Other alignment settings, such as a 45 degree rotation with respect to the coaxial alignment or coplanar, reduce the coupling factor between coils and thus the achievable distance [31]. Second, when the technology is extended to charge multiple devices, mutual coupling among the receiving coils and other objects may cause interference, and therefore careful tuning is necessary.

Recent Advances. Since the first demo by Kurs *et al.* in 2007, there have been some new advances in MRC to make it suitable for commercial applications. In 2008 (see Fig. 1.3), engineers at Intel demonstrated MRC by using flat coils, which are easier to fit into a mobile device than the helix coils used in [31]. Kurs *et al.* launched a start-up company called Witricity Corp. [67], and at the TED Global 2009 conference, they demonstrated MRC for portable devices such as cell

[2]This efficiency between source coil and load is the most important component of the system efficiency. System efficiency also includes AC-DC conversion efficiency and other system factors (such as rectifier, drivers) [5].

phones [19] (see Fig. 1.3). Further, Kurs *et al.* developed an enhanced technology (by properly tuning coupled resonators) that allows energy to be transferred wirelessly to multiple receiving coils at the same time [32]. This technology allows for broader home and office applications, e.g., charging multiple mobile devices (laptops, tablets, cell phones) simultaneously.

In 2010, home appliance maker Haier exhibited an all wireless HDTV without power cords and signal cables [40] (see Fig. 1.2(c)). More recently, several leading automakers (e.g. Rolls-Royce, Audi, Nissan, Toyota, Mitsubishi) have been working to power electric or plug-in hybrid vehicles wirelessly. In 2011, Rolls-Royce unveiled an electric version of its Phantom car. The development of WET technology allows these electric vehicles to be charged while they are parked along the street or in a garage without any power cord. This WET technology, when fully mature, could help boost the electric car industry, and would further revolutionize how energy is replenished in our lives.

1.3 Motivation

The recent breakthrough in the area of WET technology by Kurs *et al.* has opened up a revolutionary approach to address energy and lifetime problems in WSNs. Kurs *et al.*'s work showed that by exploiting the novel technique of MRC, WET is both feasible and practical. They experimentally showed that the source energy storage device does not need to be in contact with the energy receiving device (e.g., a distance of 2 meters) for efficient energy transfer. Moreover, MRC has the advantages of offering a much higher power transfer efficiency even under omni-direction, and not requiring LOS. Further, MRC overcomes the limitation of energy harvesting, which is prone to environmental conditions.

The impact of MRC on WSNs and other energy-constrained wireless networks is immense. Instead of generating energy locally at a node (as in the case of energy-harvesting), one can bring clean electric energy that is efficiently generated elsewhere to a sensor node periodically and charge its battery without the constraints of wires and plugs. As one can imagine, the applications of MRC

are numerous. For example, WET has already been applied to replenish battery energy in medical sensors and implantable devices [72] in the healthcare industry.

Inspired by this emerging WET technology, this dissertation focuses on applying the MRC technology to a WSN and on studying how to optimally use this technology to address the important energy challenge that hinders the operation and deployment of a WSN. We envision employing a mobile vehicle carrying a wireless power charging station to periodically visit the sensor nodes and charge them wirelessly. This mobile wireless charging vehicle (WCV) can either be manned by a human or be entirely autonomous. In this dissertation, our goal is to exploit such a WCV to remove the lifetime bottleneck for a WSN.

1.4 Related Work

Related work on applying WET to WSNs has mainly focused on omni-directional EM radiation technology. Omni-directional EM radiation has been used for harvesting energy for a WSN [3, 21, 44, 59, 73] when the locations of sensor nodes are either unknown or uncontrollable. In this section, we briefly describe these efforts.

In [59], Tong *et al.* conducted a preliminary experiment for charging sensor node via Powercast chips, which are commercially available RF-based WET products [45]. Their results showed that the power transfer efficiency for a single node is very low (less than 1% and 20 cm away from the energy transmitter). Based on the same WET technology, Peng *et al.* employed a mobile robot carrying a wireless charger to charge a WSN [44]. They studied the charging schedule problem for the mobile charger (i.e., when and how long to charge a node) to prolong network lifetime. In [44], the data routing was given *a priori*, while the data routing topology was assumed to be static. To prolong network lifetime, the authors proposed a heuristic algorithm, with the basic idea of charging nodes in the order of their expected lifetimes, whichever ends first. They conducted prototype experiments for a small-scale network and ran simulations for a large-scale network. Both experimental and simulation results showed that EM radiation could prolong network lifetime. But

the low power transfer efficiency was shown to be the bottleneck.

In [21], He *et al.* studied how to design an infrastructure of wireless chargers for a WSN. The authors assumed that the basic unit for deploying wireless chargers followed a triangular structure, with a wireless charger at each vertex of the triangle. The problem is to determine the side length of the triangle so that the required number of wireless chargers is minimized while the power reception rate of any sensor node in the WSN does not fall below its average energy consumption rate. They offered a solution for deployment and derived an upper bound on an asymptotic approximation ratio of the number of wireless chargers to the optimal solution. They also showed that if sensor nodes were mobile, the required number of wireless chargers could be reduced. Due to the low power transfer efficiency of EM radiation, the proposed solution still required dense deployment of wireless chargers (e.g., more than 100 wireless chargers over a 100 m $\times$ 100 m area).

Recently, Ajmal *et al.* [3] designed a compact RF energy harvester, which passively absorbs energy from ambient RF signals. Through simulation, they showed that an ultra-low power ($\sim \mu$W) node can be supported without a power outage as long as it is within the charging range of a high power transmitter (e.g., within 120 km of a 150 kW transmitter). In contrast to active power transfer [21, 44, 59], this approach can be used to charge ultra-low power nodes located in an inaccessible area.

Very recently, Zhang and Ho [73] explored using RF signals to achieve simultaneous wireless information and power transfer in a MIMO broadcasting system. Specifically, they studied a simplified three-node setup, and presented a theoretical tradeoff in designing MIMO systems for maximizing the information rate and energy transfer rate. Their work demonstrated the possibility of using multi-antenna energy beamforming to improve the power efficiency of EM radiation. This energy transfer technology is still in its infancy and further investigation is needed to fully understand its potential and limits.

In summary, radiative technology has a number of limitations when applied to a WSN. First and

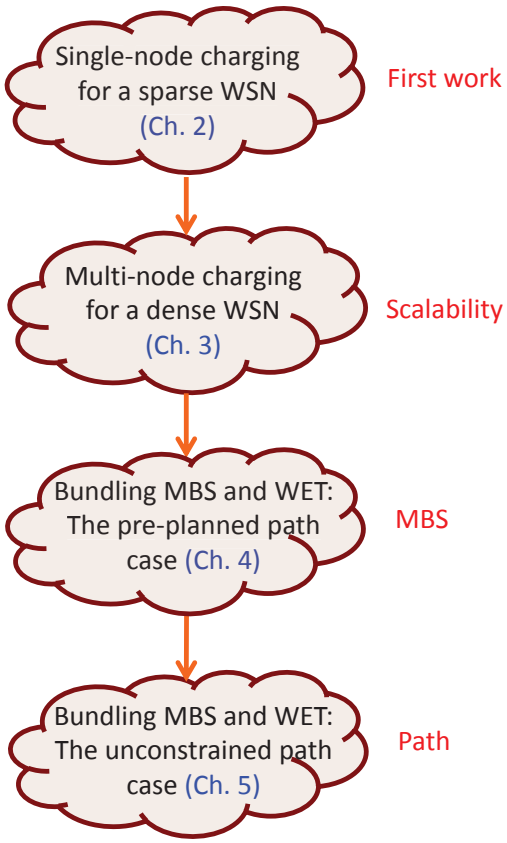

Figure 1.4: Flow chart of key chapters in the dissertation.

foremost, omnidirectional radiation has very low efficiency in WET. Second, radiative technology is sensitive to obstruction between the energy source and the receiver. Finally, active radiative technology may pose safety concern to humans. Therefore, this technology is only suitable to a WSN with ultra low-power requirements.

Compared to EM radiation, MRC enjoys significant advantages including much higher efficiency in WET (under omni-direction), immunity to neighboring environments, and no requirement of LOS [31, 32]. Although MRC has great potential for a WSN, there has been hardly any result in the literature. This dissertation is devoted to this fascinating area, and offers the first systematic investigation on applying MRC to WSNs.

1.5 Contributions and Dissertation Outline

Fig. 1.4 shows the flow chart of key chapters in this dissertation. Specifically, we address several important problems: single-node charging for a sparse WSN, multi-node charging for a dense WSN, and bundling WET and mobile base station (in two cases, i.e. the pre-planned path case and the unconstrained path case). Each piece by itself contributes to the common theme, and evolves in depth with new advances of the MRC technology and the capability of a mobile base station (MBS). The main contributions of this dissertation are summarized as follows:

- Chapter 2 lays the foundation of this dissertation. By applying MRC to a WSN, we explore the possibility of having a WSN remain operational forever. We consider the scenario where a mobile WCV periodically travels inside the WSN and chargers each sensor node's battery wirelessly. We introduce the concept of renewable energy cycle, which enables perpetual operation of a WSN, and offer both necessary and sufficient conditions for such a cycle. We study an optimization problem, with the objective of maximizing the ratio of the WCV's vacation time over the cycle time. For this problem, we prove that the optimal traveling path for the WCV is the shortest Hamiltonian cycle and provide a number of important properties. Subsequently, we develop a near-optimal solution by a piecewise linear approximation technique and establish its performance guarantee. In short, Chapter 2 shows that MRC may offer infinite network lifetime to a WSN.
- In Chapter 3, we exploit recent advances in MRC that allows multiple sensor nodes to be charged at the same time, and show how MRC with multi-node charging capability can address the scalability problem associated with the single-node charging technology. Based on the charging range of the WCV, we propose a cellular structure that partitions the two-dimensional plane into a tessellation of hexagonal cells. We pursue a formal optimization framework by jointly optimizing traveling path of the WCV, flow routing among the sensor nodes, and charging time within each hexagonal cell. By employing discretization and a novel Reformulation-Linearization Technique (RLT), we develop a provably near-optimal

solution for any desired level of accuracy. Through numerical results, we demonstrate that our solution can indeed address the scalability problem for WET in a dense WSN.

- In Chapters 2 and 3, we employed a mobile vehicle to charge sensor nodes and also assumed that the location of the base station was fixed. On the other hand, it has been recognized that a MBS can offer significant advantages over a fixed one. But having two separate vehicles, one for WET and one for MBS, could be expensive and hard to manage. So a natural question to ask is: can we bundle WET and MBS on the same vehicle? This is the focus of Chapter 4. The motivation is to take advantage of the mobility feature of the WCV and use it as a carrying platform for the MBS at the same time. The goal is to minimize energy consumption of the entire system while ensuring that none of the sensor nodes run out of energy.

  To simplify the problem, we assume that the path for the vehicle is given *a priori*. We develop a mathematical model for this problem. Instead of studying the general problem formulation (called CoP-t), which is time-dependent, we show that it is sufficient to study a special subproblem (called CoP-s), which only involves space-dependent variables. Subsequently, we develop a provable near-optimal solution to CoP-s with the development of several novel techniques including discretizing a continuous path into a finite number of segments and representing each segment with worst-case energy bounds.

- As a sequel to Chapter 4, Chapter 5 further studies the co-location problem of the MBS on the WCV in the general setting where the WCV's traveling path is unplanned and unconstrained. That is, we study an optimization problem that jointly optimizes the traveling path, stopping points, charging schedule, and flow routing. For this problem, we propose a two-step solution. First, we study an idealized problem that assumes zero traveling time, and develop a provably near-optimal solution to this idealized problem. In the second step, we show how to develop a practical solution with non-zero traveling time and quantify the performance gap between this solution and the unknown optimal solution to the original problem.

This dissertation offers the first systematic investigation of how WET (in particular, MRC) can fundamentally address lifetime bottleneck of a WSN. It lays the foundation for further research on WET for WSNs and other energy-constrained wireless networks. On the mathematical side, each problem investigated in this dissertation is formulated as a non-convex non-linear optimization problem and is NP-hard in general. The theoretical and algorithmic aspects of this research include novel network and energy modeling, development of near-optimal solutions with performance guarantee, and exploration of performance limits. In particular, this dissertation has developed several mathematical techniques that are of both theoretical and practical significance of their own. These techniques include employing piecewise linear approximation or RLT to convert a non-linear program to a mixed integer linear program, downsizing solution space without compromising optimal objective value, discretizing a continuous path/space into a finite number of logical points and representing each logical point with the worst-case bounds. We believe these techniques have the potential to address a broad class of optimization problems in wireless networks.

Chapter 2

Single-node Charging for a Sparse Sensor Network

2.1 Introduction

In this chapter, we study how the new MRC technology can be applied to a WSN. We envision employing a mobile vehicle carrying a power charging station to periodically visit each sensor node and charge it wirelessly. This mobile wireless charging vehicle (WCV) can either be manned by a human or be entirely autonomous. We investigate the fundamental question of whether the MRC technology can be applied to remove the lifetime performance bottleneck of a WSN. The main contributions of this chapter are as follows:

- We introduce the concept of *renewable energy cycle* where the remaining energy level in a sensor node's battery exhibits some periodicity over a time cycle. We offer both necessary and sufficient conditions for renewable energy cycle and show that feasible solutions satisfying these conditions can offer renewable energy cycles and thus, unlimited sensor network lifetime.
- We investigate an optimization problem, with the objective of maximizing the ratio of the WCV's vacation time (time spent at its home station) over the cycle time. In terms of achiev-

ing the maximum ratio, we prove that the optimal traveling path for the WCV in each renewable cycle is the shortest Hamiltonian cycle. We also derive several interesting properties associated with an optimal solution, such as the optimal objective being independent of traveling direction on the shortest Hamiltonian cycle and the existence of an energy bottleneck node in the network.

- Under the optimal traveling path, our optimization problem now only needs to consider flow routing and the charging time for each sensor node. We formulate an optimization problem for joint flow routing and charging schedule for each sensor node. The problem is shown to be a nonlinear optimization problem and is NP-hard in general. We apply a piecewise linear approximation technique for each nonlinear term and obtain a tight linear relaxation. Based on this linear relaxation, we obtain a feasible solution and prove that it can achieve near-optimality for any desired level of accuracy.

The remainder of this chapter is organized as follows. In Section 2.2, we describe the scope of our problem for a renewable sensor network. Section 2.3 introduces the concept of renewable energy cycle and presents some interesting properties. Section 2.4 shows that an optimal traveling path should be along the shortest Hamiltonian path. In Section 2.5, we present our problem formulation and a near-optimal solution. Section 2.6 shows how to construct the initial transient cycle preceding the first renewable cycle. In Section 2.7, we present numerical results to demonstrate the properties of a renewable wireless sensor network under our solution. Section 2.8 summarizes this chapter.

2.2 Problem Description

We consider a set of sensor nodes $\mathcal{N}$ distributed over a two-dimensional area (see Fig. 2.1). Each sensor node has a battery capacity of $E_{\max}$ and is fully charged initially.[1] Also, denote $E_{\min}$ as

[1]To simplify the model, we assume that there is no limit on the number of times batteries can be re-charged. In practice, rechargeable batteries can be re-charged only for a limited number of times. The battery capacity also decreases and batteries may eventually need to be replaced.

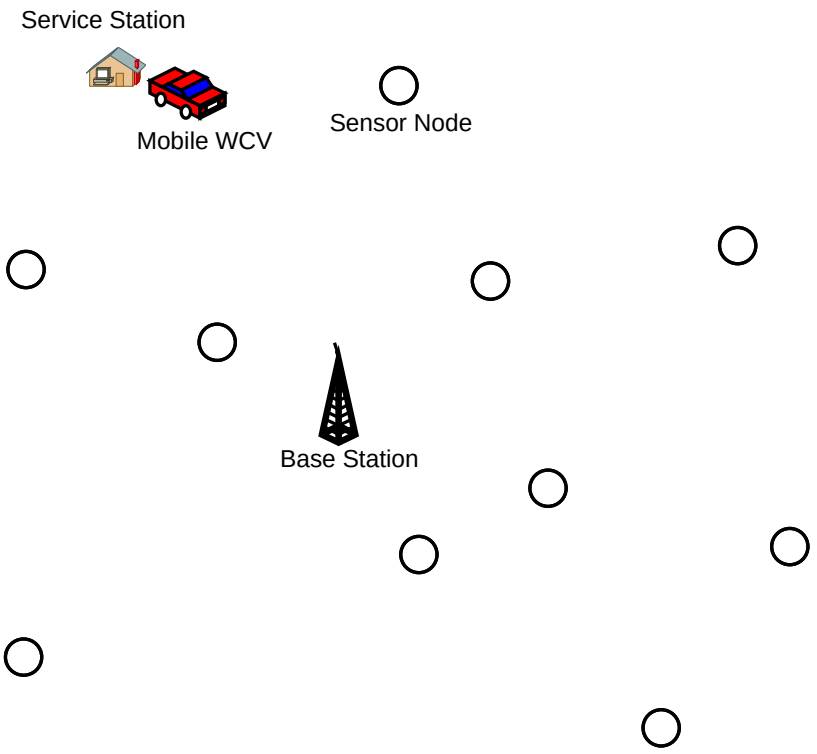

Figure 2.1: An example sensor network with a mobile WCV.

the minimum energy at a sensor node battery (for it to be operational). For simplicity, we define network lifetime as the time until the energy level of any sensor node in the network falls below $E_{\min}$ [11, 47, 65].[2] Although a more general definition of network lifetime (e.g., [12]) is available, we decided to choose a simple network lifetime definition in this chapter, which is sufficient to show the potential of MRC in a sensor network.

Each sensor node i generates sensing data with a rate of R_i (in b/s), $i \in \mathcal{N}$. Within the sensor network, there is a fixed base station (B), which is the sink node for all data generated by all sensor nodes. Multi-hop data routing is employed for forwarding data by the sensor nodes. Denote f_{ij} as the flow rate from sensor node i to sensor node j and f_{iB} as the flow rate from sensor node i to the base station B, respectively. Then we have the following flow balance constraint at each

[2] In the listed references as well as many other references, $E_{\min}$ is typically set to 0.

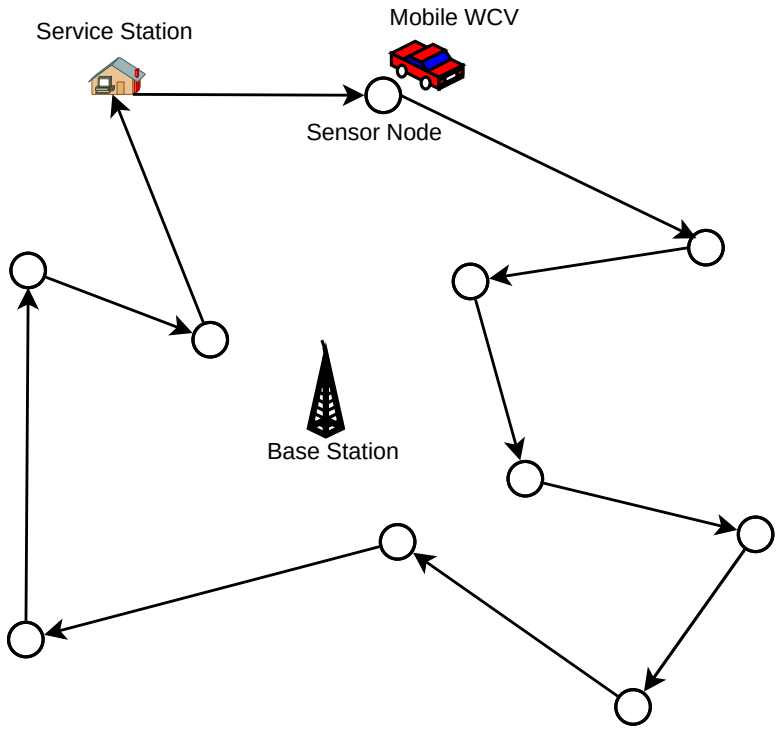

Figure 2.2: A WCV periodically visits each sensor node and charges its battery via WET.

sensor node i.

$$\sum_{k\in\mathcal{N}}^{k\neq i} f_{ki} + R_i = \sum_{j\in\mathcal{N}}^{j\neq i} f_{ij} + f_{iB} \quad (i \in \mathcal{N}). \tag{2.1}$$

Each sensor node consumes energy for data transmission and reception. Denote r_i as the energy consumption rate at sensor node $i \in \mathcal{N}$. In this chapter, we use the following power consumption model [11, 23]:

$$r_i = \rho \sum_{k\in\mathcal{N}}^{k\neq i} f_{ki} + \sum_{j\in\mathcal{N}}^{j\neq i} C_{ij} f_{ij} + C_{iB} f_{iB} \quad (i \in \mathcal{N}) \,, \tag{2.2}$$

where ρ is the energy consumption for receiving one unit of data rate, C_{ij} (or C_{iB}) is the energy consumption for transmitting one unit of data rate from node i to node j (or the base station B). Further, $C_{ij} = \beta_1 + \beta_2 D_{ij}^{\alpha}$, where D_{ij} is the distance between nodes i and j, β_1 is a distance-independent constant term, β_2 is a coefficient of the distance-dependent term, and α is the path loss

Table 2.1: General Notation.

Symbol	Definition
B	Base station
C_{ij} (or C_{iB})	Energy consumption for transmitting one unit of data rate from node i to node j (or the base station B)
D_{ij}	Distance from node i and node j
$D_{\mathcal{P}}$	Distance of path $\mathcal{P}$
E_{max}	Full battery capacity at a sensor node
E_{min}	Minimum energy required to keep a sensor node operational
$e_i(t)$	Energy level of sensor node i at time t
f_{ij} (or f_{iB})	Flow rate from sensor node i to sensor node j (or base station B)
$\mathcal{N}$	The set of sensor nodes in the network
$\mathcal{P}$	Traveling path of the WCV in a cycle
R_i	Data rate generated at sensor node i
r_i	Energy consumption rate at sensor node i
S	Service station
V	Traveling speed of the WCV
(x_i, y_i)	Coordinates of node i
α	Path loss index
β_1	A constant in energy consumed for data transmission
β_2	A coefficient in energy consumed for data transmission
ρ	Power consumption coefficient for receiving data
ϵ	Targeted performance gap ($0 < \epsilon \ll 1$)
η_{vac}	Ratio of the vacation time to the cycle time
τ	Cycle time
τ_{vac}	Vacation time at the service station S
$\tau_{\mathcal{P}}$	WCV's traveling time on path $\mathcal{P}$ in a cycle

index. In the model, $\rho \sum_{k\in\mathcal{N}}^{k\neq i} f_{ki}$ is the energy consumption rate for reception, and $\sum_{j\in\mathcal{N}}^{j\neq i} C_{ij} f_{ij} + C_{iB} f_{iB}$ is the energy consumption rate for transmission.

To recharge the battery at each sensor node, a mobile WCV is employed in the network. The WCV starts from a service station (S), and its traveling speed is V (in m/s). When it arrives at a sensor node, say i, it will spend τ_i amount of time to charge the sensor node's battery wirelessly via WET [31]. Denote U as the energy transfer rate of the WCV. After τ_i, the WCV leaves node i and travels to the next node on its path. We assume that the WCV has sufficient energy to charge all sensor nodes in the network.

After the WCV visits all the sensor nodes in the network, it will return to its service station to

Table 2.2: Notation in Chapter 2.

Symbol	Definition
a_i	Arrival time of the WCV at node i during the first renewable cycle
$\hat{a}_i$	Arrival time of the WCV at node i in the initial transient cycle
D_{TSP}	The minimum traveling distance during a renewable cycle
E_i	Initial energy of sensor node i at the beginning of a renewable cycle
h	$= \frac{1}{\tau}$
m	The number of piecewise linear segments used to approximate a quadratic curve
U	Full charge rate of the WCV at a sensor node
u_i	Charge rate at sensor node i during the initial transient cycle
$z_{i,k}$	A binary variable indicating whether η_i falls within the kth segment, $i \in \mathcal{N}$ and $1 \leq k \leq m$
η_i	The ratio of the charging time at node i to the entire cycle time.
ζ_i	A piecewise linear approximation of η_i^2
$\lambda_{i,k}$	The weight of the grid point $\frac{k}{m}$ for η_i, $0 \leq \lambda_{i,k} \leq 1$, $1 \leq k \leq m$, and $i \in \mathcal{N}$
π_i	The ith node traversed by the WCV along path $\mathcal{P}$
τ_i	Time span for the WCV to be present at the sensor node i for re-charging battery
τ_{TSP}	Minimum traveling time of the WCV for an optimal renewable cycle
φ^*	Denotes an optimal solution
φ^*_{Full}	Denotes an optimal solution with fully re-charged battery in each cycle

be serviced (e.g., replacing or recharging its battery) and get ready for the next tour. We call this resting period *vacation time*, denoted as τ_{vac}. After this vacation, the WCV will go out for its next tour.

Denote τ as the time for a trip cycle of the WCV. A number of important questions need to be addressed for such a network. First and foremost, one would ask whether it is possible to have each sensor node never run out of its energy. If this is possible, then the sensor network will have unlimited lifetime and will never cease to be operational. Second, if the answer to the first question is positive, then is there any optimal plan (including traveling path, stopping schedule) such that some useful objective can be maximized or minimized? For example, in this chapter, we would like to maximize the percentage of time in a cycle that the WCV spends on its vacation (i.e., $\frac{\tau_{\text{vac}}}{\tau}$), or equivalently, to minimize the percentage of time that the WCV is out in the field. Table 2.1 lists

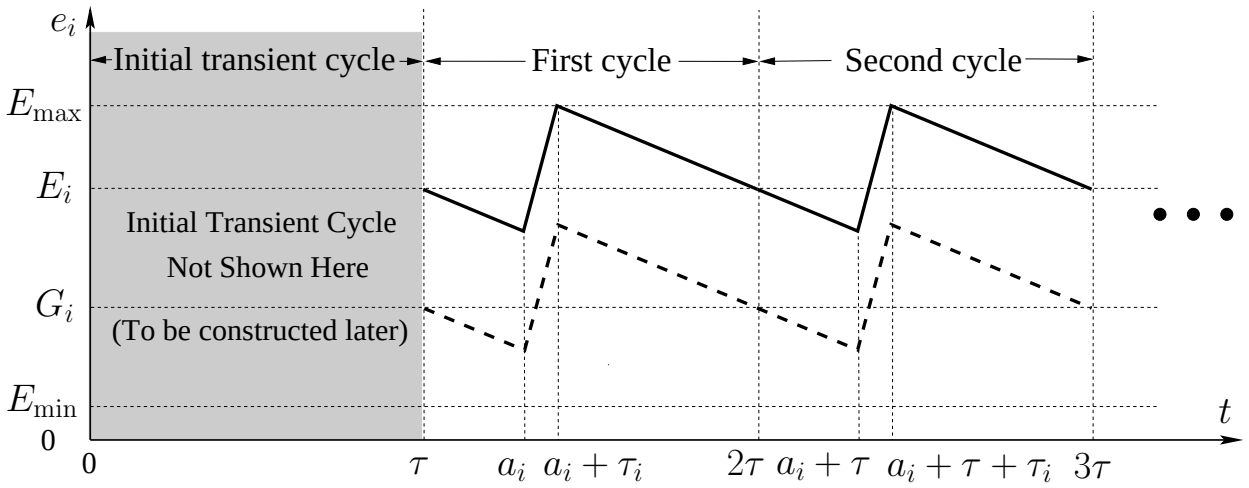

Figure 2.3: The energy level of a sensor node i during the first two renewable cycles (partially re-charged v.s. fully re-charged).

general notation used in this dissertation, and Table 2.2 lists the notation only used in this chapter.

2.3 Constructing Renewable Cycles

In this section, we focus on the renewable cycle construction. We assume that the WCV starts from the service station, visits each sensor node once in a cycle and ends at the service station (see Fig. 2.2). Further, we assume that the data flow routing in the network is invariant with time, with both routing and flow rates being part of our optimization problem.

The middle sawtooth graph (in dashed line) in Fig. 2.3 shows the energy level of a sensor node i during the first two renewable cycles. Note that there is an initialization cycle (marked in the grey area) before the first renewable cycle. That initialization cycle will be constructed in Section 2.6 once we have a solution to the renewable cycles.

Denote $\mathcal{P} = (\pi_0, \pi_1, \ldots, \pi_N, \pi_0)$ as the physical path traversed by the WCV over a trip cycle, which starts from and ends at the service station (i.e., $\pi_0 = S$) and the ith node traversed by the WCV along path $\mathcal{P}$ is π_i, $1 \leq i \leq |\mathcal{N}|$. Denote $D_{\pi_0\pi_1}$ as the distance between the service station

and the first sensor node visited along $\mathcal{P}$ and $D_{\pi_k \pi_{k+1}}$ as the distance between the kth and $(k+1)$th sensor nodes, respectively. Denote a_i as the arrival time of the WCV at node i in the first renewable energy cycle. We have

$$a_{\pi_i} = \tau + \sum_{k=0}^{i-1} \frac{D_{\pi_k \pi_{k+1}}}{V} + \sum_{k=1}^{i-1} \tau_{\pi_k} \ . \tag{2.3}$$

Denote $D_{\mathcal{P}}$ as the physical distance of path $\mathcal{P}$ and $\tau_{\mathcal{P}} = D_{\mathcal{P}}/V$ as the time spent for traveling over distance $D_{\mathcal{P}}$. Recall that τ_{vac} is the vacation time the WCV spends at its service station. Then the cycle time τ can be written as

$$\tau = \tau_{\mathcal{P}} + \tau_{\text{vac}} + \sum_{i \in \mathcal{N}} \tau_i \ , \tag{2.4}$$

where $\sum_{i \in \mathcal{N}} \tau_i$ is the total amount of time the WCV spends near all the sensor nodes in the network for WET.

We formally define a renewable energy cycle as follows:

Definition 2.1 *The energy level of a sensor node $i \in \mathcal{N}$ exhibits a renewable energy cycle if it meets the following two requirements: (i) it starts and ends with the same energy level over a period of τ; and (ii) it never falls below E_{min}.*

During a renewable cycle, the amount of charged energy at a sensor node i during τ_i must be equal to the amount of energy consumed in the cycle (so as to ensure the first requirement in Definition 2.1). That is,

$$\tau \cdot r_i = \tau_i \cdot U \quad (i \in \mathcal{N}) \ . \tag{2.5}$$

Note that when the WCV visits a node i at time a_i during a renewable energy cycle, it does not have to re-charge the sensor node's battery to E_{max}. This is illustrated in Fig. 2.3, where G_i denotes the starting energy of sensor node i in a renewable cycle and $g_i(t)$ denotes the energy level at time t (dashed sawtooth graph). During a cycle $[\tau, 2\tau]$, we see that the energy level has only two slopes:

(i) a slope of $-r_i$ when the WCV is not at this node (i.e., non-charging period), and (ii) a slope of $(U - r_i)$ when the WCV is charging this node at a rate of U (i.e., charging period). It is clear that $g_i(a_i) \leq g_i(t) \leq g_i(a_i + \tau_i)$, i.e., node i's energy level is lowest at time a_i and is highest at time $a_i + \tau_i$.

Also shown in Fig. 2.3 is another renewable energy cycle (in solid sawtooth graph) where the battery energy is charged to $E_{\max}$ during a WCV's visit. For this energy curve, denote E_i as the starting energy of node i in a renewable cycle and $e_i(t)$ as the energy level at time t, respectively. Let φ^*_{Full} be an optimal solution with fully re-charged batteries in each cycle that maximizes the ratio of the WCV's vacation time over the cycle time. Let φ^* be an optimal solution, where there is no requirement on whether or not a node's battery is fully re-charged. Naturally, the optimal objective obtained by φ^*_{Full} is no more than the optimal objective obtained by φ^* due to the additional requirement (batteries are fully re-charged) in φ^*_{Full}. Surprisingly, the following lemma shows that φ^*_{Full} is equally good as φ^* in terms of maximizing the ratio of the WCV's vacation time over the cycle time. Thus, for our optimization problem, it is sufficient to consider a solution with fully re-charged batteries.

Lemma 2.1 *The solution φ^*_{Full} achieves the same maximum ratio of vacation time to the cycle time as that achieved by the solution φ^*.*

Proof Our proof has two parts. (i) First, we show that the maximal ratio of vacation time to the cycle time achieved by solution φ^* is greater than or equal to that achieved by solution φ^*_{Full}. (ii) Second, we show that the converse is also true, i.e., the maximal ratio of vacation time to the cycle time achieved by solution φ^*_{Full} is also greater than or equal to that achieved by solution φ^*. If both (i) and (ii) hold, then the lemma is proved.

Since φ^*_{Full} is an optimal solution with the additional requirement (fully re-charged batteries in each cycle), the maximal ratio of vacation time to the cycle time obtained by φ^*_{Full} is no more than that obtained by φ^*. Thus, (i) holds.

We now prove (ii). Instead of considering the optimal solution φ^*, we will prove that any ratio achieved by a feasible solution φ can also be achieved by a feasible fully re-charged solution $\hat{\varphi}$. If this is true, in the special case that $\varphi = \varphi^*$ is an optimal solution, we have that the maximal ratio achieved by φ^* can also be achieved by a feasible fully re-charged solution. Therefore, (ii) will hold.

The proof is based on construction. Suppose $\varphi = (\mathcal{P}, a_i, G_i, f_{ij}, f_{iB}, \tau, \tau_i, \tau_{\mathcal{P}}, \tau_{\text{vac}}, r_i)$ is a feasible solution to our problem. We construct $\hat{\varphi} = (\hat{\mathcal{P}}, \hat{a}_i, E_i, \hat{f}_{ij}, \hat{f}_{iB}, \hat{\tau}, \hat{\tau}_i, \hat{\tau}_{\hat{\mathcal{P}}}, \hat{\tau}_{\text{vac}}, \hat{r}_i)$ by letting $\hat{\mathcal{P}} = \mathcal{P}$, $\hat{a}_i = a_i$, $E_i = E_{\text{max}} + r_i(a_i + \tau_i - \tau) - U\tau_i$, $\hat{f}_{ij} = f_{ij}$, $\hat{f}_{iB} = f_{iB}$, $\hat{\tau} = \tau$, $\hat{\tau}_i = \tau_i$, $\hat{\tau}_{\hat{\mathcal{P}}} = \tau_{\mathcal{P}}$, $\hat{\tau}_{\text{vac}} = \tau_{\text{vac}}$, and $\hat{r}_i = r_i$. Note that under $\hat{\varphi}$, the maximal energy level of node i occurs at time $(\hat{a}_i + \hat{\tau}_i)$, which is $e_i(\hat{a}_i + \hat{\tau}_i) = E_i + U\hat{\tau}_i - r_i(\hat{a}_i + \hat{\tau}_i - \hat{\tau}) = \left[E_{\text{max}} + r_i(a_i + \tau_i - \tau) - U\tau_i\right] + U\tau_i - r_i(a_i + \tau_i - \tau) = E_{\text{max}}$. Thus, $\hat{\varphi}$ is a fully re-charged solution. Moreover, it is clear that $\frac{\hat{\tau}_{\text{vac}}}{\hat{\tau}} = \frac{\tau_{\text{vac}}}{\tau}$ since $\hat{\tau} = \tau$ and $\hat{\tau}_{\text{vac}} = \tau_{\text{vac}}$. Now, all we need to do is to verify that $\hat{\varphi}$ is a feasible renewable cycle.

To show that $\hat{\varphi}$ is feasible, we need to verify that $\hat{\varphi}$ meets Constraints (2.1), (2.2), and (2.4), as well as $e_i(t) \geq E_{\text{min}}$ for $i \in \mathcal{N}$, $t \geq \tau$. Further, to show that $\hat{\varphi}$ is a renewable cycle, we need to verify that $e_i(k\tau) = E_i$ for $k \in \mathbb{N}$. We now verify each of these requirements. Since φ is a feasible solution, it satisfies (2.1), (2.2), and (2.4). In $\hat{\varphi}$, we have $\hat{\tau} = \tau$, $\hat{\tau}_i = \tau_i$, $\hat{\tau}_{\hat{\mathcal{P}}} = \tau_{\mathcal{P}}$, $\hat{\tau}_{\text{vac}} = \tau_{\text{vac}}$, $\hat{f}_{ij} = f_{ij}$, $\hat{f}_{iB} = f_{iB}$, and $\hat{r}_i = r_i$. Then $\hat{\varphi}$ also satisfies (2.1), (2.2), and (2.4).

We now show that $e_i(t) \geq E_{\text{min}}$ for $i \in \mathcal{N}$, $t \geq \tau$. Since φ is a feasible solution, $E_{\text{max}} \geq g_i(a_i + \tau_i) = G_i + U\tau_i - r_i(a_i + \tau_i - \tau)$. Thus, we have $E_{\text{max}} + r_i(a_i + \tau_i - \tau) - U\tau_i \geq G_i$. Since E_i is set as $E_i = E_{\text{max}} + r_i(a_i + \tau_i - \tau) - U\tau_i$, we have $E_i \geq G_i$. Moreover, since $\hat{r}_i = r_i$, the energy at a node i in $\hat{\varphi}$, $e_i(t)$, is parallel to $g_i(t)$ in φ. Because of this parallelism and $E_i \geq G_i$, we have that $e_i(t) \geq g_i(t)$ for $i \in \mathcal{N}$. Since φ is a feasible solution, we have $g_i(t) \geq E_{\text{min}}$ for $i \in \mathcal{N}$. Thus, $e_i(t) \geq g_i(t) \geq E_{\text{min}}$ for $i \in \mathcal{N}$. Therefore, $\hat{\varphi}$ is feasible.

Because of the parallelism and $g_i(k\tau) = G_i$ for $k = 1, 2, \cdots$, we have $e_i(k\tau) = E_i$ for $k = 1, 2, \cdots$. Thus, $\hat{\varphi}$ is a feasible renewable cycle, and (ii) holds. $\square$

Based on Lemma 2.1, we will only consider renewable cycles where each node is fully re-charged when it is visited by the WCV. Since the energy level at node i is at its lowest at time a_i, to ensure the second requirement in Definition 2.1, we must have $e_i(a_i) = E_i - (a_i - \tau)r_i \geq E_{\min}$. Since for a renewable cycle,

$$\begin{aligned} E_i = e_i(2\tau) &= e_i(a_i + \tau_i) - (2\tau - a_i - \tau_i)r_i \\ &= E_{\max} - (2\tau - a_i - \tau_i)r_i \ , \end{aligned} \tag{2.6}$$

we have $e_i(a_i) = E_{\max} - (2\tau - a_i - \tau_i)r_i - (a_i - \tau)r_i = E_{\max} - (\tau - \tau_i)r_i$. Therefore,

$$E_{\max} - (\tau - \tau_i) \cdot r_i \geq E_{\min} \quad (i \in \mathcal{N}) \ . \tag{2.7}$$

To construct a renewable energy cycle, we need to consider the traveling path $\mathcal{P}$, the arrival time a_i, the starting energy E_i, the flow rates f_{ij} and f_{iB}, time intervals τ, τ_i, $\tau_{\mathcal{P}}$, and τ_{vac}, and power consumption r_i. By (2.3) and (2.6), a_i and E_i are variables that can be derived from $\mathcal{P}$, τ, and τ_i. Thus, a_i and E_i can be excluded from a solution φ. So we have $\varphi = (\mathcal{P}, f_{ij}, f_{iB}, \tau, \tau_i, \tau_{\mathcal{P}}, \tau_{\text{vac}}, r_i)$. Although more variables can be removed from φ, we keep this representation for the sake of future discussion.

For a renewable energy cycle, we have the following lemma:

Lemma 2.2 *A cycle is a renewable energy cycle if and only if Constraints (2.4), (2.5), and (2.7) are satisfied at each sensor node $i \in \mathcal{N}$.*

Proof The "only if" part of the lemma can be proved by showing that a renewable cycle meets (2.4), (2.5), and (2.7). This has already been shown in the description of the renewable cycle.

We now prove the "if" part of the lemma, i.e., if (2.4), (2.5), and (2.7) hold, then (i) and (ii) in Definition 2.1 will also hold, thus the cycle is a renewable energy cycle. Since (2.4) holds, the given cycle satisfies the time constraint. Constraint (2.5) ensures that the amount of energy charged to each sensor node i during τ_i is equal to the amount of energy consumed by sensor node i in the

cycle. So the energy level at each sensor node i at the end of the cycle is the same as that at the beginning of the cycle. Therefore, requirement (i) in Definition 2.1 is satisfied.

During the first renewable cycle, the lowest energy level at node i occurs at time a_i, which is

$$\begin{aligned} e_i(a_i) &= e_i(\tau) - (a_i - \tau)r_i \\ &= e_i(2\tau) - (a_i - \tau)r_i \\ &= E_{\text{max}} - (2\tau - a_i - \tau_i)r_i - (a_i - \tau)r_i \\ &= E_{\text{max}} - (\tau - \tau_i)r_i \\ &\geq E_{\text{min}} \ , \end{aligned}$$

where the second equality holds by requirement (i), which we just proved, the third equality holds by (2.6), the fourth equality holds by $e_i(a_i + \tau_i) = E_{\text{max}}$ in a fully re-charged solution, and the last inequality holds by (2.7). Since the lowest energy level of node i occurs at time a_i and is still no less than E_{min}, requirement (ii) in Definition 2.1 is satisfied. The proof of the "if" part of the lemma is complete. □

The following property shows that in an optimal solution, there exists at least one energy "bottleneck" node in the network, where the energy level at this node drops exactly to E_{min} upon the WCV's arrival.

Property 2.1 *In an optimal solution, there exists at least one node in the network with its battery energy dropping to E_{min} when the WCV arrives at this node.*

Proof The proof is based on contradiction (i.e., if this is not true, then we can further increase the objective value, thus leading to a contradiction).

Suppose that there exists an optimal solution $\varphi^* = (\mathcal{P}^*, f_{ij}^*, f_{iB}^*, \tau^*, \tau_i^*, \tau_{\mathcal{P}}^*, \tau_{\text{vac}}^*, r_i^*)$ where none of the nodes in the network has its energy level drop to E_{min}, i.e., $e_i^*(t) > E_{\text{min}}$ for all $i \in \mathcal{N}$, $t \geq \tau$. Then we can construct a new solution $\hat{\varphi} = (\hat{\mathcal{P}}, \hat{f}_{ij}, \hat{f}_{iB}, \hat{\tau}, \hat{\tau}_i, \hat{\tau}_{\hat{\mathcal{P}}}, \hat{\tau}_{\text{vac}}, \hat{r}_i)$ by choosing

$\gamma = \min_{i\in\mathcal{N}}\{\frac{E_{\max}-E_{\min}}{(\tau^*-\tau_i^*)p_i^*}\}-1$ and letting $\hat{\mathcal{P}} = \mathcal{P}^*$, $\hat{f}_{ij} = f_{ij}^*$, $\hat{f}_{iB} = f_{iB}^*$, $\hat{\tau} = (1+\gamma)\tau^*$, $\hat{\tau}_i = (1+\gamma)\tau_i^*$, $\hat{\tau}_{\hat{\mathcal{P}}} = \tau_{\mathcal{P}}^*$, $\hat{\tau}_{\text{vac}} = \tau_{\text{vac}}^* + \gamma(\tau^* - \sum_{i\in\mathcal{N}}\tau_i^*)$, and $\hat{r}_i = p_i^*$.

Now we show that $\gamma > 0$. Since $e_i^*(t) > E_{\min}$ for all $i \in \mathcal{N}$, $t \geq \tau$, we have $e_i^*(a_i) = E_{\max} - (\tau^* - \tau_i^*)p_i^* > E_{\min}$ for all $i \in \mathcal{N}$, i.e., $\min_{i\in\mathcal{N}}\{E_{\max} - (\tau^* - \tau_i^*)p_i^*\} > E_{\min}$. It follows that $E_{\max} - \max_{i\in\mathcal{N}}\{(\tau^* - \tau_i^*)p_i^*\} > E_{\min}$, or $\frac{E_{\max}-E_{\min}}{\max_{i\in\mathcal{N}}\{(\tau^*-\tau_i^*)p_i^*\}} > 1$. Thus, $\gamma = \min_{i\in\mathcal{N}}\{\frac{E_{\max}-E_{\min}}{(\tau^*-\tau_i^*)p_i^*}\} - 1 = \frac{E_{\max}-E_{\min}}{\max_{i\in\mathcal{N}}\{(\tau^*-\tau_i^*)p_i^*\}} - 1 > 0$.

The feasibility of $\hat{\varphi}$ can be verified similarly as in the proof of Lemma 2.1.

We now show that this new feasible solution $\hat{\varphi}$ can offer a better (increased) objective value. By (2.4), we have $\frac{\hat{\tau}_{\text{vac}}}{\hat{\tau}} = 1 - \frac{\hat{\tau}_{\mathcal{P}}}{\hat{\tau}} - \frac{\sum_{i\in\mathcal{N}}\hat{\tau}_i}{\hat{\tau}}$. Since $\hat{\tau} = (1+\gamma)\tau^*$, $\hat{\tau}_i = (1+\gamma)\tau_i^*$, $\hat{\tau}_{\hat{\mathcal{P}}} = \tau_{\mathcal{P}}^*$, it follows that $\frac{\hat{\tau}_{\text{vac}}}{\hat{\tau}} = 1 - \frac{\tau_{\mathcal{P}}^*}{(1+\gamma)\tau^*} - \frac{\sum_{i\in\mathcal{N}}(1+\gamma)\tau_i^*}{(1+\gamma)\tau^*} > 1 - \frac{\tau_{\mathcal{P}}^*}{\tau^*} - \frac{\sum_{i\in\mathcal{N}}\tau_i^*}{\tau^*} = \frac{\tau_{\text{vac}}^*}{\tau^*}$, i.e., $\frac{\hat{\tau}_{\text{vac}}}{\hat{\tau}} > \frac{\tau_{\text{vac}}^*}{\tau^*}$. This contradicts the assumption that φ^* is an optimal solution. □

2.4 Optimal Traveling Path

In this section, we show that the WCV must move along the shortest Hamiltonian cycle in an optimal solution, which is formally stated in the following theorem:

Theorem 2.1 *In an optimal solution with the maximum $\frac{\tau_{\text{vac}}}{\tau}$, the WCV must travel along the shortest Hamiltonian cycle that connects all the sensor nodes and the service station.*

Proof Theorem 2.1 can be proved by contradiction. That is, if there is an optimal solution $\varphi^* = (\mathcal{P}^*, f_{ij}^*, f_{iB}^*, \tau^*, \tau_i^*, \tau_{\mathcal{P}^*}, \tau_{\text{vac}}^*, p_i^*)$, where the WCV does not move along the shortest Hamiltonian cycle, then we can construct a new solution $\hat{\varphi} = (\hat{\mathcal{P}}, \hat{f}_{ij}, \hat{f}_{iB}, \hat{\tau}, \hat{\tau}_i, \hat{\tau}_{\hat{\mathcal{P}}}, \hat{\tau}_{\text{vac}}, \hat{r}_i)$, with the WCV moving along the shortest Hamiltonian cycle and with an improved objective.

By assumption, $\mathcal{P}^*$ in φ^* does not follow the shortest Hamiltonian cycle. The new solution is

constructed as follows. Let $\hat{\mathcal{P}}$ follow the shortest Hamiltonian cycle (by either direction), $\hat{f}_{ij} = f^*_{ij}$, $\hat{f}_{iB} = f^*_{iB}$, $\hat{\tau} = \tau^*$, $\hat{\tau}_i = \tau^*_i$, $\hat{r}_i = p^*_i$, $\hat{\tau}_{\hat{\mathcal{P}}}$ is the traveling time on path $\hat{\mathcal{P}}$, and

$$\hat{\tau}_{\text{vac}} = \tau^*_{\text{vac}} + \tau_{\mathcal{P}^*} - \hat{\tau}_{\hat{\mathcal{P}}} \ . \tag{2.8}$$

Now we show that the constructed solution $\hat{\varphi}$ is feasible. To verify feasibility, we need to show that $\hat{\varphi}$ satisfies flow conservation constraint (2.1), time constraint (2.4), and energy constraints (2.5) and (2.7). Since φ^* is a feasible solution, it satisfies (2.1), (2.4), (2.5), and (2.7). Since we have $\hat{f}_{ij} = f^*_{ij}$, $\hat{f}_{iB} = f^*_{iB}$, $\hat{\tau} = \tau^*$, $\hat{\tau}_i = \tau^*_i$ and $\hat{r}_i = p^*_i$ in $\hat{\varphi}$, Constraints (2.1), (2.5), and (2.7) also hold by $\hat{\varphi}$. To show that $\hat{\varphi}$ also satisfies (2.4), we have $\hat{\tau}_{\hat{\mathcal{P}}} + \sum_{i\in\mathcal{N}} \hat{\tau}_i + \hat{\tau}_{\text{vac}} = \hat{\tau}_{\hat{\mathcal{P}}} + \sum_{i\in\mathcal{N}} \tau^*_i + \left(\tau^*_{\text{vac}} + \tau_{\mathcal{P}^*} - \hat{\tau}_{\hat{\mathcal{P}}}\right) = \sum_{i\in\mathcal{N}} \tau^*_i + \tau^*_{\text{vac}} + \tau_{\mathcal{P}^*} = \tau^* = \hat{\tau}$, where the first equality follows from (2.8), the second equality follows by the feasibility of φ^* and (2.4), and the third equality follows by $\hat{\tau} = \tau^*$ during construction.

To show $\frac{\hat{\tau}_{\text{vac}}}{\hat{\tau}} > \frac{\tau^*_{\text{vac}}}{\tau^*}$, recall that $\hat{\mathcal{P}}$ follows the shortest Hamiltonian cycle while $\mathcal{P}^*$ does not, i.e., the traveling distance $D_{\mathcal{P}^*} > \hat{D}_{\hat{\mathcal{P}}}$. Therefore, the traveling time $\tau_{\mathcal{P}^*} > \hat{\tau}_{\hat{\mathcal{P}}}$. Then by (2.8), $\hat{\tau}_{\text{vac}} = \tau^*_{\text{vac}} + \tau_{\mathcal{P}^*} - \hat{\tau}_{\hat{\mathcal{P}}} > \tau^*_{\text{vac}}$, or $\frac{\hat{\tau}_{\text{vac}}}{\hat{\tau}} > \frac{\tau^*_{\text{vac}}}{\hat{\tau}} = \frac{\tau^*_{\text{vac}}}{\tau^*}$. But $\frac{\hat{\tau}_{\text{vac}}}{\hat{\tau}} > \frac{\tau^*_{\text{vac}}}{\tau^*}$ contradicts the assumption that φ^* is optimal. This completes the proof. □

Theorem 2.1 says that the WCV should move along the shortest Hamiltonian cycle, which can be obtained by solving the well known Traveling Salesman Problem (TSP) (see, e.g., [10, 42]). Denote D_{TSP} as the traveling distance in the shortest Hamiltonian cycle and let $\tau_{\text{TSP}} = D_{\text{TSP}}/V$. Then with the optimal traveling path, (2.4) becomes

$$\tau_{\text{TSP}} + \tau_{\text{vac}} + \textstyle\sum_{i\in\mathcal{N}} \tau_i = \tau \ , \tag{2.9}$$

and the solution for a renewable cycle becomes $\varphi = (\mathcal{P}_{\text{TSP}}, f_{ij}, f_{iB}, \tau, \tau_i, \tau_{\text{TSP}}, \tau_{\text{vac}}, r_i)$. Since the optimal traveling path is determined, the solution can be simplified as $\varphi = (f_{ij}, f_{iB}, \tau, \tau_i, \tau_{\text{vac}}, r_i)$.

We note that the shortest Hamiltonian cycle may not be unique. Since any shortest Hamiltonian cycle has the same total path distance and traveling time τ_{TSP}, the selection of a particular shortest Hamiltonian cycle does not affect Constraint (2.9), and yields the same optimal objective. This insight is formally stated in the following corollary.

Corollary 2.1.1 *Any shortest Hamiltonian cycle achieves the same optimal objective.*

We also note that to travel the shortest Hamiltonian cycle, there are two (opposite) outgoing directions for the WCV to start from its home service station. Since the proof of Theorem 2.1 is independent of the starting direction for the WCV, either direction will yield an optimal solution with the same objective value, although some variables in each optimal solution will have different values. We have the following corollary:

Corollary 2.1.2 *The WCV can follow either direction to traverse the shortest Hamiltonian cycle, both of which will achieve the same optimal objective. There exist two optimal solutions corresponding to the two opposite directions, with identical values of* $f_{ij}, f_{iB}, \tau, \tau_i, \tau_{\text{TSP}}$, τ_{vac}, r_i, *but different values of* a_i *(by (2.3)) and* E_i *(by (2.6)) due to the difference in their respective renewable cycles, where* $i, j \in \mathcal{N}$, $i \neq j$.

2.5 Problem Formulation and Solution

2.5.1 Mathematical Formulation

Summarizing the objective and all the constraints in Sections 2.2, 2.3, and 2.4, our Single-node Charging Problem (SCP) can be formulated as follows:

SCP

$$\text{maximize} \quad \frac{\tau_{\text{vac}}}{\tau}$$

$$\text{subject to} \quad \sum_{j\in\mathcal{N}}^{j\neq i} f_{ij} + f_{iB} - \sum_{k\in\mathcal{N}}^{k\neq i} f_{ki} = R_i \qquad (i \in \mathcal{N})$$

$$\rho \cdot \sum_{k\in\mathcal{N}}^{k\neq i} f_{ki} + \sum_{j\in\mathcal{N}}^{j\neq i} C_{ij} \cdot f_{ij} + C_{iB} \cdot f_{iB} - r_i = 0 \quad (i \in \mathcal{N}) \tag{2.10}$$

$$\tau - \sum_{i\in\mathcal{N}} \tau_i - \tau_{\text{vac}} = \tau_{\text{TSP}} \tag{2.11}$$

$$\tau \cdot r_i - U \cdot \tau_i = 0 \qquad (i \in \mathcal{N}) \tag{2.12}$$

$$(\tau - \tau_i) \cdot r_i \leq E_{\text{max}} - E_{\text{min}} \qquad (i \in \mathcal{N}) \tag{2.13}$$

$$f_{ij}, f_{iB}, \tau_i, \tau, \tau_{\text{vac}}, r_i \geq 0 \qquad (i, j \in \mathcal{N}, i \neq j)\ .$$

In this problem, flow rates f_{ij} and f_{iB}, time intervals τ, τ_i, and τ_{vac}, and power consumption r_i are optimization variables, and R_i, ρ, C_{ij}, C_{iB}, U, E_{max}, E_{min}, and τ_{TSP} are constants. This problem has both nonlinear objective ($\frac{\tau_{\text{vac}}}{\tau}$) and nonlinear terms ($\tau r_i$ and $\tau_i r_i$) in Constraints (2.12) and (2.13).

Note that there are two possible outcomes for optimization problem SCP: either an optimal solution exists or SCP is infeasible. There are several scenarios where the latter outcome may occur, e.g., (i) the energy charging rate of WCV is too small or the energy consumption rate of a node is too large; (ii) the time interval between WCV's visits at any node is too large. As a result, some constraints in Problem SCP will not hold. These are physical limitations for a WCV to achieve a renewable network lifetime for a WSN.

We note that in the above formulation, only constant τ_{TSP} is related to the shortest Hamiltonian cycle. Since this value does not depend on the traveling direction along the Hamiltonian cycle, an optimal solution to Problem SCP will work for either direction and yields different renewable cycle for each direction.

2.5.2 Reformulation

We first use a change-of-variable technique to simplify the formulation. For the nonlinear objective $\frac{\tau_{\text{vac}}}{\tau}$, we define

$$\eta_{\text{vac}} = \frac{\tau_{\text{vac}}}{\tau} \ . \tag{2.14}$$

For (2.11), we divide both sides by τ and get $\tau_{\text{TSP}} \cdot \frac{1}{\tau} + \eta_{\text{vac}} + \sum_{i \in \mathcal{N}} \frac{\tau_i}{\tau} = 1$. To remove the nonlinear terms $\frac{1}{\tau}$ and $\frac{\tau_i}{\tau}$ in the above equation, we define

$$\eta_i = \frac{\tau_i}{\tau} \qquad (i \in \mathcal{N}) \ , \tag{2.15}$$

$$h = \frac{1}{\tau} \ . \tag{2.16}$$

Then (2.11) is reformulated as $\tau_{\text{TSP}} \cdot h + \eta_{\text{vac}} + \sum_{i \in \mathcal{N}} \eta_i = 1$, or equivalently,

$$h = \frac{1 - \sum_{i \in \mathcal{N}} \eta_i - \eta_{\text{vac}}}{\tau_{\text{TSP}}} \ . \tag{2.17}$$

Similarly, (2.12) and (2.13) can be reformulated (by dividing both sides by τ) as

$$r_i = U \cdot \eta_i \qquad (i \in \mathcal{N}) \ , \tag{2.18}$$

$$(1 - \eta_i) \cdot r_i \leq (E_{\text{max}} - E_{\text{min}}) \cdot h \quad (i \in \mathcal{N}) \ . \tag{2.19}$$

By (2.17) and (2.18), Constraint (2.19) can be rewritten as $(1-\eta_i) \cdot U\eta_i \leq (E_{\text{max}} - E_{\text{min}}) \frac{1 - \sum_{k \in \mathcal{N}} \eta_k - \eta_{\text{vac}}}{\tau_{\text{TSP}}}$, or

$$\eta_{\text{vac}} \leq 1 - \sum_{k \in \mathcal{N}} \eta_k - \frac{U \cdot \tau_{\text{TSP}}}{E_{\text{max}} - E_{\text{min}}} \cdot \eta_i \cdot (1 - \eta_i) \quad (i \in \mathcal{N}) \ .$$

By (2.18), Constraint (2.10) can be rewritten as

$$\rho \cdot \sum_{k\in\mathcal{N}}^{k\neq i} f_{ki} + \sum_{j\in\mathcal{N}}^{j\neq i} C_{ij} f_{ij} + C_{iB} f_{iB} - U\eta_i = 0 \qquad (i \in \mathcal{N}) \, .$$

Hence, Problem SCP is reformulated as follows:

SCP-R

$$\begin{aligned}
\text{maximize} \quad & \eta_{\text{vac}} \\
\text{subject to} \quad & \textstyle\sum_{j\in\mathcal{N}}^{j\neq i} f_{ij} + f_{iB} - \sum_{k\in\mathcal{N}}^{k\neq i} f_{ki} = R_i && (i \in \mathcal{N}) \\
& \rho \cdot \textstyle\sum_{k\in\mathcal{N}}^{k\neq i} f_{ki} + \sum_{j\in\mathcal{N}}^{j\neq i} C_{ij} f_{ij} + C_{iB} f_{iB} - U\eta_i = 0 && (i \in \mathcal{N}) \qquad (2.20) \\
& \eta_{\text{vac}} \leq 1 - \textstyle\sum_{k\in\mathcal{N}} \eta_k - \frac{U\cdot\tau_{\text{TSP}}}{E_{\max}-E_{\min}} \cdot \eta_i \cdot (1-\eta_i) && (i \in \mathcal{N}) \qquad (2.21) \\
& f_{ij}, f_{iB} \geq 0, 0 \leq \eta_i, \eta_{\text{vac}} \leq 1 && (i, j \in \mathcal{N}, i \neq j) \, .
\end{aligned}$$

In this problem, f_{ij}, f_{iB}, η_i, and η_{vac} are optimization variables, and R_i, ρ, C_{ij}, C_{iB}, U, $E_{\max}$, $E_{\min}$, and τ_{TSP} are constants. The following algorithm shows how to obtain a solution to Problem SCP once we obtain a solution to Problem SCP-R.

Algorithm 2.1 *Once we solve Problem SCP-R, we can obtain a corresponding solution to Problem SCP (i.e., calculate the values for τ, τ_i, τ_{vac}, and r_i) as follows: h by (2.17), τ by (2.16), τ_i by (2.15), τ_{vac} by (2.14), and r_i by (2.18).*

After reformulation, the objective function and the constraints become linear except (2.21), where we have a second order η_i^2 term, with $0 \leq \eta_i \leq 1$. In the next section, we present an efficient technique to approximate this second order nonlinear terms (with performance guarantee). Subsequently, we develop an efficient near-optimal solution to our optimization problem.

Remark 2.1 *In our optimization problem, data routing and charging time are closely coupled. One may want to decouple routing from the charging problem and require certain energy efficient*

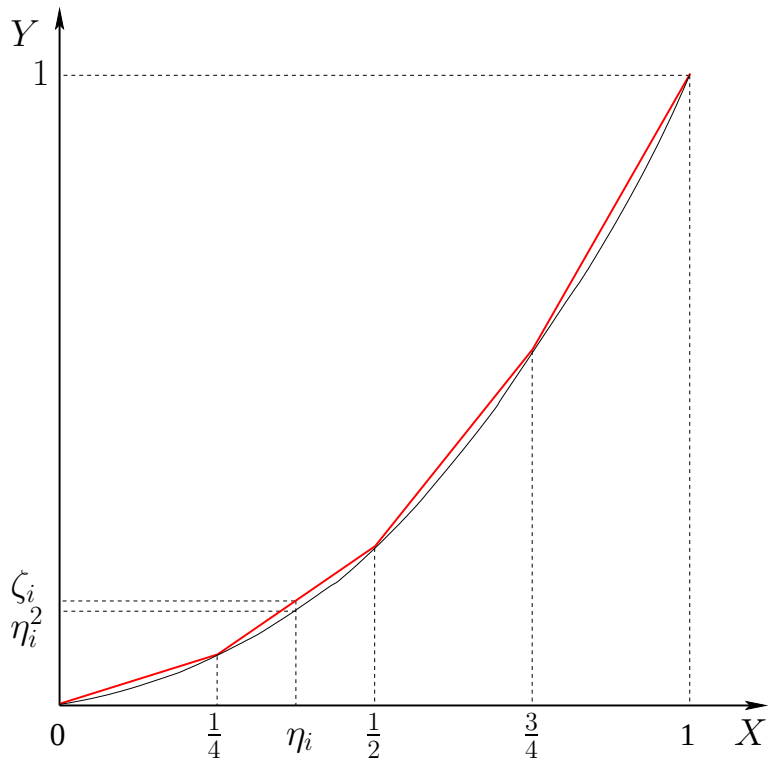

Figure 2.4: An illustration of piecewise linear approximation (with $m = 4$) for the curve (η_i, η_i^2), $0 \leq \eta_i \leq 1$.

routing, e.g., the minimum energy routing.[3] *However, minimum energy routing cannot guarantee optimality. This is because, to maximize* η_{vac}*, by (2.21), we need to minimize* $\max_{i\in\mathcal{N}}\{\sum_{k\in\mathcal{N}}\eta_k + \frac{U\cdot\tau_{\text{TSP}}}{E_{max}-E_{min}}\cdot\eta_i\cdot(1-\eta_i)\}$*, i.e., minimize* $\{\sum_{k\in\mathcal{N}}\eta_k + \max_{i\in\mathcal{N}}\{\frac{U\cdot\tau_{\text{TSP}}}{E_{max}-E_{min}}\cdot\eta_i\cdot(1-\eta_i)\}\}$*. But under minimum energy routing, we can only guarantee that* $\sum_{i\in\mathcal{N}}(\rho\cdot\sum_{k\in\mathcal{N}}^{k\neq i} f_{ki} + \sum_{j\in\mathcal{N}}^{j\neq i} C_{ij}f_{ij} + C_{iB}f_{iB})$ *is minimized. By the relationship in (2.20), minimizing* $\sum_{i\in\mathcal{N}}(\rho\cdot\sum_{k\in\mathcal{N}}^{k\neq i} f_{ki} + \sum_{j\in\mathcal{N}}^{j\neq i} C_{ij}f_{ij} + C_{iB}f_{iB})$ *is equivalent to minimizing* $\sum_{i\in\mathcal{N}}\eta_i$*, which is only part of* $\sum_{k\in\mathcal{N}}\eta_k + \max_{i\in\mathcal{N}}\{\frac{U\cdot\tau_{\text{TSP}}}{E_{max}-E_{min}}\cdot\eta_i\cdot(1-\eta_i)\}$*. Therefore, minimum energy routing cannot guarantee the optimality of our problem. This insight will be confirmed by our numerical results in Section 2.7.*

[3]Here, minimum energy routing refers to using the least energy route to transport data from its source to destination.

2.5.3 A Near-Optimal Solution

Roadmap. Our roadmap to solve Problem SCP is as follows. First, we employ a piecewise linear approximation for the quadratic terms (η_i^2) in Problem SCP-R. This approximation relaxes the corresponding nonlinear constraints into linear constraints, which allows for the problem to be solved by a solver such as CPLEX [24]. Based on the solution from CPLEX, we construct a feasible solution to Problem SCP. In Section 2.5.4, we prove the near-optimality of this feasible solution.

Piecewise Linear Approximation for η_i^2. Note that the only nonlinear terms in the formulation are η_i^2, $i \in \mathcal{N}$. Further, η_i lies in the interval $[0, 1]$, which is small. This motivates us to employ a piecewise linear approximation for the quadratic terms η_i^2.

The key idea is to use m piecewise linear segments to approximate the quadratic curve (see Fig. 2.4). That is, for curve (η_i, η_i^2), $0 \leq \eta_i \leq 1$, we construct a piecewise linear approximation (η_i, ζ_i) by connecting points ($\frac{k}{m}$,$\frac{k^2}{m^2}$), $k = 0, 1, \ldots, m$. The setting of m will determine the level of accuracy and will be studied in Section 2.5.4.

We now represent the piecewise linear curve (η_i, ζ_i) for $0 \leq \eta_i \leq 1$ mathematically. For $k = 0, 1, \ldots, m$, any point (η_i, ζ_i) on the piecewise linear curve within the kth segment (i.e., lying within two end points $(\frac{k-1}{m}, \frac{(k-1)^2}{m^2})$ and $(\frac{k}{m}, \frac{k^2}{m^2})$) can be represented by

$$\eta_i = \lambda_{i,k-1} \cdot \tfrac{k-1}{m} + \lambda_{i,k} \cdot \tfrac{k}{m} \ , \tag{2.22}$$

$$\zeta_i = \lambda_{i,k-1} \cdot \tfrac{(k-1)^2}{m^2} + \lambda_{i,k} \cdot \tfrac{k^2}{m^2} \ , \tag{2.23}$$

where $\lambda_{i,k-1}$ and $\lambda_{i,k}$ are two weights and satisfy the following constraints.

$$\lambda_{i,k-1} + \lambda_{i,k} = 1 \ , \tag{2.24}$$

$$0 \leq \lambda_{i,k-1}, \lambda_{i,k} \leq 1 \ . \tag{2.25}$$

Since $y = x^2$ is a convex function, the piecewise linear approximation curve (η_i, ζ_i) lies above the curve (η_i, η_i^2), $0 \leq \eta_i \leq 1$. Thus, we have $\zeta_i \geq \eta_i^2$ (see Fig. 2.4). The following lemma characterizes the approximation error $\zeta_i - \eta_i^2$ as a function of m.

Lemma 2.3 $\zeta_i - \eta_i^2 \leq \dfrac{1}{4m^2}$ *for* $i \in \mathcal{N}$.

The proof of this lemma is given as follows:

Proof Assume that η_i falls within the kth segment, $k = 1, 2, \cdots, m$. Then we have

$$\begin{aligned}
\zeta_i - \eta_i^2 &= \left[\lambda_{i,k-1} \cdot \frac{(k-1)^2}{m^2} + \lambda_{i,k} \cdot \frac{k^2}{m^2}\right] \\
&\quad - \left[\lambda_{i,k-1} \cdot \frac{k-1}{m} + \lambda_{i,k} \cdot \frac{k}{m}\right]^2 \\
&= (\lambda_{i,k-1} - \lambda_{i,k-1}^2) \cdot \frac{(k-1)^2}{m^2} + (\lambda_{i,k} - \lambda_{i,k}^2) \cdot \frac{k^2}{m^2} \\
&\quad -2\lambda_{i,k-1}\lambda_{i,k} \cdot \frac{k-1}{m} \cdot \frac{k}{m} \\
&= \left[(1 - \lambda_{i,k}) - (1 - \lambda_{i,k})^2\right] \cdot \frac{(k-1)^2}{m^2} \\
&\quad +(\lambda_{i,k} - \lambda_{i,k}^2) \cdot \frac{k^2}{m^2} \\
&\quad -2(1 - \lambda_{i,k})\lambda_{i,k} \cdot \frac{k-1}{m} \cdot \frac{k}{m} \\
&= (\lambda_{i,k} - \lambda_{i,k}^2) \cdot \left[\frac{(k-1)^2}{m^2} + \frac{k^2}{m^2} - 2 \cdot \frac{k-1}{m} \cdot \frac{k}{m}\right] \\
&= (\lambda_{i,k} - \lambda_{i,k}^2) \cdot \left(\frac{k}{m} - \frac{k-1}{m}\right)^2 \\
&= (\lambda_{i,k} - \lambda_{i,k}^2) \cdot \frac{1}{m^2} \\
&\leq \frac{1}{4m^2} \,,
\end{aligned}$$

where the first equality holds by (2.22) and (2.23), the third equality holds by (2.24), and the last inequality holds by $\lambda_{i,k} - \lambda_{i,k}^2 \leq \frac{1}{4}$ when $0 \leq \lambda_{i,k} \leq 1$. This completes the proof. □

Note that the mathematical representation in (2.22) to (2.25) is for a given kth segment, $k = 1, 2, \cdots, m$. We now give a mathematical formulation for the entire piecewise linear curve. Denote z_{ik}, $1 \leq k \leq m$, a binary variable indicating whether η_i falls within the kth segment, i.e., if $\frac{k-1}{m} \leq \eta_i < \frac{k}{m}$, then $z_{ik} = 1$, otherwise, $z_{ik} = 0$. Since η_i can only fall in one of the m segments, we have

$$\sum_{k=1}^{m} z_{ik} = 1 \ . \tag{2.26}$$

With the definition of z_{ik}, $1 \leq k \leq m$, we can formulate (2.22) to (2.24) for the entire piecewise linear curve. First, we show how λ_{ik} relates to z_{ik}, $1 \leq k \leq m$. Based on (2.22) to (2.24), when η_i falls within the kth segment, we can only have $\lambda_{i,k-1}$ and $\lambda_{i,k}$ positive while all other $\lambda_{i,j}$ ($j \neq k-1, k$) must be zero. That is, $\lambda_{i0} > 0$ only if $z_{i1} = 1$; $\lambda_{ik} > 0$ only if $z_{ik} = 1$ or $z_{i,k+1} = 1$, $1 \leq k < m$; and $\lambda_{im} > 0$ only if $z_{im} = 1$. These relationships can be written as follows.

$$\lambda_{i0} \leq z_{i1} \tag{2.27}$$

$$\lambda_{ik} \leq z_{ik} + z_{i,k+1} \quad (1 \leq k < m) \tag{2.28}$$

$$\lambda_{im} \leq z_{im} \tag{2.29}$$

The above three constraints ensure that there are at most two adjacent positive λ values for each η_i. Equations (2.22), (2.23), and (2.24) can now be rewritten for the entire piecewise linear curve as follows:

$$\eta_i = \sum_{k=0}^{m} \lambda_{ik} \cdot \frac{k}{m} \tag{2.30}$$

$$\zeta_i = \sum_{k=0}^{m} \lambda_{ik} \cdot \frac{k^2}{m^2} \tag{2.31}$$

$$\sum_{k=0}^{m} \lambda_{ik} = 1 \ . \tag{2.32}$$

Relaxed Linear Formulation. By replacing η_i^2 with ζ_i in (2.21), we have

$$\eta_{\text{vac}} \leq 1 - \textstyle\sum_{k\in\mathcal{N}} \eta_k - \frac{U\tau_{\text{TSP}}}{E_{\text{max}}-E_{\text{min}}}(\eta_i - \zeta_i) \quad (i \in \mathcal{N}). \tag{2.33}$$

By adding the new constraints (2.26)–(2.32) to the model, we obtain the following linear relaxed formulation:

SCP-L

maximize η_{vac}

subject to

$$\textstyle\sum_{j\in\mathcal{N}}^{j\neq i} f_{ij} + f_{iB} - \sum_{k\in\mathcal{N}}^{k\neq i} f_{ki} = R_i \qquad (i \in \mathcal{N})$$

$$\rho \cdot \textstyle\sum_{k\in\mathcal{N}}^{k\neq i} f_{ki} + \sum_{j\in\mathcal{N}}^{j\neq i} C_{ij} \cdot f_{ij} + C_{iB} \cdot f_{iB} - U \cdot \eta_i = 0 \quad (i \in \mathcal{N})$$

$$\eta_{\text{vac}} \leq 1 - \textstyle\sum_{k\in\mathcal{N}} \eta_k - \frac{U\tau_{\text{TSP}}}{E_{\text{max}}-E_{\text{min}}} \cdot (\eta_i - \zeta_i) \qquad (i \in \mathcal{N})$$

$$\textstyle\sum_{k=1}^{m} z_{ik} = 1 \qquad (i \in \mathcal{N})$$

$$\lambda_{i0} - z_{i1} \leq 0 \qquad (i \in \mathcal{N})$$

$$\lambda_{ik} - z_{ik} - z_{i,k+1} \leq 0 \qquad (i \in \mathcal{N},\ 1 \leq k < m)$$

$$\lambda_{im} - z_{im} \leq 0 \qquad (i \in \mathcal{N})$$

$$\eta_i - \textstyle\sum_{k=0}^{m} \frac{k}{m} \cdot \lambda_{ik} = 0 \qquad (i \in \mathcal{N})$$

$$\zeta_i - \textstyle\sum_{k=0}^{m} \frac{k^2}{m^2} \cdot \lambda_{ik} = 0 \qquad (i \in \mathcal{N})$$

$$\textstyle\sum_{k=0}^{m} \lambda_{ik} = 1 \qquad (i \in \mathcal{N})$$

$$f_{ij}, f_{iB} \geq 0, 0 \leq \eta_i, \eta_{\text{vac}}, \zeta_i \leq 1 \qquad (i, j \in \mathcal{N}, i \neq j)$$

$$z_{ik} \in \{0, 1\} \qquad (i \in \mathcal{N}, 1 \leq k \leq m)$$

$$0 \leq \lambda_{ik} \leq 1 \qquad (i \in \mathcal{N}, 0 \leq k \leq m),$$

where f_{ij}, f_{iB}, η_i, η_{vac}, z_{ik}, λ_{ik}, and ζ_i are variables, and R_i, ρ, C_{ij}, C_{iB}, U, E_{max}, E_{min}, and τ_{TSP} are constants. This new formulation can be solved by a solver such as CPLEX [24].

Construction of a Feasible Near-Optimal Solution. The solution to Problem SCP-L is likely to

be infeasible to Problem SCP-R (and Problem SCP). But based on this solution, we can construct a feasible solution to Problem SCP.

Suppose that $\hat{\psi}$ = ($\hat{f}_{ij}$, $\hat{f}_{iB}$, $\hat{\eta}_i$, $\hat{\eta}_{\text{vac}}$, $\hat{z}_{ik}$, $\hat{\lambda}_{ik}$, $\hat{\zeta}_i$) is the solution obtained for Problem SCP-L. By observing ($\hat{f}_{ij}$, $\hat{f}_{iB}$, $\hat{\eta}_i$, $\hat{\eta}_{\text{vac}}$), we find that it satisfies all constraints to Problem SCP-R except (2.21). To construct a feasible solution $\psi = (f_{ij}, f_{iB}, \eta_i, \eta_{\text{vac}})$ to Problem SCP-R, we let $f_{ij} = \hat{f}_{ij}$, $f_{iB} = \hat{f}_{iB}$, $\eta_i = \hat{\eta}_i$. For η_{vac}, in order to satisfy (2.21), we define

$$\eta_{\text{vac}} = \min_{i\in\mathcal{N}} \left\{ 1 - \sum_{k\in\mathcal{N}} \hat{\eta}_k - \frac{U\cdot\tau_{\text{TSP}}}{E_{\max}-E_{\min}} \hat{\eta}_i(1-\hat{\eta}_i) \right\} .$$

It is easy to verify that this newly constructed solution ψ satisfies all the constraints for Problem SCP-R. Once we have this solution to Problem SCP-R, we can easily find a solution to Problem SCP via Algorithm 2.1.

2.5.4 Proof of Near-Optimality

In this section, we quantify the performance gap between the optimal objective (unknown, denoted by η^*_{vac}) and the objective (denoted by η_{vac}) obtained by the feasible solution ψ that we derived in the last section. Naturally, we expect such a performance gap to be a function of m, i.e., the number of segments that we use in the piecewise linear approximation. This result will be stated in Lemma 2.4. Based on this result, we can obtain an important inverse result (in Theorem 2.2), which shows how to set m such that $\eta^*_{\text{vac}} - \eta_{\text{vac}} \le \epsilon$ for a given target performance gap ϵ ($0 < \epsilon \ll 1$).

Lemma 2.4 *For the feasible solution ψ with objective value η_{vac}, we have*

$$\eta^*_{\text{vac}} - \eta_{\text{vac}} \le \frac{U\cdot\tau_{\text{TSP}}}{4(E_{max}-E_{min})} \cdot \frac{1}{m^2} .$$

To prove Lemma 2.4, we need two intermediate results for $\hat{\eta}_{\text{vac}}$ and η_{vac}, which are stated in Lemmas 2.5 and 2.6, respectively.

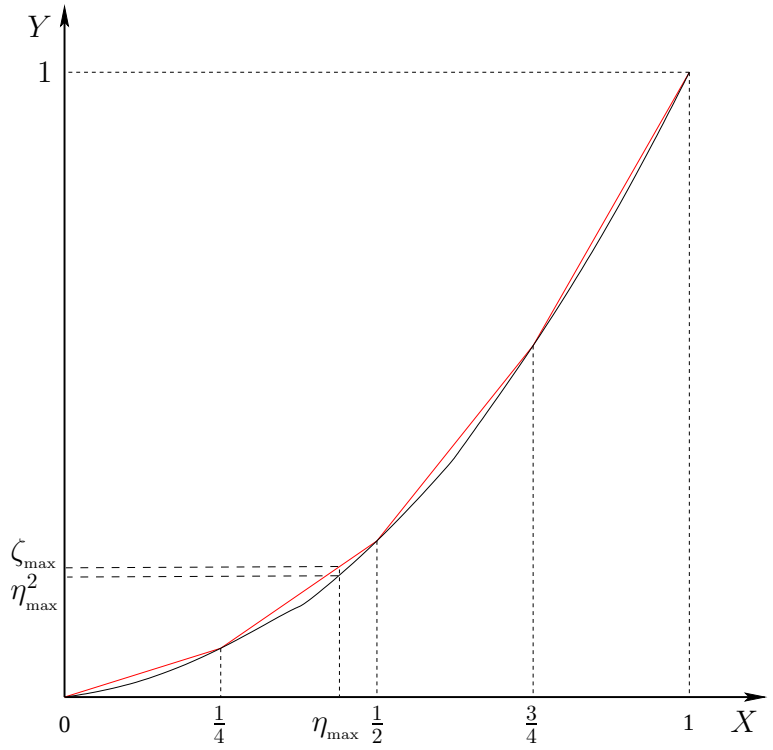

Figure 2.5: An illustration of $\eta^2_{\max}$ and its approximation $\zeta_{\max}$.

Lemma 2.5 *For the optimal solution $\hat{\psi}$ to problem SCP-L, we have*

$$\hat{\eta}_{\text{vac}} = 1 - \sum_{k \in \mathcal{N}} \hat{\eta}_k - \frac{U\tau_{\text{TSP}}}{E_{\max} - E_{\min}} \cdot (\eta_{\max} - \zeta_{\max}) \ ,$$

where

$$\eta_{\max} \equiv \max_{i \in \mathcal{N}} \{\hat{\eta}_i\}$$

and $\zeta_{\max}$ is the piecewise linear approximation of $\eta^2_{\max}$ (see Fig. 2.5).

Proof It is easy to see that in $\hat{\psi}$, $\hat{\eta}_{\text{vac}} = \min_{i \in \mathcal{N}} \{1 - \sum_{k \in \mathcal{N}} \hat{\eta}_k - \frac{U\tau_{\text{TSP}}}{E_{\max} - E_{\min}} \cdot (\hat{\eta}_i - \hat{\zeta}_i)\}$. Thus, to prove this lemma, it is sufficient to show $\max_{i \in \mathcal{N}} \{\hat{\eta}_i - \hat{\zeta}_i\} = \eta_{\max} - \zeta_{\max}$, i.e., $\hat{\eta}_i - \hat{\zeta}_i \leq \eta_{\max} - \zeta_{\max}$ for each $i \in \mathcal{N}$.

We consider the following two cases.

Case 1 $0 < \eta_{\max} \leq \frac{1}{2}$: Based on the definition of $\eta_{\max}$, we have $0 < \hat{\eta}_i \leq \eta_{\max} \leq \frac{1}{2}$ for each $i \in \mathcal{N}$. We now show that $\hat{\eta}_i - \hat{\zeta}_i$ is a non-decreasing function when $0 < \hat{\eta}_i \leq \frac{1}{2}$. Then it follows that $\hat{\eta}_i - \hat{\zeta}_i \leq \eta_{\max} - \zeta_{\max}$.

Suppose $\hat{\eta}_i$ falls within the l-th segment, i.e., $\frac{l-1}{m} \leq \hat{\eta}_i < \frac{l}{m}$ for a particular l. We have

$$\hat{\lambda}_{i,l-1} = l - m \cdot \hat{\eta}_i \text{ and } \hat{\lambda}_{i,l} = m \cdot \hat{\eta}_i - (l-1) \ .$$

Then we can express $\hat{\eta}_i - \hat{\zeta}_i$ as a function of $\hat{\eta}_i$.

$$\begin{aligned}
\hat{\eta}_i - \hat{\zeta}_i &= \hat{\eta}_i - \left(\hat{\lambda}_{i,l-1} \cdot \frac{(l-1)^2}{m^2} + \hat{\lambda}_{i,l} \cdot \frac{l^2}{m^2} \right) \\
&= \hat{\eta}_i - \left((l - m \cdot \hat{\eta}_i) \cdot \frac{(l-1)^2}{m^2} + (m \cdot \hat{\eta}_i - (l-1)) \cdot \frac{l^2}{m^2} \right) \\
&= \hat{\eta}_i - \frac{(l^2 - (l-1)^2) \cdot m\hat{\eta}_i - l(l-1)}{m^2} \\
&= \left(1 - \frac{2l-1}{m} \right) \cdot \hat{\eta}_i + \frac{l(l-1)}{m^2} \ . \qquad (2.34)
\end{aligned}$$

When $0 < \hat{\eta}_i \leq \frac{1}{2}$, we have $l \leq \frac{m+1}{2}$ if m is odd and $l \leq \frac{m}{2}$ if m is even. Then $1 - \frac{2l-1}{m} \geq 0$ for both cases. Thus, when $0 < \hat{\eta}_i \leq \frac{1}{2}$ and $\hat{\eta}_i$ falls within the l-th segment, $\hat{\eta}_i - \hat{\zeta}_i$ is a non-decreasing function. Since the non-decreasing property holds for all segments within $(0, \frac{1}{2}]$, we know that $\hat{\eta}_i - \hat{\zeta}_i$ is a non-decreasing function when $0 < \hat{\eta}_i \leq \frac{1}{2}$.

Case 2 $\frac{1}{2} < \eta_{\max} \leq 1$: Suppose $\hat{\eta}_j = \eta_{\max}$. Let $\hat{\eta}_{j'} = 1 - \hat{\eta}_j$ and denote $\hat{\zeta}_{j'}$ the approximation of $\hat{\eta}^2_{j'}$. By (2.33), we have $\hat{\eta}_i \leq 1 - \hat{\eta}_j - \left[\sum_{k \in \mathcal{N}}^{k \neq i, k \neq j} \hat{\eta}_k + \hat{\eta}_{\text{vac}} + \frac{U \tau_{\text{TSP}}}{E_{\max} - E_{\min}} \cdot (\hat{\eta}_i - \hat{\zeta}_i) \right] < 1 - \hat{\eta}_j = \hat{\eta}_{j'} < \frac{1}{2}$ for each $i \in \mathcal{N}$. Since $\hat{\eta}_i - \hat{\zeta}_i$ is a non-decreasing function for $0 < \hat{\eta}_i \leq \frac{1}{2}$, we have $\hat{\eta}_i - \hat{\zeta}_i \leq \hat{\eta}_{j'} - \hat{\zeta}_{j'}$.

We now show $\hat{\eta}_{j'} - \hat{\zeta}_{j'} = \hat{\eta}_j - \hat{\zeta}_j$. Suppose $\hat{\eta}_j$ falls within the l-th segment, i.e., $\frac{l-1}{m} \leq \hat{\eta}_j < \frac{l}{m}$

for a particular l. Then $\hat{\eta}_{j'}$ falls within the $(m-l+1)$-th segment, i.e., $\frac{m-l}{m} \leq \hat{\eta}_{j'} < \frac{m-l+1}{m}$. Then by (2.34), we have

$$\begin{aligned}
\hat{\eta}_{j'} - \hat{\zeta}_{j'} &= \left(1 - \frac{2(m-l+1)-1}{m}\right) \cdot \hat{\eta}_{j'} + \frac{(m-l+1)(m-l+1-1)}{m^2} \\
&= \frac{-m+2l-1}{m} \cdot (1-\hat{\eta}_j) + \frac{(m-l+1)(m-l)}{m^2} \\
&= \left(1 - \frac{2l-1}{m}\right) \cdot \hat{\eta}_j + \frac{(-m^2+2lm-m)+(m^2-2lm+l^2+m-l)}{m^2} \\
&= \left(1 - \frac{2l-1}{m}\right) \cdot \hat{\eta}_j + \frac{l^2-l}{m^2} \\
&= \hat{\eta}_j - \hat{\zeta}_j.
\end{aligned}$$

Therefore, we have $\hat{\eta}_i - \hat{\zeta}_i \leq \hat{\eta}_{j'} - \hat{\zeta}_{j'} = \hat{\eta}_j - \hat{\zeta}_j = \eta_{\max} - \zeta_{\max}$.

Combining both cases, we have $\hat{\eta}_i - \hat{\zeta}_i \leq \eta_{\max} - \zeta_{\max}$ for each $i \in \mathcal{N}$. This completes the proof. □

Lemma 2.6 *For the constructed solution ψ to problem SCP-R, we have*

$$\eta_{\text{vac}} = 1 - \sum_{k \in \mathcal{N}} \hat{\eta}_k - \frac{U\tau_{\text{TSP}}}{E_{\max} - E_{\min}} \cdot \eta_{\max} \cdot (1 - \eta_{\max}) \, .$$

Proof To prove the lemma, it is sufficient to show $\max_{i \in \mathcal{N}}\{\hat{\eta}_i(1-\hat{\eta}_i)\} = \eta_{max}(1-\eta_{max})$, i.e, $\hat{\eta}_i(1-\hat{\eta}_i) \leq \eta_{max}(1-\eta_{max})$ for each $i \in \mathcal{N}$.

We consider the following two cases.

Case 1 $0 < \eta_{\max} \leq \frac{1}{2}$: We have $0 < \hat{\eta}_i \leq \eta_{\max} \leq \frac{1}{2}$ for each $i \in \mathcal{N}$. Since $x(1-x)$ is an increasing function for $0 < x \leq \frac{1}{2}$, we have $\hat{\eta}_i(1-\hat{\eta}_i) \leq \eta_{\max}(1-\eta_{\max})$.

Case 2 $\frac{1}{2} < \eta_{\max} < 1$: Suppose $\hat{\eta}_j = \eta_{\max}$. By (2.33), we have $\hat{\eta}_i \leq 1 - \eta_j - \Big[\sum_{k\in\mathcal{N}, k\neq i, k\neq j} \hat{\eta}_k + \hat{\eta}_{\text{vac}} + \frac{U\tau_{\text{TSP}}}{E_{\max}-E_{\min}} \cdot (\hat{\eta}_i - \hat{\zeta}_i) \Big] < 1 - \eta_j < \frac{1}{2}$ for each $i \in \mathcal{N}$. Since $0 < \hat{\eta}_i < 1 - \eta_j < \frac{1}{2}$ and $x(1-x)$ is an increasing function for $0 < x < \frac{1}{2}$, we have $\hat{\eta}_i(1-\hat{\eta}_i) \leq (1-\eta_j)\left[1-(1-\eta_j)\right] = \eta_j(1-\eta_j) = \eta_{\max}(1-\eta_{\max})$.

Combining both cases, we have $\hat{\eta}_i(1-\hat{\eta}_i) \leq \eta_{max}(1-\eta_{max})$. This completes the proof. □

Based on Lemmas 2.5 and 2.6, we can prove Lemma 2.4.

Proof Denote $\hat{\eta}_{\text{vac}}$ as the objective value obtained by the solution $\hat{\psi}$ to the relaxed linear problem SCP-L. Since Problem SCP-L is a relaxation of Problem SCP-R, $\hat{\eta}_{\text{vac}}$ is an upper bound of η^*_{vac}, i.e., $\eta^*_{\text{vac}} \leq \hat{\eta}_{\text{vac}}$. Therefore,

$$
\begin{aligned}
& \eta^*_{\text{vac}} - \eta_{\text{vac}} \\
\leq\ & \hat{\eta}_{\text{vac}} - \eta_{\text{vac}} \\
=\ & \left[1 - \sum_{k\in\mathcal{N}} \hat{\eta}_k - \frac{U\tau_{\text{TSP}}}{E_{\max} - E_{\min}} \cdot (\eta_{\max} - \zeta_{\max})\right] - \left[1 - \sum_{k\in\mathcal{N}} \hat{\eta}_k - \frac{U\tau_{\text{TSP}}}{E_{\max} - E_{\min}} \cdot \eta_{\max} \cdot (1 - \eta_{\max})\right] \\
=\ & \frac{U\tau_{\text{TSP}}}{E_{\max} - E_{\min}} (\zeta_{\max} - \eta^2_{\max}) \\
\leq\ & \frac{U\tau_{\text{TSP}}}{4(E_{\max} - E_{\min})} \cdot \frac{1}{m^2},
\end{aligned}
$$

where the second equality holds by Lemmas 2.5 and 2.6, and the fourth inequality holds by Lemma 2.3. □

Based on Lemma 2.4, the following theorem shows how to set m such that $\eta^*_{\text{vac}} - \eta_{\text{vac}} \leq \epsilon$ for a given target performance gap ϵ ($0 < \epsilon \ll 1$).

Construction of a Near-Optimal Solution

1. Given a target performance gap ϵ.
2. Let $m = \left\lceil \sqrt{\frac{U\tau_{\rm TSP}}{4\epsilon(E_{\rm max}-E_{\rm min})}} \right\rceil$.
3. Solve Problem SCP-L with m segments by CPLEX, and obtain its solution $\hat{\psi}$ = ($\hat{f}_{ij}$, $\hat{f}_{iB}$, $\hat{\eta}_i$, $\hat{\eta}_{\rm vac}$, $\hat{z}_{ik}$, $\hat{\lambda}_{ik}$, $\hat{\zeta}_i$).
4. Construct a feasible solution ψ = (f_{ij}, f_{iB}, η_i, $\eta_{\rm vac}$) for Problem SCP-R by letting $f_{ij} = \hat{f}_{ij}$, $f_{iB} = \hat{f}_{iB}$, $\eta_i = \hat{\eta}_i$ and $\eta_{\rm vac} = \min_{i\in\mathcal{N}}\{1 - \sum_{k\in\mathcal{N}} \hat{\eta}_k - \frac{U\tau_{\rm TSP}}{E_{\rm max}-E_{\rm min}} \cdot \hat{\eta}_i \cdot (1-\hat{\eta}_i)\}$.
5. Obtain a near-optimal solution ($f_{ij}, f_{iB}, \tau, \tau_i, \tau_{\rm vac}, r_i$) to Problem SCP by Algorithm 2.1.

Figure 2.6: Procedure to construct a near-optimal solution.

Theorem 2.2 *For a given* ϵ, $0 < \epsilon \ll 1$, *if* $m = \left\lceil \sqrt{\frac{U\tau_{\rm TSP}}{4\epsilon(E_{max}-E_{min})}} \right\rceil$, *then we have* $\eta^*_{\rm vac} - \eta_{\rm vac} \le \epsilon$.

Proof Lemma 2.4 shows that the performance gap is $\eta^*_{\rm vac} - \eta_{\rm vac} \le \frac{U\tau_{\rm TSP}}{4(E_{\rm max}-E_{\rm min})} \cdot \frac{1}{m^2}$. Therefore, if we set $m = \left\lceil \sqrt{\frac{U\tau_{\rm TSP}}{4\epsilon(E_{\rm max}-E_{\rm min})}} \right\rceil \ge \sqrt{\frac{U\tau_{\rm TSP}}{4\epsilon(E_{\rm max}-E_{\rm min})}}$, then we have

$$\begin{aligned} \eta^*_{\rm vac} - \eta_{\rm vac} &\le \frac{U\tau_{\rm TSP}}{4(E_{\rm max}-E_{\rm min})} \cdot \frac{1}{m^2} \\ &\le \frac{U\tau_{\rm TSP}}{4(E_{\rm max}-E_{\rm min})} \cdot \frac{4\epsilon(E_{\rm max}-E_{\rm min})}{U\tau_{\rm TSP}} \\ &= \epsilon\ . \end{aligned}$$

This completes the proof. □

With Theorem 2.2, we display the complete solution procedure on how to obtain a near-optimal solution to Problem SCP in Fig. 2.6.

2.6 Constructing an Initial Transient Cycle

In Section 2.3, we skipped the discussion on how to construct an initial transient cycle before the first renewable cycle. Now with the optimal traveling path $\mathcal{P}$ (the shortest Hamiltonian cycle) and the feasible near-optimal solution $(f_{ij}, f_{iB}, \tau, \tau_i, \tau_{\text{vac}}, r_i)$ obtained in Section 2.5, we are ready to construct an initial transient cycle.

Unlike a renewable energy cycle at node i, which starts and ends with the same energy level E_i, the initial transient starts with $E_{\max}$ and ends with E_i. Specifically, the initial transient cycle must meet the following criterion:

Criterion 2.1 *At each node $i \in \mathcal{N}$, its initial transient cycle must meet the following criteria: (i) $e_i(0) = E_{max}$ and $e_i(\tau) = E_i$; and (ii) $e_i(t) \geq E_{min}$ for $t \in [0, \tau]$.*

We now construct an initial cycle to meet the above criterion. First, we need to calculate E_i, $i \in \mathcal{N}$. From (2.6), we have $E_i = E_{\max} - (2\tau - a_i - \tau_i)r_i$, where a_i can be obtained by (2.3).

For a solution $\varphi = (\mathcal{P}, f_{ij}, f_{iB}, \tau, \tau_i, \tau_{\mathcal{P}}, \tau_{\text{vac}}, r_i, U)$ corresponding to a renewable energy cycle for $t \geq \tau$, we construct $\hat{\varphi} = (\hat{\mathcal{P}}, \hat{f}_{ij}, \hat{f}_{iB}, \hat{\tau}, \hat{\tau}_i, \hat{\tau}_{\hat{\mathcal{P}}}, \hat{\tau}_{\text{vac}}, \hat{r}_i, u_i)$ for the initial transient cycle for $t \in [0, \tau]$ by letting $\hat{\mathcal{P}} = \mathcal{P}$, $\hat{f}_{ij} = f_{ij}$, $\hat{f}_{iB} = f_{iB}$, $\hat{\tau} = \tau$, $\hat{\tau}_i = \tau_i$, $\hat{\tau}_{\hat{\mathcal{P}}} = \tau_{\mathcal{P}}$, $\hat{\tau}_{\text{vac}} = \tau_{\text{vac}}$, $\hat{r}_i = r_i$ and

$$u_i = \frac{r_i \hat{a}_i}{\tau_i} + r_i, \tag{2.35}$$

where u_i is the charging rate at node i during the initial transient cycle and $\hat{a}_i$ is the arrival time of the WCV at node i in the initial transient cycle (see Fig. 2.7).

We now need to show that $u_i \leq U$, where U is the full charging rate. First, we have

$$\hat{a}_{\pi_i} \;=\; \sum_{k=0}^{i-1} \frac{\hat{D}_{\pi_k \pi_{k+1}}}{V} + \sum_{k=1}^{i-1} \hat{\tau}_{\pi_k} = \sum_{k=0}^{i-1} \frac{D_{\pi_k \pi_{k+1}}}{V} + \sum_{k=1}^{i-1} \tau_{\pi_k} = a_{\pi_i} - \tau \;, \tag{2.36}$$

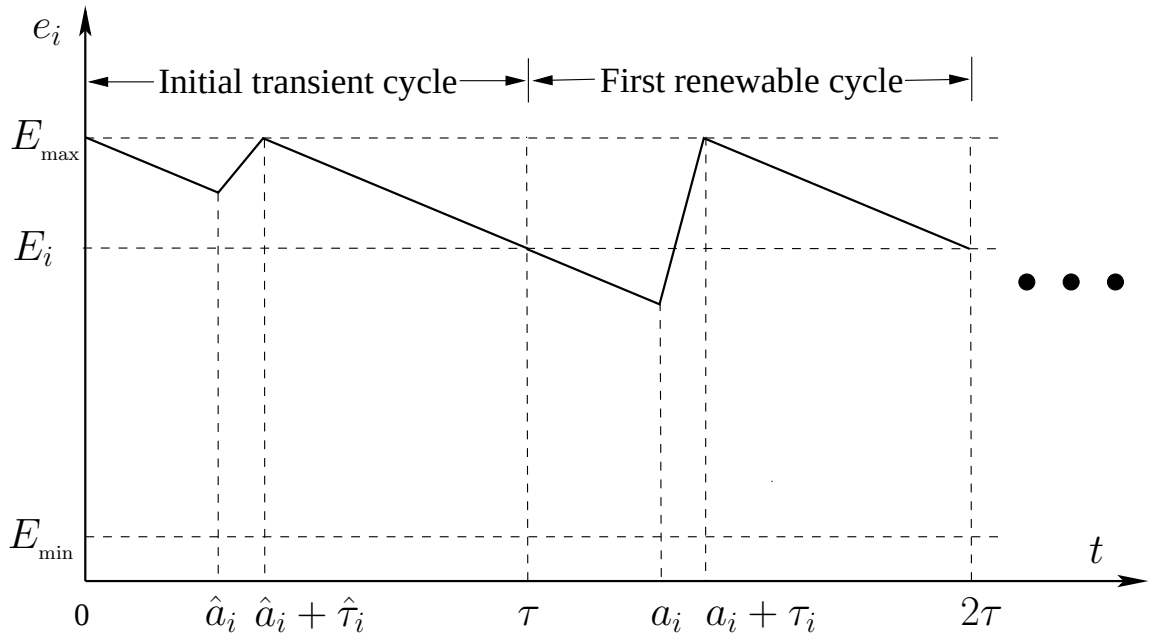

Figure 2.7: Illustration of energy behavior for the initial transient cycle and how it connects to the first renewable cycle.

where the second equality holds by $\hat{\mathcal{P}} = \mathcal{P}$ and $\hat{\tau}_i = \tau_i$, and the last equality follows from (2.3). Further, by (2.5), we have $U \cdot \tau_i = \tau \cdot r_i = (2\tau - \tau) \cdot r_i \geq (a_i + \tau_i - \tau) \cdot r_i$. It follows that

$$(a_i - \tau) \cdot r_i \leq (U - r_i) \cdot \tau_i. \tag{2.37}$$

Then, we have

$$u_i \;=\; \frac{r_i \hat{a}_i}{\tau_i} + r_i = \frac{r_i(a_i - \tau)}{\tau_i} + r_i \leq \frac{(U - r_i) \cdot \tau_i}{\tau_i} + r_i = U \ ,$$

where the first equality follows from (2.35), the second equality follows from (2.36), and the third inequality follows from (2.37).

For the newly constructed $\hat{\varphi}$, we have the following theorem:

Theorem 2.3 *The constructed $\hat{\varphi}$ is a feasible transient cycle.*

Proof To prove that $\hat{\varphi}$ is a feasible initial transient cycle, we need to show that the newly con-

structed $\hat{\varphi}$ satisfies Criterion 2.1. By our assumption, $e_i(0) = E_{\max}$. At time $(\hat{a}_i + \hat{\tau}_i)$, we have

$$\begin{aligned} e_i(\hat{a}_i + \hat{\tau}_i) &= e_i(0) - \hat{r}_i \cdot \hat{a}_i + (u_i - \hat{r}_i) \cdot \hat{\tau}_i \\ &= E_{\max} - r_i \cdot (a_i - \tau) + (u_i - r_i) \cdot \tau_i \\ &= E_{\max} - r_i \cdot (a_i - \tau + \tau_i) + u_i \cdot \tau_i = E_{\max}, \end{aligned} \tag{2.38}$$

where the second equality follows since $e_i(0) = E_{\max}$, $\hat{r}_i = r_i$, $\hat{a}_i = a_i - \tau$, and $\hat{\tau}_i = \tau_i$, the last equality follows from (2.35) and (2.36). Therefore, the battery at node i is full when the WCV leaves it at $(\hat{a}_i + \hat{\tau}_i)$. At time τ, we have

$$\begin{aligned} e_i(\tau) &= e_i(\hat{a}_i + \hat{\tau}_i) - \hat{r}_i \cdot \big(\tau - (\hat{a}_i + \hat{\tau}_i)\big) \\ &= E_{\max} - r_i \cdot [\tau - (a_i - \tau + \tau_i)] \\ &= E_{\max} - r_i \cdot [2\tau - (a_i + \tau_i)] \\ &= e_i(2\tau) = E_i, \end{aligned} \tag{2.39}$$

where the second equality follows from (2.38), and the fourth equality follows from (2.6). Therefore, Criterion 2.1(i) is met.

To show $e_i(t) \geq E_{\min}$ for $t \in [0, \tau]$, it is sufficient to show that $e_i(\hat{a}_i) \geq E_{\min}$ and $e_i(\tau) \geq E_{\min}$, since these two time instances are the local minimum for $e_i(t)$ during $t \in [0, \tau]$. We have $e_i(\hat{a}_i) = e_i(0) - \hat{r}_i \cdot \hat{a}_i = E_{\max} - r_i \cdot (a_i - \tau) \geq E_i - r_i \cdot (a_i - \tau) = e_i(a_i) \geq E_{\min}$. Also, by (2.39), $e_i(\tau) = E_i \geq E_{\min}$. Hence, $e_i(t) \geq E_{\min}$, for $t \in [0, \tau]$.

In summary, $\hat{\varphi}$ meets all the criteria of a feasible initial transient cycle. This completes the proof. □

2.7 Numerical Results

In this section, we present some numerical results to demonstrate how our solution can produce a renewable WSN and some interesting properties with such a network.

Table 2.3: Location and data rate R_i for each node in a 50-node network.

Node Index	Location (m)	R_i (kb/s)	Node Index	Location (m)	R_i (kb/s)	Node Index	Location (m)	R_i (kb/s)
1	(815, 276)	1	18	(916, 139)	10	35	(97, 917)	2
2	(906, 680)	8	19	(792, 149)	1	36	(823, 286)	2
3	(127, 655)	4	20	(959, 258)	5	37	(695, 757)	8
4	(913, 163)	6	21	(656, 841)	3	38	(317, 754)	6
5	(632, 119)	3	22	(36, 254)	10	39	(950, 380)	6
6	(98, 498)	7	23	(849, 814)	1	40	(34, 568)	2
7	(278, 960)	3	24	(934, 244)	8	41	(439, 76)	8
8	(547, 340)	7	25	(679, 929)	8	42	(382, 54)	7
9	(958, 585)	6	26	(758, 350)	9	43	(766, 531)	4
10	(965, 224)	8	27	(743, 197)	1	44	(795, 779)	6
11	(158, 751)	5	28	(392, 251)	4	45	(187, 934)	6
12	(971, 255)	1	29	(655, 616)	4	46	(490, 130)	1
13	(957, 506)	4	30	(171, 473)	9	47	(446, 569)	3
14	(485, 699)	10	31	(706, 352)	5	48	(646, 469)	2
15	(800, 891)	2	32	(32, 831)	10	49	(709, 12)	2
16	(142, 959)	9	33	(277, 585)	1	50	(755, 337)	3
17	(422, 547)	5	34	(46, 550)	3			

2.7.1 Simulation Settings

We consider two randomly generated WSNs consisting of 50 and 100 nodes, respectively. The sensor nodes are deployed over a square area of 1 km $\times$ 1 km. The data rate (i.e., R_i, $i \in \mathcal{N}$) from each node is randomly generated within $[1, 10]$ kb/s. The power consumption coefficients are $\beta_1 = 50$ nJ/b, $\beta_2 = 0.0013$ pJ$/(\mathrm{b} \cdot \mathrm{m}^4)$, $\alpha = 4$, and $\rho = 50$ nJ/b [20]. The base station is assumed to be located at (500, 500) (in m) and the home service station for the WCV is assumed to be at the origin. The traveling speed of the WCV is $V = 5$ m/s.

For the battery at a sensor node, we choose a regular NiMH battery and its nominal cell voltage and the quantity of electricity is 1.2 V/2.5 Ah. We have $E_{\max} = 1.2\,\mathrm{V} \times 2.5\,\mathrm{A} \times 3600\,\mathrm{sec} = 10.8$ KJ [33]. We let $E_{\min} = 0.05 \cdot E_{\max} = 540$ J. We assume the WET rate $U = 5$ W, which is well within feasible range [31].

We set the target $\epsilon = 0.01$ for the numerical results, i.e., our solution has an error no more than

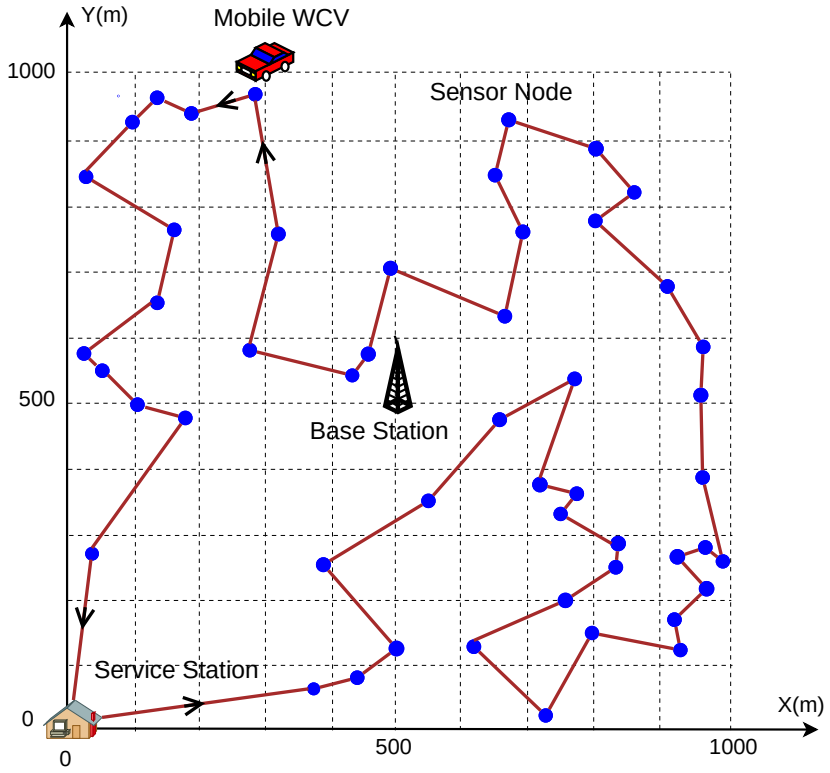

Figure 2.8: An optimal traveling path for the WCV for the 50-node sensor network, assuming traveling direction is counter clockwise.

0.01. The experiments were conducted on a DELL Precision T5400 with Intel Xeon 3.0GHz and 16GB RAM. All the network instances (with up to 100 nodes) were solved in seconds.

2.7.2 Results

50-node Network. We first present complete results for the 50-node network. Table 2.3 gives the location of each node and its data rate for a 50-node network. The shortest Hamiltonian cycle is found by using the Concorde solver [10] and is shown in Fig. 2.8. For this optimal cycle, $D_{\text{TSP}} = 5821$ m and $\tau_{\text{TSP}} = 1164.2$ s. For the target $\epsilon = 0.01$, by Theorem 2.2, we have

$$m = \left\lceil \sqrt{\frac{U \cdot \tau_{\text{TSP}}}{4\epsilon(E_{\max} - E_{\min})}} \right\rceil = \left\lceil \sqrt{\frac{5 \times 1164.2}{4 \times 0.01 \times (10800 - 540)}} \right\rceil = 4 \ ,$$

Table 2.4: The case of counter clockwise traveling direction: Node visited along the path, arrival time at each node, starting energy of each node in a renewable cycle, and charging time at each node for the 50-node network.

Node Order	a_i (s)	E_i (J)	τ_i (s)	Node Order	a_i (s)	E_i (J)	τ_i (s)
42	110702	10747	11	2	117778	10611	41
41	110725	10613	37	44	117848	10605	42
46	110777	9282	305	23	117903	10793	2
28	111113	7697	627	15	117923	10747	11
8	111776	7590	653	25	117960	10685	25
48	112461	714	2092	21	118002	10593	44
43	114579	10594	43	37	118065	8827	425
31	114660	6233	957	29	118519	8493	499
26	115627	10752	10	14	119056	10299	109
50	115639	9851	199	47	119192	10581	47
36	115855	10137	139	17	119246	9246	338
1	115997	9594	254	33	119614	4961	1287
27	116273	10551	53	38	120936	10059	164
5	116353	10646	33	7	121142	10754	10
49	116412	10610	40	45	121171	10658	31
19	116484	10660	29	16	121213	10738	14
18	116538	10622	38	35	121239	10259	120
4	116581	10329	100	32	121380	8628	483
10	116696	10596	43	11	121894	10010	176
24	116747	9648	245	3	122090	6697	924
20	116997	10773	6	40	123039	10790	2
12	117006	10794	1	34	123046	10747	12
39	117032	8565	477	6	123073	10519	63
13	117534	10020	167	30	123151	8319	563
9	117717	10613	40	22	123766	5722	1166

which is a small number. In our solution, the cycle time τ = 30.73 hours, the vacation time τ_{vac} = 26.82 hours, and the objective $\eta_{\text{vac}} = 87.27\%$.

By Corollary 2.1.2, the WCV can follow either direction of the shortest Hamiltonian cycle while achieving the same objective value $\eta_{\text{vac}} = 87.27\%$. Comparing the two solutions, the values for f_{ij}, f_{iB}, τ, τ_i, τ_{TSP}, τ_{vac} are identical while the values of a_i and E_i are different. This observation can be verified by our simulation results in Table 2.4 (counter clockwise direction) and Table 2.5 (clockwise direction). As an example, Figs. 2.9(a) and 2.9(b) show the energy cycle behavior of a

Table 2.5: The case of clockwise traveling direction: Node visited along the path, arrival time at each node, starting energy of each node in a renewable cycle, and charging time at each node for the 50-node network.

Node Order	a_i (s)	E_i (J)	τ_i (s)	Node Order	a_i (s)	E_i (J)	τ_i (s)	Node Order	a_i (s)	E_i (J)	τ_i (s)
22	110676	5032	1166	29	116590	8449	499	19	119095	10664	29
30	111894	8032	563	37	117118	8809	425	49	119156	10615	40
6	112472	10489	63	21	117561	10593	44	5	119223	10650	33
34	112550	10741	12	25	117624	10685	25	27	119283	10558	53
40	112567	10789	2	15	117674	10747	11	1	119357	9632	254
3	112594	6301	924	23	117703	10793	2	36	119613	10160	139
11	113538	9944	176	44	117718	10605	42	50	119770	9888	199
32	113744	8461	483	2	117789	10611	41	26	119972	10754	10
35	114250	10222	120	9	117852	10613	40	31	119992	6464	957
16	114382	10734	14	13	117907	10023	167	43	120986	10606	43
45	114406	10648	31	39	118099	8588	477	48	121056	1526	2092
7	114456	10751	10	12	118601	10795	1	8	123180	7927	653
38	114508	10012	164	20	118605	10773	6	28	123868	8059	627
33	114706	4676	1287	24	118617	9668	245	46	124526	9472	305
17	116024	9197	338	10	118868	10600	43	41	124846	10637	37
47	116368	10575	47	4	118928	10339	100	42	124896	10754	11
14	116443	10286	109	18	119032	10626	38				

sensor node (the 32th node) under the two opposite traveling directions, respectively.

By Property 2.1, we find that there exists an energy bottleneck node in the network with its energy dropping to $E_{\min}$ during a renewable energy cycle. This property is confirmed in our numerical results. This bottleneck node is the 48th node, whose energy behavior is shown in Fig. 2.10.

In Section 2.5.2, we showed that minimum energy routing may not be optimal for our problem (see Remark 2.1). This point is confirmed by our numerical results. In Fig. 2.11, we show that data routing in our solution differs from the minimum energy routing for the 50-node network.

100-node Network. Table 2.6 gives the location of each node and its data rate for a 100-node network. The shortest Hamiltonian cycle is shown in Fig. 2.12. For this optimal cycle, $D_{\text{TSP}} =$

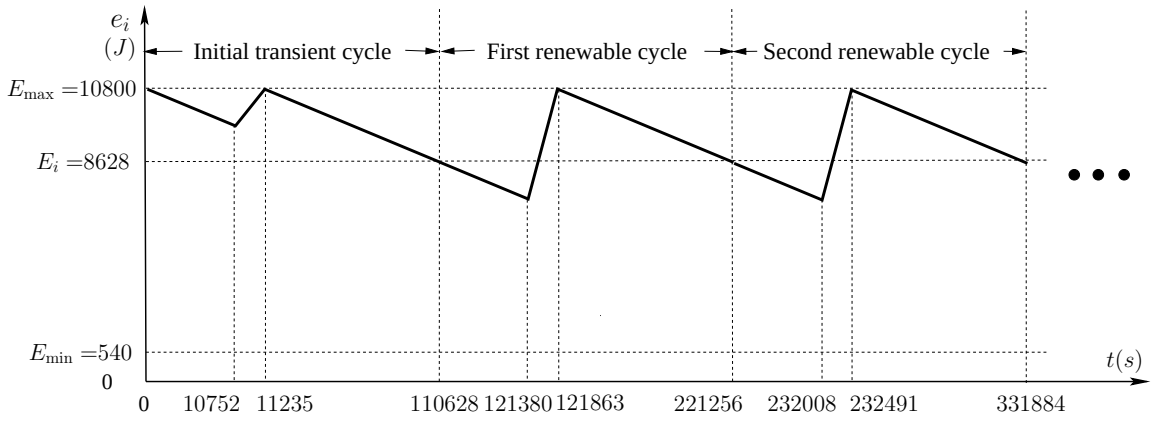

(a) Traveling direction is counter clockwise.

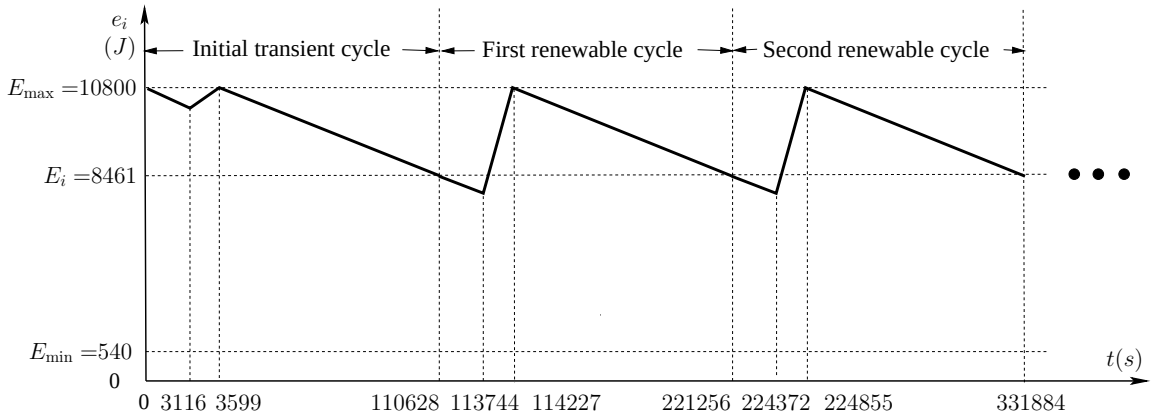

(b) Traveling direction is clockwise.

Figure 2.9: The energy behavior of a sensor node (the 32th) in the 50-node network during the initial transient cycle and the first two renewable cycles.

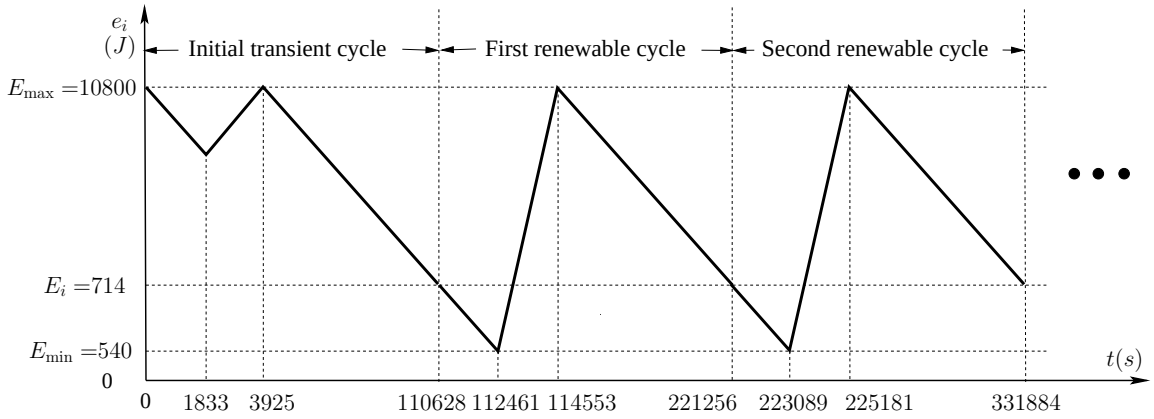

Figure 2.10: The energy behavior of the bottleneck node (48th node) in the 50-node network. Traveling direction is counter clockwise.

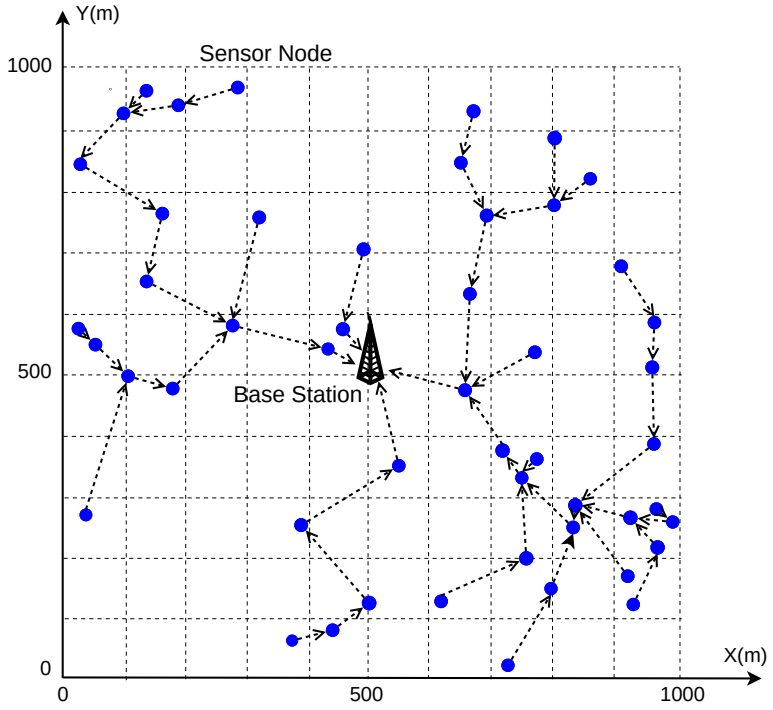

(a) Data routing in our solution.

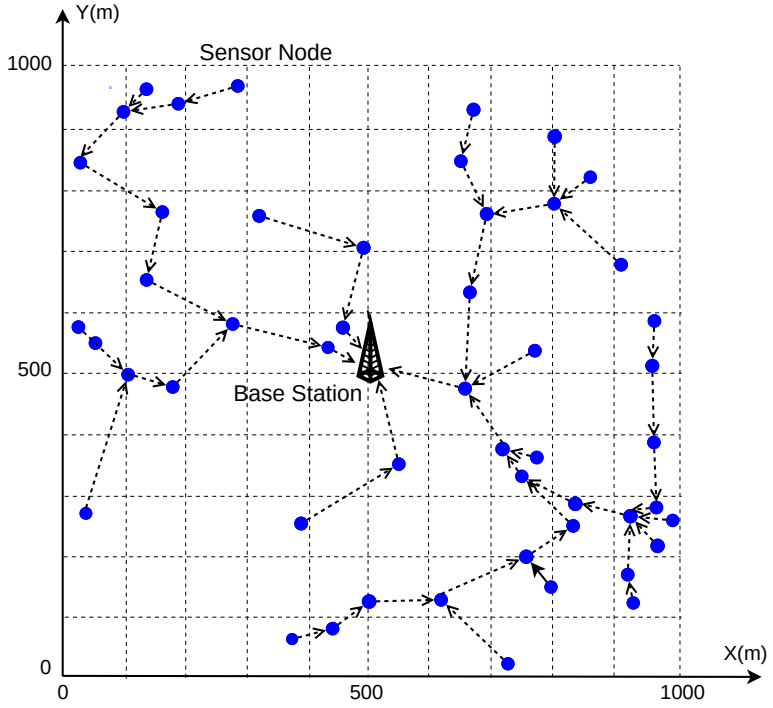

(b) Minimal energy routing.

Figure 2.11: Comparison of data routing by our solution and that by minimum energy routing for the 50-node network.

7687 m and $\tau_{\text{TSP}} = 1537.4$ s. For the target $\epsilon = 0.01$, by Theorem 2.2, we have

$$m = \left\lceil \sqrt{\frac{U\tau_{\text{TSP}}}{4\epsilon(E_{\text{max}} - E_{\text{min}})}} \right\rceil = \left\lceil \sqrt{\frac{5 \times 1537.4}{4 \times 0.01 \times (10800 - 540)}} \right\rceil = 5 \ .$$

The solution for the 100-node network includes the cycle time τ = 58.52 hours, the vacation time τ_{vac} = 50.30 hours, and the objective $\eta_{\text{vac}} = 85.95\%$. Additional results are shown in Table 2.7.

2.8 Summary

Existing WSNs have been constrained by limited battery energy at a node and thus finite lifetime is regarded as a fundamental performance bottleneck. This chapter has exploited a recent breakthrough in WET technology for a WSN and has shown that once properly designed, a WSN has the potential to remain operational forever. This is the first work that offers a systematic investigation of a sensor network operating under this new enabling energy transfer technology.

We studied a general scenario where a mobile charging vehicle periodically travels inside the network and charges each sensor node wirelessly without any plugs or wires. We introduced a new concept called renewable energy cycle and offered both necessary and sufficient conditions for renewable energy cycle. We studied a practical optimization problem with the objective of maximizing the ratio of the WCV's vacation time over the cycle time. For this problem, we proved that the optimal traveling path for the WCV in each renewable cycle is the shortest Hamiltonian cycle. Subsequently, we developed a provable near-optimal solution for flow routing, total cycle time, and individual charging time at each node. We also showed that traditional minimum energy routing cannot achieve an optimal solution. Using numerical results, we showed the detailed network behavior associated with a renewable energy cycle and demonstrated that a sensor network operating under our solution can indeed remain operational with unlimited lifetime.

Table 2.6: Location and data rate R_i for each node in a 100-node network.

Node	Location	R_i	Node	Location	R_i
1	(970, 383)	10	51	(295, 856)	7
2	(124, 85)	8	52	(306, 584)	10
3	(467, 734)	6	53	(106, 374)	8
4	(657, 332)	3	54	(594, 222)	7
5	(290, 840)	3	55	(283, 219)	10
6	(755, 372)	9	56	(155, 522)	1
7	(558, 828)	5	57	(1, 433)	3
8	(428, 177)	9	58	(284, 741)	10
9	(267, 130)	1	59	(551, 70)	8
10	(754, 880)	9	60	(871, 847)	5
11	(898, 44)	1	61	(42, 680)	7
12	(728, 687)	9	62	(905, 137)	5
13	(407, 734)	9	63	(131, 858)	4
14	(938, 437)	6	64	(834, 200)	3
15	(255, 380)	2	65	(800, 607)	4
16	(533, 980)	2	66	(918, 543)	1
17	(955, 399)	8	67	(137, 162)	5
18	(268, 440)	9	68	(505, 6)	4
19	(250, 157)	1	69	(405, 771)	10
20	(928, 326)	8	70	(174, 765)	6
21	(69, 314)	10	71	(575, 421)	9
22	(299, 895)	4	72	(606, 57)	5
23	(592, 247)	7	73	(214, 586)	5
24	(203, 311)	4	74	(520, 174)	9
25	(636, 409)	3	75	(989, 729)	10
26	(798, 708)	8	76	(490, 534)	6
27	(502, 144)	8	77	(695, 253)	10
28	(651, 871)	3	78	(411, 917)	8
29	(796, 83)	6	79	(35, 758)	6
30	(233, 462)	5	80	(293, 887)	10
31	(601, 30)	1	81	(801, 69)	9
32	(112, 753)	1	82	(347, 184)	10
33	(516, 700)	5	83	(83, 737)	7
34	(838, 215)	3	84	(511, 697)	4
35	(921, 680)	4	85	(367, 777)	5
36	(498, 557)	3	86	(739, 502)	10
37	(278, 851)	2	87	(525, 425)	1
38	(653, 559)	4	88	(805, 611)	2
39	(917, 902)	7	89	(817, 856)	5
40	(510, 420)	3	90	(189, 671)	6
41	(974, 358)	7	91	(124, 524)	1

Continued on next page

Table 2.6 – continued from previous page

Node	Location	R_i	Node	Location	R_i
42	(197, 489)	5	92	(821, 299)	7
43	(111, 256)	5	93	(638, 704)	9
44	(297, 929)	2	94	(16, 382)	2
45	(396, 467)	2	95	(896, 568)	5
46	(421, 254)	7	96	(515, 888)	3
47	(311, 431)	3	97	(545, 843)	10
48	(694, 703)	6	98	(606, 899)	7
49	(92, 402)	10	99	(760, 939)	3
50	(402, 182)	8	100	(855, 815)	2

Table 2.7: The case of clockwise traveling direction: Node visited along the path, arrival time at each node, starting energy of each node in a renewable cycle, and charging time at each node for the 100-node network.

Node	a_i (s)	E_i (J)	τ_i (s)	Node	a_i (s)	E_i (J)	τ_i (s)
67	210727	10257	109	96	227822	10722	17
43	210855	9254	310	97	227850	9391	307
21	211179	10623	35	7	228162	7595	702
94	211232	10625	35	98	228880	10638	35
57	211278	10762	8	28	228926	9893	199
49	211305	10692	22	99	229151	10762	8
53	211333	9279	306	10	229171	10075	159
24	211661	8065	551	89	229344	10726	16
15	212230	8467	471	100	229371	9797	220
47	212716	4983	1181	60	229599	10613	41
18	213906	10698	21	39	229654	10687	25
30	213935	9012	364	75	229716	10581	48
42	214308	9784	207	35	229781	9415	305
56	214526	10787	3	95	230109	10561	53
91	214534	10778	4	66	230168	10790	2
61	214574	10682	24	14	230192	10720	18
79	214614	10681	24	17	230218	10723	17
83	214649	10274	107	1	230240	10287	113
32	214762	10365	89	41	230358	10716	19
63	214873	10640	33	20	230388	8701	464
70	214926	9839	196	92	230874	7791	668
90	215141	9489	268	34	231559	10732	15
73	215427	8932	383	64	231577	9786	225
52	215828	9431	281	62	231822	10614	41
45	216139	1745	1876	11	231882	10772	6

Continued on next page

Table 2.7 – continued from previous page

Node	a_i (s)	E_i (J)	τ_i (s)	Node	a_i (s)	E_i (J)	τ_i (s)
76	218038	10737	13	81	231908	10715	19
36	218056	7075	775	29	231930	9728	239
38	218862	10152	135	72	232207	10740	13
86	219018	4116	1402	31	232226	10786	3
65	220444	8386	508	68	232249	10724	17
88	220952	9402	294	59	232281	10261	120
26	221266	9845	201	27	232419	10221	129
12	221482	10546	54	74	232556	8179	587
48	221543	10725	16	54	233160	10733	15
93	221570	9030	374	23	233180	7167	817
33	221969	1095	2072	77	234018	10563	53
84	224042	1197	2072	6	234098	6861	890
3	226126	8828	427	4	235009	6073	1075
13	226565	9705	237	25	236100	5792	1146
69	226809	10424	82	71	237259	6167	1066
85	226899	9884	199	87	238335	4268	1516
58	227115	10534	58	40	239855	10743	13
5	227193	9991	176	46	239906	10677	28
37	227372	10781	4	8	239950	10321	111
51	227380	10397	88	50	240066	10481	74
80	227473	10691	24	82	240152	10643	37
22	227499	10752	11	55	240203	9350	338
44	227517	10766	7	19	240555	10785	3
78	227547	9805	217	9	240564	10775	6
16	227791	10742	13	2	240600	10658	33

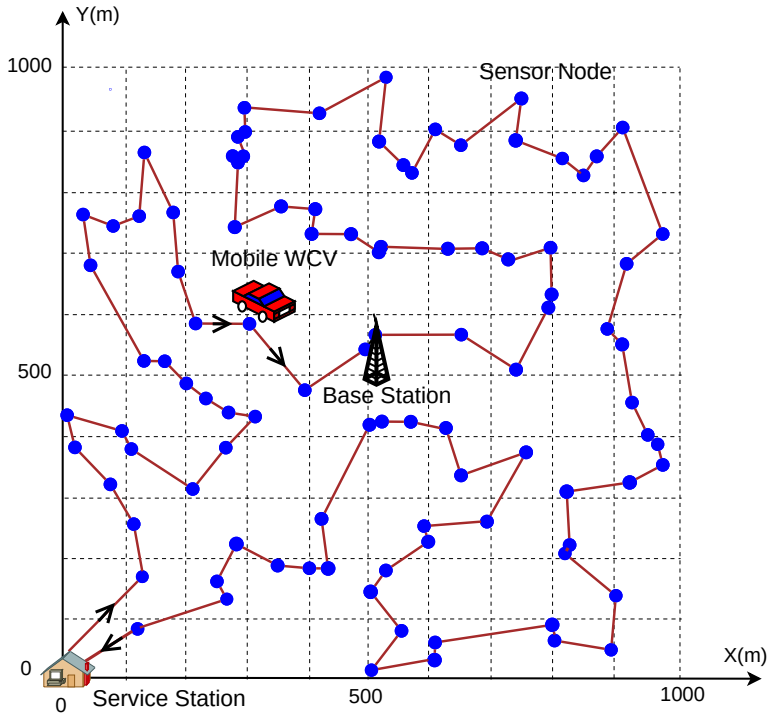

Figure 2.12: An optimal traveling path for the WCV for the 100-node sensor network, assuming traveling direction is clockwise.

Chapter 3

Multi-node Charging for a Dense Sensor Network

3.1 Introduction

In Chapter 2, we applied the MRC technology to a WSN and showed that through periodic wireless energy transfer, a WSN can remain operational forever, i.e., infinite lifetime. Specifically, we showed that by having a WCV visit each sensor node in the network and charge it periodically, one can ensure that each sensor node never runs out of energy.

An open problem in Chapter 2 is the scalability of wireless charging. That is, as the node density increases in a WSN, how can a WCV ensure that each node is charged in a timely manner before it runs out of energy? The wireless charging technology developed in [31] was limited to charging one node at a time and is not scalable as node density increases.

Kurs *et al.* also recognized this problem and recently developed an enhanced technology (by properly tuning coupled resonators) that allows energy to be transferred to *multiple* receiving nodes simultaneously [32]. Interestingly, they showed that the overall efficiency was larger when charging multiple devices than charging each device individually.

Inspired by this new advance in WET, in this chapter, we explore how such multi-node charging

technology can address the scalability problem in charging a WSN. Following the setting in Chapter 2, we consider a WCV periodically traveling inside the network and charging sensor nodes. Upon completing each trip, the WCV returns to its home service station, takes a "vacation", and starts out for its next trip. In contrast to Chapter 2, the WCV is now capable of charging multiple nodes at the same time, as long as these nodes are within its charging range. Under this setting, we ask the following fundamental question: How can such a multi-node charging technology address the scalability problem in a dense WSN?

To address this question, we propose to take a formal optimization approach. Given the limitation of a WCV's charging range, we propose a cellular structure that partitions a two-dimensional plane into hexagonal cells (similar to cellular structure for cellular telecommunications). To charge all sensor nodes in a cell, the WCV only needs to visit the center of the cell. Based on a general energy charging model, we formulate a joint optimization problem for traveling path, flow routing and charging time, with the objective of maximizing the ratio of the WCV's vacation time (time spent at its home service station) over the cycle time. We show that our optimization problem is a nonlinear program (NLP) and is NP-hard in general. By employing discretization and a novel *Reformulation-Linearization Technique* (RLT), we develop a provably near-optimal solution for any desired level of accuracy. Using numerical results, we show that our solution can indeed improve significantly upon single-node charging technology and address the charging scalability problem in a dense WSN.

The remainder of this chapter is organized as follows. In Section 3.2, we describe the mathematical model in our study. Section 3.3 presents a formulation of our optimization problem and discusses several interesting properties associated with an optimal solution. In Section 3.4, we develop a near-optimal solution, and in Section 3.5, we prove its near-optimality. In Section 3.6, we present numerical results to demonstrate our solution. Section 3.7 summarizes this chapter.

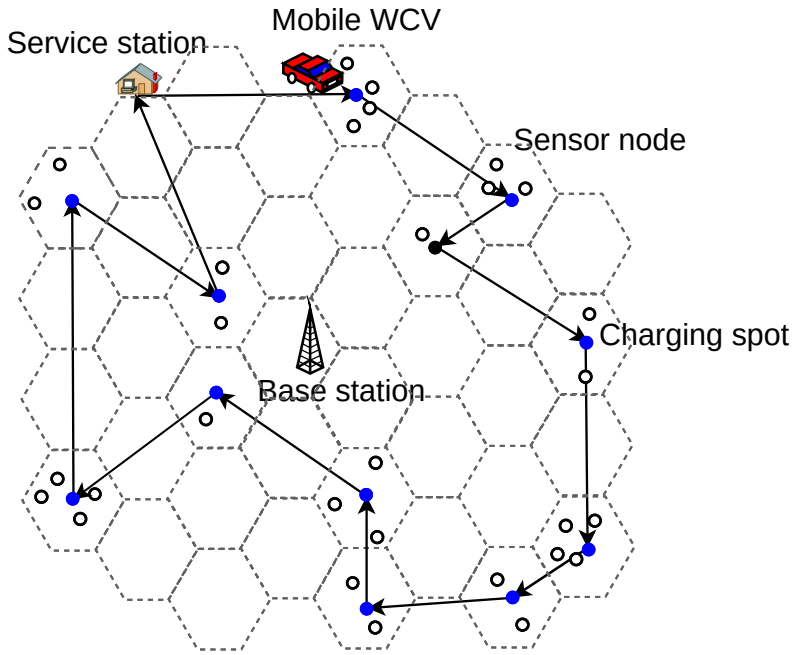

Figure 3.1: An example sensor network with a mobile WCV. Solid dots represent cell centers and empty circles represent sensor nodes.

3.2 Mathematical Modeling

3.2.1 Cellular Structure and Energy Charging Behavior

We consider a set of sensor nodes $\mathcal{N}$ distributed over a two-dimensional area. Each sensor node has a battery capacity of E_{max} and is fully charged initially. Denote E_{min} as the minimum energy at a sensor node battery for it to be operational. Each sensor node i generates sensing data with a rate R_i (in b/s), $i \in \mathcal{N}$. Within the sensor network, there is a fixed base station (B), which is the sink node for all data generated by all sensor nodes. Multi-hop data routing is employed for forwarding all data streams to the base station.

To recharge the battery at each sensor node, a mobile WCV is employed. The WCV starts at the service station (S), and travels (at a speed of V m/s) to various spots inside the network to charge batteries of sensor nodes. As discussed, the WCV can charge multiple nodes simultaneously as long as they are within its charging range, denoted as D_δ. The charging range D_δ is determined

Table 3.1: Notation in Chapter 3.

Symbol	Definition
a_k	Arrival time of the WCV at cell k in the first cycle
D_δ	WCV's charging range
D_i	Distance from node i to its cell center
D_{TSP}	The minimum traveling distance during a cycle
L	Number of points used in discretizing η_k
$\mathcal{N}_k$	The set of sensor nodes in the k-th cell
$\mathcal{Q}$	The set of cells with at least one sensor node
R_v	Energy consumption rate for carrying the WCV when the WCV is outside its service station
U_{max}	Maximum output power from the WCV to charge a single sensor node
U_i	Power reception rate at sensor node i
δ	A threshold for a sensor's power reception rate
η_k	The ratio of the charging time at cell k to the cycle time
η_{kl}	Discrete points used for discretizing η_k
π_k	The k-th cell traversed by the WCV along path $\mathcal{P}$
τ_k	The time that the WCV stays at the center of cell k
τ_{TSP}	Minimum traveling time of the WCV in a cycle
z_{kl}	A binary variable indicating whether or not η_{kl} is chosen, $k \in \mathcal{Q}, l = 0, \cdots, L$
γ_{ikl}	$\gamma_{ikl} \triangleq z_{kl} \cdot r_i$
$\mu(D_i)$	The power transfer efficiency from the WCV to a sensor node that is at a distance D_i away

by having the power reception rate at a sensor node be at least over a threshold (denoted as δ). The power reception rate at a sensor node i, denoted as U_i, is a distance-dependent parameter, and decreases with distance between itself and the WCV. When a sensor node is more than a distance of D_δ away from the WCV, we assume its power reception rate is too low to make magnetic resonant coupling work properly at the sensor node's battery. D_δ is determined by the state-of-the-art in WET research [32], which will be given in Section 3.6.

Ideally, we would like to solve a problem where the WCV can stop anywhere within the two-dimensional plane and charges sensor nodes wirelessly. However, this problem has an infinite number of possible locations, thus leading to an infinite size of search space. To make a concrete step in understanding the multi-node charging technology, we simplify the problem by introducing

a logical cellular structure and assume the WCV can only stop at the center of a cell. Specifically, we partition the two-dimensional plane with hexagonal cells with a side length of D_δ (see Fig. 3.1). Therefore, when the WCV makes a stop at the center of a cell, all sensor nodes in the cell can be charged simultaneously. We ignore the edge effect where a sensor node residing outside the cell but inside a circle with a radius of D_δ can still be charged from this cell. Note that such an omission of over-charging will not affect the feasibility of our solution.

Under the cellular structure, denote D_i the distance from node i to its cell center. Then nodes i's power reception rate is $U_i = \mu(D_i) \cdot U_{\text{max}}$, where U_{max} is the maximum output power from WCV for a single sensor node and $\mu(D_i)$ is the efficiency of WET. Note that $\mu(D_i)$ is a decreasing function of D_i and $0 \leq \mu(D_i) \leq 1$.

Under this setting, we are interested in finding out how the WCV should travel and charge from these cell centers so that (i) none of the sensor nodes runs out of energy, and (ii) some performance objective can be optimized. In the rest of this section, we present a mathematical characterization of the WCV's traveling path and cycle time (Section 3.2.2), data flow routing and energy consumption model (Section 3.2.3), and energy dynamics at a sensor node (Section 3.2.4). Table 3.1 lists notation that is used in this chapter.

3.2.2 WCV's Traveling Path and Cycle Time

Denote $\mathcal{Q}$ as the set of hexagonal cells containing at least one sensor node (see Fig. 3.2). Re-index these cells in $\mathcal{Q}$ as $k = 1, 2, \cdots, |\mathcal{Q}|$ and denote $\mathcal{N}_k$ the set of sensor nodes in the kth cell. Then $\mathcal{N} = \bigcup_{k \in \mathcal{Q}} \mathcal{N}_k$.

Denote τ_k as the time that the WCV stays at the center of cell $k \in \mathcal{Q}$. Throughout τ_k, the WCV recharges all sensor nodes within this cell simultaneously via multi-node charging technology [32]. After τ_k, the WCV leaves the current cell and travels to the next cell on its path. In our formulation, we assume that the WCV visits a cell only once during a cycle. Denote $\mathcal{P} = (\pi_0, \pi_1, \ldots, \pi_{|\mathcal{Q}|}, \pi_0)$

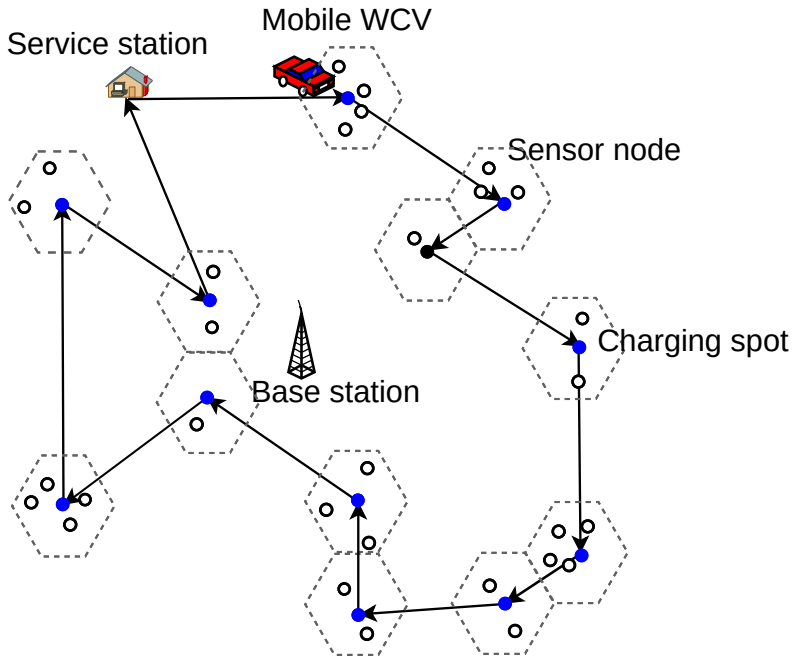

Figure 3.2: An example sensor network with a WCV. Only those cells with sensor nodes are shown in this figure.

as the physical path traversed by the WCV during a cycle, which starts from and ends at the service station (i.e., $\pi_0 = S$) and the kth cell traversed by the WCV along path $\mathcal{P}$ is π_k, $1 \leq k \leq |\mathcal{Q}|$. Denote $D_{\mathcal{P}}$ as the physical distance of path $\mathcal{P}$ and $\tau_{\mathcal{P}} = D_{\mathcal{P}}/V$ as the time spent for traveling over distance $D_{\mathcal{P}}$.

After the WCV visits the $|\mathcal{Q}|$ cells in the network, it will return to its service station to be serviced (e.g., replacing its battery, taking a vacation) and get ready for the next trip. We call this resting period *vacation time*, denoted by τ_{vac}. Denote τ as the time of a cycle spent by the WCV. Then this cycle time τ can be written as

$$\tau = \tau_{\mathcal{P}} + \tau_{\text{vac}} + \textstyle\sum_{k \in \mathcal{Q}} \tau_k \ , \tag{3.1}$$

where $\sum_{k \in \mathcal{Q}} \tau_k$ is the total amount of time the WCV spends at the $|\mathcal{Q}|$ cells for battery charging. We assume that the WCV has sufficient energy to charge all sensor nodes in a cycle.

3.2.3 Data Flow Routing and Energy Consumption

To model multi-hop data routing, denote f_{ij} and f_{iB} the flow rates from sensor node i to sensor node j and the base station B, respectively. Then we have the following flow balance constraint at each sensor node i.

$$\sum_{k\in\mathcal{N}}^{k\neq i} f_{ki} + R_i = \sum_{j\in\mathcal{N}}^{j\neq i} f_{ij} + f_{iB} \quad (i \in \mathcal{N}) \; . \tag{3.2}$$

Although both flow routing and flow rates are part of our optimization problem, we assume they do not change with time.

In this chapter, we use the following energy consumption model at each sensor node [23]. To transmit a flow rate of f_{ij} from node i to node j, the transmission power is $C_{ij} \cdot f_{ij}$, where C_{ij} is the rate of energy consumption for transmitting one unit of data rate from node i to node j, and is modeled as:

$$C_{ij} = \beta_1 + \beta_2 D_{ij}^{\alpha} \; ,$$

where D_{ij} is the distance between nodes i and j, β_1 is a distance-independent constant term, β_2 is a coefficient of the distance-dependent term and α is the path loss index. Similarly, denote C_{iB} as the rate of energy consumption for transmitting one unit of data rate from node i to the base station B. Then the aggregate energy consumption rate for transmission at node i is $\sum_{j\in\mathcal{N}}^{j\neq i} C_{ij} \cdot f_{ij} + C_{iB} \cdot f_{iB}$.

The energy consumption rate for reception at node i is modeled as $\rho \sum_{k\in\mathcal{N}}^{k\neq i} f_{ki}$, where ρ is the rate of energy consumption for receiving one unit of data rate.

Denote r_i as the energy consumption rate at sensor node $i \in \mathcal{N}$, which includes energy consumption for transmission and reception. We have,

$$r_i = \rho \sum_{k\in\mathcal{N}}^{k\neq i} f_{ki} + \sum_{j\in\mathcal{N}}^{j\neq i} C_{ij} f_{ij} + C_{iB} f_{iB} \quad (i \in \mathcal{N}) \; . \tag{3.3}$$

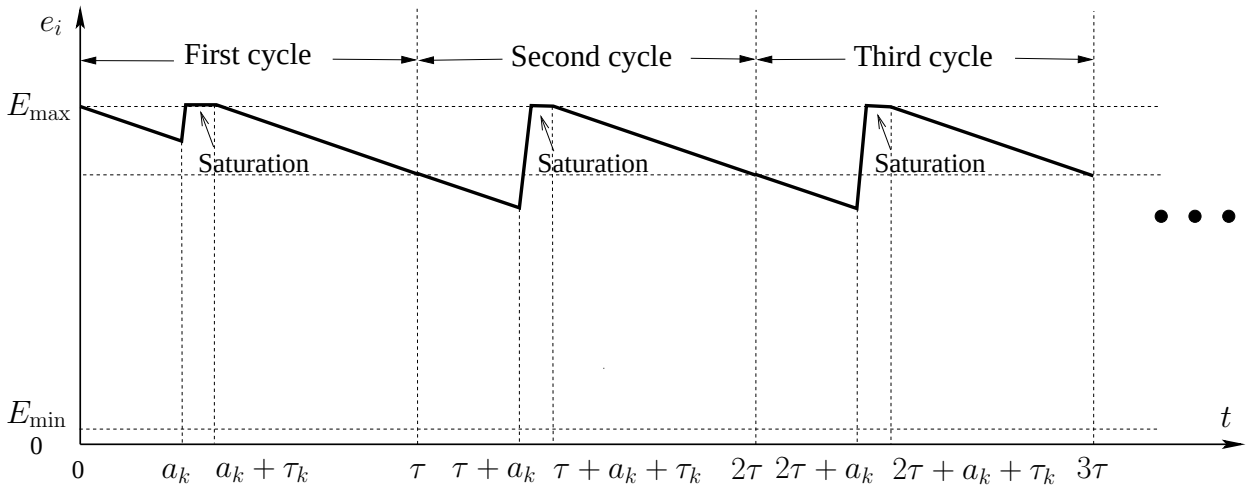

Figure 3.3: The energy level of node $i \in \mathcal{N}_k$ during the first three cycles.

3.2.4 Energy Dynamics at a Sensor Node

In Section 3.2.2, we discussed the WCV's behavior over a cycle time τ, during which the WCV starts from the service station, travels to those cells with sensor nodes, and returns to the service station (see Fig. 3.2).

Multi-Node Charging v.s. Single-Node Charging. In Chapter 2, we considered a WCV visiting each node and charging it individually. In that context, we introduced a concept called *renewable energy cycle* during which the energy level at each node exhibits a periodic behavior with a cycle time τ. Specifically, the energy level of a sensor node exhibits a renewable energy cycle if it meets the following two requirements: (i) it starts and ends with the same energy level over a period of τ; and (ii) it never falls below $E_{\min}$. A central idea in achieving a renewable energy cycle in Chapter 2 is that the amount of energy being charged to a node is equal to the amount of energy that the node expends in a cycle. However, such an idea cannot be extended to our multi-node charging context here. This is because, for each node in the same cell, its remaining energy level (when the WCV arrives at the cell) differs, so do energy charging rate and consumption rate at each node. As a result, nodes in the same cell will not complete their battery charging at the same time and those nodes that finish early will run into a "saturation" state (i.e., battery level remains at $E_{\max}$) until the

WCV departs this cell (see Fig. 3.3). Due to this "saturation" phenomenon, the idea of achieving a renewable energy cycle cannot be applied here.

Cell-based Energy Constraints. We now develop constraints to capture the saturation phenomenon while ensuring that the energy level of each node never falls below E_{min}. Denote $e_i(t)$ as node i's energy level at time t. The energy curve of node $i \in \mathcal{N}_k$ in a cell k for the first three cycles is shown in Fig. 3.3. For any cycle, we see that there can be only three possible slopes: (i) a slope of $-r_i$ when the WCV is not in node i's cell, (ii) a slope of $(U_i - r_i)$ when the WCV is at node i's cell and is charging node i at rate U_i,[1] and (iii) a slope of 0 (i.e., saturation period) when node i is already fully charged while the WCV is still in the same cell.

Denote a_k as the arrival time of the WCV at cell k in the first cycle. Denote $D_{\pi_0\pi_1}$ as the distance between the service station and the first cell visited along $\mathcal{P}$ and $D_{\pi_l\pi_{l+1}}$ as the distance between the lth and $(l+1)$th cells, respectively. Then we have

$$a_{\pi_k} \;=\; \sum_{l=0}^{k-1} \frac{D_{\pi_l\pi_{l+1}}}{V} + \sum_{l=1}^{k-1} \tau_{\pi_l}\ , k = 1, 2, \ldots, |\mathcal{Q}|.$$

Note that $e_i(m\tau + a_k)$, $m \in \mathbb{N}$, is a local minimum for $e_i(t)$. To have $e_i(t) \geq E_{\text{min}}$ for all $t \geq 0$, it is sufficient to have

$$e_i(m\tau + a_k) = e_i(m\tau) - a_k \cdot r_i \geq E_{\text{min}}$$

for all $m \in \mathbb{N}$, $i \in \mathcal{N}_k$, $k \in \mathcal{Q}$.

When $m = 0$, $e_i(a_k) = e_i(0) - a_k \cdot r_i = E_{\text{max}} - a_k \cdot r_i$. For $e_i(a_k) \geq E_{\text{min}}$, we must have

$$E_{\text{max}} - a_k \cdot r_i \geq E_{\text{min}} \quad (i \in \mathcal{N}_k, k \in \mathcal{Q})\ . \tag{3.4}$$

[1] Note that it is necessary to have $U_i \geq r_i$, for $i \in \mathcal{N}$, to achieve a feasible solution.

When $m \geq 1$,

$$\begin{aligned} e_i(m\tau + a_k) &= e_i(m\tau) - a_k \cdot r_i \\ &= e_i((m-1)\tau + a_k + \tau_k) - \{m\tau - [(m-1)\tau + a_k + \tau_k]\} \cdot r_i - a_k \cdot r_i \\ &= e_i((m-1)\tau + a_k + \tau_k) - (\tau - \tau_k) \cdot r_i \\ &\leq E_{\max} - (\tau - \tau_k) \cdot r_i \ , \end{aligned} \tag{3.5}$$

where the last inequality holds since e_i cannot exceed $E_{\max}$. For (3.5), if $e_i(m\tau + a_k) \geq E_{\min}$ for all $m \geq 1$, then we must have

$$E_{\max} - (\tau - \tau_k) \cdot r_i \geq E_{\min} \quad (i \in \mathcal{N}_k, k \in \mathcal{Q}) \ . \tag{3.6}$$

Now we show that once (3.6) holds, (3.4) must also hold. Therefore, we can remove (3.4) in the formulation. To see this, we have $a_k + \tau_k < \tau$, which leads to $E_{\max} - a_k \cdot r_i > E_{\max} - (\tau - \tau_k) \cdot r_i$.

Note that (3.6) is a necessary condition for $e_i(t) \geq E_{\min}$. The following is a second necessary condition for $e_i(t) \geq E_{\min}$:

$$\tau \cdot r_i - U_i \cdot \tau_k \leq 0 \quad (i \in \mathcal{N}_k, k \in \mathcal{Q}) \ , \tag{3.7}$$

which says that $U_i \cdot \tau_k$, the amount of energy being charged to node $i \in \mathcal{N}_k$ during the time period of τ_k, must be greater than or equal to $\tau \cdot r_i$, the amount of energy consumed during the cycle. (3.7) can be easily proved by showing that if $\tau \cdot r_i - U_i \cdot \tau_k > 0$, then $e_i(t)$ will fall below $E_{\min}$ eventually at some time t.

We have shown that (3.6) and (3.7) are necessary conditions for $e_i(t) \geq E_{\min}$. It turns out that they are also sufficient conditions. We state this result in the following lemma.

Lemma 3.1 *$e_i(t) \geq E_{min}$ for all $t \geq 0$, $i \in \mathcal{N}$, if and only if both the constraints (3.6) and (3.7) are satisfied.*

Proof The "only if" part of the lemma (i.e., (3.6) and (3.7) are necessary conditions) was already

proved in earlier discussion. We now prove the "if" part of the lemma, i.e., if (3.6) and (3.7) hold, then $e_i(t) \geq E_{\min}$ for all $t \geq 0$, $i \in \mathcal{N}$.

Recall that, to have $e_i(t) \geq E_{\min}$, $i \in \mathcal{N}$, it is sufficient to have $e_i(m\tau + a_k) \geq E_{\min}$, for $m \in \mathbb{N}$, $i \in \mathcal{N}$. We consider $e_i(a_k)$ and $e_i(m\tau + a_k)$ for $m \geq 1$, respectively. The first cycle (i.e., $m = 0$) is solely considered since it starts with $E_{\max}$, and the succeeding cycle (i.e., $m \geq 1$) starts with a non-full energy level. Note that for all cycles, the traveling path $\mathcal{P}$, time intervals τ, $\tau_{\mathcal{P}}$, τ_{vac}, and τ_k, the flow rates f_{ij} and f_{iB}, and power consumption r_i are identical.

When $m = 0$, we show that $e_i(a_k) \geq E_{\min}$. We see that

$$\begin{aligned} e_i(a_k) &= e_i(0) - r_i \cdot a_k = E_{\max} - r_i \cdot a_k \\ &> E_{\max} - r_i \cdot (\tau - \tau_k) \geq E_{\min} \quad (i \in \mathcal{N}) \,, \end{aligned}$$

where the second equality holds due to $e_i(0) = E_{\max}$, the third inequality holds due to $a_k + \tau_k < \tau$, and the last inequality holds due to (3.6). That is, each sensor has sufficient energy to support itself until the WCV's first arrival.

Now we show $e_i(m\tau + a_k)$, $m \geq 1$. It is sufficient to show $e_i(\tau + a_k) \geq E_{\min}$ and $e_i(2\tau) = e_i(\tau)$. It follows that $e_i(m\tau + a_k) \geq E_{\min}$ for all $m \geq 1$ due to periodicity.

To show $e_i(\tau + a_k) \geq E_{\min}$, we have

$$\begin{aligned} e_i(\tau + a_k) &= e_i(a_k + \tau_k) - [(\tau + a_k) - (a_k + \tau_k)] \cdot r_i \\ &= e_i(a_k + \tau_k) - (\tau - \tau_k) \cdot r_i \,, \end{aligned}$$

where $e_i(a_k + \tau_k) = \min\left\{e_i(a_k) + (U_i - r_i) \cdot \tau_k, E_{\max}\right\}$ considering that node $i \in \mathcal{N}_k$ may be under saturation state during $[a_k, a_k + \tau_k]$. We find that

$$\begin{aligned} e_i(a_k) + (U_i - r_i) \cdot \tau_k = e_i(0) - a_k \cdot r_i + (U_i - r_i) \cdot \tau_k &= E_{\max} - (a_k + \tau_k) \cdot r_i + U_i \cdot \tau_k \\ &> E_{\max} - \tau \cdot r_i + U_i \cdot \tau_k \geq E_{\max} \,, \end{aligned}$$

where the second equality holds due to $e_i(0) = E_{\text{max}}$, the third inequality holds due to $a_k + \tau_k < \tau$, and the last inequality holds due to (3.7). We then have

$$e_i(a_k + \tau_k) = E_{\text{max}} \ , \tag{3.8}$$

Therefore,

$$\begin{aligned} e_i(\tau + a_k) &= e_i(a_k + \tau_k) - (\tau - \tau_k) \cdot r_i \\ &= E_{\text{max}} - (\tau - \tau_k) \cdot r_i \\ &\geq E_{\text{min}} \ , \end{aligned} \tag{3.9}$$

where the last inequality holds by (3.6).

We also show that $e_i(2\tau) = e_i(\tau)$. We find that

$$\begin{aligned} e_i(\tau) &= e_i(a_k + \tau_k) - (\tau - a_k - \tau_k) \cdot r_i \\ &= E_{\text{max}} - (\tau - a_k - \tau_k) \cdot r_i \ , \end{aligned} \tag{3.10}$$

where the second equality holds by (3.8). We also have

$$\begin{aligned} e_i(2\tau) &= e_i(\tau + a_k + \tau_k) - [2\tau - (\tau + a_k + \tau_k)] \cdot r_i \\ &= e_i(\tau + a_k + \tau_k) - (\tau - a_k - \tau_k) \cdot r_i \ , \end{aligned}$$

where $e_i(\tau + a_k + \tau_k) = \min\{e_i(\tau + a_k) + (U_i - r_i) \cdot \tau_k, E_{\text{max}}\}$. It follows that

$$\begin{aligned} & e_i(\tau + a_k) + (U_i - r_i) \cdot \tau_k \\ = \ & E_{\text{max}} - (\tau - \tau_k) \cdot r_i + (U_i - r_i) \cdot \tau_k \\ = \ & E_{\text{max}} - \tau \cdot r_i + U_i \cdot \tau_k \\ \geq \ & E_{\text{max}} \ , \end{aligned}$$

where the first equality holds by (3.9), and the last inequality holds due to (3.7). We then have

$$e_i(\tau + a_k + \tau_k) = E_{\text{max}} \ , \tag{3.11}$$

and it follows that

$$\begin{aligned} e_i(2\tau) &= e_i(\tau + a_k + \tau_k) - (\tau - a_k - \tau_k) \cdot r_i \\ &= E_{\text{max}} - (\tau - a_k - \tau_k) \cdot r_i \\ &= e_i(\tau) \ , \end{aligned}$$

where the second equality holds by (3.11), and the last equality holds by (3.10).

Therefore, if both constraints (3.6) and (3.7) are satisfied, $e_i(t) \geq E_{\text{min}}$ for all $t \geq 0$, $i \in \mathcal{N}$. □

The following corollary follows from the proof of Lemma 3.1.

Corollary 3.1.1 *When the WCV departs cell k, $k \in \mathcal{Q}$, each sensor node $i \in \mathcal{N}_k$ is fully charged to E_{max}.*

3.3 Problem Formulation and Properties

Based on the constraints that we have discussed in Section 3.2, we consider optimizing some global performance objective. In particular, we would like to minimize the rate of energy consumption for the entire system, which encompasses all energy consumption at the WCV as follows:[2]

- The energy consumption rate for carrying the WCV to move along $\mathcal{P}$ during τ is

$$\frac{R_v \cdot \left[\tau_{\mathcal{P}} + \sum_{k \in \mathcal{Q}} \tau_k\right]}{\tau} \ , \tag{3.12}$$

[2]Note that except their initial energy, the energy consumed in the WSN comes from the WCV.

where $\tau_{\mathcal{P}} + \sum_{k \in \mathcal{Q}} \tau_k$ is the time that the WCV is at work during τ (i.e., outside its service station), and R_v denotes the energy consumption rate for carrying the WCV in this period. Note that the energy consumed at the WCV when it makes stops along $\mathcal{P}$ should be included as the vehicle's engine is still on.

- The rate of energy transferred from the WCV to the sensor nodes in the network is at most $\frac{\sum_{i \in \mathcal{N}} r_i}{\delta / U_{\max}}$, where $\sum_{i \in \mathcal{N}} r_i$ is the sum of energy consumption rates at the sensor nodes, and $\delta / U_{\max}$ is the minimum efficiency for effective wireless charging.[3]

To date, the most fuel-efficient vehicle has an energy consumption of 17.4 kW-h per 100 km [61], which indicates that R_v is on the order of 1 kW. In contrast, the rate of energy transferred to sensor nodes is roughly on the order of 0.1 to 1 W (see Section 3.6). Since the energy consumed to carry the WCV is the dominant source of energy consumption, we only need to consider this dominant part, i.e., minimizing (3.12). Since R_v is a constant factor, we can remove it from the objective function.

It is interesting that, by (3.1), minimizing $\frac{\tau_{\mathcal{P}} + \sum_{k \in \mathcal{Q}} \tau_k}{\tau}$ is equivalent to maximizing $\frac{\tau_{\text{vac}}}{\tau}$, which is the percentage of time that the WCV is on vacation at its service station. This is intuitive. Mathematically, this is a very challenging objective, as it involves a ratio of two variables. Therefore, a successful solution to this optimization problem will help pave the way to solve many other optimization problems with simpler objectives.

We now summarize our optimization problem as follows.

$$
\begin{array}{ll}
\text{maximize} & \frac{\tau_{\text{vac}}}{\tau} \\
\text{subject to} & \text{Time constraint: (3.1);} \\
& \text{Flow routing constraints: (3.2);} \\
& \text{Energy consumption model: (3.3);} \\
& \text{Cell-based energy constraints: (3.6), (3.7);} \\
& \tau, \tau_{\mathcal{P}}, \tau_{\text{vac}}, \tau_k, f_{ij}, f_{iB} \geq 0 \quad (i, j \in \mathcal{N}, i \neq j); \\
& 0 \leq r_i \leq U_i \quad (i \in \mathcal{N}) \, .
\end{array}
$$

[3] From experimental results in [32], the ratio of δ to $U_{\max}$ can be set as 20% (see Section 3.6).

In this problem, time intervals τ, $\tau_{\mathcal{P}}$, τ_{vac} and τ_k, flow rates f_{ij} and f_{iB}, and power consumption rate r_i are optimization variables; R_i, ρ, C_{ij}, C_{iB}, U_i, E_{max}, and E_{min} are constants. Note that $\tau_{\mathcal{P}}$ can be determined once the traveling path $\mathcal{P}$ is determined.

This problem is a nonlinear program (NLP), with nonlinear objective ($\frac{\tau_{\text{vac}}}{\tau}$) and nonlinear terms ($\tau \cdot r_i$ and $\tau_k \cdot r_i$) in Constraints (3.6) and (3.7). An NLP is NP-hard in general. Nevertheless, we can still find several useful properties associated with an optimal solution.

Property 3.1 *In an optimal solution with the maximal $\frac{\tau_{\text{vac}}}{\tau}$, the WCV must move along the shortest Hamiltonian cycle that connects the service station and the centers of cells $k \in \mathcal{Q}$. If the shortest Hamiltonian cycle is not unique, then any shortest Hamiltonian cycle can achieve the same optimal objective. Further, the WCV can follow either clockwise or counterclockwise direction of the shortest Hamiltonian cycle, both of which will achieve the same optimal objective.*

A proof of this property can be developed based on contradiction. That is, if there is an optimal solution where the WCV does not move along the shortest Hamiltonian cycle, then we can construct a new solution with the WCV moving along the shortest Hamiltonian cycle and with an improved objective. Since it shares a similar idea to a proof in Chapter 2, we omit it here to conserve space.

The shortest Hamiltonian cycle can be obtained by solving the well known Traveling Salesman Problem (TSP) [4, 10]. Denote D_{TSP} as the total path distance for the shortest Hamiltonian cycle and $\tau_{\text{TSP}} = D_{\text{TSP}}/V$. Then (3.1) becomes

$$\tau - \textstyle\sum_{k\in\mathcal{Q}} \tau_k - \tau_{\text{vac}} = \tau_{\text{TSP}} \ . \tag{3.13}$$

The solution to our problem becomes $\varphi = (\mathcal{P}_{\text{TSP}}, \tau, \tau_{\text{TSP}}, \tau_{\text{vac}}, \tau_k, f_{ij}, f_{iB}, r_i)$. Since the optimal traveling path is determined, we simplify the notation for φ as $\varphi = (\tau, \tau_{\text{vac}}, \tau_k, f_{ij}, f_{iB}, r_i)$.

For (3.13), we divide both sides by τ and have $1 - \sum_{k\in\mathcal{Q}} \frac{\tau_k}{\tau} - \frac{\tau_{\text{vac}}}{\tau} = \tau_{\text{TSP}} \cdot \frac{1}{\tau}$. We define $\eta_{\text{vac}} = \frac{\tau_{\text{vac}}}{\tau}$, where η_{vac} represents the ratio of the vacation time to the entire cycle time, and is our objective function in the optimization problem. Similarly, we define $\eta_k = \frac{\tau_k}{\tau}$, for $k \in \mathcal{Q}$, and $h = \frac{1}{\tau}$, where

η_k represents the ratio of the charging time at cell k to the entire cycle time. Then (3.13) is written as $1 - \sum_{k\in\mathcal{Q}} \eta_k - \eta_{\text{vac}} = \tau_{\text{TSP}} \cdot h$, or equivalently, $h = \frac{1-\sum_{k\in\mathcal{Q}} \eta_k - \eta_{\text{vac}}}{\tau_{\text{TSP}}}$.

Similarly, by dividing both sides by τ, replacing $\frac{\tau_k}{\tau}$ with η_k, and replacing $\frac{1}{\tau}$ with $\frac{1-\sum_{k\in\mathcal{Q}} \eta_k - \eta_{\text{vac}}}{\tau_{\text{TSP}}}$, (3.6) and (3.7) can be reformulated as:

$$\begin{aligned} (1-\eta_k)\cdot r_i \le (E_{\text{max}} - E_{\text{min}}) \cdot \tfrac{1-\sum_{j\in\mathcal{Q}} \eta_j - \eta_{\text{vac}}}{\tau_{\text{TSP}}} \quad & (i \in \mathcal{N}_k, k \in \mathcal{Q}) \,, \\ r_i - U_i \cdot \eta_k \le 0 \quad & (i \in \mathcal{N}_k, k \in \mathcal{Q}) \,. \end{aligned} \tag{3.14}$$

We can rewrite (3.14) as:

$$\eta_{\text{vac}} \le 1 - \sum_{j\in\mathcal{Q}} \eta_j - \frac{\tau_{\text{TSP}}}{E_{\text{max}} - E_{\text{min}}}(1-\eta_k)\cdot r_i \quad (i \in \mathcal{N}_k, k \in \mathcal{Q}).$$

Now the Multi-node Charging Problem (MCP) is reformulated as follows:

MCP

$$\begin{aligned} \text{maximize} \quad & \eta_{\text{vac}} \\ \text{subject to} \quad & \textstyle\sum_{j\in\mathcal{N}}^{j\neq i} f_{ij} + f_{iB} - \sum_{k\in\mathcal{N}}^{k\neq i} f_{ki} = R_i \quad (i \in \mathcal{N}) \\ & \rho \cdot \textstyle\sum_{k\in\mathcal{N}}^{k\neq i} f_{ki} + \sum_{j\in\mathcal{N}}^{j\neq i} C_{ij}\cdot f_{ij} + C_{iB}\cdot f_{iB} - r_i = 0 \quad (i \in \mathcal{N}) \\ & \eta_{\text{vac}} \le 1 - \textstyle\sum_{j\in\mathcal{Q}} \eta_j - \frac{\tau_{\text{TSP}}}{E_{\text{max}} - E_{\text{min}}}(1-\eta_k)\cdot r_i \quad (i \in \mathcal{N}_k, k \in \mathcal{Q}) \quad (3.15) \\ & r_i - U_i \cdot \eta_k \le 0 \quad (i \in \mathcal{N}_k, k \in \mathcal{Q}) \quad (3.16) \\ & f_{ij}, f_{iB} \ge 0, 0 \le r_i \le U_i, 0 \le \eta_k, \eta_{\text{vac}} \le 1 \quad (i, j \in \mathcal{N}, i \neq j) \,. \end{aligned}$$

In this problem, f_{ij}, f_{iB}, r_i, η_{vac}, and η_k are optimization variables; R_i, ρ, C_{ij}, C_{iB}, U_i, E_{max}, E_{min} and τ_{TSP} are constants. Once we obtain a solution to Problem MCP, we can recover τ, τ_k, and τ_{vac}

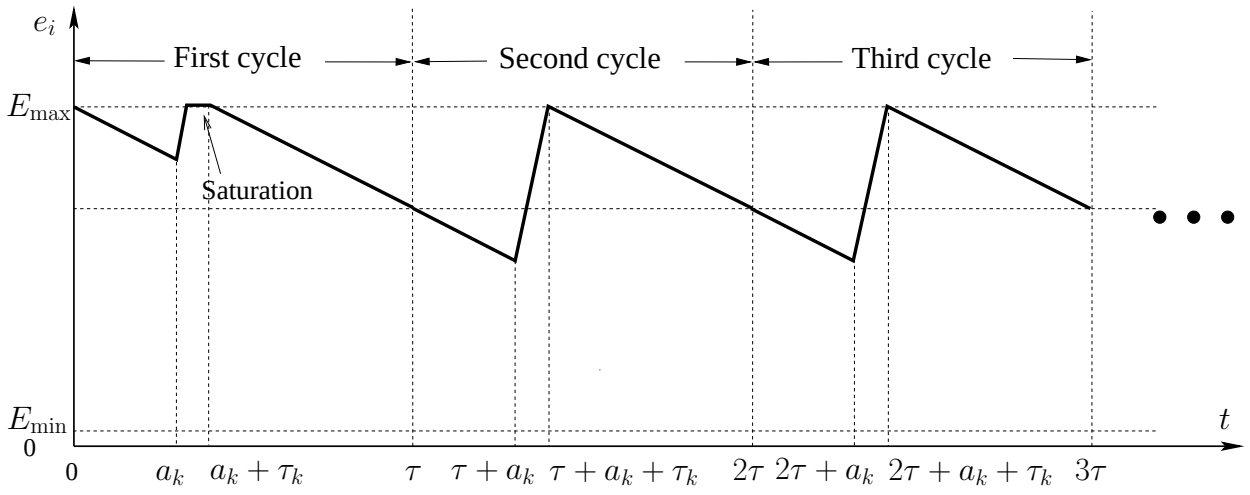

Figure 3.4: The energy level of an equilibrium node $i \in \mathcal{N}_k$ in the first three cycles.

as follows:

$$\tau = \frac{\tau_{\text{TSP}}}{1 - \sum_{k \in \mathcal{Q}} \eta_k - \eta_{\text{vac}}} , \tag{3.17}$$

$$\tau_k = \tau \cdot \eta_k , \tag{3.18}$$

$$\tau_{\text{vac}} = \tau \cdot \eta_{\text{vac}} . \tag{3.19}$$

In an optimal solution to MCP, we shows that there exists at least one *bottleneck node*, which is defined as the node whose energy level drops exactly to E_{min} upon WCV's arrival.

Property 3.2 *In an optimal solution to MCP, there exists at least one bottleneck node in the network.*

Proof The proof is based on contradiction. Suppose there exists an optimal solution $\varphi^* = (\tau^*, \tau^*_{\text{vac}}, \tau^*_k, f^*_{ij}, f^*_{iB}, r^*_i)$, where none of the nodes in the network has its energy level ever drops to E_{min}, i.e., $e^*_i(\tau^* + a^*_k) > E_{\text{min}}$ for all $i \in \mathcal{N}$. Then we can construct a new solution $\hat{\varphi} = (\hat{\tau}, \hat{\tau}_{\text{vac}}, \hat{\tau}_k, \hat{f}_{ij}, \hat{f}_{iB}, \hat{r}_i)$ by choosing $\gamma = \min_{i \in \mathcal{N}_k, k \in \mathcal{Q}} \{ \frac{E_{\text{max}} - E_{\text{min}}}{(\tau^* - \tau^*_k) p^*_i} \} - 1$ and letting $\hat{\tau} = (1 + \gamma)\tau^*$, $\hat{\tau}_k = (1 + \gamma)\tau^*_k$, $\hat{\tau}_{\text{vac}} = \tau^*_{\text{vac}} + \gamma(\tau^* - \sum_{k \in \mathcal{Q}} \tau^*_k)$, $\hat{f}_{ij} = f^*_{ij}$, $\hat{f}_{iB} = f^*_{iB}$, and $\hat{r}_i = p^*_i$.

Now we show $\gamma > 0$. Since $e_i^*(\tau^* + a_k^*) > E_{\min}$ for all $i \in \mathcal{N}$, we have $e_i^*(\tau^* + a_k^*) = E_{\max} - (\tau^* - \tau_k^*)p_i^* > E_{\min}$ for all $i \in \mathcal{N}$, i.e., $\min_{i\in\mathcal{N}_k, k\in\mathcal{Q}}\{E_{\max} - (\tau^* - \tau_k^*)p_i^*\} > E_{\min}$. It follows $E_{\max} - \max_{i\in\mathcal{N}_k, k\in\mathcal{Q}}\{(\tau^* - \tau_k^*)p_i^*\} > E_{\min}$, or $\frac{E_{\max}-E_{\min}}{\max_{i\in\mathcal{N}_k, k\in\mathcal{Q}}\{(\tau^*-\tau_k^*)p_i^*\}} > 1$. Thus, $\gamma = \min_{i\in\mathcal{N}_k, k\in\mathcal{Q}}\{\frac{E_{\max}-E_{\min}}{(\tau^*-\tau_k^*)p_i^*}\} - 1 = \frac{E_{\max}-E_{\min}}{\max_{i\in\mathcal{N}_k, k\in\mathcal{Q}}\{(\tau^*-\tau_k^*)p_i^*\}} - 1 > 0$.

The feasibility of $\hat{\varphi}$ can be verified similarly as that in the proof of Property 3.3. We now show that this new feasible solution $\hat{\varphi}$ can offer a better (increased) objective value. By (3.13), we have $\frac{\hat{\tau}_{\text{vac}}}{\hat{\tau}} = 1 - \frac{\hat{\tau}_{\mathcal{P}}}{\hat{\tau}} - \frac{\sum_{k\in\mathcal{Q}}\hat{\tau}_k}{\hat{\tau}}$. Since $\hat{\tau} = (1+\gamma)\tau^*$, $\hat{\tau}_k = (1+\gamma)\tau_k^*$, $\hat{\tau}_{\hat{\mathcal{P}}} = \tau_{\mathcal{P}}^*$, it follows that $\frac{\hat{\tau}_{\text{vac}}}{\hat{\tau}} = 1 - \frac{\tau_{\mathcal{P}}^*}{(1+\gamma)\tau^*} - \frac{\sum_{k\in\mathcal{Q}}(1+\gamma)\tau_k^*}{(1+\gamma)\tau^*} > 1 - \frac{\tau_{\mathcal{P}}^*}{\tau^*} - \frac{\sum_{k\in\mathcal{Q}}\tau_k^*}{\tau^*} = \frac{\tau_{\text{vac}}^*}{\tau^*}$, i.e., $\frac{\hat{\tau}_{\text{vac}}}{\hat{\tau}} > \frac{\tau_{\text{vac}}^*}{\tau^*}$. This contradicts the assumption that φ^* is an optimal solution. The proof is complete. □

Based on Corollary 3.1.1, we know that when the WCV departs a cell k, $k \in \mathcal{Q}$, each sensor node in this cell is fully charged to $E_{\max}$. Further, some nodes may experience saturation state during each cycle. The following property says that in an optimal solution, at least one sensor node in each cell $k \in \mathcal{Q}$ will have saturation-free cycles except its initial first cycle (see Fig. 3.4).

Property 3.3 *In an optimal solution to MCP, there exists at least one node in each cell $k \in \mathcal{Q}$ such that, starting from the second cycle, the amount of energy reception at the node is the same as the amount of energy consumption in the cycle.*

We call the node in Property 3.3 as *equilibrium node.* Note that the definition of equilibrium node is different from the bottleneck node. The proof of Property 3.3 is given as follows.

Proof The proof is based on contradiction. Suppose there exists an optimal solution $\varphi = (f_{ij}, f_{iB}, r_i, \eta_{\text{vac}}, \eta_k)$ to Problem MCP, where there is no equilibrium node in some cell $k \in \mathcal{Q}$, i.e., $r_i - U_i \cdot \eta_k < 0$ for all $i \in \mathcal{N}_k$. Let $\mathcal{Q}_{\text{nb}} = \{k | r_i - U_i \cdot \eta_k < 0, i \in \mathcal{N}_k\}$ be the set of these cells. We show how to construct a new solution $\hat{\varphi}$ with a better objective value, thus leading to contradiction.

Define $\hat{\varphi} = (\hat{f}_{ij}, \hat{f}_{iB}, \hat{r}_i, \hat{\eta}_{\text{vac}}, \hat{\eta}_k)$ by letting

$$\hat{f}_{ij} = f_{ij}, \quad \hat{f}_{iB} = f_{iB}, \quad \hat{r}_i = r_i \ , \tag{3.20}$$

$$\hat{\eta}_k = \begin{cases} \eta_k, & \text{if } k \notin \mathcal{Q}_{\text{nb}} \ , \\ \frac{\max\{r_i | i \in \mathcal{N}_k\}}{U_i}, & \text{if } k \in \mathcal{Q}_{\text{nb}} \ , \end{cases} \tag{3.21}$$

$$\hat{\eta}_{\text{vac}} = \ \min_{i \in \mathcal{N}_k, k \in \mathcal{Q}} \left\{ 1 - \sum_{j \in \mathcal{Q}} \hat{\eta}_j - \frac{\tau_{\text{TSP}}}{E_{\text{max}} - E_{\text{min}}} (1 - \hat{\eta}_k) \cdot \hat{r}_i \right\} . \tag{3.22}$$

Now we show that $\hat{\varphi}$ is feasible to Problem MCP. By feasibility, we mean that it meets the flow conservation constraint (3.2), and the energy constraints (3.3), (3.15), (3.16). Since φ is a feasible solution, it satisfies (3.2), (3.3), (3.15), and (3.16). By (3.20), $\hat{\varphi}$ also satisfies Constraints (3.2) and (3.3). Constraints (3.15) can be verified directly from (3.22). Now we consider Constraint (3.16), which can be easily verified for $k \notin \mathcal{Q}_{\text{nb}}$ due to $\hat{r}_i = r_i$ and (3.21). For $k \in \mathcal{Q}_{\text{nb}}$, $\hat{r}_i - U_i \cdot \hat{\eta}_k = r_i - \max\{r_j | j \in \mathcal{N}_k\} \leq 0$, where the equality holds due to $\hat{r}_i = r_i$ and (3.21). Therefore, $\hat{\varphi}$ is feasible to Problem MCP.

We now show that this new feasible solution $\hat{\varphi}$ can offer a better (increased) objective value, i.e., $\hat{\eta}_{\text{vac}} > \eta_{\text{vac}}$. Let $g(\eta_1, \eta_2, ..., \eta_{|\mathcal{Q}|}) = 1 - \sum_{j \in \mathcal{Q}} \eta_j - \frac{\tau_{\text{TSP}}}{E_{\text{max}} - E_{\text{min}}} \cdot \max_{i \in \mathcal{N}_k, k \in \mathcal{Q}} \{(1 - \eta_k) \cdot r_i\}$, and assume that $q \in \mathcal{Q}$ is a particular cell such that $(1 - \eta_q) \cdot \max_{i \in \mathcal{N}_q} \{r_i\} = \max_{i \in \mathcal{N}_k, k \in \mathcal{Q}} \{(1 - \eta_k) \cdot r_i\}$. Then we have

$$\frac{\partial g(\cdot)}{\partial \eta_k} = \begin{cases} -1 + \frac{\tau_{\text{TSP}}}{E_{\text{max}} - E_{\text{min}}} \cdot \max_{i \in \mathcal{N}_q} \{r_i\}, & \text{if } k = q \ , \\ -1, & \text{otherwise} \ . \end{cases}$$

We show $g(\cdot)$ is a decreasing function of variables η_k for $k \in \mathcal{Q}$. It is sufficient to show that $\frac{\partial g(\cdot)}{\partial \eta_k} < 0$ for $k \in \mathcal{Q}$. Clearly, we only need to consider the case of $k = q$. We see $\tau_{\text{TSP}} \cdot r_i < (\tau - \tau_k) \cdot r_i \leq E_{\text{max}} - E_{\text{min}}$, $i \in \mathcal{N}$, where the first inequality holds due to $\tau_{\text{TSP}} + \tau_k < \tau$, and the second inequality due to (3.6) (which is a reformulation reversely from (3.15)). We have $\frac{\tau_{\text{TSP}}}{E_{\text{max}} - E_{\text{min}}} \cdot \max_{i \in \mathcal{N}_q} \{r_i\} < 1$, or $\frac{\partial g(\cdot)}{\partial \eta_k} < 0$ for the case of $k = q$.

Now we are ready to show $\hat{\eta}_{\text{vac}} > \eta_{\text{vac}}$. For $k \in \mathcal{Q}_{\text{nb}}$, we have $\hat{\eta}_k = \frac{\max\{r_i | i \in \mathcal{N}_k\}}{U_i} < \eta_k$, where the equality holds by (3.21) and the inequality holds by the definition of $\mathcal{Q}_{\text{nb}}$. By (3.21), $\hat{\eta}_k = \eta_k$ for $k \notin \mathcal{Q}_{\text{nb}}$. Since $g(\cdot)$ is a decreasing function of variables η_k and $\mathcal{Q}_{\text{nb}} \neq \emptyset$, we have $g(\hat{\eta}_1, \hat{\eta}_2, ..., \hat{\eta}_{|\mathcal{Q}|}) > g(\eta_1, \eta_2, ..., \eta_{|\mathcal{Q}|})$. Therefore, $\hat{\eta}_{\text{vac}} = g(\hat{\eta}_1, \hat{\eta}_2, ..., \hat{\eta}_{|\mathcal{Q}|}) > g(\eta_1, \eta_2, ..., \eta_{|\mathcal{Q}|}) \geq \eta_{\text{vac}}$, where the equality holds due to (3.22), and the last inequality holds since φ satisfies (3.15). This contradicts the assumption that φ is an optimal solution. Therefore, there exists at least one equilibrium node in any hexagonal cell $k \in \mathcal{Q}$ in an optimal solution. This completes the proof. □

3.4 A Near-Optimal Solution

3.4.1 Approach

Problem MCP is a nonlinear program (NLP), with bilinear terms ($\eta_k \cdot r_i$) in Constraints (3.15). This nonlinear (bilinear) program is nonconvex [15], and cannot be solved by existing off-the-shelf solvers.

A natural analytical approach is to employ branch-and-bound algorithm [22, 41, 60]. Although branch-and-bound algorithms are able to address general nonlinear optimization problems, their performance highly depend on tightness of relaxations at each branching node and requires careful algorithm design. Specifically, common relaxations includes linear relaxation ([8, 14, 54]) and piecewise linear relaxation via bivariate partitioning of variables [13]. A poor relaxation, however, may yield loose bounds and thus slow down the convergence of the algorithm.

Another approach is to convert the NLP to a mixed-integer linear program (MILP), which can then be solved efficiently by an off-the-shelf solver such as CPLEX [24]. This is the approach that we take in this chapter. First, we discretize variable η_k in the bilinear term $\eta_k \cdot r_i$ using binary variables. This converts Problem MCP to a 0-1 mixed-integer nonlinear program (MINLP). By exploiting the special structures of the 0-1 MINLP, we employ a powerful technique called *Reformulation-Linearization Technique* (RLT) [53] to eliminate all bilinear terms. Subsequently, we have a 0-1

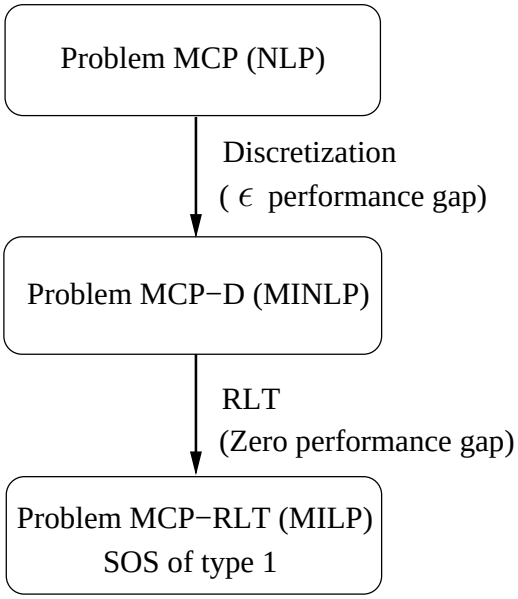

Figure 3.5: A flow chart of our solution roadmap to Problem MCP.

MILP, and we show that this new 0-1 MILP and the 0-1 MINLP have zero performance gap. This MILP has special ordered sets (SOS), which can be efficiently solved by CPLEX solver [24]. We quantify performance gap (due to discretization) and prove near-optimality of our solution. A flow chart of our solution roadmap is given in Fig. 3.5.

3.4.2 Discretization

As a first step to reformulate the NLP to MILP, we consider the bilinear term $\eta_k \cdot r_i$. Since η_k is a continuous variable within $[0, 1]$, we discretize it by using $L + 1$ discrete points $\eta_{kl} = \frac{l}{L}$, $l = 0, 1, \cdots, L$. Then we write

$$\eta_k = \sum_{l=0}^{L} \eta_{kl} \cdot z_{kl}, \qquad k \in \mathcal{Q}, \tag{3.23}$$

$$\sum_{l=0}^{L} z_{kl} = 1, \qquad k \in \mathcal{Q}, \tag{3.24}$$

where z_{kl} is a binary variable that indicates whether or not η_{kl} is chosen. By (3.23), the term $\eta_k \cdot r_i$ in (3.15) can be rewritten as $\eta_k \cdot r_i = \sum_{l=0}^{L} \eta_{kl} \cdot z_{kl} \cdot r_i$, which remains a bilinear term involving

binary variables z_{kl}, $l = 1, 2, \cdots, L$. This makes the problem a 0-1 MINLP, which is formulated as follows.

MCP-D

$$\begin{aligned}
\text{maximize} \quad & \eta_{\text{vac}} \\
\text{subject to} \quad & \textstyle\sum_{j\in\mathcal{N}}^{j\neq i} f_{ij} + f_{iB} - \sum_{k\in\mathcal{N}}^{k\neq i} f_{ki} = R_i && (i \in \mathcal{N}) \\
& \rho \cdot \textstyle\sum_{k\in\mathcal{N}}^{k\neq i} f_{ki} + \sum_{j\in\mathcal{N}}^{j\neq i} C_{ij} \cdot f_{ij} + C_{iB} \cdot f_{iB} - r_i = 0 && (i \in \mathcal{N}) \\
& \eta_{\text{vac}} \leq 1 - \textstyle\sum_{j\in\mathcal{Q}} \sum_{l=0}^{L} \eta_{jl} \cdot z_{jl} - \frac{\tau_{\text{TSP}}}{E_{\max} - E_{\min}} \\
& \qquad \cdot (r_i - \textstyle\sum_{l=0}^{L} \eta_{kl} \cdot z_{kl} \cdot r_i) && (i \in \mathcal{N}_k, k \in \mathcal{Q}) \qquad (3.25) \\
& r_i - U_i \textstyle\sum_{l=0}^{L} \eta_{kl} \cdot z_{kl} \leq 0 && (i \in \mathcal{N}_k, k \in \mathcal{Q}) \qquad (3.26) \\
& \textstyle\sum_{l=0}^{L} z_{kl} = 1 && (k \in \mathcal{Q}) \\
& f_{ij}, f_{iB} \geq 0, 0 \leq r_i \leq U_i, 0 \leq \eta_{\text{vac}} \leq 1 && (i, j \in \mathcal{N}, i \neq j) \\
& z_{kl} \in \{0, 1\} && (i \in \mathcal{N}_k, k \in \mathcal{Q}, l = 0, \cdots, L) \, .
\end{aligned}$$

3.4.3 Reformulation and Linearization

To remove the nonlinear terms $z_{kl} \cdot r_i$ in the 0-1 MINLP, we employ a powerful technique called *Reformulation-Linearization Technique (RLT)* [53] as follows. Define

$$\gamma_{ikl} \triangleq z_{kl} \cdot r_i, \quad i \in \mathcal{N}_k, k \in \mathcal{Q}, l = 0, \cdots, L. \tag{3.27}$$

Then $\sum_{l=0}^{L} \eta_{kl} \cdot z_{kl} \cdot r_i$ can be is rewritten as $\sum_{l=0}^{L} \eta_{kl} \cdot z_{kl} \cdot r_i = \sum_{l=0}^{L} \eta_{kl} \cdot \gamma_{ikl}$, $i \in \mathcal{N}_k, k \in \mathcal{Q}$.

To replace the nonlinear constraint (3.27), we need to add RLT constraints, which are linear. The new linear constraints are generated by multiplying existing linear constraints for variables z_{kl} and r_i, which are $1 - \sum_{l=0}^{L} z_{kl} = 0$, $z_{kl} \geq 0$, $r_i \geq 0$ and $U_i - r_i \geq 0$. It is worth pointing out that RLT in [54] typically refers to multiplying each pair of these constraints (i.e., reformulation)

and generating linear constraints via variable substitution (i.e., linearization). For our problem, this will produce several redundant or null constraints. To reduce such redundancy, we exploit a special structure of our problem, i.e., the presence of equality constraints $1 - \sum_{l=0}^{L} z_{kl} = 0$. It is only necessary to multiply these constraints (and $z_{kl} \geq 0$) by $r_i \geq 0$ and $U_i - r_i \geq 0$. Multiplying $1 - \sum_{l=0}^{L} z_{kl} = 0$ by $r_i \geq 0$ gives us:

$$\sum_{l=0}^{L} z_{kl} \cdot r_i = r_i, \qquad i \in \mathcal{N}_k, k \in \mathcal{Q},$$

which can be written as

$$\sum_{l=0}^{L} \gamma_{ikl} = r_i, \quad i \in \mathcal{N}_k, k \in \mathcal{Q}. \tag{3.28}$$

Multiplying $1-\sum_{l=0}^{L} z_{kl} = 0$ by $U_i - r_i \geq 0$ simply produces constraint (3.28), or $1-\sum_{l=0}^{L} z_{kl} = 0$ if $U_i - r_i > 0$, or $U_i - r_i = 0$, none of which is new.

Multiplying $r_i \geq 0$ and $U_i - r_i \geq 0$ by $z_{kl} \geq 0$, respectively, we have the following RLT constraints:

$$0 \leq z_{kl} \cdot r_i \leq U_i z_{kl}, \qquad i \in \mathcal{N}_k, k \in \mathcal{Q}, l = 0, \cdots, L,$$

which can be written as:

$$0 \leq \gamma_{ikl} \leq U_i z_{kl}, \quad i \in \mathcal{N}_k, k \in \mathcal{Q}, l = 0, \cdots, L. \tag{3.29}$$

In summary, the new RLT constraints are (3.28) and (3.29). By substituting (3.27) for $z_{kl} \cdot r_i$, and adding the new RLT constraints (3.28) and (3.29), we obtain the following 0-1 MILP.

MCP-RLT

$$\begin{aligned}
&\text{maximize} && \eta_{\text{vac}} \\
&\text{subject to} && \textstyle\sum_{j \in \mathcal{N}}^{j \neq i} f_{ij} + f_{iB} - \sum_{k \in \mathcal{N}}^{k \neq i} f_{ki} = R_i && (i \in \mathcal{N}) \\
& && \rho \cdot \textstyle\sum_{k \in \mathcal{N}}^{k \neq i} f_{ki} + \sum_{j \in \mathcal{N}}^{j \neq i} C_{ij} \cdot f_{ij} + C_{iB} \cdot f_{iB} - r_i = 0 && (i \in \mathcal{N})
\end{aligned}$$

$$\eta_{\text{vac}} \leq 1 - \sum_{j\in\mathcal{Q}} \sum_{l=0}^{L} \eta_{jl} \cdot z_{jl} - \frac{\tau_{\text{TSP}}}{E_{\text{max}} - E_{\text{min}}} \cdot (r_i - \sum_{l=0}^{L} \eta_{kl} \cdot \gamma_{ikl}) \quad (i \in \mathcal{N}_k, k \in \mathcal{Q}) \tag{3.30}$$

$$r_i - U_i \sum_{l=0}^{L} \eta_{kl} \cdot z_{kl} \leq 0 \qquad (i \in \mathcal{N}_k, k \in \mathcal{Q})$$

$$\sum_{l=0}^{L} z_{kl} = 1 \qquad (k \in \mathcal{Q})$$

$$\sum_{l=0}^{L} \gamma_{ikl} - r_i = 0 \qquad (i \in \mathcal{N}_k, k \in \mathcal{Q})$$

$$\gamma_{ikl} - U_i z_{kl} \leq 0, \qquad (i \in \mathcal{N}_k, k \in \mathcal{Q}, l = 0, \cdots, L)$$

$$f_{ij}, f_{iB} \geq 0, 0 \leq r_i \leq U_i, 0 \leq \eta_{\text{vac}} \leq 1 \qquad (i, j \in \mathcal{N}, i \neq j)$$

$$\gamma_{ikl} \geq 0, z_{kl} \in \{0, 1\} \qquad (i \in \mathcal{N}_k, k \in \mathcal{Q}, l = 0, \cdots, L)\ .$$

In this problem, f_{ij}, f_{iB}, r_i, η_{vac}, and γ_{ikl} are continuous variables; z_{kl} are binary variables; R_i, ρ, C_{ij}, C_{iB}, U_i, η_{kl}, E_{max}, E_{min}, and τ_{TSP} are constants. The integer variables z_{kl}, $l = 0, 1, \cdots, L$, are constrained by (3.24) and form a special ordered set (SOS) of type 1 (meaning that at most one of the variables in the set may be non-zero) [7]. It turns out that such special type of MILP is particularly suitable for CPLEX solver as CPLEX can use special branching strategies to improve performance [24].

Through RLT, we have eliminated all bilinear terms in the 0-1 MINLP and have obtained a 0-1 MILP. A natural question to ask is how much the performance gap is between the optimal solutions under MINLP and MILP. The following lemma says that the performance gap between the two is zero, thus substantiating the benefits of employing RLT in our solution approach. By zero performance gap, we mean there is a bijection from the feasible region of Problem MCP-D to the feasible region of Problem MCP-RLT and vice versa; and any two feasible solutions corresponding to this one-to-one mapping achieve the same objective value.

Lemma 3.2 *Problem MCP-RLT and Problem MCP-D have zero performance gap.*

Proof Our proof consists of two parts:

(i) If a solution $\psi_{\text{D}} = (f_{ij}, f_{iB}, r_i, \eta_{\text{vac}}, z_{kl})$ is feasible to Problem MCP-D, then the solution

$\psi_{\text{RLT}} = (f_{ij}, f_{iB}, r_i, \eta_{\text{vac}}, z_{kl}, \gamma_{ikl})$ is also feasible to Problem MCP-RLT, where $\gamma_{ikl} = r_i \cdot z_{kl}$.

(ii) If a solution $\psi_{\text{RLT}} = (f_{ij}, f_{iB}, r_i, \eta_{\text{vac}}, z_{kl}, \gamma_{ikl})$ is feasible to Problem MCP-RLT, then the solution $\psi_{\text{D}} = (f_{ij}, f_{iB}, r_i, \eta_{\text{vac}}, z_{kl})$ is also feasible to Problem MCP-D.

We shall prove that if both (i) and (ii) hold, then there is a bijection from the feasible region of Problem MCP-D to the feasible region of Problem MCP-RLT and vice verse; and for any one-to-one solution mapping between ψ_{D} and ψ_{RLT}, their objective values are the same.

For the first part, suppose we have a solution $\psi_{\text{D}} = (f_{ij}, f_{iB}, r_i, \eta_{\text{vac}}, z_{kl})$ that is feasible to Problem MCP-D. To show that $\psi_{\text{RLT}} = (f_{ij}, f_{iB}, r_i, \eta_{\text{vac}}, z_{kl}, \gamma_{ikl})$ is feasible to Problem MCP-RLT, we need to show that ψ_{RLT} satisfies Constraints (3.2), (3.3), (3.24), (3.26), (3.28), (3.29), and (3.30). Since ψ_{D} is feasible to Problem MCP-D, ψ_{D} satisfies Constraints (3.2), (3.3), (3.24), (3.25), and (3.26). For ψ_{RLT}, since the value of f_{ij}, f_{iB}, r_i, and z_{kl} are the same as those in ψ_{D}, ψ_{RLT} must also satisfy Constraints (3.2), (3.3), (3.24), and (3.26). To verify Constraint (3.28), we multiply (3.24) by r_i on both sides, and have $\sum_{l=0}^{L} z_{kl} \cdot r_i = r_i$, or equivalently, $\sum_{l=0}^{L} \gamma_{ikl} = r_i$. Similarly, we can verify (3.29) by multiplying $0 \leq r_i \leq U_i$ by z_{kl} on both sides. From (3.25), since $\gamma_{ikl} = r_i \cdot z_{kl}$, (3.30) holds. This completes the proof of (i).

For the second part, suppose we have a solution $\psi_{\text{RLT}} = (f_{ij}, f_{iB}, r_i, \eta_{\text{vac}}, z_{kl}, \gamma_{ikl})$ that is feasible to Problem MCP-RLT. To show that ψ_{D} is a feasible solution to Problem MCP-D, we need to show that ψ_{D} satisfies Constraints (3.2), (3.3), (3.24), (3.25), and (3.26). Since ψ_{RLT} is feasible to Problem MCP-RLT, ψ_{RLT} satisfies Constraints (3.2), (3.3), (3.24), (3.26), (3.28), (3.29), and (3.30). For ψ_{D}, since the value of f_{ij}, f_{iB}, r_i, and z_{kl} are the same as those in ψ_{RLT}, ψ_{D} must also satisfy Constraints (3.2), (3.3), (3.24), and (3.26). Now we show that ψ_{D} satisfies (3.25). Since ψ_{RLT} satisfies (3.30), it is sufficient to show that $\gamma_{ikl} = r_i \cdot z_{kl}$. To have $\gamma_{ikl} = r_i \cdot z_{kl}$, we need to show that $\gamma_{ikl} = 0$ if $z_{kl} = 0$ and $\gamma_{ikl} = r_i$ if $z_{kl} = 1$. There are assured by (3.24), (3.28) and (3.29). By (3.24), for each $k \in \mathcal{Q}$, there is only one $z_{km} = 1$, $0 \leq m \leq L$, and other z_{kl} ($l \neq m$) equal 0. By (3.29), the corresponding γ_{ikl} must be 0, for all $i \in \mathcal{N}_k$, $l \neq m$. Then by (3.28), the single z_{km} that equals 1 suggests $\gamma_{ikm} = r_i$, for all $i \in \mathcal{N}_k$. This completes the proof of (ii). $\square$

A Near-Optimal Solution Procedure

7. Given a target performance gap ϵ.
8. Let $L = \left\lceil \frac{|\mathcal{Q}|}{\epsilon} \right\rceil$.
9. Solve Problem MCP-RLT by CPLEX with a solution $\psi_{\text{RLT}} = (f_{ij}, f_{iB},$. $r_i, \eta_{\text{vac}}, z_{kl}, \gamma_{ikl})$.
10. Construct a feasible solution ψ = (f_{ij}, f_{iB}, r_i, η_{vac}, η_k) to Problem MCP via Lemma 3.3.
11. Recover $\tau, \tau_k, \tau_{\text{vac}}$ by (3.17), (3.18) and (3.19), respectively.

Figure 3.6: A summary of the proposed near-optimal solution procedure.

3.4.4 Recovering a Solution to the Original Problem

By now, we have obtained a solvable 0-1 MILP. Once we have an optimal solution to this MILP, the question to ask is how to recover a feasible solution to the original problem (MCP). Assuming we have a solution $\psi_{\text{RLT}} = (f_{ij}, f_{iB}, r_i, \eta_{\text{vac}}, z_{kl}, \gamma_{ikl})$ that is optimal to Problem MCP-RLT, by Lemma 3.2, the solution $\psi_{\text{D}} = (f_{ij}, f_{iB}, r_i, \eta_{\text{vac}}, z_{kl})$ is also feasible to Problem MCP-D. Based on ψ_{D}, we can construct a solution $\psi = (f_{ij}, f_{iB}, r_i, \eta_{\text{vac}}, \eta_k)$ to Problem MCP by letting $\eta_k = \sum_{l=0}^{L} \eta_{kl} \cdot z_{kl}$, and f_{ij},f_{iB}, r_i and η_{vac} unchanged from ψ_{D}. Note that ψ is a feasible solution to Problem MCP since the constraints in Problem MCP are the same as those in Problem MCP-D after we replace η_k by $\sum_{l=0}^{L} \eta_{kl} \cdot z_{kl}$. Since ψ is only a feasible solution to Problem MCP, its objective value η_{vac} is a lower bound for Problem MCP. We summarize our discussion in the following lemma.

Lemma 3.3 *For a given optimal solution $\psi_{\text{RLT}} = (f_{ij}, f_{iB}, r_i, \eta_{\text{vac}}, z_{kl}, \gamma_{ikl})$ to Problem MCP-RLT, we can construct a solution $\psi = (f_{ij}, f_{iB}, r_i, \eta_{\text{vac}}, \eta_k)$ that is feasible to Problem MCP by letting $\eta_k = \sum_{l=0}^{L} \eta_{kl} \cdot z_{kl}$. Furthermore, η_{vac} is a lower bound for the optimal objective value of Problem MCP.*

We summarize our near-optimal solution procedure to MCP in Fig. 3.6.

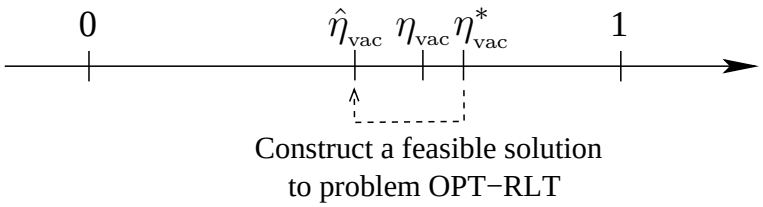

Figure 3.7: An illustration of main idea in the proof of Lemma 3.4. η^*_{vac} is the objective value under an optimal (unknown) solution ψ^* to Problem MCP; η_{vac} is the objective value under an optimal solution ψ_{RLT} to Problem MCP-RLT that is obtained by solving the 0-1 MILP (MCP-RLT); $\hat{\eta}_{\text{vac}}$ is the objective value obtained by the constructed feasible solution $\hat{\psi}_{\text{RLT}}$ to Problem MCP-RLT.

3.5 Proof of Near-Optimality

Recall that our original problem is MCP, which is a NLP. We converted this NLP to a 0-1 MINLP via discretization (Problem MCP-D) and then to a 0-1 MILP via RLT (Problem MCP-RLT). We proved that Problem MCP-D and Problem MCP-RLT have zero performance gap. So the performance gap between Problems MCP and MCP-RLT could only occur during discretization.

Quantifying Performance Gap. By solving Problem MCP-RLT, we obtain an optimal solution ψ_{RLT} to Problem MCP-RLT. Denote ψ^* the optimal (unknown) solution to Problem MCP. Denote η_{vac} the optimal objective value obtained by ψ_{RLT} and η^*_{vac} the optimal objective value obtained by ψ^*, respectively. Naturally, the gap between η_{vac} and η^*_{vac} is closely tied to L, which is the number of discrete points used in discretization. We quantify this gap in the following lemma.

Lemma 3.4 *For a given L, we have $\eta^*_{\text{vac}} - \eta_{\text{vac}} \leq \frac{|\mathcal{Q}|}{L}$.*

Proof We consider two cases, depending on whether $\eta^*_{\text{vac}} \leq \frac{|\mathcal{Q}|}{L}$ or $\eta^*_{\text{vac}} > \frac{|\mathcal{Q}|}{L}$.

Case i. Suppose $\eta^*_{\text{vac}} \leq \frac{|\mathcal{Q}|}{L}$. This is the trivial case. Since $\eta_{\text{vac}} \geq 0$, we have $\eta^*_{\text{vac}} - \eta_{\text{vac}} \leq \frac{|\mathcal{Q}|}{L}$.

Case ii. Suppose $\eta^*_{\text{vac}} > \frac{|\mathcal{Q}|}{L}$. This is the most common case. The rest of the proof is devoted to this case and its main idea is illustrated in Fig. 3.7. Denote $\hat{\psi}_{\text{RLT}}$ as a feasible solution to Problem

MCP-RLT and $\hat{\eta}_{\text{vac}}$ as the objective value under $\hat{\psi}_{\text{RLT}}$. Since η_{vac} is the objective value of an optimal solution ψ_{RLT} to MCP-RLT, we have $0 \leq \hat{\eta}_{\text{vac}} \leq \eta_{\text{vac}}$. To show that $\eta^*_{\text{vac}} - \eta_{\text{vac}} \leq \frac{|\mathcal{Q}|}{L}$, it is sufficient to show that $\eta^*_{\text{vac}} - \hat{\eta}_{\text{vac}} \leq \frac{|\mathcal{Q}|}{L}$ for some feasible solution $\hat{\psi}_{\text{RLT}}$. In the following proof, we will construct such a feasible solution $\hat{\psi}_{\text{RLT}}$ to Problem MCP-RLT so that $\eta^*_{\text{vac}} - \hat{\eta}_{\text{vac}} \leq \frac{|\mathcal{Q}|}{L}$.

Recall that an optimal (unknown) solution ψ^* to Problem MCP consists of $(f^*_{ij}, f^*_{iB}, r^*_i, \eta^*_{\text{vac}}, \eta^*_k)$. For a given L, we construct a solution $\hat{\psi}_{\text{RLT}} = (\hat{f}_{ij}, \hat{f}_{iB}, \hat{r}_i, \hat{\eta}_{\text{vac}}, \hat{z}_{kl}, \hat{\gamma}_{ikl})$ for Problem MCP-RLT based on $\psi^* = (f^*_{ij}, f^*_{iB}, r^*_i, \eta^*_{\text{vac}}, \eta^*_k)$ as follows. First, we let $\hat{f}_{ij} = f^*_{ij}, \hat{f}_{iB} = f^*_{iB}$, and $\hat{r}_i = r^*_i$. Then for the rest of the solution $\hat{\psi}_{\text{RLT}}$ (i.e., $\hat{\eta}_{\text{vac}}$, $\hat{z}_{kl}$, and $\hat{\gamma}_{ikl}$), we do the following. First, we round "up" η^*_k to the nearest discrete point $\eta_{k\xi} = \frac{\xi}{L}$, where $\xi = \lceil \eta^*_k \cdot L \rceil$. The rounding error for each $k \in \mathcal{Q}$ is

$$\eta_{k\xi} - \eta^*_k \;\; \leq \;\; \frac{1}{L} \, . \tag{3.31}$$

For $\hat{z}_{kl}$, we set $\hat{z}_{k\xi} = 1$ and $\hat{z}_{kl} = 0$, for $l = 0, \ldots, L$, $l \neq \xi$. Then for $\hat{\gamma}_{ikl}$, we set $\hat{\gamma}_{ikl} = \hat{z}_{kl} \cdot \hat{r}_i$, for $i \in \mathcal{N}_k$, $k \in \mathcal{Q}$, $l = 0, 1, \ldots, L$. Finally, for $\hat{\eta}_{\text{vac}}$, based on (3.30), we set it to

$$\hat{\eta}_{\text{vac}} = \min_{i \in \mathcal{N}_k, k \in \mathcal{Q}} \left\{ 1 - \sum_{j \in \mathcal{Q}} \sum_{l=0}^{L} \eta_{jl} \cdot \hat{z}_{jl} - \frac{\tau_{\text{TSP}}}{E_{\text{max}} - E_{\text{min}}} \cdot (\hat{r}_i - \sum_{l=0}^{L} \eta_{kl} \cdot \hat{\gamma}_{ikl}) \right\} . \tag{3.32}$$

Now we prove that the above newly constructed $\hat{\psi}_{\text{RLT}} = (\hat{f}_{ij}, \hat{f}_{iB}, \hat{r}_i, \hat{\eta}_{\text{vac}}, \hat{z}_{kl}, \hat{\gamma}_{ikl})$ is indeed a feasible solution to Problem MCP-RLT. That is, we will show that $\hat{\psi}_{\text{RLT}}$ satisfies Constraints (3.2), (3.3), (3.24), (3.26), (3.28), (3.29), and (3.30). Since ψ^* is an optimal solution to Problem MCP, ψ^* satisfies (3.2), (3.3), (3.15), and (3.16). Since $\hat{f}_{ij} = f^*_{ij}, \hat{f}_{iB} = f^*_{iB}$, and $\hat{r}_i = r^*_i$, $\hat{\psi}_{\text{RLT}}$ also satisfies (3.2) and (3.3). From the construction of $\hat{z}_{kl}$ and $\hat{\gamma}_{ikl}$, we know that $\hat{\psi}_{\text{RLT}}$ satisfies Constraints (3.24) and (3.28). Now we consider (3.26). We have $\hat{r}_i - U_i \sum_{l=0}^{L} \eta_{kl} \cdot \hat{z}_{kl} \leq r^*_i - U_i \cdot \eta^*_k \leq 0$, where the first inequality holds due to $\hat{r}_i = r^*_i$ and $\sum_{l=0}^{L} \eta_{kl} \cdot \hat{z}_{kl} = \eta_{k\xi} \geq \eta^*_k$ (because $\hat{z}_{k\xi} = 1$

and $\hat{z}_{kl} = 0$, $l = 0, 1, \ldots, L$, $l \neq \xi$), the second inequality holds since ψ^* satisfies (3.16). To verify Constraint (3.29), we multiply $0 \leq \hat{r}_i \leq U_i$ by $\hat{z}_{kl}$, and have $0 \leq \hat{z}_{kl} \cdot \hat{r}_i \leq U_i \cdot \hat{z}_{kl}$, or equivalently, $0 \leq \hat{\gamma}_{ikl} \leq U_i \cdot \hat{z}_{kl}$. Constraint (3.30) can be verified directly from (3.32). Thus, the newly constructed solution $\hat{\psi}_{\text{RLT}}$ is indeed a feasible solution to Problem MCP-RLT.

Now we show that $\eta^*_{\text{vac}} - \hat{\eta}_{\text{vac}} \leq \frac{|\mathcal{Q}|}{L}$. Since ψ^* is an optimal solution to Problem MCP, Constraint (3.15) must be binding for some $i \in \mathcal{N}$ under ψ^*. That is,

$$\eta^*_{\text{vac}} = \min_{i \in \mathcal{N}_k, k \in \mathcal{Q}} \left\{ 1 - \sum_{j \in \mathcal{Q}} \eta^*_j - \frac{\tau_{\text{TSP}}}{E_{\text{max}} - E_{\text{min}}} (1 - \eta^*_k) \cdot r^*_i \right\}. \tag{3.33}$$

We have

$$\begin{aligned}
\eta^*_{\text{vac}} - \hat{\eta}_{\text{vac}} &= \min_{i \in \mathcal{N}_k, k \in \mathcal{Q}} \left\{ 1 - \sum_{j \in \mathcal{Q}} \eta^*_j - \frac{\tau_{\text{TSP}}}{E_{\text{max}} - E_{\text{min}}} (1 - \eta^*_k) \cdot r^*_i \right\} - \\
&\quad \min_{i \in \mathcal{N}_k, k \in \mathcal{Q}} \left\{ 1 - \sum_{j \in \mathcal{Q}} \sum_{l=0}^{L} \eta_{jl} \cdot \hat{z}_{jl} - \frac{\tau_{\text{TSP}}}{E_{\text{max}} - E_{\text{min}}} \cdot (\hat{r}_i - \sum_{l=0}^{L} \eta_{kl} \cdot \hat{\gamma}_{ikl}) \right\} \\
&= \Big(\sum_{j \in \mathcal{Q}} \sum_{l=0}^{L} \eta_{jl} \cdot \hat{z}_{jl} - \sum_{j \in \mathcal{Q}} \eta^*_j \Big) - \frac{\tau_{\text{TSP}}}{E_{\text{max}} - E_{\text{min}}} \cdot \max_{i \in \mathcal{N}_k, k \in \mathcal{Q}} \left\{ (1 - \eta^*_k) \cdot r^*_i \right\} \\
&\quad + \frac{\tau_{\text{TSP}}}{E_{\text{max}} - E_{\text{min}}} \cdot \max_{i \in \mathcal{N}_k, k \in \mathcal{Q}} \left\{ \hat{r}_i - \sum_{l=0}^{L} \eta_{kl} \cdot \hat{\gamma}_{ikl} \right\} \\
&= \Big(\sum_{j \in \mathcal{Q}} \eta_{j\xi} - \sum_{j \in \mathcal{Q}} \eta^*_j \Big) - \frac{\tau_{\text{TSP}}}{E_{\text{max}} - E_{\text{min}}} \cdot \max_{i \in \mathcal{N}_k, k \in \mathcal{Q}} \left\{ (1 - \eta^*_k) \cdot r^*_i \right\} \\
&\quad + \frac{\tau_{\text{TSP}}}{E_{\text{max}} - E_{\text{min}}} \cdot \max_{i \in \mathcal{N}_k, k \in \mathcal{Q}} \left\{ \hat{r}_i - \sum_{l=0}^{L} \eta_{kl} \cdot \hat{z}_{kl} \cdot \hat{r}_i \right\} \\
&= \sum_{j \in \mathcal{Q}} \Big(\eta_{j\xi} - \eta^*_j \Big) - \frac{\tau_{\text{TSP}}}{E_{\text{max}} - E_{\text{min}}} \cdot \max_{i \in \mathcal{N}_k, k \in \mathcal{Q}} \left\{ (1 - \eta^*_k) \cdot r^*_i \right\} \\
&\quad + \frac{\tau_{\text{TSP}}}{E_{\text{max}} - E_{\text{min}}} \cdot \max_{i \in \mathcal{N}_k, k \in \mathcal{Q}} \left\{ (1 - \eta_{k\xi}) \cdot r^*_i \right\}
\end{aligned}$$

$$
\begin{aligned}
&= \sum_{j\in\mathcal{Q}}\left(\eta_{j\xi}-\eta_j^*\right)+\frac{\tau_{\text{TSP}}}{E_{\max}-E_{\min}}\cdot\left\{\max_{i\in\mathcal{N}_k,k\in\mathcal{Q}}\left\{(1-\eta_{k\xi})\cdot r_i^*\right\}-\max_{i\in\mathcal{N}_k,k\in\mathcal{Q}}\left\{(1-\eta_k^*)\cdot r_i^*\right\}\right\}\\
&\leq \sum_{j\in\mathcal{Q}}\left(\eta_{j\xi}-\eta_j^*\right)\\
&\leq \frac{|\mathcal{Q}|}{L},
\end{aligned}
$$

where the first equality holds by (3.33) and (3.32), the third equality holds due to $\sum_{l=0}^{L}\eta_{jl}\cdot\hat{z}_{jl}=\eta_{j\xi}$ (since only $\hat{z}_{j\xi}=1$ and $\hat{z}_{jl}=0$, $l=0,1,\ldots,L$, $l\neq\xi$) and $\hat{\gamma}_{ikl}=\hat{z}_{kl}\cdot\hat{r}_i$, the fourth equality holds due to $\hat{r}_i=r_i^*$ and $\sum_{l=0}^{L}\eta_{kl}\cdot\hat{z}_{kl}=\eta_{k\xi}$, the sixth inequality holds due to $\eta_{k\xi}\geq\eta_k^*$ for $k\in\mathcal{Q}$, and the last inequality holds by (3.31). This completes the proof. □

Performance Guarantee. Lemma 3.4 gives an upper bound of the performance gap between η_{vac} and η_{vac}^* for a given L. The following lemma shows how to choose L so that this performance gap is no more than ϵ ($0<\epsilon\ll 1$).

Lemma 3.5 *For a given* ϵ, $0<\epsilon\ll 1$, *if* $L=\left\lceil\frac{|\mathcal{Q}|}{\epsilon}\right\rceil$, *we have* $\eta_{\text{vac}}^*-\eta_{\text{vac}}\leq\epsilon$.

Proof By Lemma 3.4, we know $\eta_{\text{vac}}^*-\eta_{\text{vac}}\leq\frac{|\mathcal{Q}|}{L}$. To have $\eta_{\text{vac}}^*-\eta_{\text{vac}}\leq\epsilon$, it is sufficient to have $\frac{|\mathcal{Q}|}{L}\leq\epsilon$, or $L=\left\lceil\frac{|\mathcal{Q}|}{\epsilon}\right\rceil$. This completes the proof. □

3.6 Numerical Results

In this section, we present some numerical results to demonstrate our proposed solution. We also demonstrate how our solution can address the scalability issue when the density of sensor nodes increases.

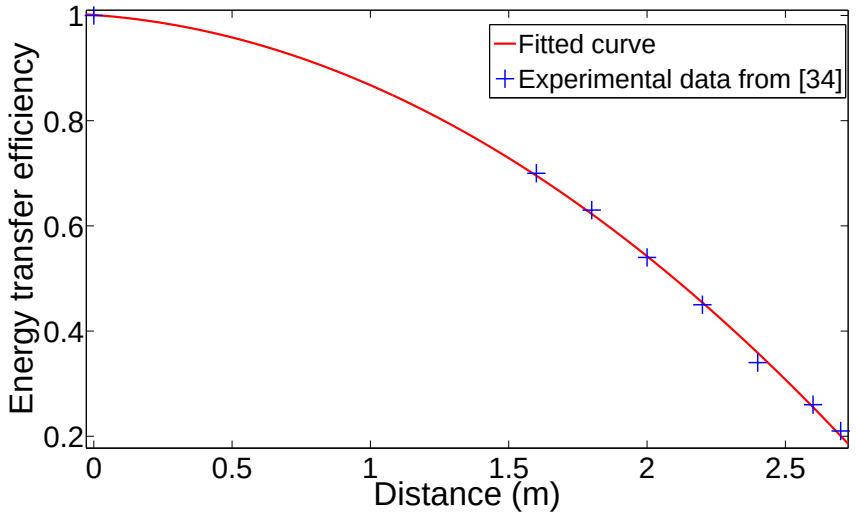

Figure 3.8: Efficiency of energy transfer as a function of distance between a sensor node and the WCV. This figure is based on averaging energy transfer efficiencies for two devices in the experimental study in [32].

.

Table 3.2: Location and data rate R_i for each node in a 100-node network.

Node index	Location (m)	R_i (kb/s)	Node index	Location (m)	R_i (kb/s)
1	(140.8,905.4)	3	51	(613.9,474.1)	9
2	(977.8,913.0)	5	52	(837.1,6.1)	2
3	(679.9,92.7)	4	53	(635.8,216.4)	4
4	(325.8,378.1)	5	54	(165.7,109.6)	7
5	(196.2,526.8)	8	55	(634.9,218.4)	1
6	(546.5,967.0)	2	56	(747.2,33.2)	7
7	(323.4,329.4)	7	57	(821.4,608.6)	5
8	(747.7,33.4)	3	58	(250.1,839.1)	10
9	(838.3,678.0)	1	59	(990.6,617.0)	6
10	(692.5,461.4)	9	60	(977.9,909.0)	4
11	(918.4,517.9)	1	61	(585.6,623.4)	5
12	(613.6,476.1)	1	62	(678.6,91.7)	1
13	(586.2,621.8)	4	63	(613.5,475.9)	1
14	(440.2,17.7)	4	64	(438.8,17.3)	2
15	(813.3,749.9)	7	65	(836.5,680.4)	10
16	(886.2,612.7)	7	66	(321.9,331.2)	3
17	(804.9,329.4)	5	67	(752.3,714.6)	9
18	(633.7,218.4)	4	68	(679.6,93.7)	8
19	(753.3,713.0)	9	69	(838.0,677.4)	6

Continued on next page

Table 3.2 – continued from previous page

Node index	Location (m)	R_i (kb/s)	Node index	Location (m)	R_i (kb/s)
20	(163.7,108.6)	2	70	(897.2,709.2)	2
21	(672.0,318.1)	10	71	(750.8,712.4)	3
22	(250.2,840.1)	1	72	(635.5,217.4)	7
23	(732.3,965.0)	4	73	(585.4,622.0)	6
24	(197.4,672.2)	6	74	(732.0,966.2)	3
25	(92.7,967.7)	1	75	(91.5,971.3)	2
26	(990.1,617.4)	4	76	(918.6,514.1)	2
27	(804.3,352.0)	7	77	(166.0,109.0)	8
28	(821.5,609.8)	7	78	(90.6,967.7)	10
29	(898.3,708.4)	6	79	(813.4,749.7)	1
30	(688.4,59.1)	3	80	(686.9,59.7)	10
31	(837.3,4.5)	2	81	(587.1,622.4)	2
32	(451.2,135.5)	1	82	(838.2,680.4)	4
33	(979.3,911.8)	8	83	(249.7,842.5)	3
34	(678.9,93.3)	8	84	(139.9,902.0)	7
35	(751.6,714.2)	6	85	(691.4,459.4)	3
36	(633.8,217.0)	9	86	(747.3,36.0)	5
37	(452.9,133.7)	3	87	(803.9,327.0)	7
38	(633.6,217.8)	1	88	(164.6,108.4)	3
39	(884.4,613.9)	1	89	(197.8,670.4)	5
40	(197.1,523.2)	6	90	(820.8,610.2)	3
41	(813.8,747.7)	5	91	(140.8,904.6)	9
42	(804.1,326.6)	4	92	(546.3,965.4)	4
43	(732.9,966.2)	3	93	(886.8,613.1)	8
44	(690.1,460.2)	7	94	(671.5,318.9)	8
45	(669.9,319.1)	7	95	(248.7,842.9)	4
46	(195.9,670.2)	10	96	(670.6,318.1)	7
47	(440.7,17.1)	2	97	(613.3,477.1)	9
48	(670.2,319.3)	10	98	(614.2,475.7)	5
49	(585.1,624.2)	1	99	(452.2,133.1)	7
50	(896.5,708.4)	8	100	(197.4,670.6)	4

3.6.1 Results of a 100-node Network

We assume sensor nodes are deployed over a 1000 m $\times$ 1000 m square area. The number of nodes in the network will be specified for each instance in the study. The base station is at (500, 500) (in m) and the WCV's home service station is assumed to be at the origin. The traveling speed of the

Table 3.3: Cells index, location of cell center, sensor nodes in each cell, cell traveling order along the path, and charging time at each cell for the 100-node network.

Cell index	Location of cell center (m)	Sensor nodes in the cell	Travel order	τ_k (s)
1	(140.4, 904.1)	1, 84, 91	26	157
2	(452.3, 134.8)	32, 37, 99	2	314
3	(837.0, 6.2)	31, 52	6	157
4	(687.1, 60.0)	30, 80	4	157
5	(897.8, 710.1)	29, 50, 70	21	157
6	(820.8, 609.5)	28, 57, 90	17	628
7	(804.6, 352.3)	27	10	157
8	(990.9, 618.9)	26, 59	20	157
9	(91.8, 969.6)	25, 75, 78	25	157
10	(197.1, 670.3)	24, 46, 89, 100	28	2510
11	(731.7, 964.9)	23, 43, 74	23	314
12	(249.8, 841.0)	22, 58, 83, 95	27	471
13	(670.9, 317.2)	21, 45, 48, 94, 96	8	314
14	(164.7, 109.1)	20, 54, 77, 88	32	471
15	(751.9, 714.7)	19, 35, 67, 71	14	314
16	(634.5, 216.7)	18, 36 ,38, 53, 55, 72	7	157
17	(804.6, 328.9)	17, 42, 87	9	157
18	(885.6, 614.2)	16, 39, 93	18	157
19	(812.7, 749.8)	15, 41, 79	15	157
20	(440.1, 15.6)	14, 47, 64	1	157
21	(585.9, 623.5)	13, 49, 61, 73, 81	13	157
22	(614.3, 476.2)	12, 51, 63, 97, 98	12	314
23	(918.0, 516.0)	11, 76	19	157
24	(691.2, 459.9)	10, 44, 85	11	157
25	(837.0, 679.7)	9, 65, 69, 82	16	157
26	(747.9, 34.3)	8, 56, 86	5	157
27	(322.6, 331.3)	7, 66	31	2353
28	(545.4, 964.9)	6, 92	24	157
29	(197.1, 525.3)	5, 40	29	784
30	(326.7, 380.4)	4	30	157
31	(679.0, 92.8)	3, 34, 62,68	3	157
32	(978.8, 911.1)	2, 33, 60	22	314

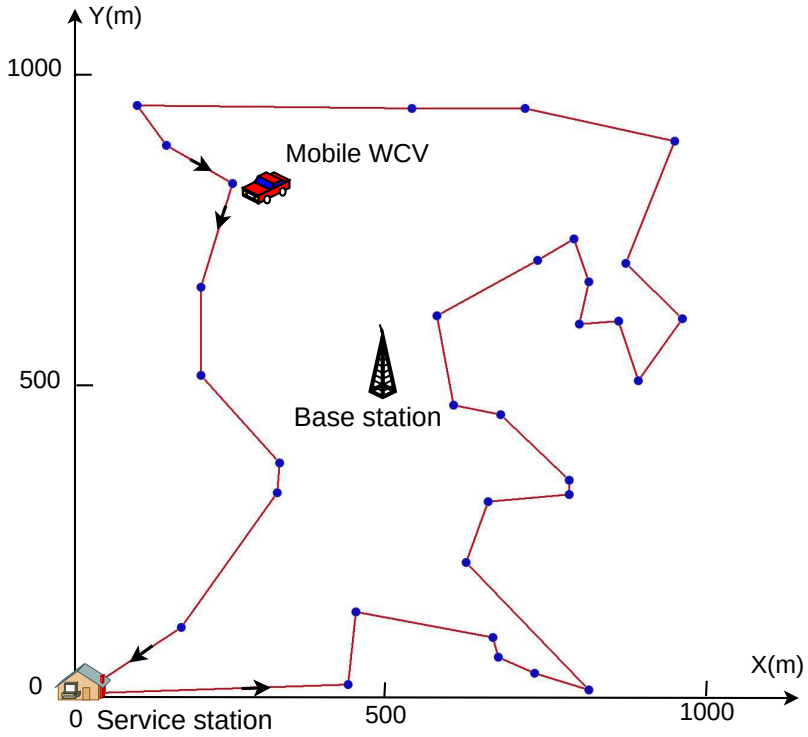

Figure 3.9: An optimal traveling path (assuming counter clockwise direction) for the 100-node sensor network. The 100 nodes are distributed in 32 cells, with the center of each cell being represented as a point in the figure.

WCV is $V = 5$ m/s. The data rate R_i, $i \in \mathcal{N}$, from each node is randomly generated within $[1, 10]$ kb/s. The power consumption coefficients are $\beta_1 = 50$ nJ/b, $\beta_2 = 0.0013$ pJ$/(\text{b} \cdot \text{m}^4)$, and $\rho = 50$ nJ/b. The path loss index is $\alpha = 4$.

For the battery at a sensor node, we choose a regular NiMH battery and its nominal cell voltage and electricity volume is 1.2 V/2.5 Ah. We have $E_{\max} = 1.2$ V $\times$ 2.5 A $\times$ 3600 sec $= 10.8$ kJ [33]. We let $E_{\min} = 0.05 \cdot E_{\max} = 540$ J. For $\mu(D_i)$, we refer to the experimental data on WET efficiency in [32] (see Fig. 3.8). Through curve fitting, we obtain $\mu(D_i) = -0.0958 D_i^2 - 0.0377 D_i + 1.0$. Assuming $U_{\max} = 5$ W and $\delta = 1$ W, we have $D_\delta = 2.7$ m for a cell's side length. We set $\epsilon = 0.1$ for the numerical results.

We first present complete results for a 100-node network. Table 3.2 gives the location of each node and its data rate for the 100-node network. These 100 nodes are distributed in $|\mathcal{Q}| = 32$ selected

cells and Table 3.3 gives the location of each cell as well as the number of sensor nodes it contains. The shortest Hamiltonian cycle that threads all cells $k \in \mathcal{Q}$ and the service station is found by the Concorde TSP solver [10], which is shown in Fig. 3.9. For this optimal cycle, $D_{\text{TSP}} = 5110$ m and $\tau_{\text{TSP}} = 1022$ s ≈ 0.28 h. For the target performance gap $\epsilon = 0.1$, we have cycle time $\tau = 13.95$ h, vacation time $\tau_{\text{vac}} = 10.26$ h, total charing time $13.95 - 10.26 - 0.28 = 3.41$ h, and the objective $\eta_{\text{vac}} = 73.55\%$.

Corollary 3.1.1 says that each sensor node in the network is fully charged to E_{max} when the WCV departs its cell, which is confirmed by our numerical results. By Property 3.3, we find that in an optimal solution, there exists at least one equilibrium node in each cell $k \in \mathcal{Q}$. In our numerical results, all 32 cells contain equilibrium nodes.

To examine energy behavior at sensor nodes, consider sensor nodes in cell 10. There are 4 sensor nodes in this cell, nodes 24 and 46 are equilibrium nodes while nodes 89 and 100 are not. Fig. 3.10 shows the energy behavior of node 24 (solid curve) and node 89 (dashed curve). Note that node 24 does not have any saturation period except in the initial first cycle while node 89 has saturation period in every cycle.

By Property 3.2, we find that there exists an energy bottleneck node in the network with its energy dropping to E_{min} during a cycle. This property is also confirmed in our numerical results. This bottleneck node is the 89th node, whose energy behavior is shown in Fig. 3.10.

3.6.2 Scalability Comparison

In this section, we demonstrate how multi-node charging can address the scalability problem in WET. We consider $|\mathcal{Q}| = 25$ cells and increase node density in these cells from 1 to 8 per cell. For each density, we compare multi-node charging with single-node charging. Fig. 3.11 shows the numerical results. We have two observation: (i) The achievable objective value under multi-node charging remains steady when node density increases from 1 to 8, with only slight decrease. On

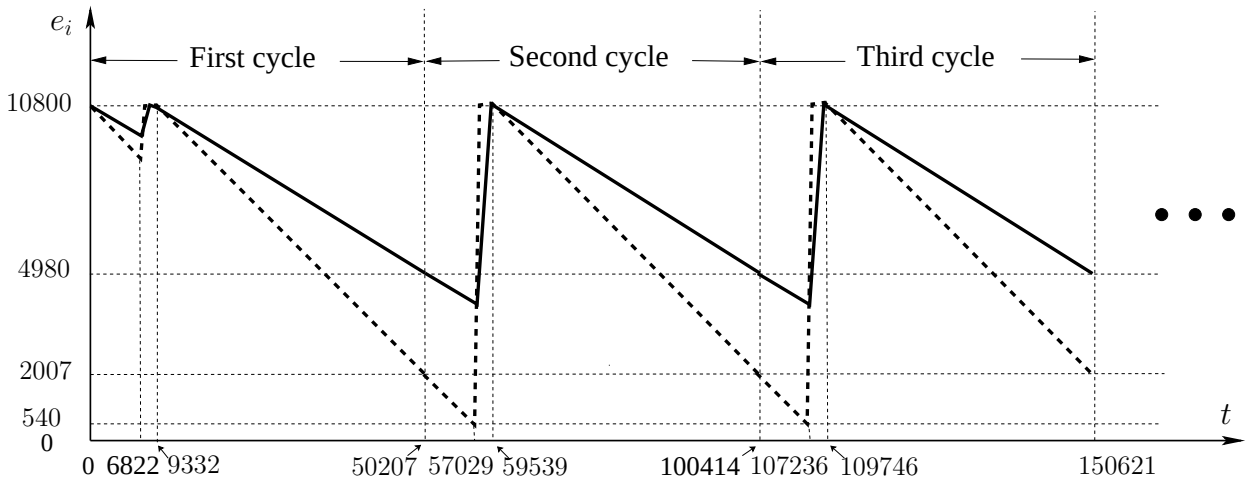

Figure 3.10: Energy cycle behavior of an equilibrium node (node 24, in solid curve) and a non-equilibrium node (node 89, in dashed curve) in the 100-node network. Node 89 is also a bottleneck node.

the other hand, the achievable objective value under single-node charging drops very quickly when node density increases and a feasible solution does not exist when node density is beyond 5. (ii) Over the entire density range (from 1 to 8), the objective value under multi-node charging is always higher than that under single-node charging and the gap between them widens as density increases.

Table 3.4 gives more details for the study shown in Fig. 3.11. Note that under multi-node charging, the achievable objective value at density 6 is slightly larger than that at density 5. This local fluctuation is due to more possibilities for routing when density increases. However, this is only a local fluctuation. The prevailing trend is that η_{vac} decreases as density increases.

3.7 Summary

In this chapter, we have exploited recent advances in multi-node WET technology to charge the batteries of sensor nodes in a dense WSN. Our approach was to develop a formal optimization framework by jointly optimizing traveling path, flow routing and charging time at each cell. By employing discretization and a novel reformulation-linearization technique, we developed a prov-

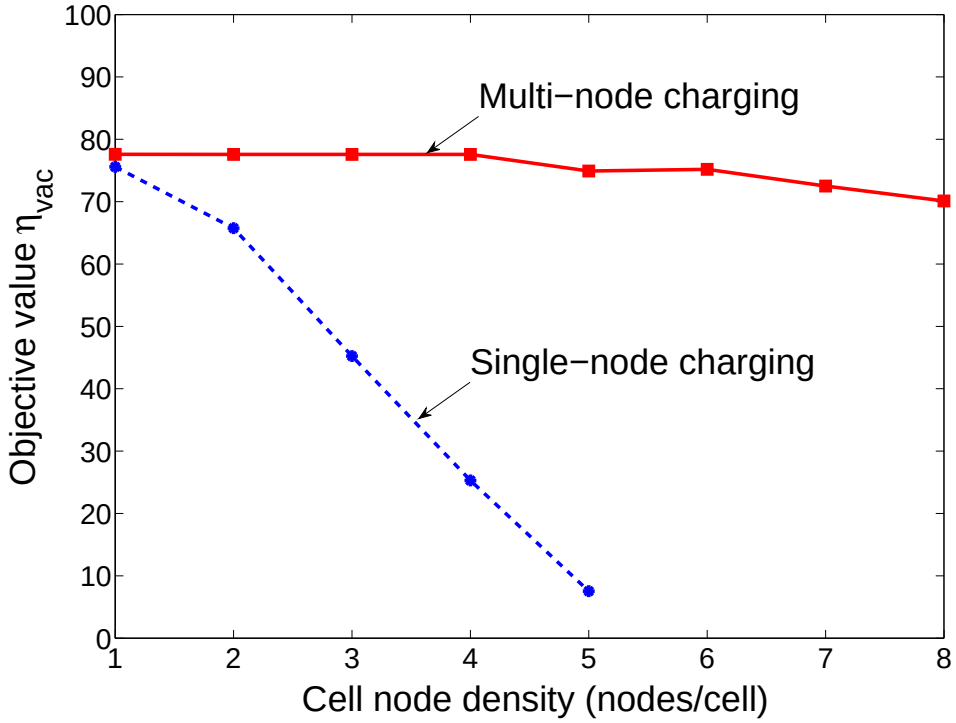

Figure 3.11: Achievable objective value as a function of node density under multi-node and single-node charging technologies.

Table 3.4: Details of comparison between multi-node charging and single-node charging.

Density	Multi-node Charging			Single-node Charging		
(Nodes /Cell)	τ (h)	$\sum_{k\in\mathcal{Q}}\tau_k$ (h)	η_{vac}	τ (h)	$\sum_{k\in\mathcal{Q}}\tau_k$ (h)	η_{vac}
1	8.28	1.59	77.59%	8.12	1.84	75.58%
2	8.27	1.59	77.58%	4.72	1.46	65.75%
3	8.22	1.58	77.57%	7.32	3.86	45.24%
4	8.24	1.58	77.57%	5.64	4.06	25.29%
5	7.21	1.76	74.91%	6.20	5.58	7.54%
6	8.28	1.79	75.19%	–	–	–
7	7.33	1.75	72.50%	–	–	–
8	6.83	1.77	70.11%	–	–	–

ably near-optimal solution for any desired level of accuracy. Using numerical results, we demonstrated the advantage of multi-node WET technology and showed how it addressed the charging scalability problem in a dense WSN.

Chapter 4

Bundling Mobile Base Station and Wireless Energy Transfer: The Pre-planned Path Case

4.1 Introduction

In Chapters 2 and 3, MRC was shown to be a promising technology to fundamentally address energy and lifetime problems in a WSN. To maintain high efficiency in WET, a vehicle is needed to carry the wireless charger to travel inside the network. Note that in Chapters 2 and 3, although the WCV is mobile, the base station in the WSN is fixed.

On the other hand, it has been well recognized that a *mobile base station* (MBS) can achieve significant energy saving and network lifetime extension [36, 37, 51, 69]. Given that a MBS needs to be carried on a vehicle, we explore the possibility of having the base statio co-locate on the same vehicle used for carrying the wireless charger.[1] This is the main motivation of this investigation.

In this chapter, we explore problems centered around bundling MBS and WET. When there is no ambiguity, we still call the combined two systems as WCV. We envision that the WCV starts from its home service station, travels along a pre-planned path and returns to its home service station at

[1] Although two separate vehicles may be employed (one for WET and the other for MBS), the costs (both equipment and energy) associated with the two vehicles will be much higher.

the end of a trip. While traveling on its path, the WCV can make a number of stops and charge sensor nodes near those stops. At any time, all data collected by the sensor nodes are relayed (via multi-hop) to the MBS (on WCV). Apparently this is a very complex system, involving variables across multiple dimensions — time, space, and energy. A basic requirement is that by employing WET, none of the sensor nodes run out of energy while all sensing data are relayed to the base station in real time. A more aggressive goal is to minimize energy consumption of the entire system (see Section 4.5 for more details).

This is a challenging optimization problem that involves several subproblems, each of which is interesting on its own. First, the WCV's stopping and charging behavior needs to be optimized, which will tell us where the WCV will make stops along its path and how long it will stay at each stop. Second, the flow routing among sensor nodes need to be optimized, which depends on the location of WCV (and time). Finally, the energy transfer behavior of the WCV depends on its stopping locations and their distances to neighboring sensor nodes. Apparently, these subproblems are tightly coupled together (both in time/space and under a global optimization objective).

The main contributions of this chapter are as follows:

- We develop a mathematical model for co-locating the MBS on the WCV. This includes energy criteria to ensure that the energy level at each sensor node never falls below some minimum threshold, and a general optimization problem formulation (CoP-t) involving the WCV's stopping behavior, energy charging, and data flow routing. We also show that the goal of minimizing energy consumption associated with the WCV is equivalent to maximizing the fraction of the WCV's vacation time at the service station.
- The general problem CoP-t has a time-dependent formulation, for which it is difficult to devise a solution procedure. We show that a special case of CoP-t, where data flow routing and energy consumption of sensor nodes only depend on the WCV's location, can in fact offer the same optimal objective value as that for CoP-t. Therefore, we propose to study this simpler formulation, denoted as CoP-s, which only involves location-dependent variables.

- For Problem CoP-s, we develop an $(1-\epsilon)$-optimal solution with any desired level of accuracy ϵ. Our solution involves discretizing path into a finite number of segments and representing each segment as a logical point. By exploiting the worst case and the best case representation for each logical point, we can find a lower bound and an upper bound for CoP-s by solving two linear programs (LPs). Depending on the required accuracy, we show how to discretize segments into smaller segments. We prove that the gap between the lower and upper bounds will close as the number of iterations increases and we will eventually obtain an $(1-\epsilon)$-optimal solution.

The remainder of this chapter is organized as follows. In Section 4.2, we review related work on MBS. In Section 4.3, we describe some basic models for the WCV's stopping behavior, flow routing, and energy charging and consumption in a WSN. Section 4.4 presents energy criteria to ensure that each sensor node is always operational. A general optimization formulation (CoP-t) is given in Section 4.5. In Section 4.6, we show that we can study a special case of CoP-t that only involves space-dependent formulation, which we denote as CoP-s. Section 4.7 presents an $(1-\epsilon)$-optimal solution to CoP-s. Section 4.8 presents numerical results and Section 4.9 summarizes this chapter.

4.2 Related Work

The benefits of offering mobility to a base station in a sensor network have been well recognized [6, 35, 36, 51, 70]. Due to the complexity associated with a MBS, early efforts either simplified the problem by limiting the locations of the base station to a finite set of points and assuming negligible traveling time between points [6, 36], or developed heuristic solutions under some simplified assumptions (e.g., a heuristic move of the base station toward sensor nodes with high traffic [70] or decoupling the base station's movement and data routing [35]). A major breakthrough in MBS research was made by Shi and Hou in [51], in which they proposed a provably $(1-\epsilon)$-optimal

solution. Even in [51], it was assumed that the time for the base station to move from one location to another is negligible.

It is worth contrasting this chapter with [51] in terms of problem scope and solution techniques. In [51], only a MBS problem was investigated while in this chapter, we investigate the WCV and MBS co-location problem. In [51], it was assumed that the time for the base station to move from one point to another is negligible while in this chapter we explicitly consider the traveling time in problem formulation and solution. Further, in this chapter, we generalize the "fictitious cost point" concept proposed in [51], which only considered energy consumption. That is, the so-called "logical point" concept in this chapter considers *both* energy reception *and* energy consumption.

Further, it is worth pointing out that the MBS discussed in this dissertation differs fundamentally from some other mobile stations/relays in the literature. First, mobile stations such as data MULEs [50], message ferry [74], and SenCar [38, 75] are employed in the so-called delay-tolerant network (DTN) [26], in which frequent network disconnectivity or partitioning is expected. In essence, the goal of DTN is to exploit intermediate nodes (e.g., mobile nodes) to perform intermittent routing "over time" (i.e., delay tolerant) so as to achieve "eventual delivery". Applications under DTN are expected to tolerate large delays. In contrast, the MBS considered in this dissertation collects real-time data flow from sensor nodes with negligible delays. The MBS in this dissertation is also different from the mobile relay mechanism in [65], which employs a mobile node to help relay data from sensor nodes to a static base station.

4.3 Basic Network and Energy Models

In this section, we present some basic models for the WCV's stopping behavior, flow routing, and energy charging and consumption in a WSN. Table 4.1 lists the notation used in this chapter.

Table 4.1: Notation in Chapter 4.

Symbol	Definition
$C_{iB}(p)(C_{iB}(p(t)))$	Energy consumption for transmitting one unit of data rate from node i to base station B when B is at point p (or $p(t)$)
$C_{iB}(p_m)$	$= \max_{p \in \mathcal{S}_m}\{C_{iB}(p)\}$
D_δ	Maximum charging distance of the WCV
$D_{iB}(p)$	Distance from node i to the WCV when the WCV is at p
$D(\mathcal{S}_m)$	The length of segment $\mathcal{S}_m$
$f_{ij}(t)$ (or $f_{iB}(t)$)	Flow rate from sensor node i to sensor node j (or base station B) at time t
$f_{ij}(p)$ (or $f_{iB}(p)$)	Flow rate from sensor node i to sensor node j (or base station B) when the WCV is at point p
M_i	Number of segments at the i-th iteration of the algorithm
$p(t)$	Location of the WCV at time t
p_m	A logical point that represents segment $\mathcal{S}_m$
p_{vac}	Location of the service station
R_i	Data rate generated at sensor node i
$r_i(t)$	Energy consumption rate at sensor node i at time t
$r_i(p)$	Energy consumption rate at sensor node i when the WCV is at point p
$s(t)$	Distance traversed by the WCV up to time t
$\mathcal{S}_m$	The m-th segment of path $\mathcal{P}$
$U_{\max}$	Maximum output power from the WCV for a single sensor node
$U_{iB}(p)$	Power reception rate at node i when the WCV is at p
$U_{iB}(p_m)$	$= \min_{p \in \mathcal{S}_m}\{U_{iB}(p)\}$
W	$= \frac{1}{V}$
$(x, y)(t)$	Coordinates of $p(t)$
δ	A threshold of power reception rate
$\omega(p)$	Aggregate amount of time the WCV stops at point $p \in \mathcal{P}$
$\omega(p_m)$	Stopping time that the WCV is in segment $\mathcal{S}_m$
$\tau(p_m)$	Total time that the WCV spends at p_m (including stopping time and traveling time)
$\mu(\cdot)$	The efficiency function of WET from the WCV to a sensor node
$\psi_{\text{CoP-t}}$ (or $\psi^*_{\text{CoP-t}}$)	A feasible solution (or an optimal solution) to Problem CoP-t
$\psi_{\text{CoP-s}}$ (or $\psi^*_{\text{CoP-s}}$)	A feasible solution (or an optimal solution) to Problem CoP-s
$\eta_{\text{CoP-s}}$ (or $\eta^*_{\text{CoP-s}}$)	The objective value achieved by $\psi_{\text{CoP-s}}$ (or $\psi^*_{\text{CoP-s}}$)

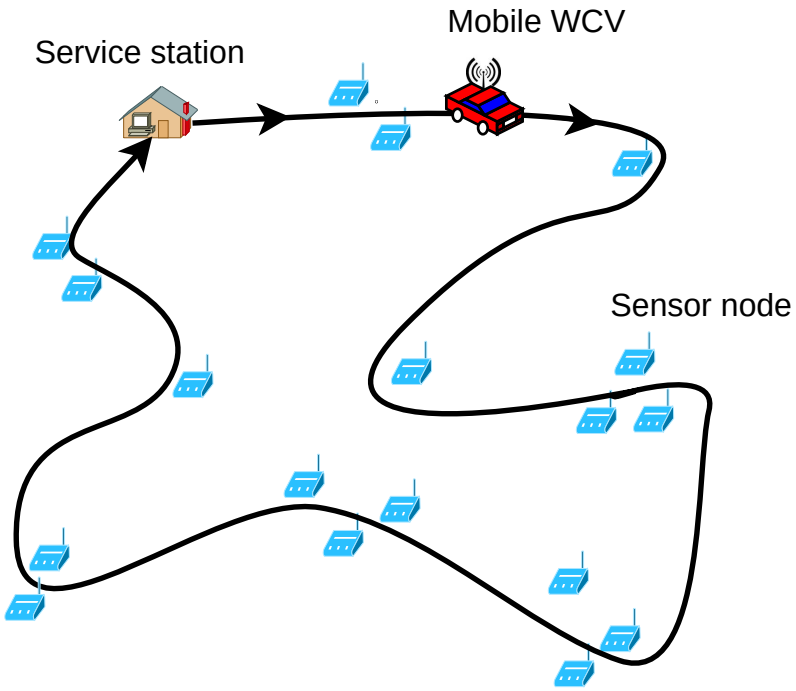

Figure 4.1: A WCV, where a MBS and a wireless charger are located, traveling in a WSN.

4.3.1 WCV and Traveling Path

Suppose we have a sensor network $\mathcal{N}$ deployed over a two-dimensional area, with the location of each node $i \in \mathcal{N}$ being (x_i, y_i). A WCV is employed to charge sensor nodes in the network. This WCV starts from a service station, travels along a pre-planned path in the area and returns to the service station at the end of its trip. While on its path, the WCV can make a number of stops and charge sensor nodes near those stops (see Fig. 4.1). The detailed energy charging model will be described in Section 4.3.4.

Denote $\mathcal{P}$ as the traveling path and τ as the total amount of time for the WCV to complete the trip. Then τ includes three components:

- The total traveling time along path $\mathcal{P}$ is $D_{\mathcal{P}}/V$, where $D_{\mathcal{P}}$ is the distance of path $\mathcal{P}$ and V is the traveling speed of WCV.
- The vacation time τ_{vac}, which refers to the amount of time that the WCV stays at the service

station (at point p_{vac}) before leaving for the next trip.

- The total stopping time along path $\mathcal{P}$. Denote $\omega(p)$ as the aggregate amount of time the WCV stops at point $p \in \mathcal{P}$. Since the WCV may stops at p more than once during τ, we have:

$$\omega(p) = \int_{\{t\in[0,\tau]:(x,y)(t)=p\}} 1 \ \mathrm{d}t \ , \tag{4.1}$$

  where $(x, y)(t)$ is the location of the WCV at time t. Then the total stopping time is $\sum_{p\in\mathcal{P},\, p\neq p_{\text{vac}}}^{\omega(p)>0} \omega(p)$.

Then we have:

$$\tau = \frac{D_{\mathcal{P}}}{V} + \tau_{\text{vac}} + \sum_{p\in\mathcal{P},\, p\neq p_{\text{vac}}}^{\omega(p)>0} \omega(p) \ . \tag{4.2}$$

4.3.2 Mobile Base Station and Data Flow Routing

As discussed, we assume that the base station is co-located at the WCV. Therefore, the base station is also mobile and serves as the sink node for all data collected by the WSN. To conserve energy, multi-hop data routing is employed among the sensor nodes in the network.

Suppose each sensor node i produces its local data with a constant rate R_i (in b/s), $i \in \mathcal{N}$. Denote $f_{ij}(t)$ and $f_{iB}(t)$ as the flow rates from node i to node j and the base station at time t, respectively. Then we have the following flow balance at each sensor node i:

$$\sum_{k\in\mathcal{N}}^{k\neq i} f_{ki}(t) + R_i = \sum_{j\in\mathcal{N}}^{j\neq i} f_{ij}(t) + f_{iB}(t) \quad (i \in \mathcal{N}) \ . \tag{4.3}$$

Note that we are dealing with real-time flow routing rather than delay-tolerant data MULEs [50]

or message ferry [74] type of communications.

4.3.3 Sensor Energy Consumption

At a sensor node, we assume that communications are the dominant source for the node's energy consumption. Denote C_{ij} as the energy consumption rate for transmitting one unit of data flow from sensor node i to sensor node j. Then C_{ij} can be modeled as [11, 23]:

$$C_{ij} = \beta_1 + \beta_2 D_{ij}^{\alpha} ,$$

where D_{ij} is the distance between nodes i and j, β_1 and β_2 are constant terms, and α is the path loss index. Suppose all sensor nodes are stationary. Then the inter-sensor distance D_{ij} and C_{ij} are all constants.

Denote $C_{iB}(p(t))$ as the energy consumption rate for transmitting one unit of data flow from sensor node i to base station B when B is at location $p(t)$. Then we have

$$C_{iB}(p(t)) = \beta_1 + \beta_2 \left[\sqrt{(x(t) - x_i)^2 + (y(t) - y_i)^2}\right]^{\alpha} , \tag{4.4}$$

where $(x(t), y(t))$ and (x_i, y_i) are the coordinates of $p(t)$ and node i, respectively. Note that unlike the C_{ij} parameters, which are all constants, $C_{iB}(p(t))$ varies with the base station's location over time.

Denote ρ as the rate of energy consumption for receiving one unit of data flow. Then the total energy consumption rate for both transmission and reception at node i, denoted as $r_i(t)$, is

$$r_i(t) = \rho \sum_{k \in \mathcal{N}}^{k \neq i} f_{ki}(t) + \sum_{j \in \mathcal{N}}^{j \neq i} C_{ij} \cdot f_{ij}(t) + C_{iB}(p(t)) \cdot f_{iB}(t) \quad (i \in \mathcal{N}, t \geq 0) . \tag{4.5}$$

4.3.4 Energy Charging Model

We assume that the WCV can only perform its charging function when it makes a full stop somewhere along path $\mathcal{P}$ (except p_{vac}). Denote $U_{iB}(p)$ as the power reception rate at node i when the WCV is located at $p \in \mathcal{P}$. Denote the efficiency of wireless charging by $\mu(D_{iB}(p))$, which is a decreasing function of $D_{iB}(p)$, the distance from node i to the WCV when the WCV is at p. Then the wireless charging model is:

$$U_{iB}(p) = \begin{cases} \mu(D_{iB}(p)) \cdot U_{\text{max}} & \text{if } D_{iB}(p) \leq D_\delta \\ 0 & \text{if } D_{iB}(p) > D_\delta \ , \end{cases} \tag{4.6}$$

where U_{max} is the maximum output power for a single sensor node and D_δ is the charging range of the WCV, below which wireless charging cannot be performed. In other words, D_δ is defined in a way such that the power reception rate at a sensor node is at least over a threshold value δ. We assume that a sensor node can be charged only if it is within a distance of D_δ from path $\mathcal{P}$.

When multiple nodes receive power from the WCV simultaneously, interference may occur due to resonant coupling between receiving nodes. The interference can be handled by adjusting the resonance frequencies at the source and receiving nodes [1].

4.4 Energy Criteria for Cycles

We assume that the WCV follows a fixed travel schedule along $\mathcal{P}$ with a period of τ. Then we have $p(t) = p(t + k\tau)$ for $0 \leq t \leq \tau$, $k = 1, 2, \cdots$. Further, we assume that the flow routing in the network also follows a periodic cycle, i.e., $f_{ij}(t) = f_{ij}(t + k\tau)$ and $f_{iB}(t) = f_{iB}(t + k\tau)$ for $0 \leq t \leq \tau$, $k = 1, 2, \cdots$. Then by (4.5), the energy consumption rate at each node also follows a periodic cycle, i.e., $r_i(t) = r_i(t + k\tau)$ for $0 \leq t \leq \tau$, $i \in \mathcal{N}$. Since the WCV's charging behavior only depends on its travel schedule, then the charging behavior also forms a periodic cycle. In summary, the travel schedule of the WCV, its charging behavior along its path, flow routing among

the nodes, and energy consumption at each node are all cyclic and repeat themselves with a period of τ.

Suppose that each sensor node has a battery capacity of $E_{\max}$ and is fully charged initially. Denote $E_{\min}$ as the minimum energy at a sensor node battery for it to be operational. We are interested in developing a particular travel cycle so that the energy level at each sensor node at time t, denoted as $e_i(t)$, $i \in \mathcal{N}$, never falls below $E_{\min}$. In the following, we will offer two constraints for the *first* cycle. We will show that once these two constraints hold for the first cycle, then $e_i(t) \geq E_{\min}$ for $t \geq \tau$, i.e., all future cycles.

The first constraint ensures that $e_i(t)$, which starts from $E_{\max}$ at $t = 0$, will not fall below $E_{\min}$ at $t = \tau$,

$$E_{\max} - \Big\{ \int_{\{t\in[0,\tau]:\omega(p(t))=0\}} r_i(t)\ \mathrm{d}t + \int_{\{t\in[0,\tau]:\omega(p(t))>0,\ D_{iB}(p(t))>D_\delta\}} r_i(t)\ \mathrm{d}t \Big\} \geq E_{\min} \quad (i \in \mathcal{N}), \tag{4.7}$$

where $\int_{\{t\in[0,\tau]:\omega(p(t))=0\}} r_i(t)\ \mathrm{d}t$ is the amount of energy consumed at node i when the WCV is moving along path $\mathcal{P}$ while $\int_{\{t\in[0,\tau]:\omega(p(t))>0,\ D_{iB}(p(t))>D_\delta\}} r_i(t)\ \mathrm{d}t$ is the amount of energy consumed at node i when the WCV is making stops but node i is outside the WCV's charging range.

The second constraint ensures that $e_i(t)$, which starts from $E_{\max}$ at $t = 0$, will be charged back to $E_{\max}$ before the end of the first cycle τ. We have

$$\int_0^\tau r_i(t)\ \mathrm{d}t \leq \sum_{p\in\mathcal{P}}^{\omega(p)>0,\ D_{iB}(p)\leq D_\delta} U_{iB}(p)\cdot\omega(p) \quad (i \in \mathcal{N}), \tag{4.8}$$

where the left-hand side is the amount of energy consumed at node i during τ and the right-hand side is the maximum possible amount of energy received by node i in a cycle. Note that the actual

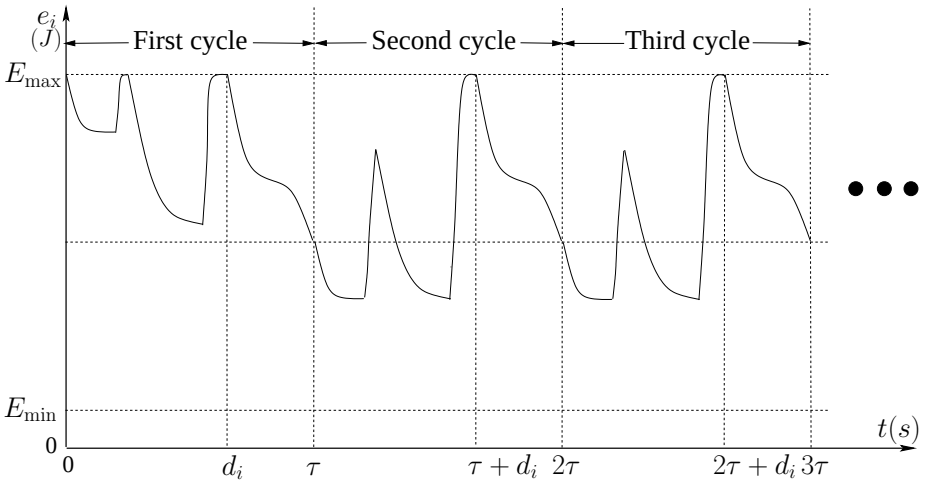

Figure 4.2: The energy level of node $i \in \mathcal{N}$ during the first three cycles.

amount of energy received by node i in the first cycle may be less than the right-hand side due to potential battery overflow.[2]

Note that (4.7) and (4.8) characterize the energy consumption and reception in the first cycle. The following lemma says that if both (4.7) and (4.8) hold for the first cycle, then we have $e(t) \geq E_{\min}$ for all cycles.

Lemma 4.1 (Energy Criteria) *If both (4.7) and (4.8) are satisfied for the first cycle, then* $e_i(t) \geq E_{min}$ *for all* $t \geq 0$, $i \in \mathcal{N}$.

Proof We consider the first cycle and the other cycles, separately. The first cycle (i.e., $t \in [0, \tau]$) is solely considered since it starts with $E_{\max}$, and the succeeding cycle (i.e., $t \in [k\tau, (k+1)\tau]$, $k \in \mathbb{N}^+$) starts with a non-full energy level. Note that for all cycles, the time intervals τ, $D_{\mathcal{P}}$, V, τ_{vac}, and $\omega(p)$ are identical, and the location $p(t)$, the flow rates $f_{ij}(t)$ and $f_{iB}(t)$, and the power consumption rate $r_i(t)$ repeat in a cycle of τ.

For the first cycle, $e_i(0) = E_{\max}$, $i \in \mathcal{N}$. Considering that node i may be under saturation state, denote $\gamma(t)$ as the last time before t such that $E(\gamma(t)) = E_{\max}$, i.e., $e(t') < E_{\max}$ for $\gamma(t) < t' \leq t$.

[2]Once a battery is charged to $E_{\max}$, its energy level cannot be further increased.

Since there is no battery overflow over $(\gamma(t), t]$, this yields

$$e_i(t) = \min\{E_{\max}, E_{\max} - \int_{\{t' \in [\gamma(t),t]\}} r_i(t')\ \mathrm{d}t' + \int_{\{t' \in [\gamma(t),t]:\omega(p(t'))>0,\ D_{iB}(p(t')) \le D_\delta\}} U_{iB}(p(t'))\ \mathrm{d}t'\}\ . \tag{4.9}$$

There always exists a $\gamma(t)$ for $t \in (0, \tau]$ as $e_i(0) = E_{\max}$.

To show that $e_i(t) \ge E_{\min}$, $t \in [0, \tau]$, it is sufficient to show that the second item on the right-hand side of (4.9) not below $E_{\min}$. We have

$$\begin{aligned}
& E_{\max} - \int_{\{t' \in [\gamma(t),t]\}} r_i(t')\ \mathrm{d}t' + \int_{\{t' \in [\gamma(t),t]:\omega(p(t'))>0,\ D_{iB}(p(t')) \le D_\delta\}} U_{iB}(p(t'))\ \mathrm{d}t' \\
= \ & E_{\max} - \Big(\int_{\{t' \in [\gamma(t),t]:\omega(p(t'))=0\}} r_i(t')\ \mathrm{d}t' + \int_{\{t' \in [\gamma(t),t]:\omega(p(t'))>0,\ D_{iB}(p(t'))>D_\delta\}} r_i(t')\ \mathrm{d}t' \\
& + \int_{\{t' \in [\gamma(t),t]:\omega(p(t'))>0,\ D_{iB}(p(t')) \le D_\delta\}} r_i(t')\ \mathrm{d}t' \Big) + \int_{\{t' \in [\gamma(t),t]:\omega(p(t'))>0,\ D_{iB}(p(t')) \le D_\delta\}} U_{iB}(p(t'))\ \mathrm{d}t' \\
= \ & E_{\max} - \Big(\int_{\{t' \in [\gamma(t),t]:\omega(p(t'))=0\}} r_i(t')\ \mathrm{d}t' + \int_{\{t' \in [\gamma(t),t]:\omega(p(t'))>0,\ D_{iB}(p(t'))>D_\delta\}} r_i(t')\ \mathrm{d}t' \Big) \\
& + \int_{\{t' \in [\gamma(t),t]:\omega(p(t'))>0,\ D_{iB}(p(t')) \le D_\delta\}} \Big[U_{iB}(p(t')) - r_i(t') \Big]\ \mathrm{d}t' \\
\ge \ & E_{\max} - \Big(\int_{\{t' \in [\gamma(t),t]:\omega(p(t'))=0\}} r_i(t')\ \mathrm{d}t' + \int_{\{t' \in [\gamma(t),t]:\omega(p(t'))>0,\ D_{iB}(p(t'))>D_\delta\}} r_i(t')\ \mathrm{d}t' \Big) \\
\ge \ & E_{\max} - \Big(\int_{\{t' \in [0,t]:\omega(p(t'))=0\}} r_i(t')\ \mathrm{d}t' + \int_{\{t' \in [0,t]:\omega(p(t'))>0,\ D_{iB}(p(t'))>D_\delta\}} r_i(t')\ \mathrm{d}t' \Big) \\
\ge \ & E_{\min},
\end{aligned} \tag{4.10}$$

where the first equality holds since the amount of energy consumed by node i is divided into three parts, i.e., energy consumed when the WCV travels, sojourns while charging other nodes or at the service station, and charging node i, the third inequality holds due to $U_{iB}(p(t')) - r_i(t') \ge 0$, the fourth inequality holds since $[\gamma(t), t] \subseteq [0, t]$ and $r_i(t) \ge 0$, and the last inequality holds by (4.7).

We next show that $e_i(t) \geq E_{\min}$ in the subsequent cycles, i.e., $t \geq \tau$. It is sufficient to show that $e_i(t) \geq E_{\min}$ for $t \in [\tau, 2\tau]$, and then show that $e_i(2\tau) = e_i(\tau)$. It will follow that $e_i(t) \geq E_{\min}$ for all $t \geq \tau$ due to periodicity.

To show that $e_i(t) \geq E_{\min}$, $t \in [\tau, 2\tau]$, for each $i \in \mathcal{N}$, we need to show that node i can be charged back to $E_{\max}$ in both the first and the second cycle. For the first cycle, we show that there exists at least one time instance $\tilde{t} \in (0, \tau]$ such that $E(\tilde{t}) = E_{\max}$ (See Fig. 4.2). This can be proved by contradiction. Suppose that $e_i(t) < E_{\max}$ for $t \in (0, \tau]$. That is, there is no battery overflow and thus for $t \in (0, \tau]$, we have

$$e_i(t) = E_{\max} - \int_{\{t' \in [0,t]\}} r_i(t')\ \mathrm{d}t' + \int_{\{t' \in [0,t]: \omega(p(t'))>0,\ D_{iB}(p(t')) \leq D_\delta\}} U_{iB}(p(t'))\ \mathrm{d}t' < E_{\max}\ ,$$

or equivalently,

$$\int_{\{t' \in [0,t]: \omega(p(t'))>0,\ D_{iB}(p(t')) \leq D_\delta\}} U_{iB}(p(t'))\ \mathrm{d}t' < \int_{\{t' \in [0,t]\}} r_i(t')\ \mathrm{d}t'\ .$$

This contradicts the assumption that (4.8) is satisfied. Therefore, there exists at least one time instance $\tilde{t} \in (0, \tau]$ such that $E(\tilde{t}) = E_{\max}$. Let T_i be the $\tilde{t}$ with the largest value.

For the second cycle, we need the following intermediate result.

Proposition 4.1 *We have $E(T_i + \tau) = E_{max}$, where $0 < T_i \leq \tau$.*

Now we prove this intermediate result. By the same token as for $(0, \tau]$, we can show that there exists at least one time instance $\tilde{t} \in (T_i, T_i + \tau]$ such that $E(\tilde{t}) = E_{\max}$ due to $E(T_i) = E(0) = E_{\max}$ and energy charging/consumption periodicity. Since T_i is the last time in the first cycle when node i is recharged back to $E_{\max}$, the range of $\tilde{t}$ can be narrowed as $(\tau, T_i + \tau]$.

Next we prove that $E(T_i + \tau) = E_{\max}$ by contradiction. Suppose that $E(T_i + \tau) < E_{\max}$. Since we have shown that there exist a $\tilde{t} \in (\tau, T_i + \tau]$ so that $E(\tilde{t}) = E_{\max}$, we have $\tilde{t} \in (\tau, T_i + \tau)$.

To be specific, we let $\tilde{t} = T_i' + \tau$ be the last time instance, where $0 < T_i' < T_i$. By having $E(T_i' + \tau) = E_{\max}$, it is straightforward to have $E(T_i') = E_{\max}$ since for a node's initial energy level, $E(0) = E_{\max} \geq E(\tau)$.

In the first cycle, the energy level reaches $E_{\max}$ at both T_i' and T_i. In the second cycle, the energy level also reaches $E_{\max}$ at $T_i' + \tau$. Due to periodicity, we have $E(T_i + \tau) = E_{\max}$, which contradicts the assumption. That is, we must have $E(T_i + \tau) = E_{\max}$.

Subsequently, we show $e_i(t) \geq E_{\min}$ for $t \in [\tau, T_i + \tau]$ and $t \in [T_i + \tau, 2\tau]$, respectively. For $t \in [\tau, T_i + \tau]$, we have

$$\begin{aligned} e_i(t) &\geq E_{\max} - \left\{ \int_{\{t' \in [\tau,t]:\omega(p(t'))=0\}} r_i(t')\ \mathrm{d}t' + \int_{\{t' \in [\tau,t]:\omega(p(t'))>0,\ D_{iB}(p(t'))>D_\delta\}} r_i(t')\ \mathrm{d}t' \right\} \\ &= E_{\max} - \left\{ \int_{\{t' \in [0,t-\tau]:\omega(p(t'))=0\}} r_i(t')\ \mathrm{d}t' + \int_{\{t' \in [0,t-\tau]:\omega(p(t'))>0,\ D_{iB}(p(t'))>D_\delta\}} r_i(t')\ \mathrm{d}t' \right\} \\ &\geq E_{\max} - \left\{ \int_{\{t' \in [0,\tau]:\omega(p(t'))=0\}} r_i(t')\ \mathrm{d}t' + \int_{\{t' \in [0,\tau]:\omega(p(t'))>0,\ D_{iB}(p(t'))>D_\delta\}} r_i(t')\ \mathrm{d}t' \right\} \\ &\geq E_{\min}, \end{aligned} \tag{4.11}$$

where the first inequality holds since the nonnegative amount of energy received over $[\tau, t]$ is not counted, the second equality holds due to $p(t) = p(t - \tau)$ and $r_i(t) = r_i(t - \tau)$ for $t \in [\tau, 2\tau]$, the third inequality holds due to $[0, t - \tau] \subseteq [0, \tau]$ and $r_i(t) \geq 0$, and the last inequality holds due to (4.7).

In addition to $t \in [\tau, T_i + \tau]$, we show that $e_i(t) \geq E_{\min}$ for $t \in [T_i + \tau, 2\tau]$. Since T_i is the last moment over $[0, \tau]$ that node i is charged back to $E_{\max}$, we further have that $T_i + \tau$ is the last moment with battery fully recharged over $[\tau, 2\tau]$ by contradiction (i.e., if not true, then T_i is not

the last moment with battery fully recharged over $[0, \tau]$). Thus, we have

$$\begin{aligned} e_i(t) &= E(T_i + \tau) - \int_{\{t' \in [T_i+\tau, t]\}} r_i(t')\ \mathrm{d}t' + \int_{\{t' \in [T_i+\tau, t]: \omega(p(t'))>0,\ D_{iB}(p(t')) \le D_\delta\}} U_{iB}(p(t'))\ \mathrm{d}t' \\ &= e_i(T_i) - \int_{\{t' \in [T_i, t-\tau]\}} r_i(t')\ \mathrm{d}t' + \int_{\{t' \in [T_i, t-\tau]: \omega(p(t'))>0,\ D_{iB}(p(t')) \le D_\delta\}} U_{iB}(p(t'))\ \mathrm{d}t' \\ &= e_i(t - \tau) \qquad (4.12) \\ &\ge E_{\text{min}}\ , \end{aligned}$$

where the second equality holds due to $E(T_i + \tau) = E_{\text{max}} = E(T_i)$, $p(t) = p(t - \tau)$ and $r_i(t) = r_i(t - \tau)$ for $t \in [\tau, 2\tau]$, and the last inequality holds by (4.10).

By (4.12), we can easily deduce that $e_i(2\tau) = e_i(\tau)$. Therefore, if both the constraints (4.7) and (4.8) are satisfied, then $e_i(t) \ge E_{\text{min}}$ for all $t \ge 0$, $i \in \mathcal{N}$. □

4.5 Problem Formulation

In Section 4.4, we explained energy criteria for cycles. Under Lemma 4.1, we showed that under certain conditions, $e_i(t) \ge E_{\text{min}}$ for all $t \ge 0$, $i \in \mathcal{N}$. In addition to these constraints, we can also consider optimizing some global performance objective. In particular, we want to minimize energy consumption of the entire system, which encompasses all energy consumption at the WCV.

Since the energy consumed to carry the WCV to move along $\mathcal{P}$ is the dominant source of energy consumption (when compared its wireless charging to sensor nodes, see Section 3.3), we aim to minimize the fraction of time that the WCV is outside its service station, i.e.,

$$\frac{D_{\mathcal{P}}/V + \sum_{p \in \mathcal{P},\ p \ne p_{\text{vac}}}^{\omega(p)>0} \omega(p)}{\tau}\ .$$

It is interesting that, by (4.2), minimizing $\frac{D_{\mathcal{P}}/V + \sum_{p \in \mathcal{P},\ p \ne p_{\text{vac}}}^{\omega(p)>0} \omega(p)}{\tau}$ is equivalent to maximizing $\frac{\tau_{\text{vac}}}{\tau}$,

which is the percentage of time that the WCV is on vacation at its service station. Therefore, we have the following Co-location Problem based on time (CoP-t):

$$
\begin{array}{rl}
\textbf{CoP-t:} & \\
\text{maximize} & \frac{\tau_{\text{vac}}}{\tau} \\
\text{subject to} & \text{Time constraints: (4.1), (4.2);} \\
& \text{Flow routing constraints: (4.3);} \\
& \text{Energy consumption model: (4.4), (4.5);} \\
& \text{Energy criteria constraints: (4.7), (4.8);} \\
\multicolumn{2}{c}{\tau, \tau_{\text{vac}}, \omega(p) \geq 0, (x,y)(t) \in \mathcal{P} \quad (p \in \mathcal{P}, 0 \leq t \leq \tau);} \\
\multicolumn{2}{c}{f_{ij}(t), f_{iB}(t), C_{iB}(p(t)), r_i(t) \geq 0, \ (i,j \in \mathcal{N}, i \neq j, 0 \leq t \leq \tau)\ .}
\end{array}
$$

In this formulation, $\mathcal{P}$, $D_{\mathcal{P}}$, V, R_i, β_1, β_2, α, x_i, y_i, ρ, C_{ij}, E_{max}, and E_{min} are given *a priori*, and $U_{iB}(p)$ can be computed by (4.6). The time intervals τ, τ_{vac}, and $\omega(p)$, the WCV's location $(x,y)(t)$, the flow rates $f_{ij}(t)$ and $f_{iB}(t)$, the unit cost rate $C_{iB}(p(t))$, and the power consumption rate $r_i(t)$ are optimization variables. Among these variables, there are three sets of variables that constitute the solution space: (i) the WCV's location (i.e., $(x,y)(t)$); (ii) the WCV's sojourn time at each location $p \in \mathcal{P}$ and $p \neq p_{\text{vac}}$ (i.e., $\omega(p)$) or vacation time at the service station (i.e., τ_{vac}); (iii) the corresponding flow routing (i.e., $f_{ij}(t)$ and $f_{iB}(t)$). Problem CoP-t is a continuous-time nonlinear program [71], and is NP-hard in general.

4.6 Downsizing Solution Space: A Location-based Formulation

Roadmap. CoP-t is a general formulation of our problem. It is difficult as its variables are time-dependent (e.g., $(x,y)(t)$, $f_{ij}(t)$). In this general formulation, CoP-t allows data flow routing and energy consumption of sensor nodes to vary over time, even when the WCV visits the same location.

In this section, we consider a special case of Problem CoP-t, where data flow routing and energy consumption of sensor nodes only depend on the WCV's location. That is, as long as the WCV

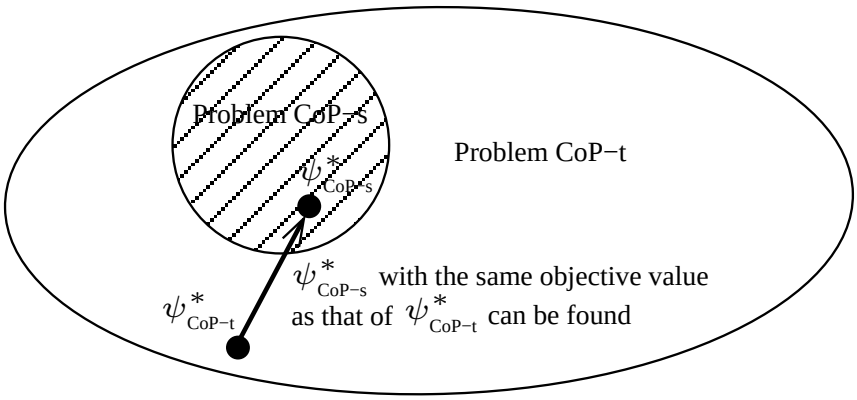

Figure 4.3: Solution space for Problems CoP-t and CoP-s. $\psi^*_{\text{CoP-t}}$ and $\psi^*_{\text{CoP-s}}$ are optimal solutions to CoP-t and CoP-s, respectively.

visits a location $p \in \mathcal{P}$, the data flow routing and energy consumption of sensor nodes are the same regardless when the WCV visits this location. This location (space)-dependent problem is a special case of Problem CoP-t. We denote this problem as CoP-s. The solution space for CoP-s and CoP-t is shown in Fig. 4.3, in which the solution space for CoP-s is completely contained in that for CoP-t.

We will show that the optimal objective value for CoP-s is the same as that for CoP-t, despite that its solution space is smaller (Theorem 4.1). This result is significant as it allows us to study CoP-s, which has a simpler formulation that only involves location-dependent variables.

Location-dependent Formulation. We now formulate CoP-s. First, we need some new notations. Denote $f_{ij}(p)$ and $f_{iB}(p)$ as flow rates from sensor node i to sensor node j and to the base station when the WCV is at location $p \in \mathcal{P}$, respectively. Then (4.3) is rewritten as

$$\sum_{k\in\mathcal{N}}^{k\neq i} f_{ki}(p) + R_i = \sum_{j\in\mathcal{N}}^{j\neq i} f_{ij}(p) + f_{iB}(p) \quad (i \in \mathcal{N}, p \in \mathcal{P}). \tag{4.13}$$

Similarly, denote $C_{iB}(p)$ and $r_i(p)$ as the energy consumption for transmitting one unit of data flow from node i to the base station and the energy consumption rate at node i when the WCV is

at location $p \in \mathcal{P}$, respectively. Then (4.5) can be rewritten as:

$$r_i(p) = \rho \sum_{k \in \mathcal{N}}^{k \neq i} f_{ki}(p) + \sum_{j \in \mathcal{N}}^{j \neq i} C_{ij} \cdot f_{ij}(p) + C_{iB}(p) \cdot f_{iB}(p) \quad (i \in \mathcal{N}, p \in \mathcal{P}) \; . \tag{4.14}$$

Now we rewrite (4.7) and (4.8) into location-based constraints. We start with (4.8). In (4.8), $\int_0^\tau r_i(t) \; \mathrm{d}t$ can be split into two parts:

- energy consumed when WCV makes stops (including vacation at the service station), which is, $r_i(p_{\text{vac}}) \cdot \tau_{\text{vac}} + \sum_{p \in \mathcal{P},\, p \neq p_{\text{vac}}}^{\omega(p)>0} r_i(p) \cdot \omega(p)$;
- energy consumed when WCV travels along $\mathcal{P}$, i.e.,

$$\int_{t \in [0,\tau]}^{\omega(p(t))=0} r_i(t) \; \mathrm{d}t = \int_{s \in [0, D_{\mathcal{P}}]}^{\omega(p(s))=0} r_i(p(s)) \, \frac{dt}{ds} \, ds \; , \tag{4.15}$$

  where $s \in [0, D_{\mathcal{P}}]$ is the distance traversed by the WCV along $\mathcal{P}$ (starting from its service station), and $p(s)$ is the WCV's location corresponding to s. Denote $W = \lim_{\Delta \to 0} \frac{\Delta t}{\Delta s}$. Then $W = \frac{1}{V}$, and (4.15) can be rewritten as:

$$\int_{t \in [0,\tau]}^{\omega(p(t))=0} r_i(t) \; \mathrm{d}t = \int_{s \in [0, D_{\mathcal{P}}]}^{\omega(p(s))=0} W \cdot r_i(p(s)) ds \; .$$

Based on the above discussion, (4.8) can be rewritten as:

$$\begin{aligned} r_i(p_{\text{vac}}) \cdot \tau_{\text{vac}} + \sum_{p \in \mathcal{P},\, p \neq p_{\text{vac}}}^{\omega(p)>0} r_i(p) \cdot \omega(p) + \int_{s \in [0, D_{\mathcal{P}}]}^{\omega(p(s))=0} W \cdot r_i(p(s)) ds \\ \leq \sum_{p \in \mathcal{P}}^{\omega(p)>0,\; D_{iB}(p) \leq D_\delta} U_{iB}(p) \cdot \omega(p) \quad (i \in \mathcal{N}), \end{aligned} \tag{4.16}$$

which is a location-dependent formulation.

Similarly, (4.7) can be rewritten as:

$$r_i(p_{\text{vac}}) \cdot \tau_{\text{vac}} + \sum_{p \in \mathcal{P},\, p \neq p_{\text{vac}}}^{\omega(p)>0,\, D_{iB}(p)>D_\delta} r_i(p) \cdot \omega(p)$$

$$+ \int_{s \in [0, D_{\mathcal{P}}]}^{\omega(p(s))=0} W \cdot r_i(p(s)) ds \leq E_{\text{max}} - E_{\text{min}} \quad (i \in \mathcal{N}). \tag{4.17}$$

We now have a formulation for CoP-s, which only involves location-dependent variables.

CoP-s:

$$\begin{aligned}
\text{maximize} \quad & \tfrac{\tau_{\text{vac}}}{\tau} \\
\text{subject to} \quad & \text{Time constraint: (4.2);} \\
& \text{Flow routing constraints: (4.13);} \\
& \text{Energy consumption model: (4.14);} \\
& \text{Energy criteria constraints: (4.16), (4.17);} \\
& \tau, \tau_{\text{vac}}, \omega(p) \geq 0 \qquad (p \in \mathcal{P}); \\
& f_{ij}(p), f_{iB}(p), r_i(p) \geq 0 \quad (i, j \in \mathcal{N}, i \neq j, p \in \mathcal{P}).
\end{aligned}$$

Proof of Equivalence. We now show that the optimal objective value of CoP-s is the same as that for CoP-s (see Fig. 4.3). For Problem CoP-t, denote $\psi_{\text{CoP-t}}$ and $\psi^*_{\text{CoP-t}}$ as a feasible solution and an optimal solution, respectively. Similarly, for Problem CoP-s, denote $\psi_{\text{CoP-s}}$ and $\psi^*_{\text{CoP-s}}$ as a feasible solution and an optimal solution, respectively.

Theorem 4.1 *The optimal objectives achieved by $\psi^*_{\text{CoP-s}}$ and $\psi^*_{\text{CoP-t}}$ are identical.*

The proof of this theorem is based on two results. First, we show that the optimal objective achieved by $\psi^*_{\text{CoP-t}}$ is no less than that achieved by solution $\psi^*_{\text{CoP-s}}$. This is straightforward as CoP-s is a subproblem of CoP-t. Second, we show that the converse is also true. Instead of considering an optimal solution, we will show that for *any* objective value achieved by a feasible solution $\psi_{\text{CoP-t}}$, we can always find a feasible solution $\psi_{\text{CoP-s}}$, which achieves the same objective value (Lemma 4.2). If this is true, in the special case when the feasible solution $\psi_{\text{CoP-t}}$ is the optimal solution $\psi^*_{\text{CoP-t}}$, the objective by $\psi^*_{\text{CoP-t}}$ can also be achieved by some feasible solution $\psi_{\text{CoP-s}}$.

Lemma 4.2 *Given a feasible $\psi_{\text{CoP-t}}$, we can construct a feasible $\psi_{\text{CoP-s}}$ with the same objective value.*

Proof Our proof is based on construction. Given a path $\mathcal{P}$ and $\psi_{\text{CoP}} = (\tau, \tau_{\text{vac}}, \omega(p), (x,y)(t), f_{ij}(t), f_{iB}(t), C_{iB}(t), r_i(t))$, we let the WCV adopt the same path $\mathcal{P}$ and construct a solution $\psi_{\text{CoP-s}} = (\hat{\tau}, \hat{\tau}_{\text{vac}}, \hat{\omega}(p), \hat{f}_{ij}(p), \hat{f}_{iB}(p), \hat{r}_i(p))$ by letting $\hat{\tau} = \tau$, $\hat{\tau}_{\text{vac}} = \tau_{\text{vac}}$, $\hat{\omega}(p) = \omega(p)$, and considering two cases:

- If $\omega(p) > 0$, i.e., the WCV has sojourned in location p, we set

$$\hat{f}_{ij}(p) = \frac{\int_{\{t\in[0,\tau]:(x,y)(t)=p\}} f_{ij}(t)\ \mathrm{d}t}{\hat{\omega}(p)} \tag{4.18}$$

$$\hat{f}_{iB}(p) = \frac{\int_{\{t\in[0,\tau]:(x,y)(t)=p\}} f_{iB}(t)\ \mathrm{d}t}{\hat{\omega}(p)}\ . \tag{4.19}$$

- If $\omega(p) = 0$, i.e., the WCV traverses p (maybe multiple times) but never sojourns, we set

$$\hat{f}_{ij}(p) = \frac{\sum_{s\in\mathcal{Z}(p)} f_{ij}(t(s))}{|\mathcal{Z}(p)|} \tag{4.20}$$

$$\hat{f}_{iB}(p) = \frac{\sum_{s\in\mathcal{Z}(p)} f_{iB}(t(s))}{|\mathcal{Z}(p)|}\ , \tag{4.21}$$

  where $\mathcal{Z}(p)$ is denoted as the set of distances $s \in [0, D_{\mathcal{P}}]$ that correspond to the same location p, and $t(s)$ is denoted as time instance at distance s.

For either $\omega(p) > 0$ or $\omega(p) = 0$, we set $\hat{r}_i(p)$ by (4.14).

Now, all we need to do is to verify that $\psi_{\text{CoP-s}}$ is a feasible solution to Problem CoP-s and to show that the objective value of $\psi_{\text{CoP-s}}$ is equivalent to that of ψ_{CoP}. To show the feasibility of $\psi_{\text{CoP-s}}$, we need to verify that $\psi_{\text{CoP-s}}$ satisfies Constraints (4.2), (4.13), (4.14), (4.16), and (4.17). Since (4.2) remains unchanged, and $\hat{\tau} = \tau$, $\hat{\tau}_{\text{vac}} = \tau_{\text{vac}}$, $\hat{\omega}(p) = \omega(p)$, we have that $\psi_{\text{CoP-s}}$ satisfies (4.2). To

verify (4.13) for those $p \in \mathcal{P}$ with $\omega(p) > 0$, we have

$$\begin{aligned}
\sum_{k\in\mathcal{N}}^{k\neq i} \hat{f}_{ki}(p) + G_i &= \sum_{k\in\mathcal{N}}^{k\neq i} \frac{\int_{\{t\in[0,\tau]:(x,y)(t)=p\}} f_{ki}(t)\ \mathrm{d}t}{\hat{\omega}(p)} + \frac{\int_{\{t\in[0,\tau]:(x,y)(t)=p\}} G_i\ \mathrm{d}t}{\hat{\omega}(p)} \\
&= \frac{\int_{\{t\in[0,\tau]:(x,y)(t)=p\}} \left[\sum_{k\in\mathcal{N}}^{k\neq i} f_{ki}(t) + G_i\right]\ \mathrm{d}t}{\hat{\omega}(p)} \\
&= \frac{\int_{\{t\in[0,\tau]:(x,y)(t)=p\}} \left[\sum_{j\in\mathcal{N}}^{j\neq i} f_{ij}(t) + f_{iB}(t)\right]\ \mathrm{d}t}{\hat{\omega}(p)} \\
&= \sum_{j\in\mathcal{N}}^{j\neq i} \frac{\int_{\{t\in[0,\tau]:(x,y)(t)=p\}} f_{ij}(t)\ \mathrm{d}t}{\hat{\omega}(p)} + \frac{\int_{\{t\in[0,\tau]:(x,y)(t)=p\}} f_{iB}(t)\ \mathrm{d}t}{\hat{\omega}(p)} \\
&= \sum_{j\in\mathcal{N}}^{j\neq i} \hat{f}_{ij}(p) + \hat{f}_{iB}(p)\ ,
\end{aligned}$$

where the first equality holds by (4.18), the third equality holds since ψ_{CoP} meets (4.3), and the last equality holds by (4.18) and (4.19).

Similarly, to verify (4.13) for those $p \in \mathcal{P}$ with $\omega(p) = 0$, we have

$$\begin{aligned}
\sum_{k\in\mathcal{N}}^{k\neq i} \hat{f}_{ki}(p) + G_i &= \sum_{k\in\mathcal{N}}^{k\neq i} \frac{\sum_{s\in\mathcal{Z}(p)} f_{ki}(t(s))}{|\mathcal{Z}(p)|} + \frac{\sum_{s\in\mathcal{Z}(p)} G_i}{|\mathcal{Z}(p)|} \\
&= \frac{\sum_{s\in\mathcal{Z}(p)} \left[\sum_{k\in\mathcal{N}}^{k\neq i} f_{ki}(t(s)) + G_i\right]}{|\mathcal{Z}(p)|} \\
&= \frac{\sum_{s\in\mathcal{Z}(p)} \left[\sum_{j\in\mathcal{N}}^{j\neq i} f_{ij}(t(s)) + f_{iB}(t(s))\right]}{|\mathcal{Z}(p)|} \\
&= \sum_{j\in\mathcal{N}}^{j\neq i} \frac{\sum_{s\in\mathcal{Z}(p)} f_{ij}(t(s))}{|\mathcal{Z}(p)|} + \frac{\sum_{s\in\mathcal{Z}(p)} f_{iB}(t(s))}{|\mathcal{Z}(p)|} = \sum_{j\in\mathcal{N}}^{j\neq i} \hat{f}_{ij}(p) + \hat{f}_{iB}(p)\ ,
\end{aligned}$$

where the first equality holds by (4.20), the third equality holds since ψ_{CoP} meets (4.3), and the last equality holds by (4.20) and (4.21).

Since $\hat{r}_i(p)$ is set by (4.14), $\psi_{\text{CoP-s}}$ must satisfy Constraint (4.14). To verify that $\psi_{\text{CoP-s}}$ satisfies Constraints (4.16) and (4.17), we first show that, for $p \in \mathcal{P}$ with $\omega(p) > 0$, we have

$$\begin{aligned}
\hat{r}_i(p) &= \rho \sum_{k \in \mathcal{N}}^{k \neq i} \hat{f}_{ki}(p) + \sum_{j \in \mathcal{N}}^{j \neq i} C_{ij} \cdot \hat{f}_{ij}(p) + C_{iB}(p) \cdot \hat{f}_{iB}(p) \\
&= \rho \sum_{k \in \mathcal{N}}^{k \neq i} \frac{\int_{\{t \in [0,\tau]:(x,y)(t)=p\}} f_{ki}(t)\ \mathrm{d}t}{\hat{\omega}(p)} + \sum_{j \in \mathcal{N}}^{j \neq i} C_{ij} \cdot \frac{\int_{\{t \in [0,\tau]:(x,y)(t)=p\}} f_{ij}(t)\ \mathrm{d}t}{\hat{\omega}(p)} \\
&\quad + C_{iB}(p) \cdot \frac{\int_{\{t \in [0,\tau]:(x,y)(t)=p\}} f_{iB}(t)\ \mathrm{d}t}{\hat{\omega}(p)} \\
&= \frac{\int_{\{t \in [0,\tau]:(x,y)(t)=p\}} \left[\rho \cdot \sum_{k \in \mathcal{N}}^{k \neq i} f_{ki}(t) + \sum_{j \in \mathcal{N}}^{j \neq i} C_{ij} \cdot f_{ij}(t) + C_{iB}(p) \cdot f_{iB}(t)\right]\ \mathrm{d}t}{\hat{\omega}(p)} \\
&= \frac{\int_{\{t \in [0,\tau]:(x,y)(t)=p\}} r_i(t)\ \mathrm{d}t}{\hat{\omega}(p)}\,, \qquad (4.22)
\end{aligned}$$

where the first equality holds since $\hat{r}_i(p)$ is set by (4.14), the second equality holds by (4.18) and (4.19), and the last equality holds since ψ_{CoP} meets (4.5). Similarly, for $p \in \mathcal{P}$ with $\omega(p) = 0$, we have

$$\hat{r}_i(p) = \frac{\sum_{s \in \mathcal{Z}(p)} r_i(t(s))}{|\mathcal{Z}(p)|}\,. \qquad (4.23)$$

By (4.22) and (4.23), we can verify (4.16) as follows:

$$\hat{r}_i(p_{\text{vac}}) \cdot \hat{\tau}_{\text{vac}} + \sum_{p \in \mathcal{P},\ p \neq p_{\text{vac}}}^{\hat{\omega}(p)>0} \hat{r}_i(p) \cdot \hat{\omega}(p) + \int_{s \in [0, D_{\text{p}}]}^{\hat{\omega}(p(s))=0} W \cdot \hat{r}_i(p(s))ds$$

$$
\begin{aligned}
&= \frac{\int_{\{t\in[0,\tau]:(x,y)(t)=p_{\text{vac}}\}} r_i(t)\ \mathrm{d}t}{\hat{\tau}_{\text{vac}}} \cdot \hat{\tau}_{\text{vac}} + \sum_{p\in\mathcal{P},\ p\neq p_{\text{vac}}}^{\hat{\omega}(p)>0} \frac{\int_{\{t\in[0,\tau]:(x,y)(t)=p\}} r_i(t)\ \mathrm{d}t}{\hat{\omega}(p)} \cdot \hat{\omega}(p) \\
&\quad + \int_{s\in[0,D_{\text{p}}]}^{\hat{\tau}_{\text{B}}(p(s))=0} W \cdot \frac{\sum_{s\in\mathcal{Z}(p)} r_i(t(s))}{|\mathcal{Z}(p)|}\, ds \\
&= \int_{\{t\in[0,\tau]:(x,y)(t)=p_{\text{vac}}\}} r_i(t)\ \mathrm{d}t + \sum_{p\in\mathcal{P},\ p\neq p_{\text{vac}}}^{\omega(p)>0} \int_{\{t\in[0,\tau]:(x,y)(t)=p\}} r_i(t)\ \mathrm{d}t \\
&\quad + \int_{p\in\mathcal{P}}^{\omega(p)=0} \sum_{s\in\mathcal{Z}(p)} W \cdot \frac{\sum_{s\in\mathcal{Z}(p)} r_i(t(s))}{|\mathcal{Z}(p)|}\, ds \\
&= \int_{\{t\in[0,\tau]:(x,y)(t)=p_{\text{vac}}\}} r_i(t)\ \mathrm{d}t + \sum_{p\in\mathcal{P},\ p\neq p_{\text{vac}}}^{\omega(p)>0} \int_{\{t\in[0,\tau]:(x,y)(t)=p\}} r_i(t)\ \mathrm{d}t \\
&\quad + \int_{p\in\mathcal{P}}^{\omega(p)=0} \int_{\{t\in[0,\tau]:(x,y)(t)=p\}} r_i(t)\, dt \\
&= \int_0^{\tau} r_i(t)\ \mathrm{d}t \\
&\leq \sum_{p\in\mathcal{P}}^{\omega(p)>0} U_{iB}(p)\cdot\omega(p) = \sum_{p\in\mathcal{P}}^{\hat{\omega}(p)>0} U_{iB}(p)\cdot\hat{\omega}(p)\ ,
\end{aligned}
$$

where the first equality holds by (4.22) and (4.23), the second equality holds due to $\omega(p) = \hat{\omega}(p)$, the third equality holds due to the following equation:

$$
\begin{aligned}
\sum_{s\in\mathcal{Z}(p)} W \cdot \frac{\sum_{s\in\mathcal{Z}(p)} r_i(t(s))}{|\mathcal{Z}(p)|}\, ds &= |\mathcal{Z}(p)| \cdot \frac{dt}{ds} \cdot \frac{\sum_{s\in\mathcal{Z}(p)} r_i(t(s))}{|\mathcal{Z}(p)|}\, ds \\
&= \sum_{s\in\mathcal{Z}(p)} r_i(t(s))\, dt = \int_{\{t\in[0,\tau]:(x,y)(t)=p\}} r_i(t)\, dt\ ,
\end{aligned}
$$

the fourth equality holds since every possible location along $\mathcal{P}$ is covered, the fifth inequality holds since ψ_{CoP} meets (4.8), and the last equality holds due to $\hat{\omega}(p) = \omega(p)$. The proof of (4.17) is very

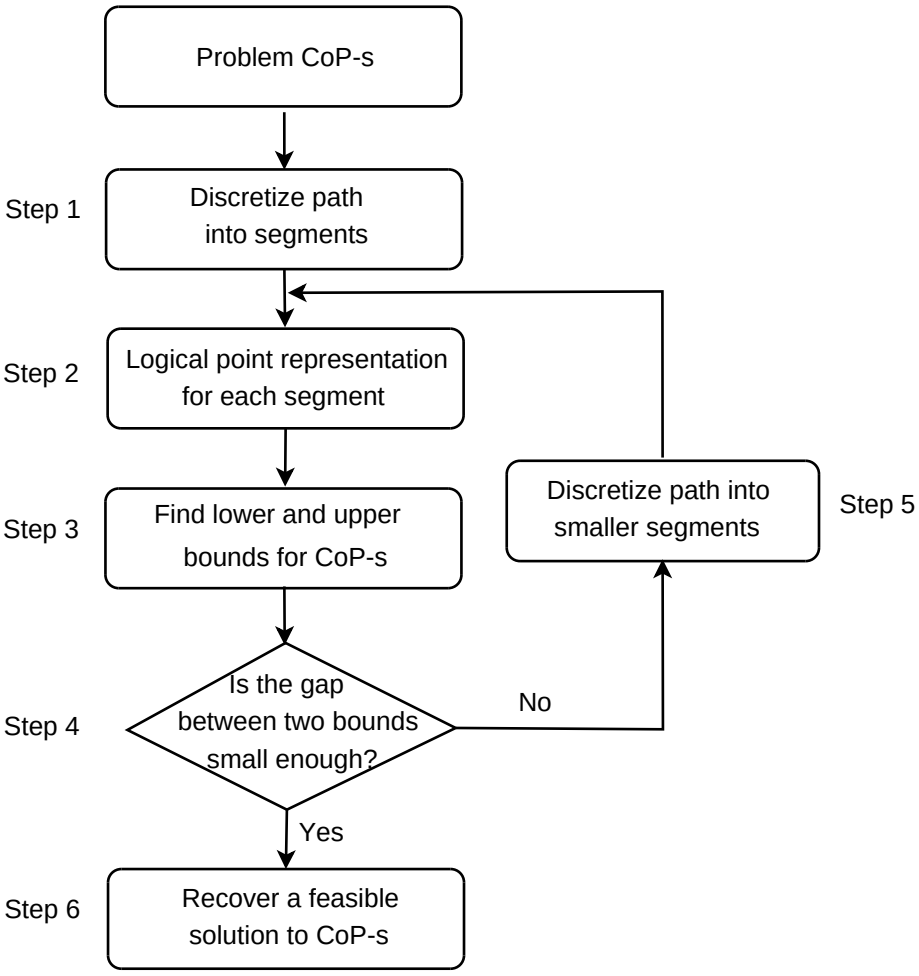

Figure 4.4: A flow-chart of our algorithm to Problem CoP-s.

similar to the above proof of (4.16), and thus omitted to conserve space.

We have thus shown that $\psi_{\text{CoP-s}}$ is a feasible solution to Problem CoP-s. We also have

$$\frac{\hat{\tau}_{\text{vac}}}{\hat{\tau}} = \frac{\tau_{\text{vac}}}{\tau} \ ,$$

where the equality holds simply due to $\hat{\tau} = \tau$ and $\hat{\tau}_{\text{vac}} = \tau_{\text{vac}}$, i.e., the objective value of $\psi_{\text{CoP-s}}$ is equal to that of ψ_{CoP}. This completes the proof. □

Based on Theorem 4.1, we know that as long as our objective is concerned, it is sufficient to study CoP-s, which has a simpler formulation than CoP-t.

4.7 A Near-Optimal Solution to Problem CoP-s

Although CoP-s is simpler than CoP-t, path $\mathcal{P}$ still has infinite number of points. In this section, by discretizing path $\mathcal{P}$ into a finite number of segments and representing each segment as a *logical* point, we develop a provably $(1-\epsilon)$ near-optimal solution.

4.7.1 Basic Idea

Fig. 4.4 shows the flow-chart of our proposed algorithm. In Step 1, we discretize path $\mathcal{P}$ into M_1 segments of equal distance, i.e., $D_{\mathcal{P}}/M_1$. For each segment, we represent it as a *logical* point. Once the WCV is within a segment, we say that it is visiting the corresponding logical point, regardless the specific location within this segment. Note that the time that the WCV spends at a logical point includes both its traveling time over this segment as well as stopping time at any point in this segment.

Since each sensor node's energy consumption and charging behaviors depend on the specific location of the WCV within a segment, it is not obvious to characterize these energy behaviors for the corresponding logical point. Fortunately, we find that for the purpose of developing an $(1-\epsilon)$-optimal algorithm, it is sufficient to use the worst case behavior. That is, to characterize a sensor node's energy consumption and charging behaviors when the WCV is at a logical point, it is sufficient to consider maximum energy consumption and minimum energy charging.

Once we have a worst case representation for each logical point, in Step 3, we can find a lower bound for CoP-s by solving a LP. Also in Step 3, by developing a best case representation for each logical point (following the same token for the worst case representation), we can find an upper bound for CoP-s by solving another LP.

In Step 4, we check the gap between objective values of the lower and upper bounds. If the gap is within ϵ of the upper bound, we have an $(1-\epsilon)$-optimal solution (corresponding to the lower bound solution, which is feasible); otherwise, we increase the number of segments (Step 5) linearly and

return to Step 2.

As the iteration continues, we expect the gap between lower and upper bounds gets closer and closer and we shall have an $(1-\epsilon)$-optimal solution (when the lower bound is within $(1-\epsilon)$ of the upper bound). From the solution corresponding to the final lower bound, we can construct a feasible solution to Problem CoP-s (Step 6).

4.7.2 Some Details

In this section, we give some details on each step of our algorithm.

Path Discretization (Step 1). In the first iteration, path $\mathcal{P}$ is equally divided into M_1 segments, each of which is indexed in increasing order following the WCV's traveling direction. Denote $\mathcal{S}_m$ and $D(\mathcal{S}_m)$, $m = 1, 2, \ldots, M_1$, as the m-th segment and its length, with $D(\mathcal{S}_m) = D_{\mathcal{P}}/M_1$, $m = 1, 2, \ldots, M_1$.

Logical Point Representation (Step 2). For segment $\mathcal{S}_m$, $m = 1, 2, \ldots, M$, we represent it as a logical point p_m. The traveling time by the WCV on segment $\mathcal{S}_m$ (excluding stopping time) is $D(\mathcal{S}_m)/V$. Denote $\omega(p_m)$ as the total stopping time that the WCV is in segment $\mathcal{S}_m$, i.e., $\omega(p_m) = \sum_{p\in\mathcal{S}_m}^{\omega(p)>0} \omega(p)$. Denote $\tau(p_m)$ as the total time that the WCV spends at p_m, which includes traveling time and stopping time. Then,

$$\tau(p_m) = \frac{D(\mathcal{S}_m)}{V} + \sum_{p\in\mathcal{S}_m}^{\omega(p)>0} \omega(p) \ .$$

Note that energy consumption rate $C_{iB}(p)$ and energy charging rate $U_{iB}(p)$ may vary at different point in the same segment. To develop an $(1-\epsilon)$-optimal solution, we use the worst case values of energy consumption rate and energy charging rate within the segment to characterize a logical

point. That is, for $i \in \mathcal{N}$, define $U_{iB}(p_m)$ and $C_{iB}(p_m)$ as

$$U_{iB}(p_m) \triangleq \min_{p \in \mathcal{S}_m} \{U_{iB}(p)\} \ , \ C_{iB}(p_m) \triangleq \max_{p \in \mathcal{S}_m} \{C_{iB}(p)\} \ .$$

Since there are $|\mathcal{N}|$ sensor nodes in the network, a logical point p_m is represented by $2|\mathcal{N}|$-tuple vector $[U_{1B}(p_m), \ldots, U_{|\mathcal{N}|B}(p_m), C_{1B}(p_m), \ldots, C_{|\mathcal{N}|B}(p_m)]$.

Find Lower and Upper Bounds (Step 3). Once we have a worst case representation of each logical point, we can obtain a formulation for a lower bound to CoP-s, which we denote as CoP-lb. Through a systematic change-of-variable technique (similar to that in Chapter 2), CoP-lb can be reformulated into an LP and can be solved in polynomial time.

Following the same token, we can find an upper bound to CoP-s by developing a best case representation for each logical point. This is done by defining

$$\bar{U}_{iB}(p_m) \triangleq \max_{p \in p_m} \{U_{iB}(p)\} \ , \ \bar{C}_{iB}(p_m) \triangleq \min_{p \in \mathcal{S}_m} \{C_{iB}(p)\}.$$

Based on this best-base representation, we obtain a formulation for an upper bound to CoP-s, denoted as CoP-ub. Similar to CoP-lb, CoP-ub can be reformulated into an LP and can be solved in polynomial time.

Termination Condition (Step 4) and Discretizing into Smaller Segments (Step 5). We can check the gap between the lower and upper bounds. If the gap is within desired accuracy (denoted by ϵ), the algorithm terminates and returns an $(1-\epsilon)$-optimal solution; otherwise, we need to further discretize existing segments into smaller ones and perform another iteration and so forth.

For discretization, we denote M_i, $i = 1, 2, \cdots$, as the number of segments in the i-th iteration. By intuition, among all variables, $\omega(p_m)$'s directly determine the WCV's stopping behavior at p_m and thus the final objective value. Thus, we sort segments p_m, $m = 1, 2, \ldots, M_i$, in decreasing values of $\omega(p_m)$ (with ties broken randomly). From the ordered segments, we pick the first $|\mathcal{N}|$ segments

and equally subdivide each of them into two segments.[3] As a result, at most $|\mathcal{N}|$ segments are added at each iteration, i.e., a linear increase in the number of segments.

Denote $\psi^{(M_i)}_{\text{CoP-lb}}$ and $\psi^{(M_i)}_{\text{CoP-ub}}$ as the optimal solutions to CoP-lb and CoP-ub at the end of the i-th iteration, respectively. Denote $\eta^{(M_i)}_{\text{vac}}$ and $\bar{\eta}^{(M_i)}_{\text{vac}}$ as the objective values in $\psi^{(M_i)}_{\text{CoP-lb}}$ and $\psi^{(M_i)}_{\text{CoP-ub}}$, respectively. Then we have the following lemma:

Lemma 4.3 *For $i \geq 1$, $\eta^{(M_{i+1})}_{vac} > \eta^{(M_i)}_{vac}$, and $\bar{\eta}^{(M_{i+1})}_{vac} < \bar{\eta}^{(M_i)}_{vac}$.*

Lemma 4.3 says that as the number of segments increases with the number of iterations, the lower bound to CoP-s strictly increases while the upper bound strictly decreases. Lemma 4.3 can be proved by construction. The proof is intuitive and is omitted here to conserve space.

Recover a Feasible Solution to CoP-s (Step 6). Once the lower bound is within $(1-\epsilon)$ of the upper bound, the algorithm terminates. With the current lower bound solution to CoP-lb (denoted as $\psi_{\text{CoP-lb}}$), we can construct a feasible solution to CoP-s (denoted as $\psi_{\text{CoP-s}}$). Solution $\psi_{\text{CoP-s}}$ consists of several components, including (i) cycle time τ; (ii) for $p \neq p_{\text{vac}}$, stopping time $\omega(p)$, flow routing $f_{ij}(p)$ and $f_{iB}(p)$, and energy consumption rate $r_i(p)$; and (iii) vacation time at the service station τ_{vac}, and corresponding flow routing $f_{ij}(p_{\text{vac}})$ and $f_{iB}(p_{\text{vac}})$, and energy consumption rate $r_i(p_{\text{vac}})$. From $\psi_{\text{CoP-lb}}$, $\psi_{\text{CoP-s}}$ can be constructed as follows:

- It has the same cycle time τ as that in $\psi_{\text{CoP-lb}}$.
- For $p \neq p_{\text{vac}}$, the WCV may traverse segment $\mathcal{S}_m$ with or without any stop. To see if the WCV makes any stop in $\mathcal{S}_m$, we calculate $\tau(p_m) - D(\mathcal{S}_m)/V$. If the difference is greater than 0, then the WCV stops within $\mathcal{S}_m$ and in $\psi_{\text{CoP-s}}$ the WCV may stop at any point $p \in \mathcal{S}_m$. For this p, the WCV will stay for $\tau(p_m) - D(\mathcal{S}_m)/V$ amount of time. Otherwise (i.e., $\tau(p_m) - D(\mathcal{S}_m)/V = 0$), the WCV does not stop within $\mathcal{S}_m$. Regardless of stopping or not,

[3] As there are $|\mathcal{N}|$ sensor nodes, the number of stops by the WCV (for charging) should be on the same order of $|\mathcal{N}|$. If $M_i < |\mathcal{N}|$, then we just divide all M_i segments.

the flow routing solution at a point $p \in \mathcal{S}_m$ is: $f_{ij}(p) = f_{ij}(p_m)$ and $f_{iB}(p) = f_{iB}(p_m)$. Corresponding to $p \in \mathcal{S}_m$, $r_i(p)$ is defined by (4.14).

- For $p = p_{\text{vac}}$, we have that τ_{vac}, $f_{ij}(p_{\text{vac}})$, $f_{iB}(p_{\text{vac}})$, and $r_i(p_{\text{vac}})$ are the same as those in $\psi_{\text{CoP-lb}}$.

Denote $\eta_{\text{CoP-lb}}$ and $\eta_{\text{CoP-s}}$ as the objective values achieved by $\psi_{\text{CoP-lb}}$ and $\psi_{\text{CoP-s}}$, respectively. Since τ and τ_{vac} are unchanged in the foregoing solution construction, we have

$$\eta_{\text{CoP-s}} = \eta_{\text{CoP-lb}} \ . \tag{4.24}$$

4.7.3 Proof of $(1-\epsilon)$ Optimality

Let $\eta^*_{\text{CoP-s}}$ be the (unknown) optimal objective value to CoP-s. The following theorem says that the constructed solution $\psi_{\text{CoP-s}}$ is $(1-\epsilon)$-optimal.

Theorem 4.2 *For any* $0 < \epsilon \ll 1$, $\eta_{\text{CoP-s}} \geq (1-\epsilon)\eta^*_{\text{CoP-s}}$.

Proof Upon termination, we have $\eta_{\text{CoP-lb}} \geq (1-\epsilon)\eta_{\text{CoP-ub}}$, where $\eta_{\text{CoP-lb}}$ and $\eta_{\text{CoP-ub}}$ are the objective values achieved by the lower bound solution to CoP-lb and the upper bound solution to CoP-ub, respectively. Therefore, we have

$$\eta_{\text{CoP-s}} = \eta_{\text{CoP-lb}} \geq (1-\epsilon)\eta_{\text{CoP-ub}} \geq (1-\epsilon)\eta^*_{\text{CoP-s}} \ ,$$

where the first equality holds by (4.24), and the last inequality holds since $\eta_{\text{CoP-ub}}$ is an upper bound for CoP-s. This completes the proof. □

4.8 Numerical Results

In this section, we use numerical results to demonstrate how our algorithm solves the WCV and MBS co-location problem.

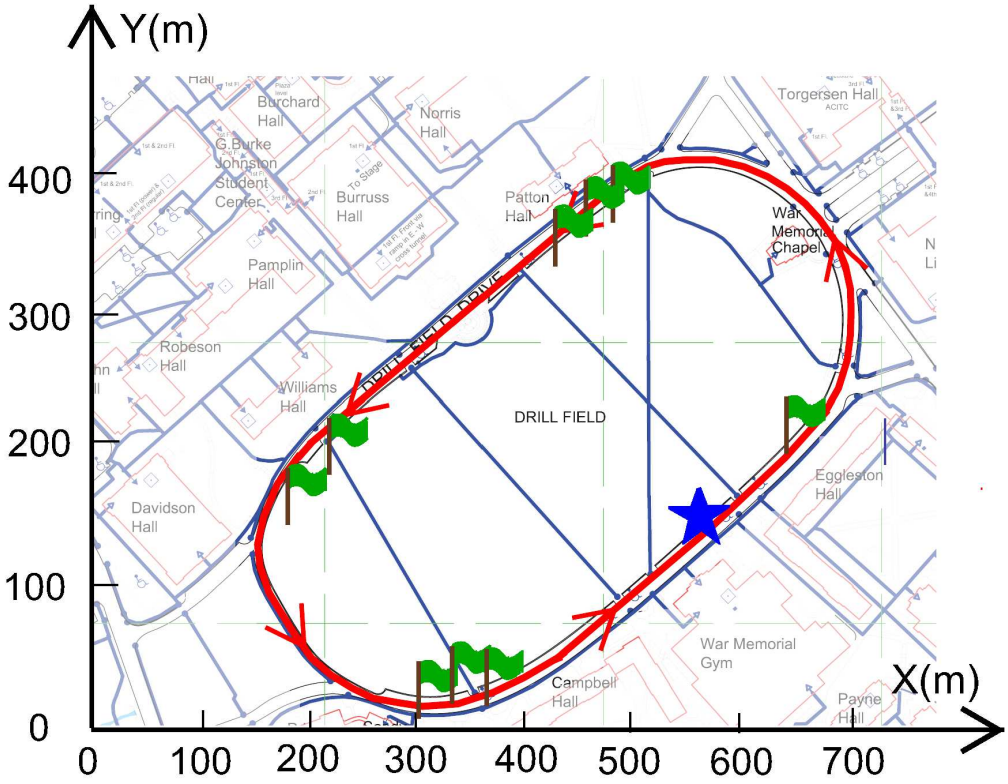

Figure 4.5: Drillfield driveway on Virginia Tech campus. A star represents the WCV's home service station. A flag represents a stopping point in the case study (Section 4.8.2).

Table 4.2: Location and data rate R_i for each node in a 25-node network.

Node Index	Location (m)	R_i (Kb/s)	Node Index	Location (m)	R_i (Kb/s)
1	(626.0, 236.1)	1	14	(247.6, 181.6)	7
2	(623.3, 235.6)	7	15	(245.9, 180.4)	4
3	(624.0, 237.2)	1	16	(247.7, 181.0)	10
4	(625.6, 237.1)	1	17	(220.5, 118.0)	5
5	(460.8, 357.8)	1	18	(220.5, 121.1)	2
6	(462.6, 361.9)	4	19	(219.5, 119.8)	7
7	(459.8, 359.0)	2	20	(220.7, 118.3)	6
8	(461.1, 359.0)	3	21	(328.8, 12.2)	2
9	(435.7, 337.8)	2	22	(335.2, 13.2)	9
10	(433.3, 337.7)	4	23	(334.2, 13.0)	4
11	(435.2, 338.5)	5	24	(333.2, 13.9)	8
12	(434.8, 337.4)	5	25	(331.5, 13.7)	8
13	(245.1, 180.3)	1			

Table 4.3: Index of stopping point along the path, location and time spent at each stopping point for the 25-node network.

Visit Order	Location (m)	$\omega(p)$ (s)	Visit Order	Location (m)	$\omega(p)$ (s)
1	(625.7, 235.3)	23	6	(221.0, 119.4)	219
2	(461.1, 357.4)	358	7	(329.3, 11.9)	2
3	(464.5, 360.2)	9	8	(332.4, 12.1)	9
4	(435.4, 336.2)	98	9	(333.9, 12.4)	2318
5	(247.3, 179.3)	42			

4.8.1 Network and Parameter Settings

We use Virginia Tech's Drillfield (see Fig. 4.5) for sensor network deployment. Sensor nodes are deployed within a distance of the charging range along the side of the Drillfield driveway, which is roughly an ellipse. The home service station (marked as a star in Fig. 4.5) is located at (540,160) (in m) along the driveway. For the Drillfield path $\mathcal{P}$, $D_{\mathcal{P}} = 1228$ m. The travel speed of the WCV is $V = 5$ m/s.

The number of sensor nodes in the network will be specified later for different results. The data rate R_i, $i \in \mathcal{N}$, is randomly generated within $[1, 10]$ Kb/s. Suppose a sensor node uses a rechargeable NiMH battery (connected to an energy receiving coil). Assume $E_{\max} = 10.8$ kJ [33], and $E_{\min} = 0.05 \cdot E_{\max} = 540$ J. The power consumption coefficients are $\beta_1 = 50$ nJ/b, $\beta_2 = 0.0013$ pJ$/(\text{b} \cdot \text{m}^4)$, and $\rho = 50$ nJ/b. The path loss index is $\alpha = 4$. For the charging efficiency function $\mu(D_{iB})$, we refer to the experimental results in [32]. Through curve fitting (see Fig. 3.8), we obtain $\mu(D_{iB}) = -0.0958 D_{iB}^2 - 0.0377 D_{iB} + 1.0$. Letting $U_{\max} = 5$ W and $\delta = 1$ W, we have $D_\delta = 2.7$ m for a maximum distance of effective charging.[4] We set $\epsilon = 0.05$.

4.8.2 A Case Study

We first present results for a 25-node sensor network. The location of each node and its data rate are given in Table 4.2. Applying our $(1 - \epsilon)$-optimal algorithm, we find that the algorithm

[4]The charging distance can be extended by using larger coils.

finds a solution after the third iteration. In this solution, we have τ = 17.29 h, τ_{vac} = 16.29 h, and the objective value is 94.21%.[5] Since the total traveling time along path $\mathcal{P}$ is $1228/5 = 245.6$ s ≈ 0.07 h, we have that the total stopping time for charging is $17.29 - 16.29 - 0.07 = 0.93$ h.

Upon termination, there are a total of 316 segments (corresponding to 316 logical points). However, the WCV only makes 9 stops among these segments, and merely traverses all the other segments without stop. For illustration purpose, we use a physical point (x, y) within the corresponding segment to represent the segment where the WCV makes a stop. These stopping points are marked with flags in Fig. 4.5, and the location and the amount of time at each stop are given in Table 4.3. Note that the number of stops for the WCV is much fewer than the number of sensor nodes due to multi-node charging. For example, the WCV charges nodes 1, 2, 3, and 4 at the same time when it stops at the 1st point $(625.7, 235.3)$. Also, it is possible that a node may be charged more than once in a cycle. For example, node 25 is charged when the WCV stops at both the 8th point $(332.4, 12.1)$ and the 9th point $(333.9, 12.4)$.

4.9 Summary

This chapter has explored the complex problem of co-locating a MBS on the wireless charging vehicle (WCV). The motivation was to take advantage of the mobility feature of the WCV and use it as a carrying platform for the MBS at the same time. The goal was to minimize energy consumption of the entire system while ensuring none of the sensor nodes runs out of energy. We developed a mathematical model for this problem and found that it is a highly complex problem involving time-dependent variables. Instead of studying the original problem formulation (CoP-t), we showed that it is sufficient to study a special subproblem (CoP-s) that only involves space-dependent variables. Subsequently, we developed a provable near-optimal solution to CoP-s.

There are a number of novel techniques that are worth being disseminated to the research com-

[5]The objective value achieved by the upper bound solution is 95.91%. This means that our solution achieves an objective value that is at least $0.9421/0.9591 = 99.0\%$ of the optimum.

munity, most notably, downsizing solution space without compromising optimal objective value, discretizing a continuous path into a finite number of segments and representing each segment with a logical point. These powerful techniques allow development of a provably near-optimal solution to a complex problem that is seemingly intractable at first glance. In our future work, we will further explore these techniques to address other difficult networking problems involving time-dependent movement, flow routing, and energy consumption.

Chapter 5

Bundling Mobile Base Station and Wireless Energy Transfer: The Unconstrained Path Case

5.1 Introduction

In Chapter 4, we studied the problem of co-locating the MBS on the WCV on a pre-planed path. However, the pre-planned plan may be not well-designed. In this chapter, we address this issue by investigating the traveling path and related problems for the WCV.

Following the setting in Chapter 4, we consider a WCV periodically traveling inside the WSN, making stops and charging sensor nodes near these stops. At any time, data collected from the sensor nodes are relayed to the WCV (via multi-hop). Upon completing each trip, the WCV returns to its home service station, takes a "vacation", and starts out for its next trip. In contrast to Chapter 4, the WCV in this chapter is allowed to travel anywhere over the two-dimensional area, i.e., its traveling path is unconstrained and is part of the optimization problem.

Apparently, the above problem brings in a number of technical challenges. First of all, the traveling path for the WCV is unknown and needs to be determined. Second, we need to find optimal stopping points along this path as well as the charging schedule of the WCV (i.e., how long it shall

stay at each stopping point). Finally, the data flow routing in the network is dynamic and depends on where the WCV is in the network. Among these challenges, we find that the traveling path problem is most crucial and solutions to the other sub-problems all hinge upon the determination of a traveling path. In this chapter, we address these challenges by studying an optimization problem.

The main contributions of this chapter are as follows:

- We formulate an optimization problem (TPP) that involves joint optimization of traveling path, stopping points, charging schedule, and data flow routing. This is shown to be a non-linear program (NLP).
- To tackle TPP, we first consider an idealized problem (OPT-ub) that assumes zero traveling time (i.e., infinite traveling speed) from one point to another. The optimal solution of OPT-ub gives an upper bound to TPP.
- Subsequently, we develop a provably near-optimal solution to OPT-ub for any desired level of accuracy ϵ. Our solution involves several novel techniques, such as discretization of energy reception rate and energy consumption rate, double partitioning of the smallest enclosing disk (SED) into smaller subareas with tight upper energy consumption bounds and lower energy reception bounds, and representation of each subarea by a logical point as its "worst-case" energy reception and energy consumption behavior.
- Based on the near-optimal solution to the idealized problem OPT-ub, we return to the original problem TPP by incorporating non-zero traveling time for the WCV. In particular, we determine the traveling path in TPP by finding the shortest Hamiltonian cycle to connect all the logical points that have non-zero stopping time in OPT-ub. Note that this Hamiltonian cycle is fundamentally different from the Hamiltonian cycle that connects all sensor nodes in the network. Based on this traveling path, we can obtain a feasible solution to the original problem TPP. We further quantify the performance gap between this feasible solution and an optimal solution to TPP.

The remainder of this chapter is organized as follows. In Section 5.2, we give some essential background and necessary mathematical models for this problem. We also develop a formulation for the optimization problem TPP. In Section 5.3, we study an idealized problem OPT-ub and develop a near-optimal solution. In Section 5.4, we determine a traveling path based on the solution in Section 5.3. Based on this path, we develop a feasible solution to the original problem TPP. We then quantify the performance gap between this solution and the optimal solution. Section 5.5 presents numerical results. Section 5.6 summarizes this chapter.

5.2 Modeling and Formulation

Suppose that we have a sensor network $\mathcal{N}$ deployed over a two-dimensional area. A WCV is employed to recharge sensor nodes in the network and to collect data from nodes in real time. The WCV follows a periodic schedule: In each cycle, it starts from its home service station, travels inside the network, and returns to the service station. While traveling, the WCV makes a number of stops and charges sensor nodes that are in the vicinity of those stops. For the traveling path that we are investigating in this chapter, the WCV is allowed to visit *anywhere* over the two-dimensional area, i.e., its traveling path is unconstrained and is part of the optimization problem. At any time, the data generated from the sensor nodes are relayed through multi-hops toward the WCV (in real time).

In this section, we present necessary mathematical models for this problem. Based on these models, we present a problem formulation. Table 5.1 lists the notation used in this Chapter.

5.2.1 Traveling Path and Stopping Schedule

Denote $\mathcal{P}$ as the traveling path and τ as the amount of time for each cycle. Then τ includes three components:

Table 5.1: Notation in Chapter 5.

Symbol	Definition
$\mathcal{A}$	The smallest enclosing disk covering sensor nodes in the network
$\mathcal{A}_j^u$	The j-th subarea in $\mathcal{A}$ via area partition based on energy replenishment
$\mathcal{A}_m^c$	The m-th subarea in $\mathcal{A}$ via area partition based on energy consumption
$\mathcal{A}_k^{u+c}$	The k-th subarea in $\mathcal{A}$, $k = 1, 2, \ldots, K$
B	The total number of circles in area partition
$C_{iB}(p)$	Energy consumption for transmitting one unit of data rate from node i to the WCV at location p
$C[h]$	A sequence of discretized energy consumption rate
D_δ	Maximum charging distance of the WCV
$D_{iB}(p)$	Distance from node i to the WCV at p
$D^u[h]$	A distance corresponding to $U[h]$
$D^c[h]$	A distance corresponding to $C[h]$
$\mathcal{E}_i(p_{\text{vac}})$ (or $\mathcal{E}_i(p_m)$)	Node i's weighted energy consumption rate when the WCV stays at p_{vac} (or p_m)
$f_{ij}(p)$ (or $f_{iB}(p)$)	Flow rate from sensor node i to sensor node j (or base station WCV) when the WCV is at location p
$g_{ij}(p)$ (or $g_{iB}(p)$)	Weighted data flow from node i to node j (or the WCV) when the WCV stays at p
$\mathcal{L}_m$	The m-th logical point
h	The index used in the sequence of $U[h]$ or $C[h]$
$h_i^u(\mathcal{A}_j^u)$	The index of the outer circle for a subarea $\mathcal{A}_j^u$ in Phase I area partition
$h_i^c(\mathcal{A}_m^c)$	The index of the outer circle for a subarea $\mathcal{A}_m^c$ in Phase II area partition
K	The total number of subareas
M^u	The total number of elements in the sequence of $U[h]$
M^c	The total number of elements in the sequence of $C[h]$
$O_{\mathcal{A}}$	The origin of disk $\mathcal{A}$
$\mathcal{Q}$	The set of indexes for all the traversed subareas by WCV
$\mathcal{Q}_s$	The set of indexes for those subareas that the WCV will make stops
$R_{\mathcal{A}}$	The radius of disk $\mathcal{A}$
$r_i(p)$	Energy consumption rate at sensor node i when the WCV is at location p
U_{max}	Maximum output power from the WCV for a single sensor node
$U[h]$	A discretization of energy reception rate
$U_{iB}(p)$	Power reception rate at node i when the WCV is at p
W	A parameter controlling the granularity of the discretization
(x_i, y_i)	Location of sensor node i
$\omega(p)$	Aggregate time span for the WCV to stay at location $p \in \mathcal{P}$
$\mu(\cdot)$	The efficiency function of wireless energy transfer from the WCV to a sensor node
ψ_{TPP} (or ψ^*_{TPP})	A feasible solution (or an optimal solution) to Problem TPP
$\psi_{\text{OPT-ub}}$ (or $\psi^*_{\text{OPT-ub}}$)	A feasible solution (or an optimal solution) to Problem OPT-ub
$\eta_{\text{OPT-ub}}$, $\eta^*_{\text{OPT-ub}}$	The objective value achieved by $\psi_{\text{OPT-ub}}$ and $\psi^*_{\text{OPT-ub}}$

- The total traveling time along path $\mathcal{P}$, $D_{\mathcal{P}}/V$, where $D_{\mathcal{P}}$ is the distance along path $\mathcal{P}$ and V is the traveling speed of the WCV.
- The total sojourn time along path $\mathcal{P}$, which is defined as the sum of all stopping time of the WCV when it travels on $\mathcal{P}$.
- The vacation time for the WCV at its home service station, τ_{vac}, which starts when the WCV returns to its home service station (after traveling path $\mathcal{P}$) and ends when the WCV leaves for the next trip.

Then we have:

$$\tau = \frac{D_{\mathcal{P}}}{V} + \sum_{p \in \mathcal{P},\, p \neq p_{\text{vac}}}^{\omega(p)>0} \omega(p) + \tau_{\text{vac}} \ , \tag{5.1}$$

where $\omega(p)$ denotes the aggregate amount of time the WCV stays at point $p \in \mathcal{P}$ and p_{vac} denotes the location of the home service station.

5.2.2 Energy Charging Model

We assume that the WCV can only perform its charging function when it makes a stop along path $\mathcal{P}$ (excluding p_{vac}). Based on the current charging technology [32], the WCV can charge multiple neighboring nodes simultaneously as long as they are within its charging range, although the WET rate at a sensor node decreases over the distance.

Denote $U_{iB}(p)$ as the power reception rate at node i when the WCV is located at $p \in \mathcal{P}$. Denote the efficiency of wireless charging by $\mu(D_{iB}(p))$, which is a decreasing function of $D_{iB}(p)$, the distance between node i and the WCV located at p. Then the wireless charging model is as follows:

$$U_{iB}(p) = \begin{cases} \mu(D_{iB}(p)) \cdot U_{\text{max}} & \text{if } D_{iB}(p) \leq D_\delta \\ 0 & \text{if } D_{iB}(p) > D_\delta \ , \end{cases} \tag{5.2}$$

where $U_{\max}$ is the maximum output power for a single sensor node and D_δ is the charging range of the WCV, beyond which wireless charging will not occur. In other words, D_δ is defined in a way such that the power reception rate at a sensor node is at least over a threshold value δ.

5.2.3 Dynamic Data Flow Routing

Recall that the base station is co-located at the WCV and all data generated from the sensor nodes shall be delivered to the base station. To conserve energy, multi-hop data routing is necessary among the sensor nodes in the network. Due to the mobility of the WCV, data flow routing is dynamic, with routing topology changing over time.

Suppose that each sensor node i ($i \in \mathcal{N}$) generates a constant rate R_i. Denote $f_{ij}(p)$ and $f_{iB}(p)$ as flow rates from sensor node i to sensor node j and to the base station when the WCV is at location $p \in \mathcal{P}$, respectively. Then we have the following flow balance at each sensor node i:

$$\sum_{k \in \mathcal{N}}^{k \neq i} f_{ki}(p) + R_i = \sum_{j \in \mathcal{N}}^{j \neq i} f_{ij}(p) + f_{iB}(p) \quad (i \in \mathcal{N}, p \in \mathcal{P}) \tag{5.3}$$

The above flow balance equation indicates that we are dealing with real-time flow routing, rather than DTN-like data routing (e.g., data MULEs [50] or message ferry [74]), where data can be delayed and delivered till a later time.

5.2.4 Sensor Energy Consumption

At a sensor node, we assume data communications (transmission and reception) is the dominant source for energy consumption.[1] Denote C_{ij} as the energy consumption rate for transmitting one unit of data flow from sensor node i to sensor node j. Then C_{ij} (in Joule/bit) can be modeled as

[1] Energy consumption for hardware device and information processing can be assumed to be constants and can be easily integrated into total energy consumption without major change of the problem structure.

[23, 51]:

$$C_{ij} = \beta_1 + \beta_2 D_{ij}^{\alpha} \ ,$$

where D_{ij} is the distance between nodes i and j, β_1 and β_2 are constant terms, and α is the path loss index. Given that all sensor nodes are stationary, we have that D_{ij} and C_{ij} are all constants.

Denote $C_{iB}(p)$ as the energy consumption rate for transmitting one unit of data flow from sensor node i to base station B when the WCV is at location $p \in \mathcal{P}$. We have

$$C_{iB}(p) = \beta_1 + \beta_2 \left[\sqrt{(x_p - x_i)^2 + (y_p - y_i)^2} \right]^{\alpha} , \tag{5.4}$$

where (x_p, y_p) and (x_i, y_i) are the coordinates of p and node i, respectively. Note that unlike C_{ij}'s, which are all constants, $C_{iB}(p)$ varies with the base station's position p.

Then the total energy consumption rate for both transmission and reception at node i when the WCV is at $p \in \mathcal{P}$, denoted as $r_i(p)$, is

$$r_i(p) = \rho \sum_{k \in \mathcal{N}}^{k \neq i} f_{ki}(p) + \sum_{j \in \mathcal{N}}^{j \neq i} C_{ij} \cdot f_{ij}(p) + C_{iB}(p) \cdot f_{iB}(p) \quad (i \in \mathcal{N}, p \in \mathcal{P}) \ , \tag{5.5}$$

where ρ is a constant term associated with the rate of energy consumption for receiving one unit of data.

5.2.5 Energy Cycle at a Sensor Node

We will develop a travel schedule (including charging schedule) for the WCV and data flow routing among the nodes so that no sensor node ever runs out of energy. Such travel schedule follows a periodic cycle, as discussed in Section 5.2.1, with a cycle time of τ.

Suppose that each sensor node is fully charged initially. Denote E_{max} as its battery capacity and E_{min} as the minimum energy threshold for a node to be operational. We offer two energy renewable conditions, and show that once they are met, then the energy level at each sensor node at time t,

denoted as $e_i(t)$, never falls below E_{min}.

First, we split energy consumption at node i into two parts:

- Energy consumed whenever the WCV makes any stop (including vacationing at its service station): $r_i(p_{\text{vac}}) \cdot \tau_{\text{vac}} + \sum_{p\in\mathcal{P},\, p\neq p_{\text{vac}}}^{\omega(p)>0} r_i(p) \cdot \omega(p)$,

- Energy consumed when the WCV is moving along $\mathcal{P}$, i.e., $\int_{s\in[0,D_{\mathcal{P}}]}^{\omega(p(s))=0} \frac{1}{V} \cdot r_i(p(s))\, ds$, where $s \in [0, D_{\mathcal{P}}]$ and the integration is taken over the distance traversed by the WCV along $\mathcal{P}$, and $p(s)$ is the WCV's location corresponding to s.

Following the results in Chapter 3, it can be shown that $e_i(t) \geq E_{\text{min}}$ for all $t \geq 0$, $i \in \mathcal{N}$ if the following conditions are satisfied:

$$\begin{aligned} E_{\text{max}} - \Big[& r_i(p_{\text{vac}}) \cdot \tau_{\text{vac}} + \sum_{p\in\mathcal{P},\, p\neq p_{\text{vac}}}^{\omega(p)>0,\ D_{iB}(p)>D_\delta} r_i(p) \cdot \omega(p) \\ & + \int_{s\in[0,D_{\text{p}}]}^{\omega(p(s))=0} \frac{1}{V} \cdot r_i(p(s)) ds \Big] \geq E_{\text{min}} \ , \ (i \in \mathcal{N}) \end{aligned} \tag{5.6}$$

$$\begin{aligned} & r_i(p_{\text{vac}}) \cdot \tau_{\text{vac}} + \sum_{p\in\mathcal{P},\, p\neq p_{\text{vac}}}^{\omega(p)>0} r_i(p) \cdot \omega(p) \\ & \quad + \int_{s\in[0,D_{\text{p}}]}^{\omega(p(s))=0} \frac{1}{V} \cdot r_i(p(s)) ds \\ & \leq \sum_{p\in\mathcal{P}}^{\omega(p)>0,\ D_{iB}(p)\leq D_\delta} U_{iB}(p) \cdot \omega(p) \ , \ (i \in \mathcal{N}) \end{aligned} \tag{5.7}$$

In Constraint (5.6), $\sum_{p\in\mathcal{P},\, p\neq p_{\text{vac}}}^{\omega(p)>0,\ D_{iB}(p)>D_\delta} r_i(p) \cdot \omega(p)$ is the amount of energy consumed at node i when the WCV is making stops near those nodes other than i. Constraint (5.6) ensures that $e_i(t)$, which starts from E_{max} at $t = 0$, will not fall below E_{min} at the end of the first cycle $t = \tau$. In Constraint (5.7), the left-hand side is the amount of energy consumed at node i during τ while the right-hand side is maximum amount of potential energy received by node i in a cycle. Note that the actual amount of energy received by node i in the first cycle may be less than the right-hand

side due to battery overflow.[2] Constraint (5.7) ensures that $e_i(t)$, which starts at full level $E_{\max}$, will be charged back to $E_{\max}$ before the end of the first cycle τ.

5.2.6 Problem Formulation

Based on the above mathematical models, a number of problems can be formulated and studied. As a case study, we consider an optimization problem involving joint optimization of traveling path, stopping points, charging schedule, and flow routing. For the objective function, we consider minimizing energy consumption of the entire system, which includes power used by the WCV and the power consumed for WET.[3] Since power used by the WCV is the dominant component in the overall energy consumption, our objective function will focus on this component. Specifically, we aim to minimize the fraction of time that the WCV is at work (i.e., away from its service station) in each cycle period, i.e., $\frac{D_{\mathcal{P}}/V+\sum_{p\in\mathcal{P},\, p\neq p_{\text{vac}}}^{\omega(p)>0}\omega(p)}{\tau}$.[4] Note that by (5.1), minimizing $\frac{D_{\mathcal{P}}/V+\sum_{p\in\mathcal{P},\, p\neq p_{\text{vac}}}^{\omega(p)>0}\omega(p)}{\tau}$ is equivalent to maximizing $\frac{\tau_{\text{vac}}}{\tau}$, which is the percentage of time that the WCV is on vacation at its service station. Therefore, we have the following optimization problem, called Traveling Path Problem (TPP):

$$
\begin{aligned}
&\textbf{TPP:}\\
&\text{Maximize} \quad \tfrac{\tau_{\text{vac}}}{\tau}\\
&\text{s.t.} \quad \text{Time constraints: (5.1);}\\
&\qquad\quad \text{Flow routing constraints: (5.3);}\\
&\qquad\quad \text{Energy consumption model: (5.5);}\\
&\qquad\quad \text{Energy renewable constraints: (5.6), (5.7).}\\
&\qquad\quad \tau, \tau_{\text{vac}}, \omega(p) \geq 0 \quad (p \in \mathcal{P})\\
&\qquad\quad f_{ij}(p), f_{iB}(p), r_i(p) \geq 0 \quad (i, j \in \mathcal{N}, i \neq j, p \in \mathcal{P})\ .
\end{aligned}
$$

In this formulation, V, R_i, ρ, C_{ij}, $E_{\max}$, and $E_{\min}$ are constants, and $U_{iB}(p)$ and $C_{iB}(p)$ can be computed by (5.2) and (5.4), respectively. The path $\mathcal{P}$ and $D_{\mathcal{P}}$ are to be determined in Problem TPP.

[2] Once a battery is charged to $E_{\max}$, its energy cannot be further increased.

[3] Note that except their initial energy, the energy consumed at all sensor nodes comes from the WCV.

[4] We assume the WCV keeps its engine running as long as it is away from its service station.

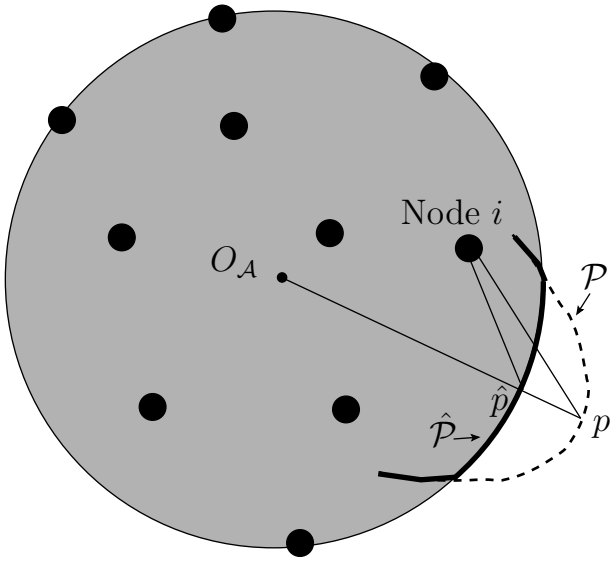

Figure 5.1: An example sensor network that illustrates Lemma 5.1.

The time intervals τ, τ_{vac}, and $\omega(p)$, the flow rates $f_{ij}(p)$ and $f_{iB}(p)$, and the power consumption rate $r_i(p)$ are also optimization variables.[5] Note that Problem TPP is a nonlinear program, and is NP-hard in general.

In Problem TPP, the WCV can travel anywhere in the two-dimensional plane. It is not hard to see that the WCV's roaming area can be narrowed down to a much smaller area. In particular, it is sufficient for the WCV to roam in the smallest enclosing disk (SED) [66], denoted as $\mathcal{A}$, which covers all the sensor nodes in the network and the home service station. This result is stated in the following lemma:

Lemma 5.1 *The optimal traveling path for the WCV must stay inside the SED $\mathcal{A}$.*

Proof This proof is based on contradiction. That is, if there exists an optimal traveling path $\mathcal{P}$ (for the WCV) with some part outside of the SED $\mathcal{A}$, we can always find a better path $\hat{\mathcal{P}}$ (in terms of higher percentage of vacation time), which leads to contradiction.

[5]Note that variables in this formulation are only dependent on the WCV's location p and are independent of the time when the WCV visits this location. In [51], Shi *et al.* showed that a time-based formulation involving a MBS like ours can be transformed into a location-based formulation. In light of that result, we start directly with a location-based formulation in this chapter without going through the details of such transformation, which are similar to those in [51].

Denote $O_{\mathcal{A}}$ as the origin of the SED $\mathcal{A}$ (See Fig. 5.1). Assuming that the WCV follows path $\mathcal{P}$. For point $p \in \mathcal{P}$ and p is outside of the SED, let $\hat{p}$ be the intersecting point between the line segment $[p, O_{\mathcal{A}}]$ and the circle of the SED. For any sensor i (all within the SED), we have $D_{iB}(\hat{p}) < D_{iB}(p)$. Subsequently, we have $C_{iB}(\hat{p}) < C_{iB}(p)$ and then by (5.5), we have $r_i(\hat{p}) < r_i(p)$. As a result, we can save energy consumption at node i, $i \in \mathcal{N}$, by relocating the WCV from p to $\hat{p}$. On the other hand, we have $U_{iB}(\hat{p}) \geq U_{iB}(p)$ by (5.2). That is, node i, $i \in \mathcal{N}$, receives more or equal amount of energy by relocating the WCV from p to $\hat{p}$.

By relocating p to $\hat{p}$, the WCV could spend less time at $\hat{p}$ than that at p while maintaining each node's energy level over $E_{\min}$ (provided that the remaining parts of the solution are unchanged). Further, it is clear that $D_{\hat{\mathcal{P}}} < D_{\mathcal{P}}$ and thus less traveling time is needed. Therefore, by (5.1), the cycle time is reduced for path $\hat{\mathcal{P}}$, which leads to a higher ratio of vacation time over cycle time. This contradicts our assumption, and completes the proof. □

5.3 A Near-Optimal Solution to an Idealized Problem

A major difficulty in Problem TPP is that the traveling path $\mathcal{P}$ is unknown and is part of the optimization problem. What further complicates this matter is that it takes time for the WCV to travel along the path. In this section, we consider an idealized problem that ignores the time for the WCV to travel from one point to another along $\mathcal{P}$. We will show that it is possible to develop a provably near-optimal solution to this idealized problem. Based on this result, in Section 5.4, we address the practical problem which considers non-zero traveling time for the WCV.

5.3.1 An Idealized Problem with Zero Traveling Time

In the idealized problem, the traveling time of the WCV is assumed to be zero. In this section, we give a formulation for this idealized problem (denoted as OPT-ub) based on our formulation for

TPP. Since $V \to \infty$, Constraint (5.1) becomes

$$\tau = \sum_{p\in\mathcal{P},\, p\neq p_{\text{vac}}}^{\omega(p)>0} \omega(p) + \tau_{\text{vac}} \ . \tag{5.8}$$

Further, since $V \to \infty$ in OPT-ub, energy consumed at a sensor node i when the WCV travels along $\mathcal{P}$ (i.e., $\int_{s\in[0,D_{\text{p}}]}^{\omega(p(s))=0} \frac{1}{V} \cdot r_i(p(s))\ ds$) degenerates to 0. Hence, (5.7) can be simplified to

$$\begin{aligned} & r_i(p_{\text{vac}}) \cdot \tau_{\text{vac}} + \sum_{p\in\mathcal{P},\, p\neq p_{\text{vac}}}^{\omega(p)>0} r_i(p) \cdot \omega(p) \\ & \leq \sum_{p\in\mathcal{P}}^{\omega(p)>0,\ D_{iB}(p)\leq D_\delta} U_{iB}(p) \cdot \omega(p) \qquad (i \in \mathcal{N}) \ , \end{aligned} \tag{5.9}$$

and (5.6) can be simplified to

$$\begin{aligned} r_i(p_{\text{vac}}) \cdot \tau_{\text{vac}} + \sum_{p\in\mathcal{P},\, p\neq p_{\text{vac}}}^{\omega(p)>0,\ D_{iB}(p)>D_\delta} r_i(p) \cdot \omega(p) \\ \leq E_{\text{max}} - E_{\text{min}} \quad (i \in \mathcal{N}) \ . \end{aligned} \tag{5.10}$$

Summarizing all these updates, OPT-ub can be written as follows:

OPT-ub:

Maximize $\frac{\tau_{\text{vac}}}{\tau}$

s.t. Time constraints: (5.8);
Flow routing constraints: (5.3);
Energy consumption model: (5.5);
Energy renewable constraints: (5.9), (5.10) .
$\tau, \tau_{\text{vac}}, \omega(p) \geq 0 \quad (p \in \mathcal{P})$
$f_{ij}(p), f_{iB}(p), r_i(p) \geq 0 \ \ (i, j \in \mathcal{N}, i \neq j, p \in \mathcal{P})$.

Denote ψ^*_{TPP} and $\psi^*_{\text{OPT-ub}}$ as an optimal solution to Problem TPP and Problem OPT-ub, respectively. Denote η^*_{TPP} as the objective value achieved by ψ^*_{TPP} and $\eta^*_{\text{OPT-ub}}$ as the objective value achieved by $\psi^*_{\text{OPT-ub}}$, respectively. The following lemma shows the relationship between $\eta^*_{\text{OPT-ub}}$ and η^*_{TPP}.

Lemma 5.2 *$\eta^*_{OPT\text{-}ub}$ is an upper bound of η^*_{TPP}, i.e., $\eta^*_{OPT\text{-}ub} > \eta^*_{TPP}$.*

A proof sketch: The proof of Lemma 5.2 can be constructed as follows. Suppose ψ^*_{TPP} is given.

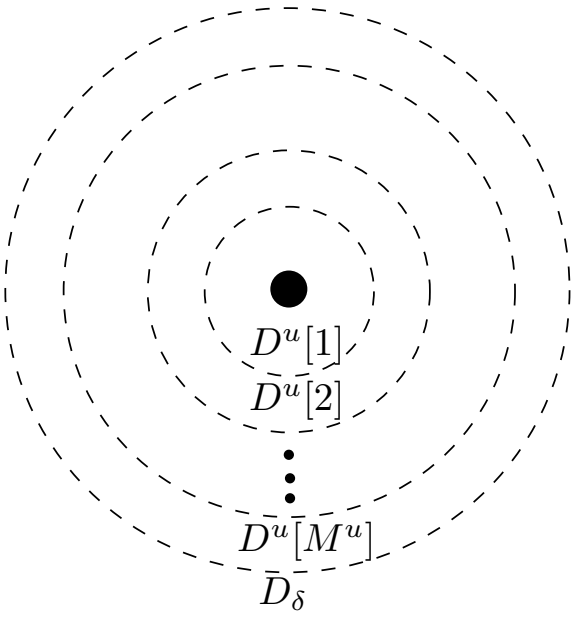

Figure 5.2: A sequence of circles centered at a node with decreasing energy charging rates.

Then we can construct a solution $\psi_{\text{OPT-ub}}$ to Problem OPT-ub with strictly greater objective value than η^*_{TPP}. Such construction of $\psi_{\text{OPT-ub}}$ is straightforward as OPT-ub is an ideal (or relaxed) case of TPP assuming zero traveling time. Since the obtained solution $\psi_{\text{OPT-ub}}$ is only feasible to OPT-ub, $\eta^*_{\text{OPT-ub}}$ (for $\psi^*_{\text{OPT-ub}}$) must be greater than η^*_{TPP}. The proof is straightforward and is omitted to conserve space.

In the rest of this section, we develop a near-optimal solution to OPT-ub. In Section 5.3.2, we partition the SED $\mathcal{A}$ into a number of smaller subareas. In Section 5.3.3, we employ the so-called *logical point* as a "worst-case" representation for each subarea in terms of energy reception and energy consumption. The logical point concept that we propose here generalizes the "fictitious cost point" proposed in [51], which only considered energy consumption. In Section 5.3.4, we propose an approximation algorithm to Problem OPT-ub, and prove it near-optimality.

5.3.2 Area Partitioning

In this section, we partition the SED $\mathcal{A}$ into a number of smaller subareas. The partition is performed in a special way such that some lower and upper bounds can be derived regarding energy charging and consumption at each sensor node.

Phase I: Area Partition based on WET. First, we discretize energy reception rate. Due to one-to-one mapping between distance and energy reception rate (see (5.2)), a discretization of energy reception rate also corresponds to a discretization of distance.

We discretize energy reception rates $U[1], U[2], \ldots, U[M^u]$ as follows:

$$U[h] = \begin{cases} U_{\max}(1 - \frac{\epsilon}{W})^h & \text{if } 0 \leq h \leq M^u \\ 0 & \text{otherwise} , \end{cases} \tag{5.11}$$

where M^u is the largest integer such that $U[M^u] > \delta$, ϵ is the allowed error margin for the near-optimal solution, W is a parameter controlling the granularity of the discretization (i.e., a large W leads to a large M^u).

Corresponding to $U[1], U[2], \ldots, U[M^u]$, we can discretize distance into $D^u[1], D^u[2], \ldots, D^u[M^u]$, and define $D^u[h]$ as follows:

$$D^u[h] = \mu^{-1}\left(\frac{U[h]}{U_{\max}}\right), \quad 1 \leq h \leq M^u ,$$

where $\mu^{-1}(\cdot)$ denotes the inverse function of (5.2).

To determine M^u, recall that M^u is the largest integer such that $U[M^u] > \delta$. By (5.11), we have

$$M^u = \left\lfloor \frac{\ln(\frac{\delta}{U_{\max}})}{\ln(1 - \frac{\epsilon}{W})} \right\rfloor . \tag{5.12}$$

For each node $i \in \mathcal{N}$, we draw M^u circles centered at node i, with each circle having an increasing

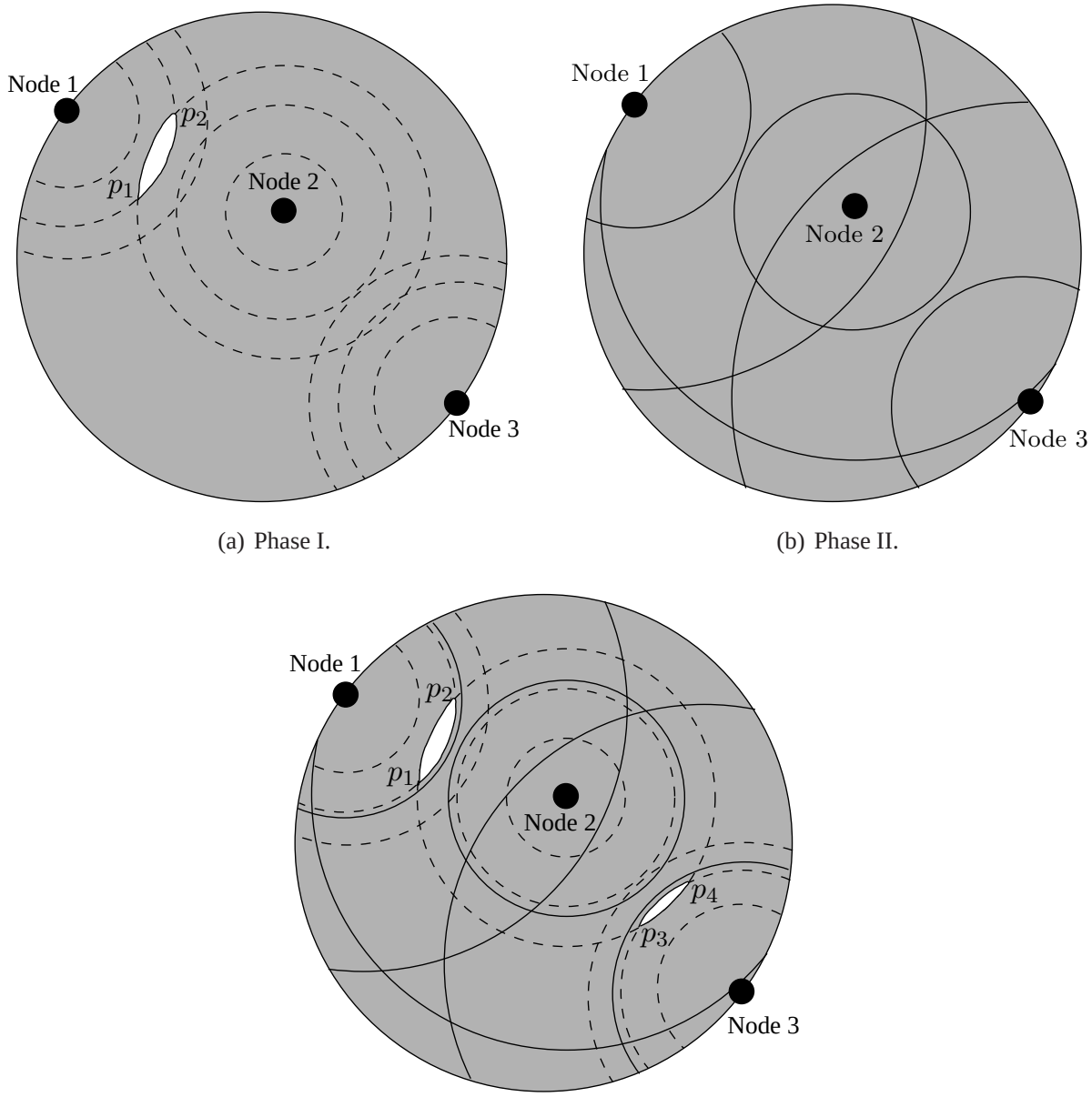

(a) Phase I.

(b) Phase II.

(c) Phase III.

Figure 5.3: An example three-node sensor network illustrating area partition in three phases. The gray region is the SED of the three nodes.

radius $D^u[h]$, $1 \leq h \leq M^u$. Based on (5.2), there is a circle with a radius of D_δ that cuts off the charging area for node i. That is, when $D_{iB}(p) = D_\delta$, $U_{iB}(p) = \delta$ (see Fig. 5.2). Note that this last cut-off circle, along with the M^u-th inner circle (i.e. the second outermost circle) partition $\mathcal{A}$ into three regions:

(i). A disk with a radius of $D^u[M^u]$, where $U[M^u] \leq U_{iB}(p) \leq U_{\max}$.

(ii). A ring bounded by these two circles with radiuses of $D^u[M^u]$ and D_δ, respectively, where $\delta \leq U_{iB}(p) < U[M^u]$.

(iii). The area outside of the cut-off circle, in which $U_{iB}(p) = 0$.

Since we have $(M^u + 1)$ circles for each node i, the intersections of these circles partition disk $\mathcal{A}$ into a number of irregular subareas. As an example, for the 3-node network in Fig. 5.3(a), suppose that $M^u = 2$. Then we draw 3 circles for each node. Disk $\mathcal{A}$ in Fig. 5.3(a) is partitioned into 19 irregular subareas. For the subarea of white color with corner points p_1 and p_2, any point p in this subarea satisfies $U[2] \leq U_{1B}(p) \leq U[1]$ with respect to node 1. With respect to nodes 2 and 3, for any point p in this same subarea, we have $\delta \leq U_{2B}(p) \leq U[2]$, and $U_{3B}(p) = 0$.

As shown in the example, the proposed area partition gives tight lower and upper bounds for each subarea. In particular, for a subarea $\mathcal{A}^u$ with $D_{iB}(p) \leq D^u[M^u]$ where $p \in \mathcal{A}^u$, we have

$$U[h_i^u(\mathcal{A}^u)] \leq U_{iB}(p) \leq U[h_i^u(\mathcal{A}^u) - 1] \ , \ p \in \mathcal{A}^u \ , \tag{5.13}$$

where $h_i^u(\mathcal{A}^u)$ denotes the index of the outer circle (centered at node i), and $h_i^u(\mathcal{A}^u) \leq M^u$. For a given subarea $\mathcal{A}^u$, $h_i^u(\mathcal{A}^u)$ can be determined by (5.11) and (5.13). We have

$$h_i^u(\mathcal{A}^u) = \left\lceil \frac{\ln\left(U_{iB}(p)/U_{\max}\right)}{\ln\left(1 - \epsilon/W\right)} \right\rceil \ , \ p \in \mathcal{A}^u \ . \tag{5.14}$$

Therefore, for any $p \in \mathcal{A}^u$, we have the lower bound for energy reception $U_{iB}(p)$ as follows:

$$U[h_i^u(\mathcal{A}^u)] = \begin{cases} U_{\max}(1-\frac{\epsilon}{W})^{h_i^u(\mathcal{A}^u)}, \text{if } D_{iB}(p) \le D^u[M^u] \ , \\ \delta, \qquad\qquad \text{if } D^u[M^u] < D_{iB}(p) \le D_\delta \ , \\ 0, \qquad\qquad \text{otherwise} \ , \end{cases} \tag{5.15}$$

where $h_i^u(\mathcal{A}^u)$ is determined by (5.14).

Phase II: Area Partition based on Energy Consumption. Following a similar token to that in Phase I, we discretize energy consumption rate, which also corresponds to a discretization of distance. Specifically, for each node $i \in \mathcal{N}$, we define a sequence of increasing energy costs $C[1], C[2], \ldots, C[M_i^c]$ as follows:

$$C[h] = \beta_1 \left(1 + \frac{\epsilon}{W}\right)^h \ , \tag{5.16}$$

where M_i^c is the largest number of elements in the sequence of $C[h]$. Corresponding to $C[h]$, $h = 1, 2, \ldots, M_i^c$, we can discretize distance into $D^c[1], D^c[2], \ldots, D^c[M_i^c]$, where

$$D^c[h] = \Big(\frac{C[h] - \beta_1}{\beta_2}\Big)^{-\alpha} \ , \quad 0 \le h \le M_i^c + 1 \ .$$

For each node $i \in \mathcal{N}$, we can draw M_i^c circles centered at node i, with increasing radii $D^c[1], D^c[2], \ldots, D^c[M_i^c]$. To determine M_i^c, denote $O_\mathcal{A}$ and $R_\mathcal{A}$ as the origin and radius of $\mathcal{A}$, respectively. Denote $D_{i,O_\mathcal{A}}$ as the distance from node i to $O_\mathcal{A}$. As $D_{iB}(p) \in [0, D_{i,O_\mathcal{A}} + R_\mathcal{A}]$, by (5.4), we have $C_{iB} \in [\beta_1, \beta_1 + \beta_2 \cdot (D_{i,O_\mathcal{A}} + R_\mathcal{A})^\alpha]$. Since the WCV can only travel within $\mathcal{A}$, M_i^c is the largest integer such that $C[M_i^c] < \beta_1 + \beta_2 \cdot (D_{i,O_\mathcal{A}} + R_\mathcal{A})^\alpha$. By (5.16), we have

$$M_i^c = \Big\lfloor \frac{\ln\left(1 + \frac{\beta_2}{\beta_1} \cdot (D_{i,O_\mathcal{A}} + R_\mathcal{A})^\alpha\right)}{\ln\left(1 + \frac{\epsilon}{W}\right)} \Big\rfloor \ . \tag{5.17}$$

Since we have M_i^c circles for $i \in \mathcal{N}$, the intersections of these circles partition $\mathcal{A}$ into a number of

subareas (see Fig. 5.3(b)). For a subarea $\mathcal{A}^c$, we have

$$C[h_i^c(\mathcal{A}^c) - 1] \leq C_{iB}(p) \leq C[h_i^c(\mathcal{A}^c)] \ , \quad p \in \mathcal{A}^c \ , \tag{5.18}$$

where $h_i^c(\mathcal{A}^c)$ denotes the index of the outer circle (centered at node i) that contains $\mathcal{A}^c$. Given a subarea $\mathcal{A}^c$, $h_i^c(\mathcal{A}^c)$ can be determined by (5.16) and (5.18). Thus, we have

$$h_i^c(\mathcal{A}^c) = \left\lceil \frac{\ln\left(1 + \frac{\beta_2}{\beta_1} \cdot D_{iB}(p)^\alpha\right)}{\ln\left(1 + \frac{\epsilon}{W}\right)} \right\rceil \ . \tag{5.19}$$

Therefore, for any $p \in \mathcal{A}^c$, a tight upper bound of $C_{iB}(p)$ is:

$$C[h_i^c(\mathcal{A}^c)] = \beta_1 \left(1 + \frac{\epsilon}{W}\right)^{h_i^c(\mathcal{A}^c)} \ , \tag{5.20}$$

where $h_i^c(\mathcal{A}^c)$ is determined by (5.19).

Phase III: Joint Area Partition. By combining the partitions in both Phases I and II, the disk $\mathcal{A}$ is partitioned into smaller subareas $\mathcal{A}_k^{u+c}$, $k = 1, 2, \ldots, K$ (see Fig. 5.3(c)). For each subarea $\mathcal{A}_k^{u+c}$, both the energy reception and consumption can be tightly bounded.

Now we give an upper bound on the number of subareas K. By (5.12), we have

$$M^u = \left\lfloor \frac{\ln\left(\frac{\delta}{U_{\max}}\right)}{\ln\left(1 - \frac{\epsilon}{W}\right)} \right\rfloor = O\left(\left\lfloor \frac{1}{\frac{\epsilon}{W}} \right\rfloor\right) = O\left(\frac{W}{\epsilon}\right) \ ,$$

where the second equality holds since $\ln\left(\delta/U_{\max}\right)$ is a negative constant and $\ln(1-\epsilon/W) \approx -\epsilon/W$ for small ϵ/W. Similarly, we have

$$M_i^c \ = \ \left\lfloor \frac{\ln\left(1 + \frac{\beta_2}{\beta_1} \cdot (D_{i,O_\mathcal{A}} + R_\mathcal{A})^\alpha\right)}{\ln\left(1 + \frac{\epsilon}{W}\right)} \right\rfloor = O\left(\left\lfloor \frac{1}{\frac{\epsilon}{W}} \right\rfloor\right) = O\left(\frac{W}{\epsilon}\right) \ .$$

For each sensor node, there are $(M^u + 1)$ circles from Phase I and M_i^c circles from Phase II.

Putting these circles and one more circle for $\mathcal{A}$ together, the total number of circles is $B = 1 + \sum_{i\in\mathcal{N}}(M^u + M_i^c + 1)$. Given B circles, the maximum number of subareas K is upper bounded by $K \leq B^2 - B + 2$ (which can be easily proved by induction). That is

$$K = O(B^2) \;\; = \;\; O\bigg(\Big[1 + \sum_{i\in\mathcal{N}}(M^u + M_i^c + 1)\Big]^2\bigg) = O\bigg(\Big(\frac{W|\mathcal{N}|}{\epsilon}\Big)^2\bigg) \; . \tag{5.21}$$

5.3.3 Logical Point Representation

For each subarea $\mathcal{A}_k^{u+c}$, $k = 1, 2, \ldots, K$, we represent it as a *logical point* $\mathcal{L}_k$. Denote $\omega(\mathcal{L}_k)$ as the total stopping time when the WCV is in subarea $\mathcal{A}_k^{u+c}$. Then we have,

$$\omega(\mathcal{L}_k) = \sum_{p\in\mathcal{A}_k^{u+c}}^{\omega(p)>0} \omega(p) \; .$$

To characterize a logical point $\mathcal{L}_k$, we use the worst case bounds of energy charging and energy consumption rates within the subarea $\mathcal{A}_k^{u+c}$. Specifically, for a logical point $\mathcal{L}_k$, we use a $|2\mathcal{N}|$-tuple to represent a logical point, where the first $|\mathcal{N}|$ components are for energy charging and the other $|\mathcal{N}|$ components are for energy consumption, i.e., $\big[U_1(\mathcal{L}_k), U_2(\mathcal{L}_k), \ldots, U_{|\mathcal{N}|}(\mathcal{L}_k), C_{1B}(\mathcal{L}_k), C_{2B}(\mathcal{L}_k), \ldots, C_{|\mathcal{N}|B}(\mathcal{L}_k)\big]$. In this vector, the first $|\mathcal{N}|$ components are

$$U_i(\mathcal{L}_k) = U[h_i^u(\mathcal{A}_k^{u+c})] \; , \tag{5.22}$$

where $U[h_i^u(\mathcal{A}_k^{u+c})]$ is the lower bound of $U_{iB}(p)$ for any $p \in \mathcal{A}_k^{u+c}$ and is determined by (5.15), while the next $|\mathcal{N}|$ components are

$$C_{iB}(\mathcal{L}_k) = C[h_i^c(\mathcal{A}_k^{u+c})] \; , \tag{5.23}$$

where $C[h_i^c(\mathcal{A}_k^{u+c})]$ is the upper bound of $C_{iB}(p)$ for any $p \in \mathcal{A}_k^{u+c}$ and is determined by (5.20).

The procedure of space partitioning and logical points representation is summarized in Algorithm 5.1.

Algorithm 5.1 (Logical Points Representation)

1. *Find the smallest enclosing disk $\mathcal{A}$ for all nodes $i \in \mathcal{N}$ and the home service station.*
2. *Centered at each node $i \in \mathcal{N}$, draw a circle of radius D_δ.*
3. *Given an $\epsilon > 0$, define a sequence of energy reception rate $U[1], U[2], \ldots, U[M^u]$ by (5.11), where M^u is determined by (5.12). Centered at each node $i \in \mathcal{N}$, draw a sequence of M^u circles corresponding to $U[h]$, $1 \leq h \leq M^u$.*
4. *For the given ϵ, define a sequence of energy costs $C[1], C[2], \ldots, C[M_i^c]$ by (5.16), where M_i^c is determined by (5.17). Centered at each node $i \in \mathcal{N}$, draw a sequence of M_i^c circles corresponding to cost $C[h]$, $1 \leq h \leq M_i^c$.*
5. *The intersection of all the circles from Steps 2–4 partition $\mathcal{A}$ into K subareas $\mathcal{A}_1^{u+c}, \mathcal{A}_2^{u+c}, \ldots, \mathcal{A}_K^{u+c}$.*
6. *For each subarea $\mathcal{A}_k^{u+c}$, $k = 1, 2, \ldots, K$, define a logical point $\mathcal{L}_k$ which is represented by a $|2\mathcal{N}|$-tuple $\big[U_1(\mathcal{L}_k), U_2(\mathcal{L}_k), \ldots, U_{|\mathcal{N}|}(\mathcal{L}_k), C_{1B}(\mathcal{L}_k), C_{2B}(\mathcal{L}_k), \ldots, C_{|\mathcal{N}|B}(\mathcal{L}_k)\big]$.*

5.3.4 A Near-Optimal Solution

Based on these logical points, we can develop a provably near-optimal solution to Problem OPT-ub. Recall that $\psi^*_{\text{OPT-ub}}$ is an optimal solution to Problem OPT-ub, and $\eta^*_{\text{OPT-ub}}$ is the objective value achieved by $\psi^*_{\text{OPT-ub}}$. Our goal is to find a feasible solution to Problem OPT-ub, denoted as $\psi_{\text{OPT-ub}}$, so that $\eta_{\text{OPT-ub}} \geq \eta^*_{\text{OPT-ub}} - \epsilon$.

A Worst-Case Formulation and Its Solution. Note that a logical point is a worst-case representation of the subarea in terms of energy charging and energy consumption. Based on these logical points, we can have a formulation, denoted as OPT-$\mathcal{L}$, that can be used to derive a lower bound to OPT-ub. Problems OPT-$\mathcal{L}$ and OPT-ub are similar to each other except the following differences:

- OPT-$\mathcal{L}$ is based on a finite number of logical points while OPT-ub is based on an infinite number of physical points.
- For $p \neq p_{\text{vac}}$, we have $\omega(\mathcal{L}_k), f_{ij}(\mathcal{L}_k), f_{iB}(\mathcal{L}_k), r_i(\mathcal{L}_k)$ in OPT-$\mathcal{L}$ rather than $\omega(p), f_{ij}(p), f_{iB}(p), r_i(p)$ in OPT-ub.
- We have $U_i(\mathcal{L}_k)$ and $C_{iB}(\mathcal{L}_k)$ in OPT-$\mathcal{L}$ rather than $U_i(p)$ and $C_{iB}(p)$ in OPT-ub.

Through a number of changes of variables, OPT-$\mathcal{L}$ can be reformulated into a linear program (LP), which can be solved in polynomial time. We show how to reformulate problem OPT-$\mathcal{L}$ to an LP via a change-of-variable technique. For the fractional objective function $\frac{\tau_{\text{vac}}}{\tau}$, we define $\eta_{\text{vac}} = \frac{\tau_{\text{vac}}}{\tau}$. We also define $\eta(\mathcal{L}_k) = \frac{\omega(\mathcal{L}_k)}{\tau}$ and $q = \frac{1}{\tau}$. For time constraint (5.8), we divide both sides by τ, and rewrite it as

$$\eta_{\text{vac}} + \sum_{k=1}^{K} \eta(\mathcal{L}_k) = 1 \tag{5.24}$$

For (5.3) and (5.5), we consider logical points $\mathcal{L}_k$, $k = 1, 2, \cdots, K$, and p_{vac} separately. First, for $\mathcal{L}_k$, we multiple both sides of (5.3) by $\eta(\mathcal{L}_k)$ and define $g_{ij}(\mathcal{L}_k) = f_{ij}(\mathcal{L}_k) \cdot \eta(\mathcal{L}_k)$ and $g_{iB}(\mathcal{L}_k) = f_{iB}(\mathcal{L}_k) \cdot \eta(\mathcal{L}_k)$. For the new nonlinear terms $r_i(\mathcal{L}_k) \cdot \eta(\mathcal{L}_k)$, we define $\mathcal{E}_i(\mathcal{L}_k) = r_i(\mathcal{L}_k) \cdot \eta(\mathcal{L}_k)$. By the new variables $g_{ij}(\mathcal{L}_k)$, $g_{iB}(\mathcal{L}_k)$, and $\mathcal{E}_i(\mathcal{L}_k)$, (5.3) is reformulated as

$$\textstyle\sum_{k\in\mathcal{N}}^{k\neq i} g_{ki}(\mathcal{L}_k) + R_i \cdot \eta(\mathcal{L}_k) = \sum_{j\in\mathcal{N}}^{j\neq i} g_{ij}(\mathcal{L}_k) + g_{iB}(\mathcal{L}_k) \ , \tag{5.25}$$

and (5.5) is rewritten as

$$\mathcal{E}_i(\mathcal{L}_k) = \rho \sum_{k\in\mathcal{N}}^{k\neq i} g_{ki}(\mathcal{L}_k) + \sum_{j\in\mathcal{N}}^{j\neq i} C_{ij} \cdot g_{ij}(\mathcal{L}_k) + C_{iB}(\mathcal{L}_k) \cdot g_{iB}(\mathcal{L}_k) \ . \tag{5.26}$$

Second, for p_{vac}, we multiply both sides of (5.3) and (5.5) by η_{vac}, and define $g_{ij}(p_{\text{vac}}) = f_{ij}(p_{\text{vac}}) \cdot \eta_{\text{vac}}$, $g_{iB}(p_{\text{vac}}) = f_{iB}(p_{\text{vac}}) \cdot \eta_{\text{vac}}$, and $\mathcal{E}_i(p_{\text{vac}}) = r_i(p_{\text{vac}}) \cdot \eta_{\text{vac}}$. Then (5.3) and (5.5) can be reformulated as

$$\sum_{k\in\mathcal{N}}^{k\neq i} g_{ki}(p_{\text{vac}}) + R_i \cdot \eta_{\text{vac}} = \sum_{j\in\mathcal{N}}^{j\neq i} g_{ij}(p_{\text{vac}}) + g_{iB}(p_{\text{vac}}) \tag{5.27}$$

$$\mathcal{E}_i(p_{\text{vac}}) = \rho \sum_{k\in\mathcal{N}}^{k\neq i} g_{ki}(p_{\text{vac}}) + \sum_{j\in\mathcal{N}}^{j\neq i} C_{ij} \cdot g_{ij}(p_{\text{vac}}) + C_{iB}(p_{\text{vac}}) \cdot g_{iB}(p_{\text{vac}}) \tag{5.28}$$

By dividing both sides by τ, constraint (5.9) can be rewritten as $r_i(p_{\text{vac}}) \cdot \eta_{\text{vac}} + \sum_{k=1}^{K} r_i(\mathcal{L}_k) \cdot \eta(\mathcal{L}_k) \leq \sum_{k=1,\ldots,K}^{D_{iB}(p)\leq D_\delta, p\in\mathcal{A}_k^{u+c}} U_{iB}(\mathcal{L}_k) \cdot \eta(\mathcal{L}_k)$, or equivalently,

$$\mathcal{E}_i(p_{\text{vac}}) + \sum_{m=1}^{K} \mathcal{E}_i(\mathcal{L}_k) \leq \sum_{k=1,\ldots,K}^{D_{iB}(p)\leq D_\delta, p\in\mathcal{A}_k^{u+c}} U_{iB}(\mathcal{L}_k) \cdot \eta(\mathcal{L}_k) \tag{5.29}$$

Similarly, by dividing both sides by τ, (5.10) can be rewritten as $r_i(p_{\text{vac}}) \cdot \eta_{\text{vac}} + \sum_{k=1,\ldots,K}^{D_{iB}(p)>D_\delta, p\in\mathcal{A}_k^{u+c}} r_i(\mathcal{L}_k) \cdot \eta(\mathcal{L}_k) \leq \frac{E_{\max}-E_{\min}}{\tau}$, or equivalently,

$$\mathcal{E}_i(p_{\text{vac}}) + \sum_{k=1,\ldots,K}^{D_{iB}(p)>D_\delta, p\in\mathcal{A}_k^{u+c}} \mathcal{E}_i(\mathcal{L}_k) \leq (E_{\max} - E_{\min}) \cdot q \ . \tag{5.30}$$

Summarizing the objective function and all constraints, we have

OPT-LP:

Maximize η_{vac}

s.t. Time constraints: (5.24);
Flow routing constraints: (5.25), (5.27);
Energy consumption model: (5.26), (5.28);
Energy renewable constraints: (5.29), (5.30) .

$$q, \eta_{\text{vac}}, \eta(\mathcal{L}_k) \geq 0 \quad (k = 1, \ldots, K)$$
$$g_{ij}(\mathcal{L}_k), g_{iB}(\mathcal{L}_k), \mathcal{E}_i(\mathcal{L}_k), g_{ij}(p_{\text{vac}}), g_{iB}(p_{\text{vac}}), \mathcal{E}_i(p_{\text{vac}}) \geq 0 \ \ (i, j \in \mathcal{N}, i \neq j, k = 1, \ldots, K) .$$

Now the new objective function and new constraints are linear, which makes an LP.

Recover a Feasible Solution to OPT-ub. After we obtain an optimal solution to Problem OPT-$\mathcal{L}$, denoted as $\psi_{\text{OPT-}\mathcal{L}}$, we need to recover a solution to OPT-ub (denoted by $\psi_{\text{OPT-ub}}$). Suppose that $\psi_{\text{OPT-ub}} = (\tau, \tau_{\text{vac}}, \omega(p), f_{ij}(p), f_{iB}(p), r_i(p))$. From $\psi_{\text{OPT-}\mathcal{L}}$, $\psi_{\text{OPT-ub}}$ can be constructed as follows:

- τ and τ_{vac} are the same as their counterparts in $\psi_{\text{OPT-}\mathcal{L}}$.
- For $p = p_{\text{vac}}$, $f_{ij}(p_{\text{vac}}), f_{iB}(p_{\text{vac}}), r_i(p_{\text{vac}})$ are the same as their counterparts in $\psi_{\text{OPT-}\mathcal{L}}$.
- For any $\omega(\mathcal{L}_k) > 0$, choose a point $p_k \in \mathcal{A}_k^{u+c}$ and set $\omega(p_k) = \omega(\mathcal{L}_k)$. Further, set flow routing $f_{ij}(p_k) = f_{ij}(\mathcal{L}_k)$ and $f_{iB}(p_k) = f_{iB}(\mathcal{L}_k)$. Determine $r_i(p_k)$ by (5.5).

Denote $\eta_{\text{OPT-}\mathcal{L}}$ and $\eta_{\text{OPT-ub}}$ as the objective values achieved by $\psi_{\text{OPT-}\mathcal{L}}$ and $\psi_{\text{OPT-ub}}$, respectively. Since τ and τ_{vac} are unchanged in the foregoing solution construction, we have

$$\eta_{\text{OPT-ub}} = \eta_{\text{OPT-}\mathcal{L}} \ . \tag{5.31}$$

The following lemma affirms the feasibility of the constructed solution $\psi_{\text{OPT-ub}}$ to Problem OPT-ub.

Lemma 5.3 *$\psi_{\text{OPT-ub}}$ is a feasible solution to Problem OPT-ub.*

Proof To show that $\psi_{\text{OPT-ub}} = (\tau, \tau_{\text{vac}}, \omega(p), f_{ij}(p), f_{iB}(p), r_i(p))$ is feasible to Problem OPT-ub, we need to verify that $\psi_{\text{OPT-ub}}$ satisfies Constraints (5.3), (5.5), (5.8), (5.9), and (5.10). To do this, we exploit the worst case bounds that are inherited in a logical point representation.

Since $\psi_{\text{OPT-}\mathcal{L}}$ is feasible to Problem OPT-$\mathcal{L}$ (based on the K logical points), we know that $\psi_{\text{OPT-}\mathcal{L}}$ satisfies Constraints (5.3), (5.5), (5.8), (5.9), and (5.10). We now verify each of these constraints for $\psi_{\text{OPT-ub}}$. Since τ and τ_{vac} remain unchanged and $\omega(p_k) = \omega(\mathcal{L}_k)$, where $p_k \in \mathcal{A}_k^{u+c}$, $1 \le k \le K$, $\psi_{\text{OPT-ub}}$ satisfies Constraint (5.8). $\psi_{\text{OPT-ub}}$ also satisfies Constraints (5.3) and (5.5) since $f_{ij}(p_{\text{vac}})$, $f_{iB}(p_{\text{vac}})$ and $r_i(p_{\text{vac}})$ remain unchanged, $f_{ij}(p_k) = f_{ij}(\mathcal{L}_k)$, $f_{iB}(p_k) = f_{iB}(\mathcal{L}_k)$, and $r_i(p_k)$ is determined by (5.5).

To verify two remaining energy constraints (5.9) and (5.10), by (5.20) and (5.23), we first have $C_{iB}(p_k) \le C_{iB}(\mathcal{L}_k)$, $1 \le k \le K$. As a result, $r_i(p_k) = \rho \sum_{k\in\mathcal{N}}^{k\neq i} f_{ki}(p_k) + \sum_{j\in\mathcal{N}}^{j\neq i} C_{ij} \cdot f_{ij}(p_k) + C_{iB}(p_k) \cdot f_{iB}(p_k) \le \rho \sum_{n\in\mathcal{N}}^{n\neq i} f_{ni}(\mathcal{L}_k) + \sum_{j\in\mathcal{N}}^{j\neq i} C_{ij} \cdot f_{ij}(\mathcal{L}_k) + C_{iB}(\mathcal{L}_k) \cdot f_{iB}(\mathcal{L}_k) = r_i(\mathcal{L}_k)$, where the first equality holds since $\psi_{\text{OPT-ub}}$ satisfies (5.5), the second equality holds since $f_{ij}(p_k) = f_{ij}(\mathcal{L}_k)$, $f_{iB}(p_k) = f_{iB}(\mathcal{L}_k)$ and $C_{iB}(p_k) \le C_{iB}(\mathcal{L}_k)$, and the last equality holds since $\psi_{\text{OPT-}\mathcal{L}}$ satisfies (5.5). By the same token, we have that $r_i(p_{\text{vac}})$ is unchanged since $C_{iB}(p_{\text{vac}})$ is unchanged.

Since $r_i(p_k) \le r_i(\mathcal{L}_k)$ and $r_i(p_{\text{vac}})$ is unchanged, we have

$$\begin{aligned} r_i(p_{\text{vac}}) \cdot \tau_{\text{vac}} + \sum_{k=1}^{K} r_i(p_k) \cdot \tau(p_k) &\le r_i(p_{\text{vac}}) \cdot \tau_{\text{vac}} + \sum_{k=1}^{K} r_i(\mathcal{L}_k) \cdot \tau(\mathcal{L}_k) \\ &\le \sum_{k=1,\ldots,K}^{D_{iB}(p)\le D_\delta, p\in\mathcal{A}_k^{u+c}} U_{iB}(\mathcal{L}_k) \cdot \tau(\mathcal{L}_k) \\ &\le \sum_{k=1,\ldots,K}^{D_{iB}(p_k)\le D_\delta} U_{iB}(p_k) \cdot \tau(p_k) \end{aligned}$$

where the first inequality holds since $r_i(p_{\text{vac}})$ and τ_{vac} are unchanged, $r_i(p_k) \le r_i(\mathcal{L}_k)$ and $\tau(p_k) = \tau(\mathcal{L}_k)$, the second inequality holds since $\psi_{\text{OPT-}\mathcal{L}}$ satisfies (5.9), the third inequality holds by $U_{iB}(\mathcal{L}_k) \le U_{iB}(p_k)$ (see (5.15) and (5.22)) and $\tau(p_k) = \tau(\mathcal{L}_k)$. Thus, Constraint (5.9) holds for $\psi_{\text{OPT-ub}}$. Similarly, we can show that Constraint (5.10) holds for $\psi_{\text{OPT-ub}}$. Therefore, the constructed solution $\psi_{\text{OPT-ub}}$ is feasible to Problem OPT-ub. This completes the proof. □

Proof of Near-Optimality. The near-optimality of $\psi_{\text{OPT-ub}}$ is stated in the following theorem:

Theorem 5.1 *For a given* $\epsilon > 0$, $\eta_{OPT\text{-}ub} \geq \eta^*_{OPT\text{-}ub} - \epsilon$.

Proof The proof is based on construction. Suppose we have known an optimal solution $\psi^*_{\text{OPT-ub}}$ to Problem OPT-ub with optimal objective value $\eta^*_{\text{OPT-ub}}$. Given an arbitrarily small $\epsilon > 0$, applying Algorithm 5.1 leads to K logical points $\mathcal{L}_k$, $k = 1, 2, \ldots, K$. Based on this set of logical points, we will show that it is possible to construct a solution $\hat{\psi}_{\text{OPT-LP}}$ to Problem OPT-LP (which is an equivalent reformation of Problem OPT-$\mathcal{L}$), such that the objective value $\hat{\eta}_{\text{OPT-LP}} \geq \eta^*_{\text{OPT-ub}} - \epsilon$. As a result, the optimal solution $\psi^*_{\text{OPT-LP}}$ to Problem OPT-LP must have its objective value $\eta^*_{\text{OPT-LP}} \geq \hat{\eta}_{\text{OPT-LP}} \geq \eta^*_{\text{OPT-ub}} - \epsilon$, where the first inequality holds since $\eta^*_{\text{OPT-LP}}$ is the optimal objective value for Problem OPT-LP while $\hat{\eta}_{\text{OPT-LP}}$ may not be. Further, we have $\eta_{\text{OPT-ub}} = \eta^*_{\text{OPT-}\mathcal{L}} = \eta^*_{\text{OPT-LP}} \geq \eta^*_{\text{OPT-ub}} - \epsilon$, where the first equality holds by (5.31).

Denote $\psi^*_{\text{OPT-}\mathcal{L}}$ as an optimal solution to Problem OPT-$\mathcal{L}$. we have $\eta_{\text{OPT-}\mathcal{L}} \geq \eta^*_{\text{OPT-ub}} - \epsilon$.

The optimal solution $\psi^*_{\text{OPT-ub}}$ is explicitly expressed as $\psi^*_{\text{OPT-ub}} = (\tau^*, \tau^*_{\text{vac}}, \omega(p)^*, f_{ij}(p)^*, f_{iB}(p)^*, p_i(p)^*)$. For $\psi^*_{\text{OPT-ub}}$, we have known specific locations where the WCV stays. Through the same change-of-variable technique as described in Section 5.3.4, we can always obtain a solution $\psi_{\text{OPT-LP}} = (h, \eta_{\text{vac}}, \eta(p), g_{ij}(p), g_{iB}(p), \mathcal{E}_i(p), g_{ij}(p_{\text{vac}}), g_{iB}(p_{\text{vac}}), \mathcal{E}_i(p_{\text{vac}}))$ to Problem OPT-LP, where $p \in \mathcal{A}$ and $\psi_{\text{OPT-LP}}$ is based on physical points.

Based upon $\psi_{\text{OPT-LP}}$, we can construct a solution $\hat{\psi}_{\text{OPT-LP}} = (\hat{h}, \hat{\eta}_{\text{vac}}, \hat{\eta}(\mathcal{L}_k), \hat{g}_{ij}(\mathcal{L}_k), \hat{g}_{iB}(\mathcal{L}_k), \hat{\mathcal{E}}_i(\mathcal{L}_k), \hat{g}_{ij}(p_{\text{vac}}), \hat{g}_{iB}(p_{\text{vac}}), \hat{\mathcal{E}}_i(p_{\text{vac}}))$ to Problem OPT-LP on the set of K logical points (generated by Algorithm 5.1), by letting

$$\hat{\eta}(\mathcal{L}_k) = \left(1 + \frac{W-2}{W} \cdot \epsilon\right) \cdot \sum_{p \in \mathcal{A}_k^{u+c}}^{\omega(p)>0} \eta(p) \ , \tag{5.32}$$

$$\hat{\eta}_{\text{vac}} = \eta_{\text{vac}} - \frac{W-2}{W} \cdot \epsilon \cdot \sum_{k=1}^{K} \sum_{p \in \mathcal{A}_k^{u+c}}^{\omega(p)>0} \eta(p) \tag{5.33}$$

and setting the weighted data flow and the weighted energy consumption rate at $\mathcal{L}_k$ as

$$\hat{g}_{ij}(\mathcal{L}_k) = \left(1 + \frac{W-2}{W} \cdot \epsilon\right) \cdot \sum_{p \in \mathcal{A}_k^{u+c}}^{\omega(p)>0} g_{ij}(p) \ , \ \hat{g}_{iB}(\mathcal{L}_k) = \left(1 + \frac{W-2}{W} \cdot \epsilon\right) \cdot \sum_{p \in \mathcal{A}_k^{u+c}}^{\omega(p)>0} g_{iB}(p) \ , \tag{5.34}$$

$$\hat{\mathcal{E}}_i(\mathcal{L}_k) \text{ determined by } (5.26) \ ,$$

and setting the weighted data flow and the weighted energy consumption rate at p_{vac} as

$$\hat{g}_{ij}(p_{\text{vac}}) = \frac{\hat{\eta}_{\text{vac}}}{\eta_{\text{vac}}} g_{ij}(p_{\text{vac}}) \ , \ \hat{g}_{iB}(p_{\text{vac}}) = \frac{\hat{\eta}_{\text{vac}}}{\eta_{\text{vac}}} g_{iB}(p_{\text{vac}}) \ , \ \hat{\mathcal{E}}_i(p_{\text{vac}}) = \frac{\hat{\eta}_{\text{vac}}}{\eta_{\text{vac}}} \mathcal{E}_i(p_{\text{vac}}) \ , \tag{5.35}$$

and letting

$$\hat{h} = \frac{\max_{i \in \mathcal{N}} \left\{ \hat{\mathcal{E}}_i(p_{\text{vac}}) + \sum_{k=1,\ldots,K}^{\mathcal{A}_k^{u+c} \not\subseteq \tilde{\mathcal{A}}_i} \hat{\mathcal{E}}_i(\mathcal{L}_k) \right\}}{E_{\max} - E_{\min}} \ , \tag{5.36}$$

where $\tilde{\mathcal{A}}_i \triangleq \{p | D_{iB}(p) \leq D_\delta\}$.

To show $\eta^*_{\text{OPT-ub}} - \epsilon \leq \eta^*_{\text{OPT-LP}}$, we have

$$\begin{aligned} \eta^*_{\text{OPT-ub}} - \eta^*_{\text{OPT-LP}} &= \eta_{\text{vac}} - [\eta_{\text{vac}} - \frac{W-2}{W} \cdot \epsilon \cdot \sum_{k=1}^{K} \sum_{p \in \mathcal{A}_k^{u+c}}^{\omega(p)>0} \eta(p)] \\ &= \frac{W-2}{W} \cdot \epsilon \cdot \sum_{k=1}^{K} \sum_{p \in \mathcal{A}_k^{u+c}}^{\omega(p)>0} \eta(p) = \frac{W-2}{W} \cdot \epsilon \cdot (1 - \eta_{\text{vac}}) \leq \epsilon \ , \end{aligned}$$

where the first equality holds by (5.33), the third equality holds since $\psi_{\text{OPT-LP}}$ satisfies Constraint (5.24), and the last inequality holds due to $\eta_{\text{vac}} \leq 1$.

To show that $\hat{\psi}_{\text{OPT-LP}}$ is a feasible solution to Problem OPT-LP on K logical points, we need to verify that $\hat{\psi}_{\text{OPT-LP}}$ satisfies Constraints (5.24), (5.25), (5.26), (5.27), (5.28), (5.29), and (5.30). Since $\psi_{\text{OPT-LP}}$ is feasible to Problem OPT-LP, $\psi_{\text{OPT-LP}}$ satisfies Constraints (5.24), (5.25), (5.26), (5.27), (5.28), (5.29), and (5.30).

We now verify each of these constraints for $\hat{\psi}_{\text{OPT-LP}}$. To show that $\hat{\psi}_{\text{OPT-LP}}$ satisfies Constraint (5.24), we see that

$$\begin{aligned}\hat{\eta}_{\text{vac}} + \sum_{k=1}^{K} \hat{\eta}(\mathcal{L}_k) &= \left(\eta_{\text{vac}} - \frac{W-2}{W} \cdot \epsilon \cdot \sum_{k=1}^{K} \sum_{p \in \mathcal{A}_k^{u+c}}^{\omega(p)>0} \eta(p)\right) + \sum_{k=1}^{K} \left[\left(1 + \frac{W-2}{W} \cdot \epsilon\right) \cdot \sum_{p \in \mathcal{A}_k^{u+c}}^{\omega(p)>0} \eta(p)\right] \\ &= \eta_{\text{vac}} + \sum_{k=1}^{K} \sum_{p \in \mathcal{A}_k^{u+c}}^{\omega(p)>0} \eta(p) = \eta_{\text{vac}} + \sum_{p \in \mathcal{A}}^{\omega(p)>0} \eta(p) = 1 \ ,\end{aligned}$$

where the first equality holds by (5.33) and (5.32), and the last equality holds since $\psi_{\text{OPT-LP}}$ satisfies Constraint (5.24).

To show that $\hat{\psi}_{\text{OPT-LP}}$ satisfies Constraint (5.25), we have

$$\begin{aligned}&\sum_{q \in \mathcal{N}}^{q \neq i} \hat{g}_{qi}(\mathcal{L}_k) + R_i \cdot \hat{\eta}(\mathcal{L}_k) \\ &= \sum_{q \in \mathcal{N}}^{q \neq i} \left[\left(1 + \frac{W-2}{W} \cdot \epsilon\right) \cdot \sum_{p \in \mathcal{A}_k^{u+c}}^{\omega(p)>0} g_{qi}(p)\right] + R_i \cdot \left(1 + \frac{W-2}{W} \cdot \epsilon\right) \cdot \sum_{p \in \mathcal{A}_k^{u+c}}^{\omega(p)>0} \eta(p) \\ &= \left(1 + \frac{W-2}{W} \cdot \epsilon\right) \cdot \sum_{p \in \mathcal{A}_k^{u+c}}^{\omega(p)>0} \left[\sum_{q \in \mathcal{N}}^{q \neq i} g_{qi}(p) + R_i \cdot \eta(p)\right] \\ &= \left(1 + \frac{W-2}{W} \cdot \epsilon\right) \cdot \sum_{p \in \mathcal{A}_k^{u+c}}^{\omega(p)>0} \left[\sum_{j \in \mathcal{N}}^{j \neq i} g_{ij}(p) + g_{iB}(p)\right]\end{aligned}$$

$$= \sum_{j\in\mathcal{N}}^{j\neq i}\left[\left(1+\frac{W-2}{W}\cdot\epsilon\right)\cdot\sum_{p\in\mathcal{A}_k^{u+c}}^{\omega(p)>0} g_{ij}(p)\right]+\left(1+\frac{W-2}{W}\cdot\epsilon\right)\cdot\sum_{p\in\mathcal{A}_k^{u+c}}^{\omega(p)>0} g_{iB}(p)$$

$$= \sum_{j\in\mathcal{N}}^{j\neq i}\hat{g}_{ij}(\mathcal{L}_k)+\hat{g}_{iB}(\mathcal{L}_k)\ ,$$

where the first equality holds by (5.34) and (5.32), the third equality holds since $\psi_{\text{OPT-LP}}$ satisfies Constraint (5.25), and the last equality holds by (5.34).

Now we show that $\hat{\psi}_{\text{OPT-LP}}$ satisfies Constraints (5.26), (5.27), (5.28). As $\psi_{\text{OPT-LP}}$ satisfies Constraints (5.27), multiplying $\frac{\hat{\eta}_{\text{vac}}}{\eta_{\text{vac}}}$ on both sides of (5.27) leads to $\sum_{k\in\mathcal{N}}^{k\neq i}\frac{\hat{\eta}_{\text{vac}}}{\eta_{\text{vac}}}g_{ki}(p_{\text{vac}})+R_i\cdot\hat{\eta}_{\text{vac}} = \sum_{j\in\mathcal{N}}^{j\neq i}\frac{\hat{\eta}_{\text{vac}}}{\eta_{\text{vac}}}g_{ij}(p_{\text{vac}})+\frac{\hat{\eta}_{\text{vac}}}{\eta_{\text{vac}}}g_{iB}(p_{\text{vac}})$, or equivalently, by (5.35),

$$\sum_{k\in\mathcal{N}}^{k\neq i}\hat{g}_{ki}(p_{\text{vac}})+R_i\cdot\hat{\eta}_{\text{vac}}=\sum_{j\in\mathcal{N}}^{j\neq i}\hat{g}_{ij}(p_{\text{vac}})+\hat{g}_{iB}(p_{\text{vac}}).$$

Thereby Constraint (5.27) holds for $\hat{\psi}_{\text{OPT-LP}}$, and so does (5.28). Since $\hat{\mathcal{E}}_i(\mathcal{L}_k)$ is determined by (5.26), we know that $\hat{\psi}_{\text{OPT-LP}}$ must meet Constraint (5.26).

To show that $\hat{\psi}_{\text{OPT-LP}}$ satisfies Constraint (5.29), we first need the following properties for a logical point $\mathcal{L}_k$.

$$(1-\frac{\epsilon}{W})\cdot U_{iB}(p)\leq U_{iB}(\mathcal{L}_k)\leq U_{iB}(p)\ ,\ p\in\mathcal{A}_k^{u+c}, \tag{5.37}$$

$$C_{iB}(p)\leq C_{iB}(\mathcal{L}_k)\leq(1+\frac{\epsilon}{W})\cdot C_{iB}(p)\ ,\ p\in\mathcal{A}_k^{u+c}. \tag{5.38}$$

The former part of (5.37) can be verify by $U_{iB}(\mathcal{L}_k)=U[h_i^{\mathcal{R}}(\mathcal{A}_k^{u+c})]=(1-\frac{\epsilon}{W})\cdot U[h_i^{\mathcal{R}}(\mathcal{A}_k^{u+c})-1]\geq(1-\frac{\epsilon}{W})\cdot U_{iB}(p)$, where the first equality holds by (5.22), the second equality holds by (5.11), and the last inequality holds by (5.15). The latter part of (5.37) can be verified by (5.15) and (5.22). Similarly, the former part of (5.38) can be verify by (5.20) and (5.23). For the latter part of (5.38),

we see $C_{iB}(\mathcal{L}_k) = C[h_i(\mathcal{A}_k^{u+c})] = (1 + \frac{\epsilon}{W}) \cdot C[h_i(\mathcal{A}_k^{u+c}) - 1] \leq (1 + \frac{\epsilon}{W}) \cdot C_{iB}(p)$, where the first equality holds by (5.23), the second equality holds by (5.16), and the last inequality holds by (5.20).

Such properties are helpful to derive upper bounds for $\hat{\mathcal{E}}_i(\mathcal{L}_k)$ and $\hat{\mathcal{E}}_i(p_{\text{vac}})$ as follows.

$$
\begin{aligned}
& \hat{\mathcal{E}}_i(\mathcal{L}_k) \\
= \;& \rho \sum_{q \in \mathcal{N}}^{q \neq i} \hat{g}_{qi}(\mathcal{L}_k) + \sum_{j \in \mathcal{N}}^{j \neq i} C_{ij} \cdot \hat{g}_{ij}(\mathcal{L}_k) + C_{iB}(\mathcal{L}_k) \cdot \hat{g}_{iB}(\mathcal{L}_k) \\
= \;& \rho \sum_{q \in \mathcal{N}}^{q \neq i} \left[\left(1 + \frac{W-2}{W} \cdot \epsilon \right) \cdot \sum_{p \in \mathcal{A}_k^{u+c}}^{\omega(p)>0} g_{qi}(p) \right] + \sum_{j \in \mathcal{N}}^{j \neq i} C_{ij} \cdot \left[\left(1 + \frac{W-2}{W} \cdot \epsilon \right) \cdot \sum_{p \in \mathcal{A}_k^{u+c}}^{\omega(p)>0} g_{ij}(p) \right] \\
& + C_{iB}(\mathcal{L}_k) \cdot \left(1 + \frac{W-2}{W} \cdot \epsilon \right) \cdot \sum_{p \in \mathcal{A}_k^{u+c}}^{\omega(p)>0} g_{iB}(p) \\
= \;& \left(1 + \frac{W-2}{W} \cdot \epsilon \right) \cdot \sum_{p \in \mathcal{A}_k^{u+c}}^{\omega(p)>0} \left[\rho \sum_{q \in \mathcal{N}}^{q \neq i} g_{qi}(p) + \sum_{j \in \mathcal{N}}^{j \neq i} C_{ij} \cdot g_{ij}(p) + C_{iB}(\mathcal{L}_k) \cdot g_{iB}(p) \right] \\
\leq \;& \left(1 + \frac{W-2}{W} \cdot \epsilon \right) \cdot \sum_{p \in \mathcal{A}_k^{u+c}}^{\omega(p)>0} \left[\rho \sum_{q \in \mathcal{N}}^{q \neq i} g_{qi}(p) + \sum_{j \in \mathcal{N}}^{j \neq i} C_{ij} \cdot g_{ij}(p) + \left(1 + \frac{\epsilon}{W} \right) \cdot C_{iB}(p) \cdot g_{iB}(p) \right] \\
\leq \;& \left(1 + \frac{W-2}{W} \cdot \epsilon \right) \cdot \left(1 + \frac{\epsilon}{W} \right) \cdot \sum_{p \in \mathcal{A}_k^{u+c}}^{\omega(p)>0} \left[\rho \sum_{q \in \mathcal{N}}^{q \neq i} g_{qi}(p) + \sum_{j \in \mathcal{N}}^{j \neq i} C_{ij} \cdot g_{ij}(p) + C_{iB}(p) \cdot g_{iB}(p) \right] \\
= \;& \left(1 + \frac{W-1}{W} \cdot \epsilon + \frac{W-2}{W^2} \cdot \epsilon^2 \right) \cdot \sum_{p \in \mathcal{A}_k^{u+c}}^{\omega(p)>0} \mathcal{E}_i(p) \;, \qquad (5.39)
\end{aligned}
$$

where the first equality holds since $\hat{\psi}_{\text{OPT-LP}}$ satisfies Constraint (5.26), the second equality holds by (5.34), the fourth inequality holds by (5.38), and the last equality holds since $\psi_{\text{OPT-LP}}$ satisfies (5.26).

For $\hat{\mathcal{E}}_i(p_{\text{vac}})$, we also have

$$\begin{aligned}\hat{\mathcal{E}}_i(p_{\text{vac}}) = \frac{\hat{\eta}_{\text{vac}}}{\eta_{\text{vac}}}\mathcal{E}_i(p_{\text{vac}}) &= \frac{\eta_{\text{vac}} - \frac{W-2}{W}\cdot\epsilon\cdot\sum_{k=1}^{K}\sum_{p\in\mathcal{A}_k^{u+c}}^{\omega(p)>0}\eta(p)}{\eta_{\text{vac}}}\cdot\mathcal{E}_i(p_{\text{vac}}) \\ &= \mathcal{E}_i(p_{\text{vac}}) - \Big(\frac{W-2}{W}\cdot\epsilon\Big)\cdot\frac{\mathcal{E}_i(p_{\text{vac}})\cdot\sum_{k=1}^{K}\sum_{p\in\mathcal{A}_k^{u+c}}^{\omega(p)>0}\eta(p)}{\eta_{\text{vac}}}, \quad (5.40)\end{aligned}$$

where the first equality holds by (5.35), the second equality holds by (5.33). Now we check the rightmost item $\frac{\sum_{k=1}^{K}\sum_{p\in\mathcal{A}_k^{u+c}}^{\omega(p)>0}\eta(p)}{\eta_{\text{vac}}}\cdot\mathcal{E}_i(p_{\text{vac}})$. If the following condition holds

$$\begin{aligned}\epsilon &\leq \frac{W}{W-2}\cdot\frac{1}{\sum_{k=1}^{K}\sum_{p\in\mathcal{A}_k^{u+c}}^{\omega(p)>0}\mathcal{E}_i(p) + \sum_{k=1,\ldots,K}^{\mathcal{A}_k^{u+c}\subseteq\tilde{\mathcal{A}}_i}\sum_{p\in\mathcal{A}_k^{u+c}}^{\omega(p)>0}U_{iB}(p)\cdot\eta(p)} \\ &\cdot\Bigg[(W-2)\cdot\frac{\mathcal{E}_i(p_{\text{vac}})\cdot\sum_{k=1}^{K}\sum_{p\in\mathcal{A}_k^{u+c}}^{\omega(p)>0}\eta(p)}{\eta_{\text{vac}}} + \\ &(W-3)\cdot\sum_{k=1,\ldots,K}^{\mathcal{A}_k^{u+c}\subseteq\tilde{\mathcal{A}}_i}\sum_{p\in\mathcal{A}_k^{u+c}}^{\omega(p)>0}U_{iB}(p)\cdot\eta(p) - (W-1)\cdot\sum_{k=1}^{K}\sum_{p\in\mathcal{A}_k^{u+c}}^{\omega(p)>0}\mathcal{E}_i(p)\Bigg], \quad (5.41)\end{aligned}$$

multiplying both sides by $\frac{W-2}{W^2}\cdot\epsilon\cdot\Big[\sum_{k=1}^{K}\sum_{p\in\mathcal{A}_k^{u+c}}^{\omega(p)>0}\mathcal{E}_i(p) + \sum_{k=1,\ldots,K}^{\mathcal{A}_k^{u+c}\subseteq\tilde{\mathcal{A}}_i}\sum_{p\in\mathcal{A}_k^{u+c}}^{\omega(p)>0}U_{iB}(p)\cdot\eta(p)\Big]$ leads to

$$\begin{aligned}&\frac{W-2}{W^2}\cdot\epsilon^2\cdot\Bigg[\sum_{k=1}^{K}\sum_{p\in\mathcal{A}_k^{u+c}}^{\omega(p)>0}\mathcal{E}_i(p) + \sum_{k=1,\ldots,K}^{\mathcal{A}_k^{u+c}\subseteq\tilde{\mathcal{A}}_i}\sum_{p\in\mathcal{A}_k^{u+c}}^{\omega(p)>0}U_{iB}(p)\cdot\eta(p)\Bigg] \\ \leq\ &\frac{W-2}{W}\cdot\epsilon\cdot\frac{\mathcal{E}_i(p_{\text{vac}})\cdot\sum_{k=1}^{K}\sum_{p\in\mathcal{A}_k^{u+c}}^{\omega(p)>0}\eta(p)}{\eta_{\text{vac}}}\end{aligned}$$

$$+\frac{W-3}{W}\cdot\epsilon\cdot\sum_{k=1,\ldots,K}^{\mathcal{A}_k^{u+c}\subseteq\tilde{\mathcal{A}}_i}\sum_{p\in\mathcal{A}_k^{u+c}}^{\omega(p)>0}U_{iB}(p)\cdot\eta(p)-\frac{W-1}{W}\cdot\epsilon\cdot\sum_{k=1}^{K}\sum_{p\in\mathcal{A}_k^{u+c}}^{\omega(p)>0}\mathcal{E}_i(p)\ ,$$

or equivalently,

$$\begin{aligned}
&\frac{W-2}{W}\cdot\epsilon\cdot\frac{\mathcal{E}_i(p_{\text{vac}})\cdot\sum_{k=1}^{K}\sum_{p\in\mathcal{A}_k^{u+c}}^{\omega(p)>0}\eta(p)}{\eta_{\text{vac}}}\\
\geq\ &\frac{W-2}{W^2}\cdot\epsilon^2\cdot\left[\sum_{k=1}^{K}\sum_{p\in\mathcal{A}_k^{u+c}}^{\omega(p)>0}\mathcal{E}_i(p)+\sum_{k=1,\ldots,K}^{\mathcal{A}_k^{u+c}\subseteq\tilde{\mathcal{A}}_i}\sum_{p\in\mathcal{A}_k^{u+c}}^{\omega(p)>0}U_{iB}(p)\cdot\eta(p)\right]\\
&-\frac{W-3}{W}\cdot\epsilon\cdot\sum_{k=1,\ldots,K}^{\mathcal{A}_k^{u+c}\subseteq\tilde{\mathcal{A}}_i}\sum_{p\in\mathcal{A}_k^{u+c}}^{\omega(p)>0}U_{iB}(p)\cdot\eta(p)+\frac{W-1}{W}\cdot\epsilon\cdot\sum_{k=1}^{K}\sum_{p\in\mathcal{A}_k^{u+c}}^{\omega(p)>0}\mathcal{E}_i(p)\ . \qquad (5.42)
\end{aligned}$$

Subsequently, by (5.40) and (5.42), we have

$$\begin{aligned}
\hat{\mathcal{E}}_i(p_{\text{vac}})\ &\leq\ \mathcal{E}_i(p_{\text{vac}})-\frac{W-2}{W^2}\cdot\epsilon^2\cdot\left[\sum_{k=1}^{K}\sum_{p\in\mathcal{A}_k^{u+c}}^{\omega(p)>0}\mathcal{E}_i(p)+\sum_{k=1,\ldots,K}^{\mathcal{A}_k^{u+c}\subseteq\tilde{\mathcal{A}}_i}\sum_{p\in\mathcal{A}_k^{u+c}}^{\omega(p)>0}U_{iB}(p)\cdot\eta(p)\right]\\
&\quad+\frac{W-3}{W}\cdot\epsilon\cdot\sum_{k=1,\ldots,K}^{\mathcal{A}_k^{u+c}\subseteq\tilde{\mathcal{A}}_i}\sum_{p\in\mathcal{A}_k^{u+c}}^{\omega(p)>0}U_{iB}(p)\cdot\eta(p)-\frac{W-1}{W}\cdot\epsilon\cdot\sum_{k=1}^{K}\sum_{p\in\mathcal{A}_k^{u+c}}^{\omega(p)>0}\mathcal{E}_i(p)\\
&=\ \mathcal{E}_i(p_{\text{vac}})-\left(\frac{W-2}{W^2}\cdot\epsilon^2+\frac{W-1}{W}\cdot\epsilon\right)\cdot\sum_{k=1}^{K}\sum_{p\in\mathcal{A}_k^{u+c}}^{\omega(p)>0}\mathcal{E}_i(p)\\
&\quad+\left(\frac{W-3}{W}\cdot\epsilon-\frac{W-2}{W^2}\cdot\epsilon^2\right)\cdot\sum_{k=1,\ldots,K}^{\mathcal{A}_k^{u+c}\subseteq\tilde{\mathcal{A}}_i}\sum_{p\in\mathcal{A}_k^{u+c}}^{\omega(p)>0}U_{iB}(p)\cdot\eta(p)\ . \qquad (5.43)
\end{aligned}$$

Now we show that Condition (5.41) can be achieved. Considering that $\psi_{\text{OPT-LP}}$ satisfies Constraint (5.29), i.e., $\mathcal{E}_i(p_{\text{vac}})+\sum_{k=1}^{K}\sum_{p\in\mathcal{A}_k^{u+c}}^{\omega(p)>0}\mathcal{E}_i(p)\leq\sum_{k=1,\ldots,K}^{\mathcal{A}_k^{u+c}\subseteq\tilde{\mathcal{A}}_i}\sum_{p\in\mathcal{A}_k^{u+c}}^{\omega(p)>0}U_{iB}(p)\cdot\eta(p)$, to have (5.41), it

is sufficient to have

$$\begin{aligned}
\epsilon \;\leq\; & \frac{W}{W-2}\cdot\frac{1}{\sum_{k=1}^{K}\sum_{p\in\mathcal{A}_k^{u+c}}^{\omega(p)>0}\mathcal{E}_i(p)+\sum_{k=1,\ldots,K}^{\mathcal{A}_k^{u+c}\subseteq\tilde{\mathcal{A}}_i}\sum_{p\in\mathcal{A}_k^{u+c}}^{\omega(p)>0}U_{iB}(p)\cdot\eta(p)} \\
& \cdot\Bigg[(W-2)\cdot\frac{\mathcal{E}_i(p_{\text{vac}})\cdot\sum_{k=1}^{K}\sum_{p\in\mathcal{A}_k^{u+c}}^{\omega(p)>0}\eta(p)}{\eta_{\text{vac}}}+(W-3)\cdot\Bigg(\mathcal{E}_i(p_{\text{vac}})+\sum_{k=1}^{K}\sum_{p\in\mathcal{A}_k^{u+c}}^{\omega(p)>0}\mathcal{E}_i(p)\Bigg) \\
& -(W-1)\cdot\sum_{k=1}^{K}\sum_{p\in\mathcal{A}_k^{u+c}}^{\omega(p)>0}\mathcal{E}_i(p)\Bigg] \\
= \;& \frac{W}{W-2}\cdot\frac{1}{\sum_{k=1}^{K}\sum_{p\in\mathcal{A}_k^{u+c}}^{\omega(p)>0}\mathcal{E}_i(p)+\sum_{k=1,\ldots,K}^{\mathcal{A}_k^{u+c}\subseteq\tilde{\mathcal{A}}_i}\sum_{p\in\mathcal{A}_k^{u+c}}^{\omega(p)>0}U_{iB}(p)\cdot\eta(p)}\cdot \\
& \Bigg[(W-2)\cdot\frac{\mathcal{E}_i(p_{\text{vac}})\cdot\sum_{k=1}^{K}\sum_{p\in\mathcal{A}_k^{u+c}}^{\omega(p)>0}\eta(p)}{\eta_{\text{vac}}}+(W-3)\cdot\mathcal{E}_i(p_{\text{vac}})-2\sum_{k=1}^{K}\sum_{p\in\mathcal{A}_k^{u+c}}^{\omega(p)>0}\mathcal{E}_i(p)\Bigg].
\end{aligned} \tag{5.44}$$

One may either set ϵ arbitrarily small (adjusting ϵ down if the given one is too large) or increase W to sufficiently large value to ensure that (5.44) holds. Subsequently, (5.41) holds, and thereby (5.43) holds.

Equations (5.39) and (5.43) are useful for verifying (5.29). We further derive

$$\begin{aligned}
& \sum_{k=1,\ldots,K}^{\mathcal{A}_k^{u+c}\subseteq\tilde{\mathcal{A}}_i}U_{iB}(\mathcal{L}_k)\cdot\hat{\eta}(\mathcal{L}_k)-\hat{\mathcal{E}}_i(p_{\text{vac}})-\sum_{k=1}^{K}\hat{\mathcal{E}}_i(\mathcal{L}_k) \\
\geq\; & \sum_{k=1,\ldots,K}^{\mathcal{A}_k^{u+c}\subseteq\tilde{\mathcal{A}}_i}(1-\frac{\epsilon}{W})\cdot U_{iB}(p)\cdot\Bigg[\Big(1+\frac{W-2}{W}\cdot\epsilon\Big)\cdot\sum_{p\in\mathcal{A}_k^{u+c}}^{\omega(p)>0}\eta(p)\Bigg]
\end{aligned}$$

$$
\begin{aligned}
&-\left\{\mathcal{E}_i(p_{\text{vac}}) - \left(\frac{W-2}{W^2}\cdot\epsilon^2 + \frac{W-1}{W}\cdot\epsilon\right)\cdot\sum_{k=1}^{K}\sum_{p\in\mathcal{A}_k^{u+c}}^{\omega(p)>0}\mathcal{E}_i(p)\right.\\
&\left.+\left(\frac{W-3}{W}\cdot\epsilon - \frac{W-2}{W^2}\cdot\epsilon^2\right)\cdot\sum_{k=1,\ldots,K}^{\mathcal{A}_k^{u+c}\subseteq\tilde{\mathcal{A}}_i}\sum_{p\in\mathcal{A}_k^{u+c}}^{\omega(p)>0}U_{iB}(p)\cdot\eta(p)\right\}\\
&-\sum_{k=1}^{K}\left(1+\frac{W-1}{W}\cdot\epsilon + \frac{W-2}{W^2}\cdot\epsilon^2\right)\cdot\sum_{p\in\mathcal{A}_k^{u+c}}^{\omega(p)>0}\mathcal{E}_i(p)\\
=\;&\left(1+\frac{W-3}{W}\cdot\epsilon - \frac{W-2}{W^2}\cdot\epsilon^2\right)\cdot\sum_{k=1,\ldots,K}^{\mathcal{A}_k^{u+c}\subseteq\tilde{\mathcal{A}}_i}\sum_{p\in\mathcal{A}_k^{u+c}}^{\omega(p)>0}U_{iB}(p)\cdot\eta(p)\\
&-\left\{\mathcal{E}_i(p_{\text{vac}}) + \left(\frac{W-3}{W}\cdot\epsilon - \frac{W-2}{W^2}\cdot\epsilon^2\right)\cdot\sum_{k=1,\ldots,K}^{\mathcal{A}_k^{u+c}\subseteq\tilde{\mathcal{A}}_i}\sum_{p\in\mathcal{A}_k^{u+c}}^{\omega(p)>0}U_{iB}(p)\cdot\eta(p)\right\} - \sum_{k=1}^{K}\cdot\sum_{p\in\mathcal{A}_k^{u+c}}^{\omega(p)>0}\mathcal{E}_i(p)\\
=\;&\sum_{k=1,\ldots,K}^{\mathcal{A}_k^{u+c}\subseteq\tilde{\mathcal{A}}_i}\sum_{p\in\mathcal{A}_k^{u+c}}^{\omega(p)>0}U_{iB}(p)\cdot\eta(p) - \mathcal{E}_i(p_{\text{vac}}) - \sum_{k=1}^{K}\sum_{p\in\mathcal{A}_k^{u+c}}^{\omega(p)>0}\mathcal{E}_i(p)\geq 0
\end{aligned}
$$

where the first inequality holds by (5.37), (5.32), (5.43) and (5.39), and the last inequality holds since $\psi_{\text{OPT-LP}}$ satisfies (5.29). Thus, Constraint (5.29) holds for $\hat{\psi}_{\text{OPT-LP}}$.

To verify the remaining energy constraint (5.30) for $\hat{\psi}_{\text{OPT-LP}}$, we have

$$
\hat{\mathcal{E}}_i(p_{\text{vac}}) + \sum_{k=1,\ldots,K}^{\mathcal{A}_k^{u+c}\not\subseteq\tilde{\mathcal{A}}_i}\hat{\mathcal{E}}_i(\mathcal{L}_k) \leq \max_{j\in\mathcal{N}}\left\{\hat{\mathcal{E}}_j(p_{\text{vac}}) + \sum_{k=1,\ldots,K}^{\mathcal{A}_k^{u+c}\not\subseteq\mathcal{A}_j}\hat{\mathcal{E}}_j(\mathcal{L}_k)\right\} = (E_{\max} - E_{\min})\cdot h\ , \quad (5.45)
$$

where the last equality holds by (5.36). Therefore, the constructed solution $\hat{\psi}_{\text{OPT-LP}}$ is feasible to Problem OPT-LP. This completes the proof. □

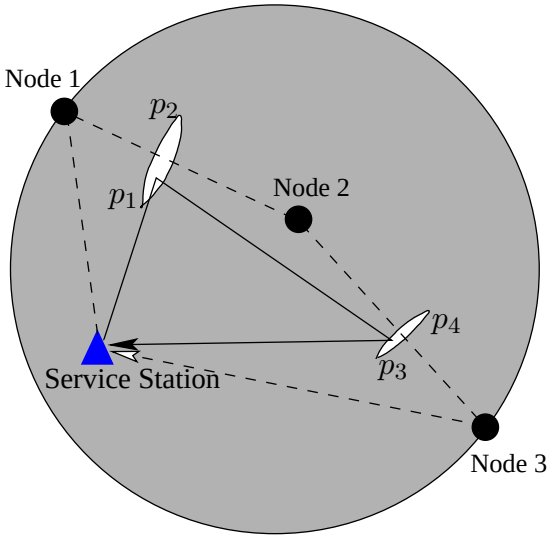

Figure 5.4: Comparison between a Hamiltonian cycle connecting the logical points and the service station and a Hamiltonian cycle connecting the sensor nodes and the service station.

5.4 A Practical Solution and Performance Gap Analysis

In Section 5.3, we have developed a near-optimal solution to an idealized problem, in which a WCV's traveling time is assumed to be zero. In this section, we incorporate traveling time and develop a practical solution to our original problem (TPP). We also quantify the performance gap between this solution and optimal (unknown) solution to TPP.

5.4.1 Fixing a Traveling Path

The near-optimal solution $\psi_{\text{OPT-ub}}$ to the idealized problem OPT-ub in Section 5.3 offers us several tools in designing a solution to the original problem TPP. First, the objective value $\eta_{\text{OPT-ub}}$ of $\psi_{\text{OPT-ub}}$ is at least $\eta^*_{\text{OPT-ub}} - \epsilon$ while $\eta^*_{\text{OPT-ub}}$ is an upper bound for the unknown objective value η^*_{TPP} of TPP. This can be used as a performance benchmark to measure the quality of the practical solution (which includes traveling time) to the original problem TPP. Second, the logical point concept in the near-optimal solution $\psi_{\text{OPT-ub}}$ offers a hint on where the WCV should make stops and charge the sensor nodes. We will exploit these stops in $\psi_{\text{OPT-ub}}$ to design a solution to Problem TPP.

For the stopping points (any physical point within a logical point that has non-zero stopping time) in $\psi_{\text{OPT-ub}}$, we propose to find a shortest Hamiltonian cycle to connect them. Note that the service station is also included in this shortest Hamiltonian cycle. Denote this path by $\mathcal{P}_{\text{OPT-lb}}$. The decision of using shortest Hamiltonian cycle is obvious as it corresponds to the least amount of traveling time (not including stopping time).

It is important to realize that the shortest Hamiltonian cycle that we find here is based on the connection of logical points, rather than the actual sensor nodes. A Hamiltonian cycle for the latter would be fundamentally different from the former. As an example, in Fig. 5.4, the solid triangle is a Hamiltonian cycle connecting two logical points (with corner points (p_1, p_2) and (p_3, p_4)) and the service station while the dotted quadrangle is a Hamiltonian cycle connecting three sensor nodes and the service station.

5.4.2 Incorporating Traveling Time

Under the selected traveling path $\mathcal{P}_{\text{OPT-lb}}$, denote G as the total number of physical points with positive stopping time. We re-index these points by traveling order under $\mathcal{P}_{\text{OPT-lb}}$, and let $\mathcal{P}_{\text{OPT-lb}} = (p_{\text{vac}}, p_1, \ldots, p_G, p_{\text{vac}})$, with the starting and ending point being the service station (p_{vac}) and the j-th stop along the path being p_j, $1 \leq j \leq G$.

To find flow routing when the WCV travels along $\mathcal{P}_{\text{OPT-lb}}$, we discretize $\mathcal{P}_{\text{OPT-lb}}$ into a sequence of segments based on $\mathcal{P}_{\text{OPT-lb}}$'s intersection with the subareas (see Figs. 5.3(c) and 5.4). Based on this path discretization, we can rewrite TPP into a new formulation (denoted as OPT-lb), in which we can obtain flow routing when the WCV is traveling on each segment along path $\mathcal{P}_{\text{OPT-lb}}$.

Note that each segment is contained by one subarea. Among these traversed subareas, the WCV makes stops at some of them while only traversing others without making any stop. Denote $\mathcal{Q}$ as the set of indexes for all the traversed subareas and $\mathcal{Q}_s$ as the set of indexes for those subareas that the WCV makes stops, respectively. For $m \in \mathcal{Q}$, the WCV's traveling time (not including stopping

time) in this subarea is $D(\mathcal{L}_m)/V$, where $\mathcal{L}_m$ is the logical point corresponding to this subarea, and $D(\mathcal{L}_m)$ denotes the distance traversed within $\mathcal{L}_m$ along $\mathcal{P}_{\text{OPT-lb}}$.

For $m \in \mathcal{Q}_s$, since the WCV makes a stop only at one point, we have $|\mathcal{Q}_s| = G$. The total time that the WCV spends in $\mathcal{L}_m$ is

$$\frac{D(\mathcal{L}_m)}{V} + \omega(\mathcal{L}_m) \ ,$$

where $\omega(\mathcal{L}_m)$ is the stopping time within $\mathcal{L}_m$. Based on $\mathcal{P}_{\text{OPT-lb}}$ and $\mathcal{L}_m$, $m \in \mathcal{Q}$, we rewrite Problem TPP to OPT-lb as follows:

OPT-lb

$$\text{Maximize} \quad \frac{\tau_{\text{vac}}}{\tau}$$

$$\text{s.t.} \quad \tau = \tau_{\text{vac}} + \sum_{m\in\mathcal{Q}_s} \omega(\mathcal{L}_m) + \sum_{m\in\mathcal{Q}} \frac{D(\mathcal{L}_m)}{V} \tag{5.46}$$

$$\sum_{k\in\mathcal{N}}^{k\neq i} f_{ki}(\mathcal{L}_m) + R_i = \sum_{j\in\mathcal{N}}^{j\neq i} f_{ij}(\mathcal{L}_m) + f_{iB}(\mathcal{L}_m) \quad (i \in \mathcal{N}, m \in \mathcal{Q})$$

$$r_i(\mathcal{L}_m) = \rho \sum_{k\in\mathcal{N}}^{k\neq i} f_{ki}(\mathcal{L}_m) + \sum_{j\in\mathcal{N}}^{j\neq i} C_{ij} \cdot f_{ij}(\mathcal{L}_m) + C_{iB}(\mathcal{L}_m) \cdot f_{iB}(\mathcal{L}_m) \quad (i \in \mathcal{N}, m \in \mathcal{Q})$$

$$r_i(p_{\text{vac}}) \cdot \tau_{\text{vac}} + \sum_{m\in\mathcal{Q}_s} r_i(\mathcal{L}_m) \cdot \omega(\mathcal{L}_m) + \sum_{m\in\mathcal{Q}} \frac{D(\mathcal{L}_m)}{V} \cdot r_i(\mathcal{L}_m) \leq \sum_{m\in\mathcal{Q}_s}^{D_{iB}(p)\leq D_\delta, p\in\mathcal{A}_m^{u+c}} U_{iB}(\mathcal{L}_m) \cdot \omega(\mathcal{L}_m) \ \ (i \in \mathcal{N}) \tag{5.47}$$

$$r_i(p_{\text{vac}}) \cdot \tau_{\text{vac}} + \sum_{m\in\mathcal{Q}_s}^{D_{iB}(p)> D_\delta, p\in\mathcal{A}_m^{u+c}} r_i(\mathcal{L}_m) \cdot \omega(\mathcal{L}_m) + \sum_{m\in\mathcal{Q}} \frac{D(\mathcal{L}_m)}{V} \cdot r_i(\mathcal{L}_m) \leq E_{\max} - E_{\min} \ \ (i \in \mathcal{N}) \tag{5.48}$$

$$\tau, \tau_{\text{vac}}, \omega(\mathcal{L}_m) \geq 0 \ \ (m \in \mathcal{Q}_s)$$

$$f_{ij}(\mathcal{L}_m), f_{iB}(\mathcal{L}_m), r_i(\mathcal{L}_m) \geq 0 \ \ (i, j \in \mathcal{N}, i \neq j, m \in \mathcal{Q})$$

$$f_{ij}(p_{\text{vac}}), f_{iB}(p_{\text{vac}}), r_i(p_{\text{vac}}) \geq 0 \ \ (i, j \in \mathcal{N}, i \neq j) \ .$$

Table 5.2: Location and data rate R_i for each node in a 50-node network.

Node Index	Location	R_i	Node Index	Location	R_i
1	(0.547,0.644)	0.1	26	(0.833,0.115)	0.2
2	(0.662,0.757)	0.7	27	(0.639,0.658)	0.1
3	(0.037,0.859)	0.4	28	(0.704,0.930)	0.6
4	(0.723,0.741)	1.0	29	(0.977,0.306)	0.8
5	(0.529,0.778)	0.9	30	(0.673,0.386)	0.5
6	(0.316,0.035)	0.4	31	(0.021,0.745)	0.7
7	(0.190,0.842)	0.8	32	(0.924,0.072)	0.6
8	(0.288,0.106)	0.8	33	(0.270,0.829)	0.1
9	(0.040,0.942)	0.2	34	(0.777,0.573)	0.8
10	(0.264,0.648)	0.4	35	(0.097,0.512)	0.9
11	(0.446,0.805)	0.5	36	(0.986,0.290)	0.2
12	(0.890,0.729)	0.5	37	(0.161,0.636)	0.7
13	(0.370,0.350)	0.1	38	(0.355,0.767)	0.9
14	(0.006,0.101)	0.7	39	(0.655,0.574)	0.5
15	(0.393,0.548)	0.1	40	(0.031,0.052)	0.4
16	(0.629,0.623)	0.1	41	(0.350,0.150)	0.3
17	(0.084,0.954)	0.5	42	(0.941,0.724)	0.1
18	(0.756,0.840)	0.2	43	(0.966,0.430)	0.2
19	(0.966,0.376)	0.7	44	(0.107,0.191)	0.3
20	(0.931,0.308)	0.6	45	(0.007,0.337)	0.3
21	(0.944,0.439)	0.1	46	(0.457,0.287)	0.4
22	(0.626,0.323)	0.4	47	(0.753,0.383)	0.1
23	(0.537,0.538)	0.2	48	(0.945,0.909)	0.1
24	(0.118,0.082)	0.3	49	(0.209,0.758)	0.3
25	(0.929,0.541)	0.2	50	(0.221,0.588)	0.8

In Problem OPT-lb, the time constraint (5.46) incorporates traveling time along $\mathcal{P}_{\text{OPT-lb}}$. Also, Constraints (5.47) and (5.48) incorporate energy consumption when the WCV is traveling.

Through a similar change-of-variable procedure to that for OPT-$\mathcal{L}$, we can reformulate OPT-lb to an LP. By solving this LP, we can obtain a feasible solution to Problem TPP. Denote $\psi_{\text{OPT-lb}}$ as this feasible solution and $\eta_{\text{OPT-lb}}$ as the objective value achieved by $\psi_{\text{OPT-lb}}$. The relationship between $\eta_{\text{OPT-lb}}$ and the optimum objective value η^*_{TPP} is given in the following lemma:

Lemma 5.4 *$\eta_{OPT\text{-}lb}$ is a lower bound of η^*_{TPP}, i.e., $\eta_{OPT\text{-}lb} \leq \eta^*_{TPP}$.*

Clearly, Lemma 5.4 holds since OPT-lb is based on a specified path $\mathcal{P}_{\text{OPT-lb}}$ and thus $\psi_{\text{OPT-lb}}$ is only a

Table 5.3: Index of stopping points along the path, location and stopping time at each stopping point for the 50-node network.

Stopping point	Location	τ_k	Stopping point	Location	τ_k
1	(0.575,0.550)	0.3	18	(0.525,0.775)	179.3
2	(0.600,0.575)	77.2	19	(0.375,0.775)	69.8
3	(0.750,0.575)	179.4	20	(0.350,0.775)	117.9
4	(0.675,0.375)	50.9	21	(0.200,0.825)	175.9
5	(0.650,0.350)	66.2	22	(0.075,0.950)	110.0
6	(0.900,0.075)	98.6	23	(0.025,0.775)	166.6
7	(0.925,0.075)	38.8	24	(0.025,0.750)	3.1
8	(0.975,0.300)	12.2	25	(0.200,0.625)	86.5
9	(0.975,0.325)	81.8	26	(0.225,0.625)	43.5
10	(0.975,0.350)	102.9	27	(0.150,0.550)	136.8
11	(0.925,0.525)	42.3	28	(0.100,0.525)	105.1
12	(0.900,0.725)	103.6	29	(0.000,0.325)	64.7
13	(0.950,0.900)	21.8	30	(0.000,0.100)	26.4
14	(0.700,0.925)	124.2	31	(0.050,0.125)	180.6
15	(0.725,0.750)	160.6	32	(0.300,0.100)	173.3
16	(0.700,0.750)	32.4	33	(0.450,0.300)	84.3
17	(0.675,0.750)	18.9	34	(0.400,0.550)	19.8

feasible solution to Problem TPP.

5.4.3 Analysis of Performance Gap and Algorithm Complexity

Denote θ as the performance gap between $\eta_{\text{OPT-lb}}$ and the unknown optimal objective η^*_{TPP}. We have the following lemma.

Lemma 5.5 $\theta \leq \epsilon + \eta_{\text{OPT-ub}} - \eta_{\text{OPT-lb}}$.

Proof By definition, $\theta = \eta^*_{\text{TPP}} - \eta_{\text{OPT-lb}}$, we have

$$\theta \leq \eta^*_{\text{OPT-ub}} - \eta_{\text{OPT-lb}} \leq \epsilon + \eta_{\text{OPT-ub}} - \eta_{\text{OPT-lb}} \ ,$$

where the first inequality holds by Lemma 5.2, and the second inequality holds by Theorem 5.1. □

In the above solution, solving two LPs (i.e., Problems OPT-$\mathcal{L}$ and OPT-lb) has the highest complexity. The problem size of either LP is decided by the maximum number of subareas, which is a polynomial in $|\mathcal{N}|$ (see (5.21)). Thus, both LPs have polynomial size and the algorithm complexity is polynomial.

5.5 Numerical Results

Network and Parameter Settings. In the numerical results, the units of distance, time, data rate, and energy are all normalized appropriately. We assume sensor nodes are randomly deployed over a unit square area. The data rate R_i, $i \in \mathcal{N}$, is randomly generated within $[0.1, 1]$. The home service station is assumed to be at (0.5,0.5), and the WCV travels at a speed $V = 0.1$.

Suppose that a sensor node uses a rechargeable battery with $E_{\text{max}} = 10,000$, and $E_{\text{min}} = 500$. For the charging efficiency function $\mu(D_{iB})$, we assume a decreasing function $\mu(D_{iB}) = -40 \cdot D_{iB}^2 - 4 \cdot D_{iB} + 1.0$. Letting $U_{\text{max}} = 50$ and $\delta = 10$, we have $D_\delta = 0.10$ for a maximum distance of effective charging. The normalized parameters in energy consumption model are $\beta_1 = \beta_2 = \rho = 1$. The path loss index is $\alpha = 4$. We set $W = 3$ and $\epsilon = 0.05$ for the numerical results.

We consider a 50-node network. The normalized location of each node and its data rate are given in Table 5.2.

Results. Table 5.3 gives the stopping points (each within a logical point with a non-zero stopping time) along the travel path for the WCV. The traveling path is shown in Fig. 5.5. For $\mathcal{P}_{\text{OPT-lb}}$, $D_{\mathcal{P}_{\text{OPT-lb}}} = 4.89$ and the traveling time $D_{\mathcal{P}_{\text{OPT-lb}}}/V = 48.9$. Table 5.3 shows the charging schedule at each stopping point on $\mathcal{P}_{\text{OPT-lb}}$. Following $\mathcal{P}_{\text{OPT-lb}}$ and this charging schedule, our solution ensures that any sensor node never runs out of energy. As an example, Fig. 5.6 shows the energy behavior of a sensor node (the 35th node) during the first three cycles. During each cycle, this node is charged by the WCV when it makes stops at two stopping points (i.e., the 27th and 28th points). Starting from the second cycle, the node's energy behavior repeats from cycle to cycle.

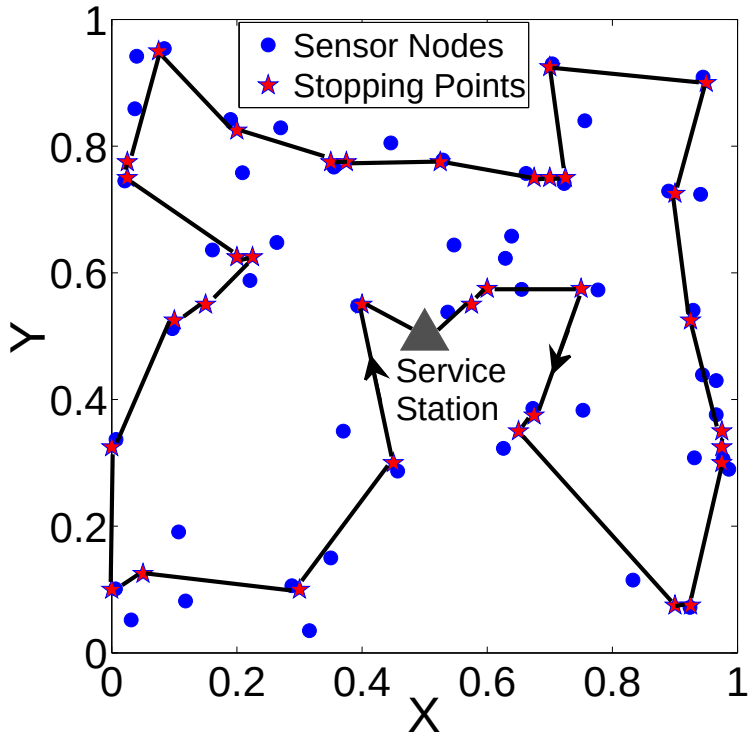

Figure 5.5: A traveling path for the WCV in the 50-node sensor network.

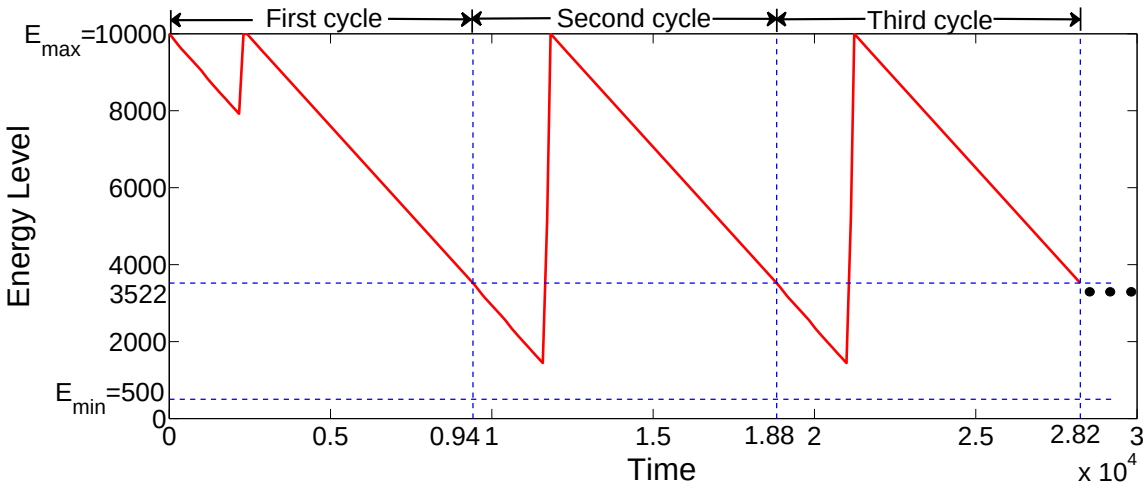

Figure 5.6: The energy behavior of the 35th sensor node in the 50-node network during the first three cycles.

For the given $\epsilon = 0.05$, we have $\eta_{\text{OPT-ub}} = 68.62\%$. For the obtained practical solution $\psi_{\text{OPT-lb}}$, the cycle time τ = 9414, the vacation time τ_{vac} = 6410, and the objective value is $\eta_{\text{OPT-lb}} = 68.09\%$. By Lemma 5.5, the performance gap $\theta \leq \epsilon + \eta_{\text{OPT-ub}} - \eta_{\text{OPT-lb}} = 0.05 + 0.6862 - 0.6809 = 0.0553$, where the given ϵ is the dominant part. This shows that the objective value by the lower bound feasible solution is very close to that by the upper bound solution.

5.6 Summary

In this chapter, we have studied the problem of co-locating the MBS on the WCV in a WSN, with a focus on the traveling path problem of the WCV. The goal was to minimize energy consumption of the the entire system while ensuring none of the sensor nodes runs out of energy. We formulated an optimization problem (TPP) that involved joint optimization of traveling path, stopping points, charging schedule, and data flow routing. We first considered an idealized problem (OPT-ub) that assumed zero traveling time. For OPT-ub, we developed a provably near-optimal solution method that involves several novel techniques, such as discretization of energy reception rate and energy consumption rate, double partitioning of the SED into smaller subareas with tight energy bounds, and representation of each subarea by a logical point as its "worst-case" energy reception and consumption behavior. Based on the near-optimal solution to the idealized problem OPT-ub, we set the traveling path as the shortest Hamiltonian cycle connecting the logical points and the service station. We then obtained a practical solution (with non-zero traveling time) to the original problem TPP, and quantified the performance gap between this feasible solution and an optimal (unknown) solution to TPP.

Chapter 6

Summary and Future Work

6.1 Summary

The focus of this dissertation was to address critical energy problems in WSNs. Motivated by recent advances in WET technology, we proposed to apply MRC to address energy problems in WSNs and explored a number of research problems in this dissertation. First, with single-node charging technology, we showed how a sparse WSN can remain operational forever when a WCV is employed. But as node density increases, single-node charging technology is not scalable to charge all the nodes in the network. Fortunately, recent advance in MRC allows WET to be performed on multiple nodes simultaneously. With the new multi-node charging technology, we showed that the scalability problem in single-node charging can be resolved successfully.

Then our attention on WET and WCV was switched to the base station location. We studied bundling WET and MBS on the same WCV, and investigated this problem both for the special pre-planned path case and the general unconstrained path case.

For each research problem, we pursued a formal optimization framework and formulated it as a complex optimization problem. Each optimization problem was a non-convex non-linear program (NLP). For these NLPs, we developed near-optimal solution procedures that convert an NLP to a simpler form such as an LP or a MILP, either of which can be solved by a solver, and we

established near-optimality for the obtained solution. There are a number of novel optimization and algorithmic techniques that are worth referring for future research, most notably, linearizing non-linear terms via piecewise linear approximation or Reformulation-Linearization Technique (RLT), downsizing solution space without compromising optimal objective value, discretizing a continuous path or space, discretizing energy reception and consumption rates, and exploiting bounding relationship among a variety of problems.

In summary, the potential of the emerging WET technology has been demonstrated to address energy problems in energy-constrained wireless networks. We showed that a successful solution to energy problems requires a coordinated effort on multiple layers and sub-components. We expect that the theoretical and algorithmic results of this research will serve as important stepping stones to exploit WET for further research on energy problems in wireless networks.

6.2 Future Work

Our work in this dissertation was among the first that brought WET to the wireless networking community. As expected, many research problems deserve further investigation. Here, we outline two problems that we are pursing following this dissertation.

Bundling WET and MBS vs. Optimal BS Placement. It is interesting to see whether co-locating a MBS on the WCV is better than placing the BS in an optimal location. In the former case, the optimal path for bundling WET and MBS may not be optimal for either WET or MBS as compared to the case when the two can be separate. For the latter, a fixed optimal location for the BS may sacrifice optimality for simplicity. It is not obvious which case is better and only a systematic investigation can reveal insights for both cases.

Energy relaying in a WSN. In this dissertation, we assumed that a mobile WCV was employed to bring a wireless charger close to the sensor nodes. Very recently, a new concept called “energy relaying” was demonstrated by Witricity [67]. In their demo, multi-hop energy transmission was

accomplished through a number of intermediate energy relays. This new concept is fairly similar to the well-known multi-hop data transmission, and may pave the way for addressing WET over long distances. To utilize energy relaying, a number of interesting questions can be raised, most notably, how many energy relay nodes are needed and where the nodes should be placed. We are currently studying this problem and will report our findings in the near future.

Bibliography

[1] D. Ahn and S. Hong, "Effect of coupling between multiple transmitters or multiple receivers on wireless power transfer," *IEEE Trans. on Industrial Electronics*, vol. 60, no. 7, pp. 2602–2613, July 2013.

[2] Y. Ammar, A. Buhrig, M. Marzencki, B. Charlot, S. Basrour, K. Matou, and M. Renaudin, "Wireless sensor network node with asynchronous architecture and vibration harvesting micro power generator," in *Proc. of Joint Conference on Smart Objects and Ambient Intelligence: Innovative Context-Aware Services: Usages and Technologies*, pp. 287–292, Grenoble, France, Oct. 12–14, 2005.

[3] T. Ajmal, D. Jazani, and B. Allen, "Design of a compact RF energy harvester for wireless sensor networks," in *IET Conference on Wireless Sensor Systems (WSS)*, pp. 1–5, London, UK, June. 2012.

[4] D. L. Applegate, R. E. Bixby, V. Chvatal, and W. J. Cook, *The Traveling Salesman Problem: A Computational Study*, Chapter 4, Princeton Univ. Press, Princeton, NJ, Jan. 2007.

[5] D.W. Baarman, and J. Schwannecke, "Understanding wireless power," White Paper, Fulton Innovation, Ada, MI, USA, Dec 2009, available [online] at http://ecoupled.com/en/wireless-power/white-papers.

[6] S. Basagni, A. Carosi, E. Melachrinoudis, C. Petrioli, and Z.M. Wang, "A new MILP formulation and distributed protocols for wireless sensor networks lifetime maximization," in *Proc. IEEE ICC*, pp. 3517–3524, Istanbul, Turkey, June 2006.

[7] E. M. L. Beale and J. J. H. Forrest, "Global optimization using special ordered sets," *Mathematical Programming*, vol. 10, no. 1, pp. 52–69, 1976.

[8] A. Ben-Tal, G. Eiger, V. Gershovitz, "Global minimization by reducing duality gap," *Mathematical Programming*, vol. 63, no. 1–3, pp. 193–212, 1994.

[9] N. Bulusu and S. Jha (eds.), *Wireless Sensor Networks: A Systems Perspective*, Chapter 9, Norwood, MA: Artech House, 2005.

[10] Concorde TSP Solver, URL: http://www.tsp.gatech.edu/concorde/.

[11] J. Chang and L. Tassiulas, "Maximum lifetime routing in wireless sensor networks," *IEEE/ACM Trans. on Networking*, vol. 12, no. 4, pp. 609–619, Aug. 2004.

[12] I. Dietrich and F. Dressler, "On the lifetime of wireless sensor networks," *ACM Trans. on Sensor Networks*, vol. 5, no. 1, pp. 1–39, Feb. 2009.

[13] M.M. Faruque Hasan and I.A. Karimi, "Piecewise linear relaxation of bilinear programs using bivariate partitioning," *American Institute of Chemical Engineers (AIChE) Journal*, vol. 56, no. 7, pp. 1880–1893, 2009.

[14] L.R. Foulds, D. Haughland, and K. Jornsten, "A bilinear approach to the pooling problem," *Optimization*, vol. 24, no. 1–2, pp. 165–180, 1992.

[15] C.A. Floudas, *Deterministic Global Optimization: Theory, Methods, and Applications*, Chapter 2, Kluwer Academic, Dec. 1999.

[16] K. Finkenzeller, *RFID Handbook: Fundamentals and Applications in Contactless Smart Cards and Identification*, 2nd ed., Chapter 4, New York, Wiley, 2003.

[17] S. Ganeriwal, I. Tsigkogiannis, H. Shim, V. Tsiatsis, M.B. Srivastava, and D. Ganesan, "Estimating clock uncertainty for efficient duty-cycling in sensor networks," *IEEE/ACM Trans. on Networking*, vol. 17, no. 3, pp. 843–856, June 2009.

[18] R.K. Ganti, P. Jayachandran, H. Luo, and T.F. Abdelzaher, "Datalink streaming in wireless sensor networks," in *Proc. ACM SenSys*, pp.209–222, Boulder, CO, Oc. 31–Nov. 3, 2006.

[19] E. Giler, "Eric Giler demos wireless electricity,"
URL: http://www.ted.com/talks/eric_giler_demos_wireless_electricity.html.

[20] W.B. Heinzelman, "Application-specific protocol architectures for wireless networks," *Ph.D. Dissertation*, Dept. Elect. Eng. Comput. Sci., MIT, Cambridge, MA, Jun. 2000.

[21] S. He, J. Chen, F. Jiang, D.K.Y. Yau, G. Xing, and Y. Sun, "Energy provisioning in wireless rechargeable sensor networks," in *Proc. IEEE INFOCOM*, pp. 2006–2014, Shanghai, China, Apr. 2011.

[22] R. Horst and H. Tuy, *Global Optimization: Deterministic Approaches*, Chapter 4, 3rd edition, Springer-Verlag, 1996.

[23] Y.T. Hou, Y. Shi, and H.D. Sherali, "Rate allocation and network lifetime problems for wireless sensor networks," *IEEE/ACM Trans. on Networking*, vol. 16, no. 2, pp. 321–334, Apr. 2008.

[24] IBM ILOG CPLEX Optimizer,
URL: http://www-01.ibm.com/software/integration/optimization/cplex-optimizer/.

[25] Intel Corp., URL: http://www.intel.com.

[26] S. Jain, K. Fall, and R. Patra, "Routing in a delay tolerant network," in *Proc. ACM SIGCOMM*, pp. 145–158, Portland, OR, Aug. 30–Sep. 3, 2004.

[27] B. Jiang, J. R. Smith, M. Philipose, S. Roy, K. Sundara-Rajan, and A. V. Mamishev, "Energy scavenging for inductively coupled passive RFID systems," *IEEE Trans. on Instrumentation and Measurement*, vol. 56, no. 1, pp. 118–125, Feb. 2007.

[28] X. Jiang, J. Polastre, and D. Culler, "Perpetual environmentally powered sensor networks," in *Proc. ACM/IEEE International Symposium on Information Processing in Sensor Networks*, pp. 463–468, Los Angeles, CA, Apr. 2005.

[29] G.W. Jull. "An Overview of SHARP,", July 1997,
URL: http://www.friendsofcrc.ca/Projects/SHARP/sharp.html.

[30] A. Kansal, J. Hsu, S. Zahedi, and M.B. Srivastava, "Power management in energy harvesting sensor networks," *ACM Trans. Embed. Comput. Syst.*, vol. 6, no. 4, article 32, Sep. 2007.

[31] A. Kurs, A. Karalis, R. Moffatt, J.D. Joannopoulos, P. Fisher, and M. Soljacic, "Wireless power transfer via strongly coupled magnetic resonances," *Science*, vol. 317, no. 5834, pp. 83–86, July 2007.

[32] A. Kurs, R. Moffatt, and M. Soljacic, "Simultaneous mid-range power transfer to multiple devices," *Appl. Phys. Lett.*, vol. 96, pp. 044102-1–044102-3, Jan. 2010.

[33] D. Linden and T.B. Reddy (eds.), *Handbook of Batteries*, 3rd ed., Chapter 1, McGraw-Hill, 2002.

[34] Z. Li, Y. Peng, W. Zhang, and D. Qiao, "J-RoC: A joint routing and charging scheme to prolong sensor network lifetime," in *Proc. IEEE ICNP*, pp. 373–382, Vancouver, Canada, Oct. 17–20, 2011.

[35] J. Luo and J.-P. Huabux, "Joint mobility and routing for lifetime elongation in wireless sensor networks," in *Proc. IEEE INFOCOM*, pp. 1735–1746, Miami, FL, March 13–17, 2005.

[36] J. Luo and J.-P. Huabux, "Joint sink mobility and routing to maximize the lifetime of wireless sensor networks: The case of constrained mobility," *IEEE/ACM Trans. on Networking*, vol. 18, no. 3, pp. 871–884, June 2010.

[37] J. Luo and L. Xiang, "Prolong the lifetime of wireless sensor networks through mobility: A general optimization framework," in *Theoretical Aspects of Distributed Computing in Sensor Networks*, pp. 553–588, Springer-Verlag, June 2010.

[38] M. Ma and Y. Yang, "SenCar: An energy-efficient data gathering mechanism for large-scale multihop sensor networks," *IEEE Trans. on Parallel and Distributed Systems*, vol. 18, no. 10, pp. 1476–1488, Oct. 2007.

[39] S. Meninger, J.O. Mur-Miranda, R. Amirtharajah, A.P. Chandrakasan, and J.H. Lang, "Vibration-to-electric energy conversion," *IEEE Trans. on Very Large Scale Integration (VLSI) Systems*, vol. 9, no. 1, pp. 64–76, Feb. 2001.

[40] J. Messina, "Haier exhibits a wireless HDTV video system at the 2010 CES," URL: www.physorg.comnews182608923.html.

[41] G. L. Nemhauser and L. A. Wolsey, *Integer and Combinatorial Optimization*, Chapter II-4, John Wiley & Sons Inc., Hoboken, NJ, July 1999.

[42] M. Padberg and G. Rinaldi, "A branch-and-cut algorithm for the resolution of large-scale symmetric traveling salesman problems," *SIAM Review*, vol. 33, no. 1, pp. 60–100, 1991.

[43] G. Park, T. Rosing, M.D. Todd, C.R. Farrar, and W. Hodgkiss, "Energy harvesting for structural health monitoring sensor networks," *J. Infrastruct. Syst.*, vol. 14, no. 1, pp. 64–79, Mar. 2008.

[44] Y. Peng, Z. Li, G. Wang, W. Zhang, and D. Qiao, "Prolonging sensor network lifetime through wireless charging," in *Proc. IEEE RTSS*, pp. 129–139, San Diego, CA, Nov. 30–Dec. 3, 2010.

[45] PowerCast, URL: http://www.powercastco.com.

[46] J. Polastre, J. Hill, and D. Culler, "Versatile low power media access for wireless sensor networks," in *Proc. ACM SenSys*,, pp. 95–107, Baltimore, MD, Nov. 2004.

[47] A. Sankar and Z. Liu, "Maximum lifetime routing in wireless ad-hoc networks," in *Proc. IEEE INFOCOM*, pp. 1089–1097, Hong Kong, China, March 7–11, 2004.

[48] A. Sample, D. Yaniel, P. Powledge, A. Mamishev, and J. Smith, "Design of an rfid-based battery-free programmable sensing platform," *IEEE Trans. on Instrumentation and Measurement*, vol. 57, no. 11, pp. 2608–2615, Nov. 2008.

[49] K. Seada, M. Zuniga, A. Helmy, and B. Krishnamachari, "Energy-efcient forwarding strategies for geographic routing in lossy wireless sensor networks," in *Proc. ACM SenSys*, pp. 108–121, Baltimore, MD, Nov. 2004.

[50] R. C. Shah, S. Roy, S. Jain, and W. Brunette, "Data MULEs: Modeling a three-tier architecture for sparse sensor networks," in *Proc. of First IEEE International Workshop on Sensor Network Protocols and Applications (SNPA)*, pp. 30–41, Anchorage, AK, May 2003.

[51] Y. Shi, and Y.T. Hou, "Theoretical results on base station movement problem for sensor network," in *Proc. IEEE INFOCOM*, pp. 376–384, Phoenix, AZ, Apr. 2008.

[52] E. Shih, S.-H. Cho, N. Ickes, R. Min, A. Sinha, A. Wang, and A. Chandrakasan, "Physical layer driven protocol and algorithm design for energy efcient wireless sensor networks," in *Proc. ACM MobiCom*, pp. 272–287, Rome, Italy, July 2001.

[53] H.D. Sherali, W.P. Adams and P.J. Driscoll, "Exploiting special structures in constructing a hierarchy of relaxations for 0-1 mixed integer problems," *Operations Research*, vol. 46, no. 3, pp. 396–405, May–June 1998.

[54] H.D. Sherali and W.P. Adams, *A Reformulation- Linearization Technique for Solving Discrete and Continuous Nonconvex Problems*, Kluwer Academic Publishers, Chapter 8, 1999.

[55] S. Cui, A.J. Goldsmith, and A. Bahai, "Energy-constrained modulation optimization," *IEEE Trans. on Wireless Communication*, vol. 4, no. 5, pp. 2349–2360, Sep. 2005.

[56] L. Summerer and O. Purcell, "Concepts for based on wireless energy transmission via laser," in *International Conf. on Space Optical Systems and Applications (ICSOS)*, article 18, Tokyo, Japan, Feb. 2009.

[57] N. Tesla, "Apparatus for transmitting electrical energy," US patent number 1,119,732, issued in Dec. 1914.

[58] B. Tong, G. Wang, W. Zhang, and C. Wang, "Node reclamation and replacement for long-lived sensor networks," *IEEE Trans. on Parallel and Distributed Syst.*, vol. 22, no. 9, pp. 1550–1563, Sep. 2011.

[59] B. Tong, Z. Li, G. Wang, and W. Zhang, "How wireless power charging technology affects sensor network deployment and routing," in *Proc. IEEE ICDCS*, pp. 438–447, Genoa, Italy, Jun. 2010.

[60] H. Tuy, *Convex Analysis and Global Optimization,* Chapter 5, Kluwer Academic, 1998.

[61] U.S. Environmental Protection Agency and U.S. Department of Energy, "2013 Scion iQ EV," URL: http://www.fueleconomy.gov.

[62] T.A. Vanderelli, J.G. Shearer, and J.R. Shearer, "Method and apparatus for a wireless power supply," U.S. patent number 7,027,311, issued in Apr. 2006.

[63] M.C. Vuran, and I.F. Akyildiz, "Spatial correlation-based collaborative medium access control in wireless sensor networks," *IEEE/ACM Trans. on Networking,* vol. 14, no. 2, pp. 316-329, Apr. 2006.

[64] G. Wang, W. Liu, M. Sivaprakasam, M. Humayun, and J. Weiland, "Power supply topologies for biphasic stimulation in inductively powered implants," in *Proc. IEEE Int. Symp. Circuits Syst. (ISCAS)*, pp. 2743–2746, Kobe, Japan, May 23–26, 2005.

[65] W. Wang, V. Srinivasan, and K.C. Chua, "Extending the lifetime of wireless sensor networks through mobile relays," *IEEE/ACM Trans. on Networking*, vol. 16, no. 5, pp. 1108–1120, Oct. 2008.

[66] E. Welzl, "Smallest enclosing disks," *Lecture Notes in Computer Science (LNCS),* vol. 555, pp. 359–370, 1991.

[67] WiTricity Corp., URL: http://www.witricity.com.

[68] Wireless Power Consortium, URL: http://www.wirelesspowerconsortium.com/.

[69] G. Xing, T. Wang, W. Jia, and M. Li, "Rendezvous design algorithms for wireless sensor networks with a mobile base station," in *Proc. ACM MobiHoc*, pp. 231–240, Hong Kong, China, May 27–30, 2008.

[70] M, Younis, M. Bangad and K. Akkaya, "Base-station repositioning for optimized performance of sensor networks," in *Proc. IEEE Vehicular Technology Conference*, pp. 2956–2960, Orlando, FL, Oct. 4–9, 2003.

[71] G.J. Zalmai, “Optimality conditions and Lagrangian duality in continuous-time nonlinear programming,” *Journal of Mathematical Analysis and Applications*, pp. 426–452, vol. 109, no. 2, Aug. 1985.

[72] F. Zhang, X. Liu, S.A. Hackworth, R.J. Sclabassi, and M. Sun, “In vitro and in vivo studies on wireless powering of medical sensors and implantable devices,” in *Proc. IEEE/NIH Life Science Systems and Applications Workshop (LiSSA)*, pp. 84–87, Apr. 2009, Bethesda, MD.

[73] R. Zhang and C.K. Ho, “MIMO broadcasting for simultaneous wireless information and power transfer,” available [online] at http://arxiv.org/abs/1105.4999

[74] W. Zhao, M. Ammar, and E. Zegura, “A message ferrying approach for data delivery in sparse mobile ad hoc networks,” in *Proc. ACM MobiHoc*, pp. 187–198, Tokyo, Japan, May 2004.

[75] M. Zhao, J. Li and Y. Yang, “Joint mobile energy replenishment and data gathering in wireless rechargeable sensor networks,” in *Proc. International Teletraffic Congress*, pp. 238–245, San Francisco, CA, Sep. 6–8, 2011.

Vita

Liguang Xie obtained his B.S. degree (with honors) from Zhejiang University, Hangzhou, China in 2006, a M.S. degree from Virginia Tech, Blacksburg, VA in 2009, both in computer science. From 2009 to 2013, Liguang was a Ph.D. student in the Bradley Department of Electrical and Computer Engineering at Virginia Tech, and was a Graduate Research Assistant in the Complex Networks and Security Research (CNSR) Lab directed by his advisor Prof. Y. Thomas Hou. During the same period, Liguang also obtained a simultaneous M.S. degree in Operations Research in 2013. Liguang's research interests include algorithm design and optimization for wired and wireless networks.

Liguang is a member of ACM and IEEE. He has been a frequent reviewer for IEEE and ACM journals and conferences. In addition, he has served (or is serving) on the Technical Program Committees of a number of international conferences. He was a recipient of Paul E. Torgersen Graduate Student Research Excellence Award from Virginia Tech in 2010, and the prestigious Chinese Government Award for Outstanding Students Abroad in 2012.

Publications

Book Chapter

[B1] L. Xie, Y. Shi, Y.T. Hou, W. Lou, H.D. Sherali, and H. Zhou, "Rechargeable sensor networks with magnetic resonant coupling," to appear in *Rechargeable Sensor Networks: Technology, Theory and Application*, J. Chen, S. He and Y. Sun (eds.), World Scientific Publishing, 2014.

Refereed Journal and Magazine Articles

[J6] L. Xie, Y. Shi, Y.T. Hou, W. Lou, H.D. Sherali, and S. F. Midkiff, "Multi-node wireless

energy charging in sensor networks" submitted to *IEEE/ACM Transactions on Networking,* under revision.

[J5] L. Xie, Y. Shi, Y.T. Hou, and H.D. Sherali, "Making sensor networks immortal: An energy-renewal approach with wireless power transfer," *IEEE/ACM Trans. on Networking*, vol. 20, no. 6, pp. 1748–1761, Dec. 2012.

[J4] L. Xie, Y. Shi, Y.T. Hou, and W. Lou, "Wireless power transfer and applications to sensor networks," *IEEE Wireless Communications*, vol. 20, no. 4, pp. 140–145, Aug. 2013.

[J3] M. Hu, Q. Peng, L. Xie, and W. Chen, "A multiple criteria framework for 3D protein shape similarity retrieval," *Chinese Journal of Computers,* vol. 29, no. 12, pp. 2208–2217, Dec. 2006.

[J2] T. Zhang, W. Chen, L. Xie, M. Hu, and Q. Peng, "Molecular structural analysis based on the topological extraction of 3D scalar fields," *Journal of Software,* vol. 17, supplement, pp. 120–125, Nov. 2006.

[J1] M. Hu, W. Chen, T. Zhang, Q. Peng, L. Xie, "A new approach for examining the similarity of protein 3D shape," *International Journal of Information Technology*, vol. 11, no. 8, pp. 6–19, 2005.

Refereed Conference Publications

[C7] L. Xie, Y. Shi, Y.T. Hou, W. Lou, and H.D. Sherali, "On traveling path and related problems for a mobile station in a rechargeable sensor network," in *Proc. ACM MobiHoc*, pp. 109–118, Bangalore, India, July 29–Aug. 1, 2013.

[C6] L. Xie, Y. Shi, Y.T. Hou, W. Lou, H.D. Sherali, and S. F. Midkiff, "Bundling mobile base station and wireless energy transfer: Modeling and optimization," in *Proc. IEEE INFOCOM*, pp. 1684–1692, Turin, Italy, Apr. 2013.

[C5] L. Xie, Y. Shi, Y.T. Hou, W. Lou, H.D. Sherali, and S. F. Midkiff, "On renewable sensor networks with wireless energy transfer: The Multi-Node Case," in *Proc. IEEE SECON*, pp. 10–18, Seoul, Korea, June 2012.

[C4] Y. Shi, L. Xie, Y.T. Hou, and H.D. Sherali, "On renewable sensor networks with wireless energy transfer," in *Proc. IEEE INFOCOM,* pp. 1350–1358, Shanghai, China, Apr. 2011.

[C3] L. Xie, B. Fang, Y. Cao, and F. Quek, “A nonlinear manifold learning framework for real-time motion estimation using low-cost sensors,” in *Proc. IEEE Applied Imagery Pattern Recognition workshop*, pp. 261–268, Washington D.C., USA, Oct. 2008.

[C2] B. Fang, L. Xie, P. Chung, Y. Cao, and F. Quek, “Human gesture tracking using an agent-based tracking system,” in *Proc. IEEE Applied Imagery Pattern Recognition workshop*, pp. 56–62, Washington D.C., USA, Oct. 2008.

[C1] L. Xie, M. Kumar, Y. Cao, D. Gracanin, and F. Quek, “Data-driven motion estimation with low-cost sensors” in *Proc. IET Visual Information Engineering*, pp. 600–605, Xi’an, China, July 29–Aug. 1, 2008.